Computational properties of cerebellar nucleus neurons: Effects of stochastic ion channel gating and input location

Maria Psarrou

Submitted to the University of Hertfordshire in partial fulfilment of the requirements of the degree of

Doctor of Philosophy

March 2018

Declaration

I have composed this thesis myself and it reports original research that has been conducted by myself unless otherwise indicated. The thesis does not contain any material that has been accepted for the award of any other degree or diploma in my name, in any university or other institution and, to the best of my knowledge does not contain any material previously published by another person, except where due reference is made in the text of the thesis.

Hatfield, 9 March 2018

Maria Psarrou

Acknowledgments

Writing the very last lines of this thesis, I would like to thank all these people who made this path an inspiring journey and in one way or another contributed to my thesis.

First and foremost, I would like to thank my principal supervisor, Volker Steuber, for his invaluable help and support, for sharing his experience and ideas, and for achieving the impossible for many, convincing me to be punctual. I would like also to express my sincere gratitude to my co-supervisors, Neil Davey (especially for his overall help with university matters and organizing the DDS meetings), Maria Schilstra, Michael Schmuker and Ben (Benjamin) Torben-Nielsen for the inspiring discussions, feedback and encouragement. I consider myself extremely lucky and fortunate to have had such a skilled supervisory team, capable of mentoring on so many different subjects (scientific or not).

I would like also to thank the University of Hertfordshire for giving me many opportunities to expand and develop my skills further and beyond my research. Many thanks to all the staff members who helped me and created a supportive and welcoming environment. I am particularly thankful to Rene te Boekhorst for his statistically (significant) help.

Further, I would like to thank my fellow PhD students and colleagues (Parivash, Weam, Parimala, Sylvia, Fariba, Anuradha, Udeshika, Ronak, Julia, Kirsty, Yi, Rebecca, Adeline, Zaheed, Ahmed, Ankur, Christoph, Jean, Alex, Sam, Marco, Deepak, Ed, Paul, Nathan, Dimitris, Karen, Damien, Cosme, Andrei, Azeemsha, Sudhir) for making the Biocomputation group (and STRI) such an enjoyable and warm work environment. I really appreciated every little help, chat, brainstorming, coffee/beer/London break (and apologies for asking so many questions in the journal club). Special thanks to Parimala, Weam and Sylvia for so many fun

moments and to Zaheed for always being the support needed, through some difficult situations, even at moment's notice.

Many special thanks also to Parivash and Alessandra for their friendship, for sharing so many experiences (or flat) and for introducing me to the Iranian and Italian culture. I couldn't have asked for better ambassadors.

So many thanks to Aliki, Valia and Vaggelio for being around the clock friends and proving that friendship has no borders.

A special thanks to Ali. I couldn't have made this journey without him being there and support me in every possible way.

Lastly, I always grateful to my family (and dogs) and especially to my parents for always believing in me and being unconditionally supportive. I also am very thankful to my uncle Emmanuel for being the best mentor.

Abstract

The function of the nervous system is shaped by the refined integration of synaptic inputs taking place at the single neuron level. Gain modulation is a computational principle that is widely used across the brain, in which the response of a neuronal unit to a set of inputs is affected in a multiplicative fashion by a second set of inputs, but without any effect on its selectivity. The arithmetic operations performed by pyramidal cells in cortical brain areas have been well characterised, along with the underlying mechanisms at the level of networks and cells, for instance background synaptic noise and dendritic saturation. However, in spite of the vast amount of research on the cerebellum and its function, little is known about neuronal computations carried out by its cellular components. A particular area of interest are the cerebellar nuclei, the main output gate of the cerebellum to the brain stem and cortical areas. The aim of this thesis is to contribute to an understanding of the arithmetic operations performed by neurons in the cerebellar nuclei. Focus is placed on two putative determinants, the location of the synaptic input and the presence of channel noise.

To analyse the effect of channel noise, the known voltage-gated ion channels of a cerebellar nucleus neuron model are translated to stochastic Markov formalisms and their electrophysiologial behaviour is compared to their deterministic Hodgkin-Huxley counterparts. The findings demonstrate that in most cases, the behaviour of stochastic channels matches the reference deterministic models, with the notable exception of voltage-gated channels with fast kinetics. Two potential explanations are suggested for this discrepancy. Firstly, channels with fast kinetics are strongly affected by the artefactual loss of gating events in the simulation that is caused by the use of a finite-length time step. While this effect can be mitigated, in part, by

using very small time steps, the second source of simulation artefacts is the rectification of the distribution of open channels, when channel kinetics characteristics allow the generation of a window current, with an temporal-averaged equilibrium close to zero. Further, stochastic gating is implemented in a realistic cerebellar nucleus neuronal model. The resulting stochastic model exhibits probabilistic spiking and a similar output rate as the corresponding deterministic cerebellar nucleus neuronal model. However, the outcomes of this thesis indicate the computational properties of the cerebellar nucleus neuronal model are independent of the presence of ion channel noise.

The main result of this thesis is that the synaptic input location determines the single neuron computational properties, both in the cerebellar nucleus and layer Vb pyramidal neuronal models. The extent of multiplication increases systematically with the distance from the soma, for the cerebellar nucleus, but not for the layer Vb pyramidal neuron, where it is smaller than it would be expected for the distance from the soma. For both neurons, the underlying mechanism is related to the combined effect of nonlinearities introduced by dendritic saturation and the synaptic input noise. However, while excitatory inputs in the perisomatic areas in the cerebellar nucleus undergo additive operations and the distal areas multiplicative, in the layer Vb pyramidal neuron the integration of the excitatory driving input is always multiplicative. In addition, the change in gain is sensitive to the synchronicity of the excitatory synaptic input in the layer Vb pyramidal neuron, but not in the cerebellar nucleus neuron. These observations indicate that the same gain control mechanism might be utilized in distinct ways, in different computational contexts and across different areas, based on the neuronal type and its function.

Contents

1 Introduction

1.1 Motivation

How does the brain compute? This is a central question in neuroscience and its answer would probably provide a fair understanding of higher cognitive functions and psychiatric and neural disorders (Adolphs, 2015). To study how the neural system acquires, maintains and utilizes its enormous computational capacity a methodical approach of three main steps could be applied.

The first step is to define the basic computational unit of the brain. In that context, a neural unit could be a neural system, such as the motor system, a brain region, such as the frontal lobe or cerebellum, a neural circuit, such as the cortical or cerebellum microcircuit, a single neuron, or a sole dendrite (Salinas and Sejnowski, 2001; Silver, 2010).

The second step is to identify the principles governing the computational operations of the neural system. The neuronal function is based on the interchange of synaptic signals between various regions of the brain that are integrated at the single neuron level. Although the basic nature of the synaptic inputs, is either excitatory or inhibitory, their integration mode could vary, from simple addition to multiplication. In fact, a brain-wide computational principle is gain modulation, where the response amplitude (sensitivity) of one neuronal unit to one set of signal inputs can undergo multiplicative transformation by the input of a second unit, without affecting the selectivity of the neuronal unit to a particular stimulus. For example, in the parietal cortex the neuronal responses depend on the retinal location of a visual stimulus and are multiplicatively modulated by gaze direction (Salinas and Sejnowski, 2001; Silver, 2010).

The third step is to elucidate the mechanisms underlying these computational principles. Again, this investigation can be carried out at the level of a brain region or single neuron, and the potential mechanisms could be related to properties either of neuronal populations or single neurons (Salinas and Sejnowski, 2001; Silver, 2010). For instance, gain modulation at the single neuron level can occur from the presence of background synaptic noise, from dendritic saturation due to the level of synaptic activation, or from synaptic non-linearities, such as short-term depression (Silver, 2010).

In addition to these steps, other factors related to the neuronal function should be considered. Such a paradigm is the presence of noise at distinct levels of the neural system, like the synaptic noise in a network of neurons, or the electric noise at the cellular level. Noise is manifested in experimental trials, *in vivo* and *in vitro*, as variability in the neuronal and behavioural responses. Although, at a first glance, its functional implications might seem destructive for the neuronal function and communication, they can be beneficial as well. As mentioned, synaptic noise underlies gain modulation and therefore supplements the potential computational operations of the neuron. In addition, electrical noise, which is generated by the stochastic gating of neuronal ion channels, could impact single neuronal dynamics and arithmetic. For example, in the presence of channel noise the amplitude of membrane potential fluctuations varies between the dendritic locations, with thinner dendrites exhibiting greater amplitudes, which affects the reliability of temporal spike patterns (Faisal et al., 2008; White et al., 2000).

The cerebellum, and in particular the cerebellar nucleus neurons, are an excellent candidate to study the computational properties of the nervous system. Cerebellar function is associated with motor control and coordination and a number of higher cognitive functions. Among the features that make it unique is that the majority of the neurons in the brain lie in the cerebellar cortex and that they are organized in a well-characterized basic pattern of a microcircuit. The cerebellum communicates bidirectionally with both the periphery and other brain areas. The cerebellar cortex output is inhibitory, via the Purkinje cells, and projects to the cerebellar nucleus neurons, in the deep cerebellar nuclei. These neurons also receive excitatory input from mossy fibres, which originate from several locations in the brain and spinal cord, and climbing fibres, which originate solely from the brain stem. After processing these inputs, they produce most of the output of the cerebellum. Cerebellar nucleus neurons are enriched by several voltage-gated ion channels and have an elaborate dendritic tree with variability in its

morphology (Apps and Garwicz, 2005; Baumel et al., 2009; Halloran et al., 2011; Saab and Willis, 2003; Uusisaari et al., 2007; Uusisaari and Knöpfel, 2012).

Untangling the integrating properties of synaptic inputs in the cerebellar nucleus neurons, by using *in silico* modelling methods and considering factors such as channel noise and input location, could provide a better understanding of cerebellar function, in a context closer to real experimental conditions, that is, in the presence of channel noise, and in more refined way, that is, input location specific arithmetic operations. Therefore, it could unravel new mechanisms underlying the computational operations of the neural system at the single neuron level, adding knowledge to the ongoing research to answer the original question: how does the brain compute?

1.2 Aims of the Thesis

The main aim of this thesis is to elucidate the computational properties of cerebellar nucleus neurons by using a systematic approach and *in silico* methods. In particular, the role of stochastic ion channel gating and input location is studied as an underlying mechanism for gain modulation.

Cerebellar nucleus neurons are the main output gateway of the cerebellum, and it has been suggested that they use different neural coding schemes, spike rate- or timing-based, to convey the information from the cerebellar cortex. Candidate mechanisms for these codes, such as post-inhibitory rebound spiking of cerebellar nucleus neurons and synchronicity or irregularity in Purkinje cells' spiking, have been identified in cerebellar nucleus neurons, by using computational models with different detail in their complexity and biological abstraction (De Zeeuw et al., 2011; Heck, 2015; Steuber and Jaeger, 2013).

Yet, the exact synaptic arithmetic operations utilized by the cerebellar nucleus neurons remain to be investigated thoroughly. A computational study using a cerebellar nucleus neuronal model with realistic morphology and a full collection of the known ionic channels, suggests that increases in the excitatory input rate from mossy fibres, or decreases in the inhibitory input rate from Purkinje cells, can control the output rate of the cerebellar nucleus neuron. In particular, inhibition from Purkinje cells performs an additive operation on the excitatory input from mossy fibres. Notably, there is no indication of multiplicative operations, in the experimental set-up used, that is, both inhibitory and excitatory synaptic inputs are

distributed along the cell, and the description of the ion channels of the neuronal model is according to the deterministic Hodgkin-Huxley formalism (Steuber et al., 2011).

Could multiplicative operations, or gain modulation occur in cerebellar nucleus neurons? Neuronal noise, such as synaptic noise, can give rise to such computations in pyramidal cells, either in a balanced background configuration (Chance et al., 2002) or in combination with dendritic saturation (Prescott and De Koninck, 2003). But, neuronal noise could also stem from stochastic ion channel gating, and affect the amplitude of the membrane potential fluctuations, especially in the thinner dendritic compartments, and as a result the synaptic integration (Cannon et al., 2010; Kole et al., 2006). Therefore, different computations could take place, in the presence of ion channel noise, based on the input location. A hypothesis could be that in the presence of channel noise, inputs in large areas, such as the soma or thick dendrites would be integrated in an additive way. However, due to the occurrence of larger voltage fluctuations, inputs in thinner dendrites would undergo multiplicative operations.

These phenomena have not been studied so far in the cerebellar nucleus neuron. Therefore, a construction of a neuronal model with stochastic ion channels and a systematic approach of stimulations in distinct dendritic locations and with different synaptic input combinations would advance the knowledge towards this direction. The following objectives are required to achieve this research aim:

1. Conduct a detailed literature review on the functional implications of neuronal noise, and particularly channel noise, and on gain modulation and the underlying mechanisms.
2. Develop a stochastic cerebellar nucleus neuronal model. The new stochastic model is based on a morphologically and biophysically realistic computational model of a cerebellar nucleus neuron, adjusted to replicate the experimentally observed electrophysiological properties of excitatory projection neurons. This model also includes a deterministic Hodgkin-Huxley description of its voltage-gated ion channels (Steuber et al., 2011). In order to introduce channel noise to the cerebellar nucleus neuronal model, its voltage-gated channels are translated to Markov formalisms, where they are described by a detailed kinetic scheme and by a probabilistic transition between the kinetic states, as in Kole et al. (2006). The development of the stochastic cerebellar nucleus neuronal model is a two-step process: firstly, each channel is described as a Markov model and is

behaviour is investigated in a simple single compartment model; secondly, the stochastic channels are incorporated and studied in the detailed cerebellar nucleus neuronal model.

3. Study the computational properties of the cerebellar nucleus neuron, in particular, its ability to perform multiplicative gain modulation. The arithmetic operations of the stochastic cerebellar nucleus neuronal model are considered, in the presence (or not) of ion channel noise and when the neuron is stimulated in the soma or different dendritic locations or regions.
4. Investigate the generality of the gain modulation mechanism by simulating another neuronal type, a layer Vb pyramidal neuron.

1.3 Contribution to knowledge

The research presented in this thesis adds to the body of knowledge of neuroscience, and especially to the better comprehension of the impact of ion channel noise and synaptic input location on single neuron computational properties, via the following main outcomes:

1. In the cerebellar nucleus neuronal model, the excitatory input is systematically modulated by the inhibitory one in a location dependent manner, where location can be a dendritic compartment or dendritic tree region. Inputs to distant locations undergo multiplicative operations, which are almost absent in the somatic and perisomatic areas. The underlying mechanism is related to the nonlinearities introduced by dendritic saturation, enhanced by the synaptic noise and synaptic input variability.
2. The same underlying mechanism for gain modulation mechanism is observed in a layer Vb pyramidal neuron. However, in this neuron the type of modulation is independent of the input location, since multiplicative operations also occur in proximal to the soma dendritic areas (basal and trunk dendrites).
3. In cerebellar nucleus neuronal model, the extent of multiplication increases systematically with the distance from the soma. However, in the layer Vb pyramidal neuronal model, the extent of multiplication is smaller than expected for the distance from the soma and related to the local input resistances.
4. The input-location dependent change in gain is correlated with the input synchronicity in the layer Vb pyramidal neuron, but not in the cerebellar nucleus neuron.

5. The choice of a modelling approach to represent the kinetics of ion channel models is subject to a trade-off between biological detail and computational cost. As in previous research, it is confirmed in this thesis that the representation of the kinetics of a single ion channel with Markov methods is possible and the average behaviour of a channel populations is a good match with the deterministic behaviour as observed with Hodgkin–Huxley counterpart models, for the majority of the cerebellar nucleus voltage-gated channels. Single channel properties, such as the specific single channel conductance, or modelling related factors, such as the integration time step, can affect the simulation results, and hence the recorded behaviour of the channel models.
6. The response of the Markov formalism of some cerebellar nucleus voltage-gated channels does not overlap with their deterministic Hodgkin–Huxley counterpart. Two possible explanations are proposed, which are not mutually excluded: Firstly, the impact of the rectification of the distribution of open channels is suggested as a factor overlooked in the implementation of the deterministic algorithms. This phenomenon could occur for ion channels if their kinetic scheme is governed by fast transition rates and it is believed to include activation and inactivation variables, which allow the generation of window current. In the presence of stochastic gating, if the current equilibrium is close to zero, and if the open channel fluctuations magnitude goes below zero, then their distribution could be rectified, and as a result the temporal average stochastic current equilibrium will not match the deterministic one. Therefore, under certain conditions the Hodgkin–Huxley model might misestimate the current flow through the voltage-gated ion channels. Secondly, even in the absence of rectification discrepancies might still occur. Due to the fast transition rates between the different kinetic states of the ion channels, there is a greater probability of multiple transitions per simulation time step, which could result in discrepancies between the response of the two models. These inconsistencies are increased with larger spans of the simulation integration step.
7. The first stochastic neuronal model of cerebellar nucleus model, where channel noise is implemented as probabilistic gating is developed and validated. The stochastic cerebellar nucleus neuronal model is detailed in terms of its morphological and biophysical features and its electrophysiological behaviour matches the available experimental data (as in Steuber et al., 2011).

8. The computational properties of the cerebellar nucleus neuronal model are independent of the presence of ion channel noise.

1.4 Overview of the Thesis

This thesis has been prepared in seven chapters. Chapter 1 is the introduction, followed by a literature review and a summary of the relevant experimental results and computational models in Chapters 2, 3 and 4. In Chapters 5 and 6, the findings of the research undertaken for this study are presented and analysed in detail. Finally, Chapter 7 contains a general discussion and conclusion of this study. The details of each chapter are summarized as follows:

- **Chapter 1** introduces briefly the background and the research questions behind the motivation for this study. In addition, the research aims are presented, the contribution to knowledge, the structure of this thesis, and its dissemination.
- **Chapter 2** presents the conductance based multi-compartmental neuronal models used for this study, the cerebellar nucleus neuron and the layer Vb pyramidal neuron. For both neurons, an overview of the function and structure of the brain area they belong to, that is, cerebellum and neocortex respectively, is given. Then, their biophysical and electrophysiological properties, which define the details of their corresponding neuronal models, are summarized.
- **Chapter 3** contains a literature review on neuronal noise, with emphasis on ion channel noise and its functional implications for neuronal function. Further, it introduces two distinct methods to model ionic channels, the classic Hodgkin-Huxley and the stochastic Markov formalisms.
- **Chapter 4** presents literature research on gain modulation. A comprehensive review is performed on the functional applications of gain modulation, as a brain-wide computational principle, followed by a detailed description of known mechanisms, with a focus on the ones at single neuron level.
- **Chapter 5** demonstrates the development of a stochastic cerebellar nucleus neuron model. In the first part, the voltage-gated ion channels of the cerebellar nucleus neuron are converted to Markov formalisms and their behaviour is studied in a simple compartmental model. In the second part, a cerebellar nucleus neuron with stochastic ion channels is implemented, and its behaviour is compared with the deterministic cerebellar nucleus neuron version.

- **Chapter 6** describes the arithmetic operations performed by the cerebellar nucleus neuron and compares them with those in the layer Vb pyramidal neuron. The chapter is divided into two main sections. Firstly, the role of channel noise in the computational operations of the cerebellar nucleus neuron is investigated. Then, a systematic study of the impact of input location on gain modulation is performed for both neuronal models, where factors such as the nature of input (synaptic or current injection), the distribution of inputs on the dendritic tree and soma, and the synaptic input synchronicity, are also considered.
- **Chapter 7** reviews the findings and presents the conclusions drawn from this research. Further, future directions are also explored.

1.5 Dissemination from the thesis

Research outcomes of this study have been presented at the following conferences:

1. Psarrou, M., Schilstra, M., Davey, N., Steuber, V. "A comparison of deterministic and stochastic ion channel representations in a model of a cerebellar nucleus neuron", Bernstein Conference 2015, Heidelberg, Germany: Poster presentation.
2. Psarrou, M., Schilstra, M., Davey, N., Torben-Nielsen, B., Steuber, V. "Input-location dependent gain modulation in cerebellar nucleus neurons", CNS 2016 Jeju, South Korea: Oral presentation.
3. Psarrou, M., Schilstra, M., Davey, N., Torben-Nielsen, B., Schmuker, M., Steuber, V. "Input-location dependent gain modulation", CNS 2017 Antwrep, Belgium: Poster presentation.

2 Neuronal models

2.1 Cerebellum

2.1.1 Function

The cerebellum (latin for “little brain”) is located at the back of the brain, underlying the occipital and temporal lobes of the cerebral cortex (Figure 2.1). There is an extended bidirectional communication between cortical areas and the cerebellum, forming cerebello-thalamo-cerebro-cortical loops, where the cerebral projections deliver output to the same cerebellar regions from which they receive input (D’Angelo and Casali, 2013; Halloran et al., 2011) (Figure 2.2).

This unique architecture of the cerebro-cerebellar pathways might underlie the diverse functions associated with cerebellum. Traditionally cerebellar function has been thought to be mostly involved in motor control and coordination, but it also extends to other cognitive functions, such as attention, language, learning, memory, visual processing, decision making and social, emotional and regulatory behaviour. Cerebellar dysfunction is linked to a variety of neuropsychiatric conditions, such as schizophrenia, autism, depression, dyslexia and motor impairments, namely, ataxias (D’Angelo et al., 2016; Halloran et al., 2011; Sokolov et al., 2017).

The computational principles that govern the function of cerebellum are often conceptualized as prediction and error-based learning, although other theories, for example related to timing, exist (Moberget and Ivry, 2016; Sokolov et al., 2017).

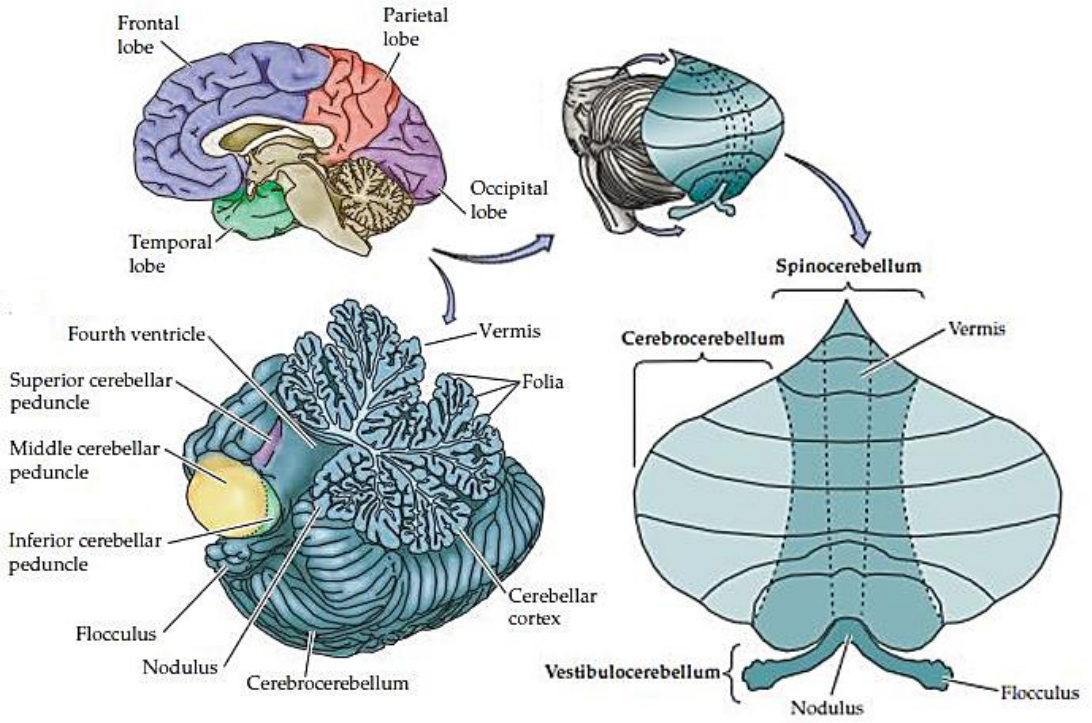

Figure 2.1 Cerebellum gross organization in the human brain. Left upper panel: Midsagittal section of the brain gross anatomy showing the four lobes of the brain and the cerebellum (below the occipital lobe and above the brain stem). Left lower panel: Paramedian sagittal section through the left cerebellar hemisphere illustrating major components of the cerebellum, such as the caudal lobes of the vestibulocerebellum and its flocculus and nodulus, the cerebellar peduncles and the organization of the cerebellum surface into folia (small gyri). Right panels: Flattened view of the cerebellar cortex surface showing its three major subdivisions (cerebrocerebellum, spinocerebellum, vestibulocerebellum) based on their source input (see also Figure 2.2 for details). Adapted from Purves et al., 2004.

2.1.2 Cerebellar circuitry

The cerebellar cortex is organized into three layers, with the same basic neuronal microcircuit: the molecular layer, the Purkinje cell layer and the granule cell layer. Purkinje and granule cells make up the main feedforward circuit of the cerebellum, but other types of neurons are also found, such as basket cells, stellate cells, Lugaro cells, unipolar brush cells and Golgi cells. The molecular layer is the outer layer and cell-poor. It is mostly made up of the axons of granule cells and the dendrites of Purkinje cells but contains basket and stellate cells as well. The innermost layer is the granule cell layer, which also contains Golgi cells. Situated between them is the Purkinje cell layer. The axons of granule cells innervate the Purkinje cell layer up to the molecular layer, where they bifurcate forming the parallel fibres. The parallel fibres are glutamatergic and send excitatory inputs onto the Purkinje cells' dendritic trees. Each parallel fibre makes contact with hundreds of Purkinje cells. Moreover, they form synapses onto the basket and stellate cells of the molecular layer, which in turn send inhibitory projections to neighbouring Purkinje neurons. Golgi cells of the inner layer also

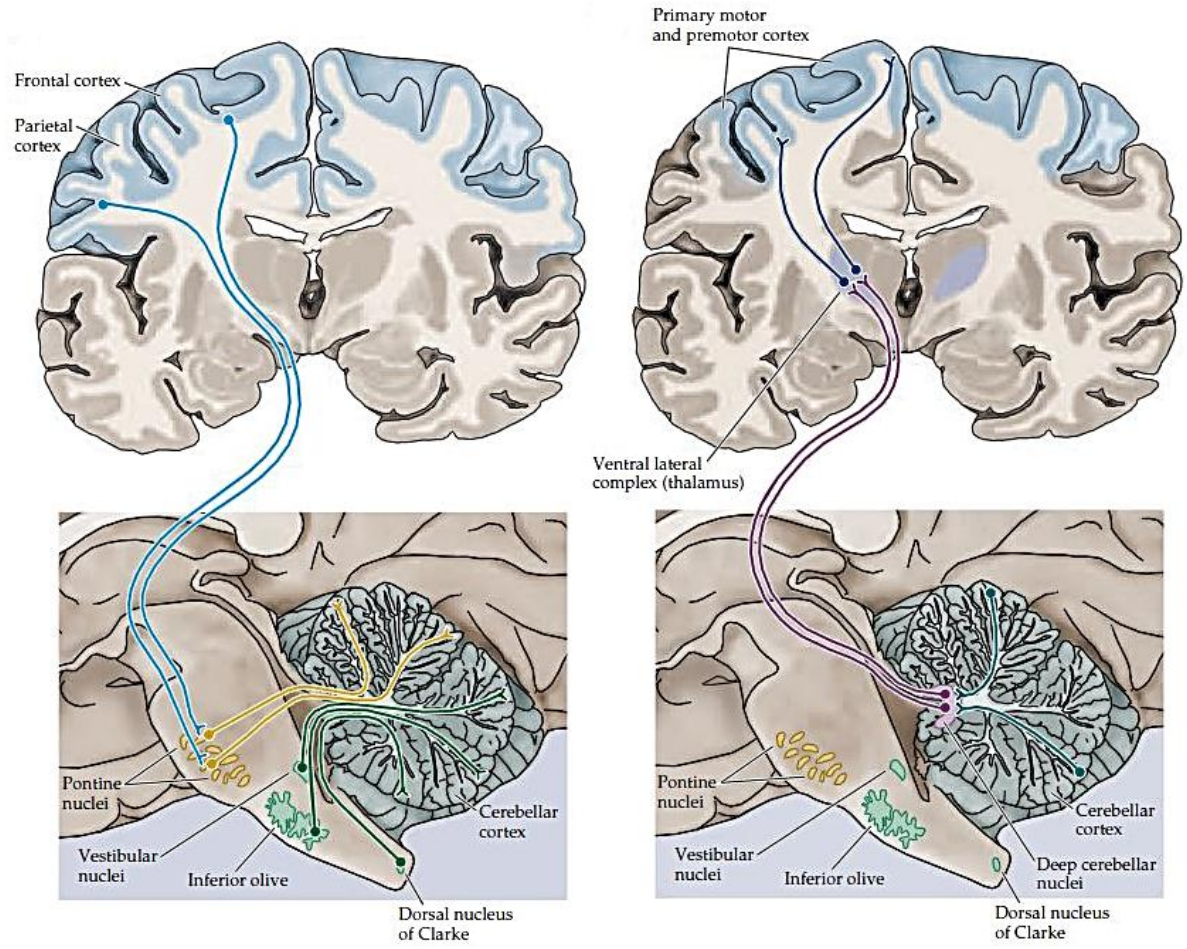

Figure 2.2 Cerebellum input and output functional organization in the human brain. Coronal (upper panels) and sagittal (lower panels) sections through the brainstem and cerebrum. Left panels: Major input projections to the cerebellum. Right panels: Major output targets of the cerebellum. Pathways leaving the deep cerebellar nuclei also project to upper motor neurons in the red nucleus, the superior colliculus, the vestibular nuclei, and the reticular formation. Adapted from Purves et al., 2004.

receive parallel fibre input and send inhibitory signals to granule cells (Apps and Garwicz, 2005; Halloran et al., 2011; Saab and Willis, 2003) (Figure 2.3).

The cerebellum receives input from the periphery through two main trajectories, the mossy fibres and the climbing fibres. This input is excitatory (glutamatergic). Mossy fibres project indirectly to Purkinje cells, via the granule cells and parallel fibres. In contrast, climbing fibres contact the Purkinje cells directly. Each Purkinje cell is contacted by merely one climbing fibre (Apps and Garwicz, 2005; Halloran et al., 2011; Saab and Willis, 2003) (Figure 2.3).

Purkinje cells have a significant role in the output of the cerebellum, since they are the source of output from the cerebellar cortex to the deep cerebellar nuclei, which are subcortical structures embedded at the centre of the cerebellum. Deep cerebellar nuclei neurons receive inhibitory (GABAergic) input from Purkinje cells, and then, after further processing this

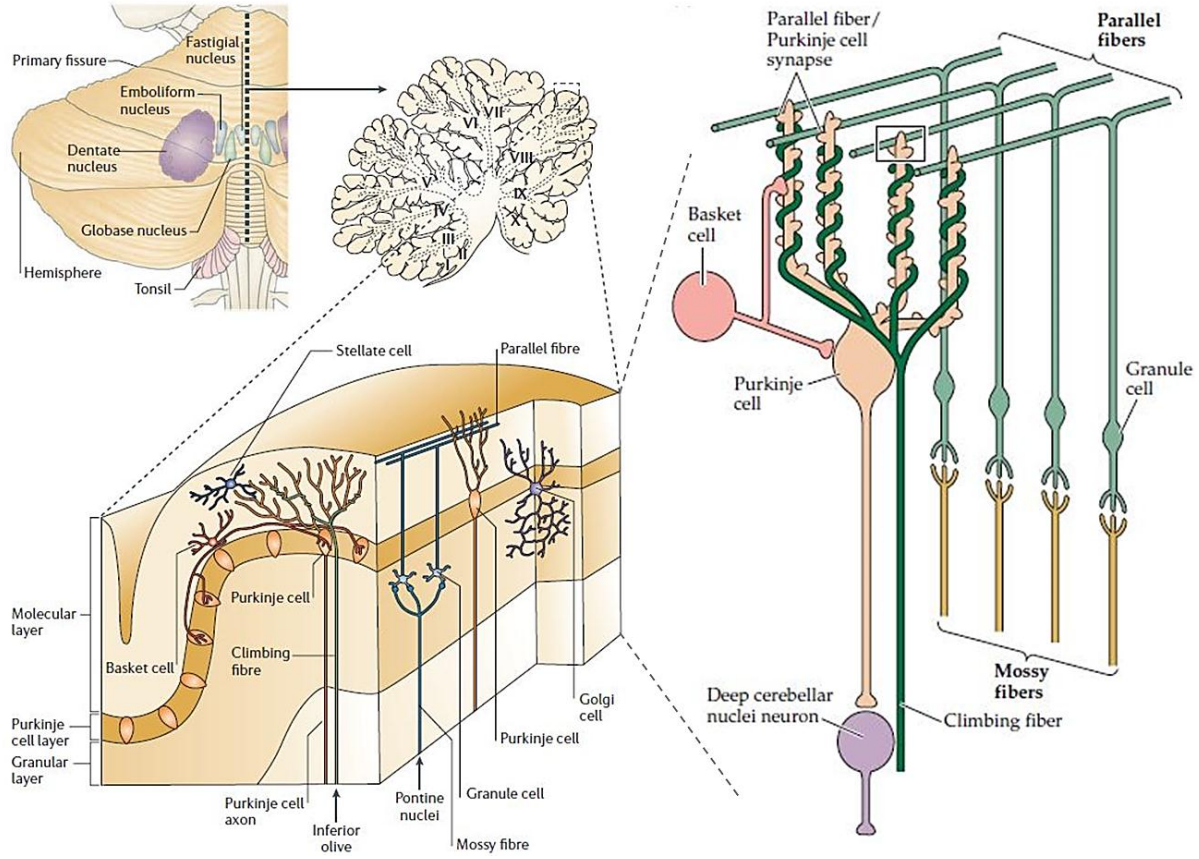

Figure 2.3 Cerebellum microstructure in the human brain. Right upper panel: Schematic of the left cerebellum hemisphere posterior view, illustrating the deep cerebellar nuclei. Left upper panel: Plane of the midsagittal cross-section with marked its lobular organization (lobes I–X). Right lower panel: Microanatomy of the cerebellar cortex. The cerebellar cortex is divided into three layers. In each one distinct types of neurons are found. Adapted from Ramnani, 2006. Right panel: Basic circuit of cerebellum. The basic pattern of the microcircuit is repeated throughout the cerebellar cortex. Adapted from Purves et al., 2004.

information, they produce most of the output of the cerebellum. Furthermore, mossy and climbing fibres project directly to the deep cerebellar nuclei (Apps and Garwicz, 2005; Halloran et al., 2011; Saab and Willis, 2003).

2.1.3 Cerebellar nuclei neuron

Cerebellar nuclei neurons (CN neurons) are the main communication gate of the entire cerebellum with the brain stem and cortical areas. Their activity is modulated by inhibitory input from Purkinje cells, and excitatory input from mossy and climbing fibres. The outputs from the deep cerebellar nuclei are inhibitory (GABAergic) signals to the inferior olivary nucleus and excitatory (glutamatergic) ones to the thalamus and brain stem (Apps and Garwicz, 2005; Baumel et al., 2009; Halloran et al., 2011; Saab and Willis, 2003; Uusisaari et al., 2007; Uusisaari and Knöpfel, 2012).

The glutamatergic projection CN neurons are characterized by complex and elaborate dendritic trees (Steuber et al., 2011; Uusisaari et al., 2007; Uusisaari and Knöpfel, 2012) (Figure 2.4). They exhibit spontaneous discharges in a regular pattern, *in vivo*, despite the presence of inhibitory input from Purkinje cells, and *in vitro*, when their synaptic inputs are blocked. The waveforms of the spontaneous action potentials are narrow and characterized by the presence of a fast after-hyperpolarization (fAHP) followed by a slow one (sAHP). When CN neurons are injected with a hyperpolarizing current, they respond with a post-hyperpolarization rebound spike burst. This rebound response can have two distinctive features: (a) a fast spike burst followed by (b) a prolonged period where the membrane is depolarized. The rate of the rebound response increases linearly with the amplitude and the duration of the hyperpolarization stimulus. Therefore, an inhibitory input to a CN neuron can produce a spike burst output. Additionally, the reproducibility of the CN response to the same input depends on the previous synaptic history (Baumel et al., 2009; Saab and Willis, 2003; Sastry et al., 1997; Steuber et al., 2011; Uusisaari et al., 2007; Uusisaari and Knöpfel, 2012).

A wide variety of voltage-gated channels, mediating Na^+, K^+ and Ca^{2+} ionic currents, is part of the CN neuron intrinsic mechanisms, shaping its electrophysiological behaviour. The Na^+ conductances underlie the fast spiking (I_{NaF}) and the maintenance of the prolonged rebound increased spiking activity (I_{NaP}). The K^+ currents have several roles. They can serve as delayed rectifiers (I_{fKdr} and I_{sKdr}) to repolarize and limit the firing frequency of action potentials, or to

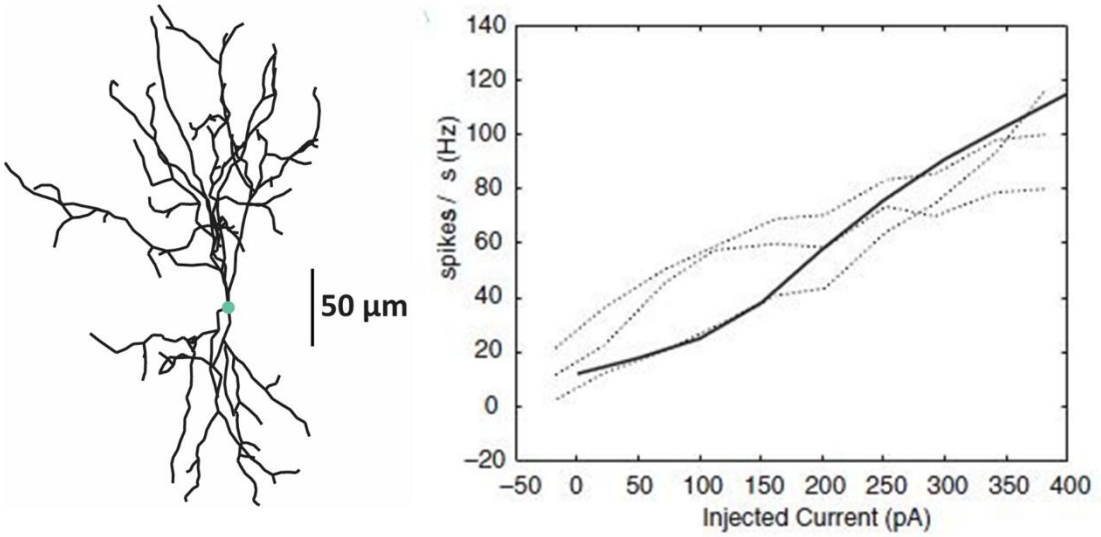

Figure 2.4 CN neuronal model. Left panel: Reconstructed neuronal morphology. The axon is not shown. Right panel: Input-Output curve for depolarizing current injection pulses for the neuronal simulated model (solid line) and experimental data from recorded neurons (dotted lines). Adapted from Steuber et al., 2011. Mint dot: soma's location (length = 32.4 µm, diameter = 14.4 µm).

introduce an after-hyperpolarization (Ca^{2+}-activated K^+ channels - I_{SK}) to spikes. There are also two Ca^{2+} conductances. The low-voltage activated T-Ca^{2+} channels (I_{CaLVA}), which can open around the resting membrane potential, generate a low-threshold Ca^{2+} regenerative current that facilitates the fast Na^+ spiking, by bringing the membrane potential to the Na^+ firing threshold after their de-inactivation by strong hyperpolarization. Subsequently, the high-voltage activated Ca^{2+} channels (I_{CaHVA}) can activate and can keep the neuron depolarized for a few milliseconds. Additionally, hyperpolarization in CN neuron can activate an inward nonselective cation hyperpolarization-activated cation (HCN) current (I_{HCN} or I_h). The effect of the I_h current is to depolarize slowly the membrane potential when it has become too negative. As a result, it can facilitate the initiation of rebound activity after strong inhibition and hyperpolarization (Hille, 2001; Sastry et al., 1997; Steuber et al., 2011; Uusisaari et al., 2007).

2.1.3.1 Cerebellar nuclei neuronal model

Several computational models have been developed with different detail in their complexity and biological abstraction, aiming to elucidate the role of CN neurons in processing their excitatory and inhibitory inputs and generating the output of the cerebellum. CN neurons integrate a range of excitatory and inhibitory inputs and they are assumed to produce output signals using different neural coding strategies (spike rate- or timing-based codes). The integration of the excitatory and inhibitory inputs that CN neurons receive could underlie their rate coding properties, and their output firing rate could be modulated by the rate, degree of irregularity and correlation (synchrony) of the inhibitory input spikes from Purkinje cells. However, temporal coding could also be the product of synchronized complex spike inputs from Purkinje cells or the CN rebound spike bursting activity following strong inhibition. The ability of CN neurons to deploy different coding schemes might depend on the behavioural task (De Zeeuw et al., 2011; Heck, 2015; Steuber and Jaeger, 2013).

For the simulations carried out in this study a CN conductance based multi-compartmental model is used; it is based on a morphological reconstruction and tuned to replicate experimentally observed electrophysiological characteristics of excitatory projection CN neuron (Steuber et al., 2011) (Figure 2.4). The model consists of 517 compartments that represent four distinct morphological areas (soma, axon, proximal dendritic and distal dendritic trees), and uniform passive properties (membrane capacitance C_m = 1.56 $\mu F/cm^2$, specific membrane resistance R_m = 3.56 Ωm^2, axial resistance R_a = 2.35 Ωm uniform for all

compartments). The active properties include eight ion channels distributed differentially over the different regions of the model: a fast sodium (NaF), a mixture of fast Kv3 (fKdr) and slow Kv2 (sKdr) delayed rectifiers, an SK-type calcium-gated potassium, an HCN current, an HVA calcium, a Cav3.1 type LVA calcium (CaT) and a persistent sodium (NaP). The intracellular calcium concentration is modelled as a sub-membrane shell with calcium influx from the HVA current. Synaptic input is modelled as biexponential postsynaptic conductance changes. The excitatory input is represented by a mixed AMPA and NMDA, and the inhibitory by a pure $GABA_A$ (Steuber et al., 2011) (Appendix A).

2.2 Neocortex

2.2.1 Function

The neocortex is part of the cerebral cortex, and in terms of evolution a mammalian innovation. The size of neocortex is believed to reflect the increasing perception and cognitive capabilities across different species and its function is related to higher cognitive functions, such as consciousness, sensory perception, reasoning, planning of behaviour, decision making, memory and language (Kaas, 2011; Marín-Padilla, 2014).

2.2.2 Cortical layers

The neocortex has a unique structure; it is arranged horizontally into cell layers, and vertically into functional columns, which include neurons with similar response properties (Harris and Shepherd, 2015; Mountcastle, 1997). The laminar structure is organized into six layers, namely, layers I-VI, counting from the superficial outer cortical surface to the deep cortex. Each layer is characterized by its distinctive neuronal types and density, and their local interconnections or connections to other cortical layers or brain regions and can be further divided to sublayers. The most superficial layer I or molecular layer contains mainly dendritic arborizations emerging from cells located in deeper layers and very few scattered neurons and glia cells. The layer II or external granule cell layer is populated by small excitatory neurons and granule (stellate) interneurons. The layer III or external pyramidal cell layer is comprised of moderate size pyramidal neurons. The layer VI or internal granule cell layer is also occupied by granule cells, and excitatory neurons. The layer V or internal pyramidal cell layer contains larger pyramidal neurons. The layer VI or polymorphic or multiform layer is inhabited by various neuronal cell types (Harris and Shepherd, 2015; Kandel et al., 2014) (Figure 2.5).

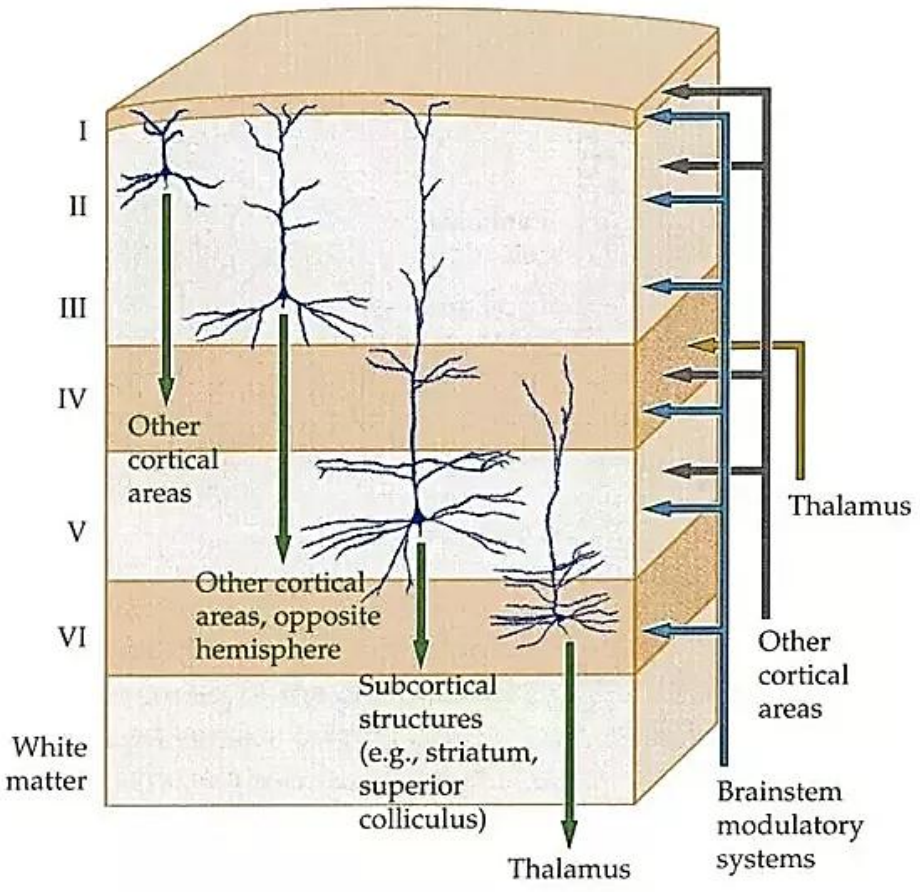

Figure 2.5 Neocortical microcircuit in the human brain. The neocortex can be divided into six laminae, based on the thickness, cell density, and other histological features. Adapted from Purves et al., 2004.

2.2.3 Layer Vb pyramidal neuron

The layer V is populated with pyramidal neurons of distinct morphological features, electrophysiological properties and axonal projections. The thick-tufted pyramidal neuron (LVb pyramidal neuron) is located in the lower part of layer V, namely, the sublayer Vb. As a pyramidal neuron, it consists of the characteristic triangle-shaped soma, two distinct dendritic trees emerging from the apex (apical tree) and base (basal tree) of the soma, and an axon with branches that bifurcate further. Both dendritic trees are elaborate, and the apical tree extends to layer I. The thick-tufted pyramidal neuron receives input from all the layers and projects to subcortical areas. Its input can be either excitatory glutamatergic on its basal, proximal and oblique apical branches, or inhibitory GABAergic, on its soma, proximal basal dendrites, axon initial segment, and terminal tufts. Due to the distinct origin of the presynaptic input, different

dendritic domains might act as distinct functional compartments (Ramaswamy and Markram, 2015; Spruston, 2008).

The response of the LVb pyramidal neuron to a depolarizing somatic current injection is a distinctive firing pattern with an initial discharge of action potentials, followed by a train with spike-frequency adaptation (Hay et al., 2011; Le Bé et al., 2007). In addition, LVb pyramidal neurons perform different integrations of their synaptic input that depend on the synaptic site and that result further in functional compartmentalization of the neuronal regions (Spruston, 2008).

Fundamental for the function and physiological properties of the LVb pyramidal neuron are the great assortment of ion channels, such as K^+ channels (A-type and persistent), Na^+ channels (transient and persistent), HCN channels, various Ca^{2+} channels, and Ca^{2+} dependent K^+ channels (small, SK, and large, BK conductances). Their distribution and density varies between the distinct neuronal regions, and their function underlies the intrinsic and integration properties of the LVb pyramidal neuron and shapes the translation of synaptic input to output firing (Ramaswamy and Markram, 2015; Spruston, 2008).

2.2.3.1 Layer Vb pyramidal neuronal model

As with the CN neuron, several models have been developed for the study of the neocortical pyramidal neurons. However, most of the them do not capture the full range of the pyramidal neurons electrophysiological properties, but are designed to replicate specific behaviours such as the impact of the HCN current on action potential (Kole et al., 2006). The pyramidal neuronal model used in this study is a conductance based multi-compartmental model with a detailed morphological reconstruction that reproduces the experimentally observed firing behaviour of a neocortical LVb pyramidal cell (Hay et al., 2011) (Figure 2.6). The model consists of 196 compartments that represent four distinct morphological areas (soma, axon, basal dendritic and apical dendritic trees). The passive properties are not uniform (membrane capacitance C_m: for the soma and axon, 1 $\mu F/cm^2$, for the basal and apical dendrites, 2 $\mu F/cm^2$, specific membrane resistance R_m is a free parameter with limits doubled for the dendrites, axial resistance R_a = 100 Ωcm uniform for all compartments). The active properties include ten ion channels distributed over the different regions of the model: a fast inactivating sodium (NaT), a persistent sodium (NaP), a muscarinic potassium (KM), a slow inactivating potassium (KP), a fast inactivating potassium (KT), a fast non-inactivating potassium (Kv3.1), a non-specific cation (HCN), an high voltage activated calcium (CaHVA), a low voltage

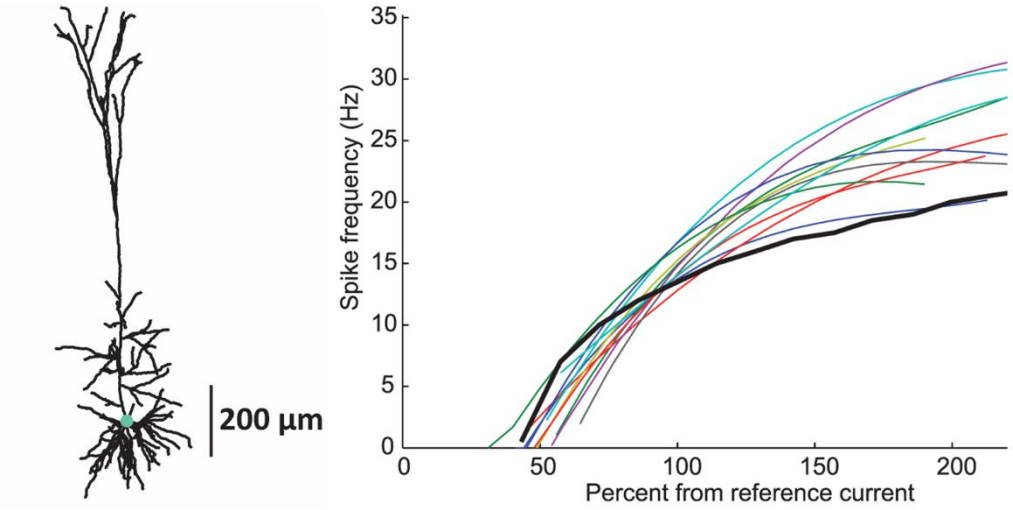

Figure 2.6 LVb pyramidal neuronal model. Left panel: Reconstructed neuronal morphology. The axon is not shown. Right panel: Input-Output curve for depolarizing current injection pulses for neuronal simulated model (black solid line) and experimental data from recorded neurons (colour lines). Adapted from Hay et al., 2011. Mint dot: soma's location (length = 23.2 µm, diameter = 13.5 µm).

activated calcium (CaLVA) and a small conductance calcium activated potassium (SK). All dendritic channels, but HCN, CaLVA and CaHVA, are uniformly distributed. The distribution of HCN channels is uniform on the basal dendrites but follows an exponential density function on the apical tree. The CaLVA and CaHVA channels are distributed based on a step function with increased conductance on the low threshold zone for Ca^{2+} spikes (located 685-885 µm from the soma). The intracellular calcium concentration is modelled as a pool in a sub-membrane shell with calcium influx from the CaLVA and CaHVA channels. Synaptic input is modelled as biexponential postsynaptic conductance changes. The excitatory synapse are a mixture of AMPA and NMDA, and the inhibitory are only $GABA_A$ (Hay et al., 2011; Hay and Segev, 2015).

3 Ion channel noise

3.1 Noise in the neural system

Noise can be defined as any random and unpredictable fluctuation that accompanies an expected signal, but is not part of it. A noisy signal varies as a function of time, and its value at any time point can be drawn from some probability distribution (Ermentrout et al., 2008; Faisal et al., 2008). In the neural system, noise can be present at various levels, externally, that is sensory noise, intrinsically, that is, cellular, synaptic noise and in the behaviour. The external noise is present in sensory stimuli that are intrinsically noisy, due to their thermodynamic or quantum mechanical nature. The perception of a sensory stimulus is usually based on its translation to a chemical one and its subsequent transduction and amplification, leading to its final conversion in an electrical signal. This process can be direct, or indirect by involving the activation of second-messenger signalling pathways. Because of the chemical basis of this process, noise is present at every step. The sources of internal noise are random events in the cell's biochemical processes, related either to housekeeping or to neuronal function, such as the stochastic gating of ion channels, namely, channel noise, or neuronal transmission, namely, synaptic noise. The final behavioural outcome is also prone to variability due to the combined effect of the noisy neuronal function and the other cell types that are involved in the behavioural implementation, such as muscle fibres (Faisal et al., 2008; Stein et al., 2005; Yarom and Hounsgaard, 2011) (Figure 3.1).

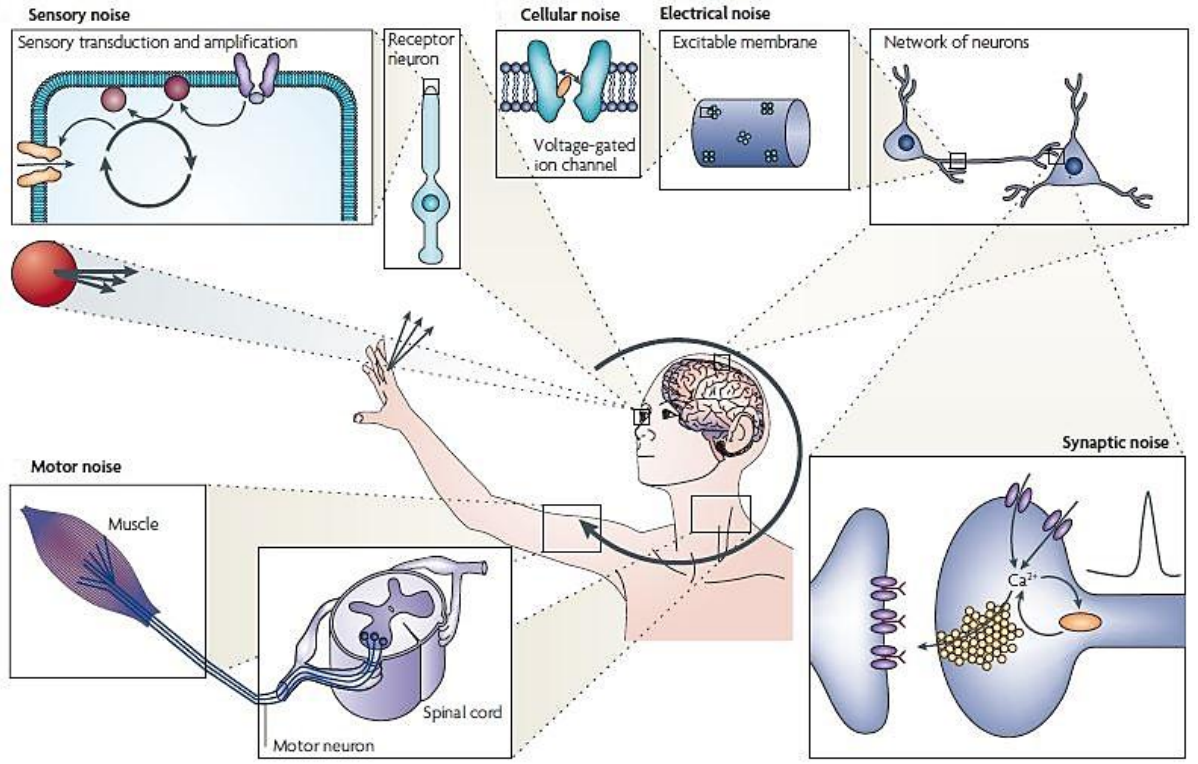

Figure 3.1 Noise in the nervous system. Even in a phenomenological simple behavioural task, such as catching a ball, various sources of noise can be identified, such as in the signal transduction, at neuronal cellular and network level and in other cell types necessary for the completion of the behaviour. Adapted from Faisal et al., 2008.

3.1.1 Functional contribution of noise

The role of noise in the neural system could be characterized as controversial (Ermentrout et al., 2008; Faisal et al., 2008; Stein et al., 2005). The traditional view suggests that noise adds unwanted variability to the neuronal and behavioural responses. In this context, the neural system should develop strategies to compensate or overcome the disruption due to noise. Since stochasticity underlies the neuronal processes, the signal would be accompanied by noise. The main principles that the neural system utilize to counter this phenomenon is averaging the sources of noise over time or space, either at the single neuron or network level, and prior knowledge of the expected features of the signal or noise, or both (Faisal et al., 2008).

However, noise could have beneficial functional consequences for the neural system. This is based on the idea that an important part of the signal might be also encoded in the timing of each spike. Thus, both rate and temporal coding should be considered to explain information processing by the neural system (Stein et al., 2005). For instance, the presence of noise in a signal can enhance weaker periodic signals (stochastic resonance) and increase the neuronal sensitivity. Moreover, the probability of subthreshold signals to be transformed into action

potentials is increased, particularly the ones close to the spiking threshold, and this results in threshold smoothing. Further, the precise timing of spikes, such as the first spike in a spike response, could be critical and encode important information. Evidence suggests that noise can facilitate the triggering of spikes and provide cues for their exact timing (Ermentrout et al., 2008; Faisal et al., 2008; Stein et al., 2005). Even at the level of a neuronal population, noise could induce oscillatory synchronization (Ermentrout et al., 2008) or prevent it (van Rossum et al., 2002). In addition, the presence of noise during the formation of neural networks endows them with the ability to maintain a robust performance of a particular function in different states (Faisal et al., 2008). Noise also underlies principles of neuronal computation, such as gain modulation (Silver, 2010). Furthermore, the probabilistic nature of the noisy neural responses could be an essential feature, and not a bug in the information processing, where the neuronal activity is based on sampling from an underlying probability distribution (Ermentrout et al., 2008).

3.1.2 Channel noise

The noise generated by the stochastic gating of ion channels has been implicated in impacting single neuron dynamics and reliability (Faisal et al., 2008; White et al., 2000). The source of this type of noise, namely, electrical or channel noise, is given by the biomolecules that constitute the ion channels of the excitable neuronal membranes (Bezanilla, 2008; Hille, 2001; White et al., 2000).

Ion channels are proteomic macromolecules that are embedded in the lipid membrane layer of the cell. The organization of these biomolecules gives rise to the formation of a pore where selected ions can pass in and out of the cell. The ions diffuse across the cell membrane according to their electrical and chemical driving force, leading to different ion concentrations between the two sides of the membrane, which generates the membrane potential and a corresponding electric field. Besides their ion selectivity, these channels are characterized by gating properties; they are not constantly open, but their gating is mediated by a specific stimulus (or stimuli). Examples of stimuli affecting the channel opening (or closing) are voltage changes across the membrane (voltage-gated channels), mechanical stress (mechanosensitive channels), or the response to a chemical signal/ligand (ligand-gated channels). Ligands can be either extracellular, such as neurotransmitters (transmitter-gated channels) or intracellular signals, such as an ion (ion-gated channels) or a nucleotide (nucleotide-gated channels).

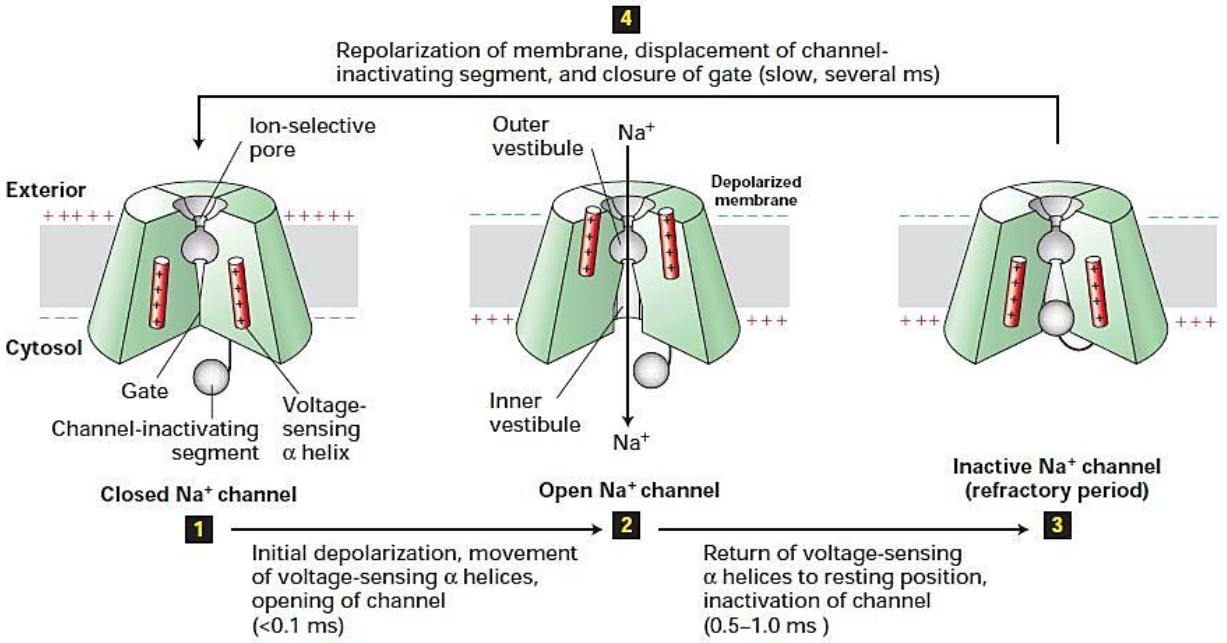

Figure 3.2 Voltage-gated Na^+ channel. An example of a voltage-gated ion channel operation model. Na^+ channels consist of transmembrane proteins, four α subunits with six α helices each (called S1-6), that form a sodium-permeable pore, and are associated with auxiliary β subunits. S4 helix contains positively charged amino acid residues, usually arginine, at every third position that endow the channel with its gating properties. These residues are attracted by the negative charge in the intracellular space and keep the channel closed. In response to depolarization, the charge distribution on each side of the membrane changes temporarily, and the residuals rotate clockwise across the membrane and towards the extracellular matrix. This results in a conformational rearrangement of the protein that opens the channel. During sustained depolarization, the voltage sensor α helices return to their original position, but the channel-inactivating segment folds into the intracellular opening of the pore and blocks it, resulting in the inactivation of the channel. When the membrane potential is repolarized, the channel-inactivating channel is displaced from the pore opening and the channel reverts to the closed position Adapted from Lodish et al., 2003.

Moreover, the activity of ionic channels is amenable to covalent protein modifications such as phosphorylation or dephosphorylation (Hille, 2001).

The function of voltage-gated ion channels as gates is based on the ability of their transmembrane proteins to sense changes of the membrane electric field. A change in the electric field, due to a depolarizing or hyperpolarizing event in the periphery of the channel, is translated into conformational changes in the channel protein units that allow the movement of ion charges through the channel, and consequently the induction of a transient current, namely, the single channel current. Each channel type consists in a different number of conformational states, with at least one functioning as the open state, where current conduction is allowed, and at least one having the opposite role, that is closed state. The rest could be intermediate or inactivated states, where in both situations the channel is impermeable to ions. The transition between the different states is a temperature-dependent biochemical reaction driven by the

thermal environment of the brain, and accordingly is a stochastic process. The transition time between states is in the order of nanoseconds, and at every given time point, a single channel can be in any of these states. Therefore, the collective behaviour of the channel population characterizes its response to an event, such as a change in membrane voltage (Bezanilla, 2008; Hille, 2001; White et al., 2000) (Figure 3.2).

3.1.2.1 Physiological and functional consequences of ion channel noise

The impact of the stochastic gating of ion channels on the biophysics and function of neurons is often overlooked, either because the neuronal output could be also explained by the assumption that the behaviour of a channel population is deterministic (Hille, 2001), or for the reason that other sources of noise, such as synaptic noise, could mask the effect of channel stochasticity (Destexhe et al., 2003; Faisal et al., 2008).

Nevertheless, growing evidence indicates that the stochasticity introduced by ion channels could influence different aspects of the neural system, from the wiring density of the brain to the neuronal arithmetic and dynamics. The fluctuations resulting from the random channel gating set a limit for the lower diameter of an unmyelinated axon, in order for it to support reliable axonal communication (Faisal et al., 2005). Stochastic gating of sodium channels can account for fluctuations in the firing threshold in the frog nodes of Ranvier, with the fluctuation magnitude being correlated with the single channel conductance and kinetic properties of the sodium channel (Sigworth, 1980). In small embryonic cultured neurons from rat hippocampus, which are characterized by a high input resistance, the random gating of ion channels underlies the generation of spontaneous action potentials (Johansson and Arhem, 1994), and the stochasticity introduced by the gating of potassium channels might be the major noise source (Diba et al., 2004). The stellate neurons in the superficial medial entorhinal cortex, which provide cortical input to the hippocampus, exhibit subthreshold membrane voltage oscillations and characteristic clustered patterns of spiking, during prolonged periods of excitation. The noise associated with the stochastic gating of persistent sodium current is essential for the generation of these oscillations, and it affects also the spike timing and the sensitivity of the neuron to weak stimuli (Dorval, 2005; White et al., 1998). Further, stochastic gating of the whole collection of the stellate neuron’s ion channels is necessary for the formation of the clustered spiking patterns (Dudman and Nolan, 2009). In rat layer IV–V pyramidal neurons, the presence of ion channel noise is the main contributor to subthreshold membrane fluctuations, and their amplitude is largely determined by the stochastic sodium

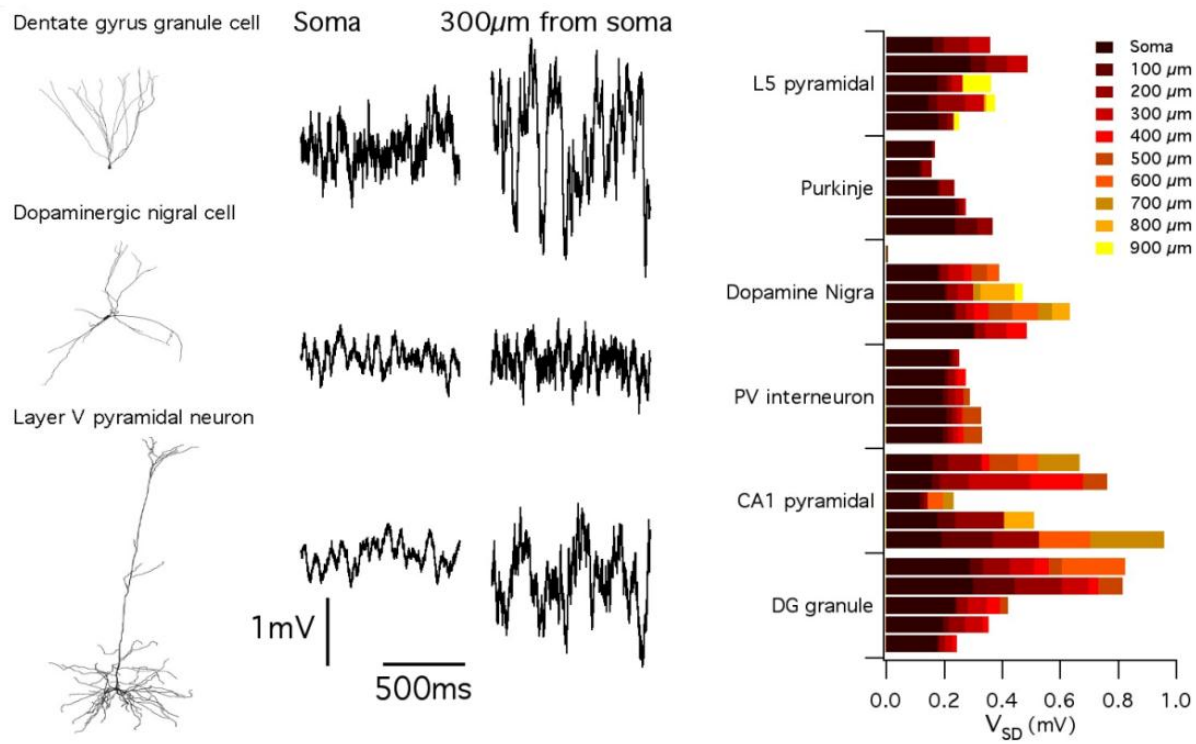

Figure 3.3 The impact of stochastic ion channel gating is related to distinct neuronal morphologies. Neuronal models with identical ion channel distribution, but distinct morphology (left panels) exhibit variability in the amplitude of resting membrane potential fluctuations (middle panels) at different regions (soma and at a dendritic location 300 μm from soma). Right panel: Resting membrane potential standard deviation for a collection of 29 reconstructed cells from six different neuronal types, plotted as a function of increasing distance along the dendrite from the soma. The amplitude of the membrane potential fluctuations increases with distance from the soma. Adapted from Cannon et al., 2010.

conductance (Jacobson et al., 2005). Furthermore, in rat cortical layer V pyramidal neurons, the stochastic gating of the nonselective hyperpolarization-activated channels is a key factor causing noisy fluctuations of the resting membrane potential, particularly in thin distal dendritic areas, and it affects the reliability of temporal spike pattern (Kole et al., 2006). Likewise, neurons with distinct morphologies, which are populated with identical stochastic ion channel distributions, exhibit significant variability in the amplitude of membrane potential fluctuations, even in various dendritic locations of the same cell type (Figure 3.3). Stochastic gating of the ion channels of hippocampal CA1 pyramidal neurons impact the transformation of synaptic input into output, by introducing or failing to evoke spikes in the firing pattern of the neuron at almost fixed time points, and injecting jitter into the interspike interval. As a result, their neuronal response to synaptic input is rather probabilistic (Figure 3.4). Moreover, the impact of the stochastic ion channels on the probabilistic spike generation and timing varies, is related to the channel type and their neuronal location, with dendritic ion channels, particularly the sodium and potassium ones, accounting for most of it (Cannon et al., 2010). In

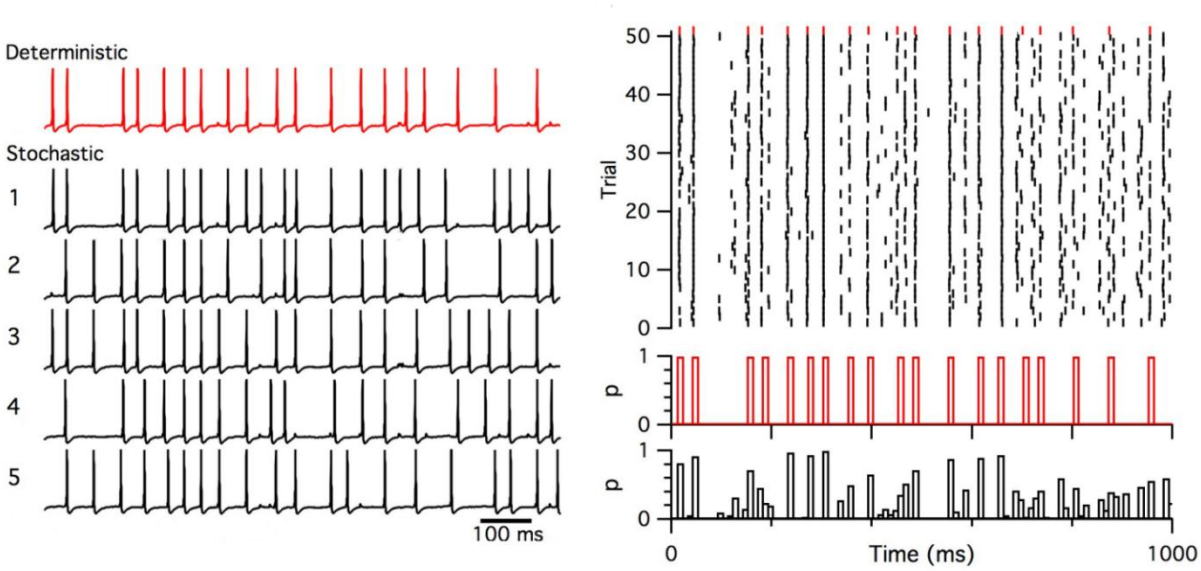

Figure 3.4 Effect of stochastic ion channel noise in synaptic integration. Left panel: Membrane voltage somatic responses of pyramidal CA1 neuronal models with deterministic or stochastic ion channels that are stimulated with the same pattern of asynchronous and distributed dendritic synaptic input. Spikes that occur at a time point with the deterministic neuronal model, might be absent in some of the stochastic trials, or additional spikes might be triggered in the stochastic models, and be absent in the deterministic one. Right panel: Spike rasters (top) of somatic responses to the synaptic simulation for the deterministic (red) and 50 stochastic trials (black). The probability of somatic spiking in 10 ms duration bins (bottom) at any time point is either one or zero in the deterministic model (red), but varies between one and zero in the stochastic one (black). Adapted from Cannon et al., 2010.

weakly excitable dendrites, such as the apical dendrites of layer V pyramidal cells, stochastic gating causes little variability in the backpropagation timing and height of single action potentials, but introduces jitter in the timing of the action potentials and variability in the dendritic calcium spike generation (Diba et al., 2006). Furthermore, channel noise in thin axons underlies random fluctuations in the width and height of the propagating action potential waveform, which translate into variability in the downstream synaptic processes (Neishabouri and Faisal, 2014).

3.1.2.2 Effect of channel properties on channel noise

The extent of subthreshold membrane fluctuations is related to the channel properties (Cannon et al., 2010; Kole et al., 2006; O'Donnell and van Rossum, 2014; White et al., 2000). An increase in the single channel conductance leads to an increase in the membrane potential fluctuations. For the same total channel conductance, a larger single channel conductance is associated with a smaller number of open channels and hence, greater current and voltage fluctuations (Donnell and Nolan, 2014; Kole et al., 2006; White et al., 2000) (Figure 3.5). Ion channels with greater open probability near the resting membrane potential provoke also larger

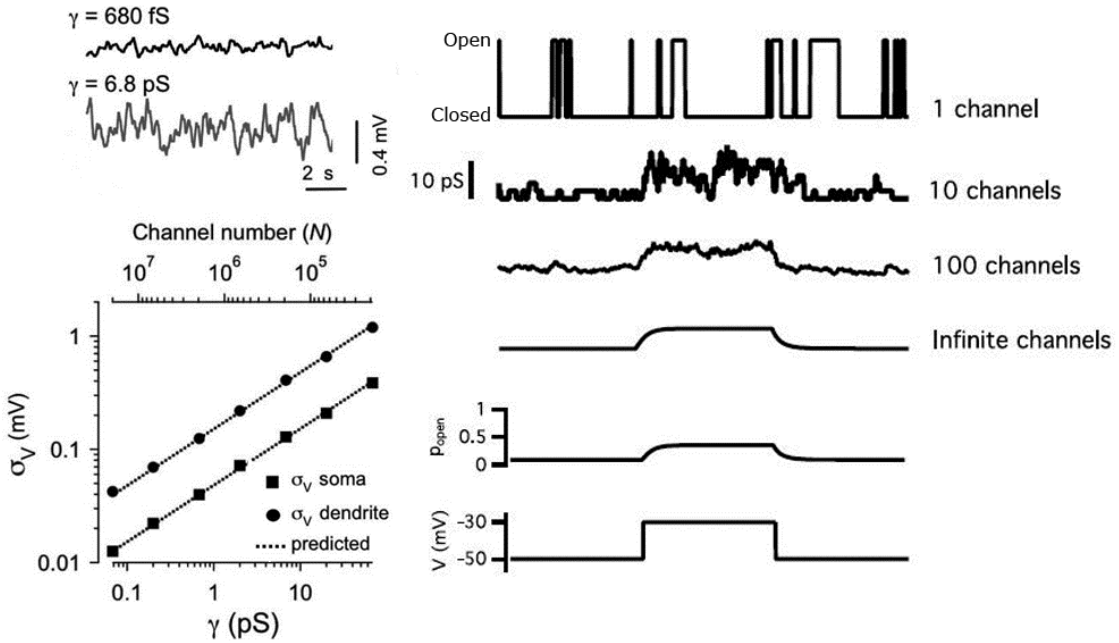

Figure 3.5 Impact of single channel conductance on voltage noise. Left panels: A morphological realistic compartmental layer V pyramidal neuronal model is simulated with all its ion channels deterministic but the hyperpolarization-activated cation channel (HCN). The somatic membrane fluctuations are greater when the single channel conductance (γ) of HCN is increased (upper panel). In the same neuronal model, the standard deviation (σ_V) of the somatic or dendritic (1000 μm from soma) resting membrane potential is systematically increased with the γ (and decreased with the total number of HCN channels) (lower panel). Adapted from Kole et al., 2006. Right panels: Simulations of Hodgkin-Huxley potassium channels. The single channel conductance response is fluctuating between discreet open and closed states (top conductance trace for one channel), even in the absence of stimulus where the probability of channel being open (P_{open}) is zero (lower panels, voltage stimulus open and probability trace respectively). For larger channel populations the conductance response becomes less noise (middle channel conductance traces), and for infinite number of channels (bottom channel conductance trace) is predictable with little trial-to-trial variability**.** Adapted from Cuntz et al., 2014.

fluctuations. Moreover, in a channel population every channel acts independently and therefore the distribution of open channels can be described by a binomial distribution. As a result, a greater total number of channels is associated with greater fluctuations in the absolute number of open channels (for a detailed explanation see also, 5.2.9 The rectified distribution of open channels results in differences between the two models), and therefore channel current. The single channel current is proportional to the channel's driving force, which is given by the difference between the channel's reversal potential and the membrane potential. Thus, ion channels with larger driving force have greater ion flow (single channel current), which is translated at the level of channel population, as current fluctuations with greater amplitude (O'Donnell and van Rossum, 2014; White et al., 2000). Slower kinetics are also associated with membrane noise, due to the low-pass filtering of the high-frequency membrane potential fluctuations by the membrane capacitance in general, the membrane fluctuations from channels with slower gating kinetics are less attenuated compared to channels with faster kinetics)

(Cannon et al., 2010; O'Donnell and van Rossum, 2014). The polarity of current flow through an open channel can contribute to the membrane noise, since the movement of ion inside or outside of the cell affects its depolarization (O'Donnell and van Rossum, 2014). Subthreshold membrane voltage fluctuations can be decreased with temperature. Increasing the temperature causes faster transitions between the channel states, and the resulting high frequency components can be filtered out by the membrane capacitance and leak resistance (Steinmetz et al., 2000).

3.2 Modelling channels

As mentioned, ionic channels have at least two states, open and closed. However, more complex gating schemes are found in nature. A lot of channels respond to a prolonged stimulation (electrical or chemical) with an inactivation state. During inactivation they are closed and refractory to further opening, until the stimulus is removed (de-inactivation) (Hille, 2001).

Modelling ionic channels is crucial for understanding the behaviour of neuronal systems either at single cell (intrinsic electrical neuronal properties) or at network (intercommunication via integration of synaptic inputs) level. The modelling approach depends on several factors, such as the aims of the study (research on single channel, neuron or neural network properties) and the desired level of detail and precision in the behaviour of model, the access to appropriate experimental data, the currently available computational and statistical tools, the computational cost and simulation time (Cannon and D'Alessandro, 2006; Hille, 2001; White et al., 2000).

Two of the formalisms that have been proposed to model ionic channels are the Hodgkin-Huxley and the Markov models. Both assume that the kinetic properties (gating) of ionic channels are based on the structure and chemical properties of the channel. The Hodgkin-Huxley model represents the notion that independent gating particles can block the channel pore and control its state (open or closed). The Markov model is more detailed in the way channels are represented and adequate to describe their stochastic behaviour. In this formalism, each channel can have several states with transitions between some of them. Although the Markov model is more accurate than the Hodgkin-Huxley one, it has a main drawback, that is, the difficulty to estimate experimentally the various parameters of channel dynamics. On the other side, Hodgkin-Huxley parameters can be determined more easily by fitting to data from electrophysiological experiments, such as voltage clamp. Furthermore, any Hodgkin-Huxley

ion channel model can be written as a Markov scheme, but the opposite is not always feasible (Cannon and D'Alessandro, 2006; Hille, 2001).

3.2.1 Hodgkin-Huxley formalism

The Hodgkin-Huxley formalism for ion channel gating was introduced by Hodgkin and Huxley in the early 1950s, in an attempt to describe the generation of the nerve output, namely, the action potential. Based on: (a) the outcome of a series of electrophysiological experiments and, (b) the fact that the electrical properties of excitable membranes, that is, membranes that can produce action potentials or spikes, can be represented by an electrical equivalent circuit (Figure 3.6), they developed a conductance-based mathematical model of ordinary differential equations that accounts for the main properties of action potentials (Hille, 2001).

In the Hodgkin-Huxley formalism each single channel of the neuronal membrane is considered to contain one or more independent particles or gates. Gates regulate the ion flow through the channel pore, and they can be in one of two states, permissive and non-permissive.

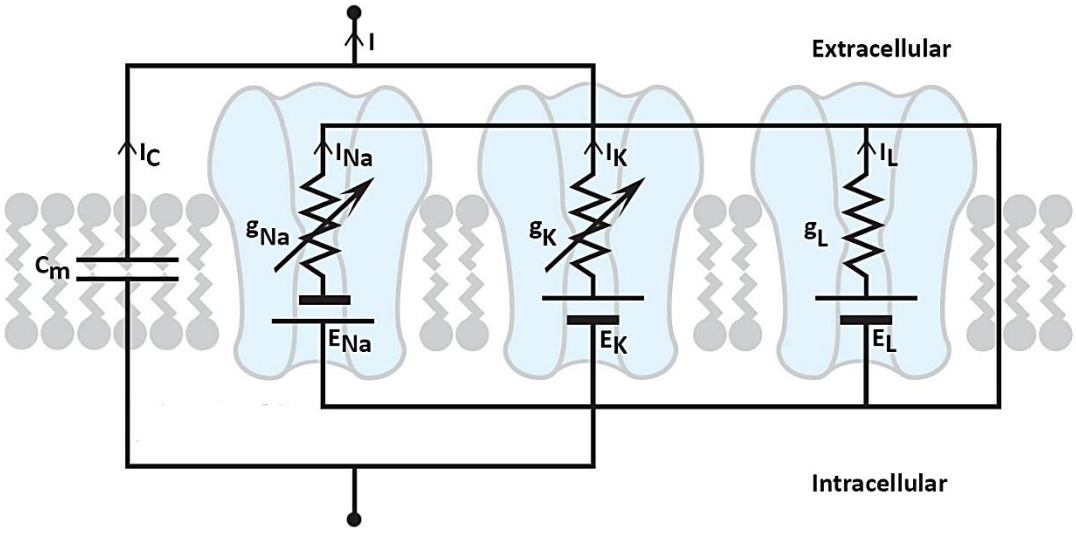

Figure 3.6 Electrical equivalent circuit of the neuronal membrane for the Hodgkin–Huxley model of the action potential. In the cell membrane of neurons are embedded ion channels and ion pumps which are protein structures that render it semipermeable, by allowing the flow of specific ions such as sodium, potassium, chloride and calcium. Due to the combined action of these biomolecules, a transmembrane electrochemical gradient is formed for each ion, and the intracellular space is charged more negative than the extracellular one. Therefore, the neuronal membrane can be considered as a capacitor (with capacitance C_m and capacitor current I_C). The permeability of the ion channels for ions such as sodium and potassium, may depend on the membrane potential, and can be represented by variable resistors with non-linear conductances (g_{Na}, current I_{Na}, and g_K, current I_K respectively) and their electrochemical gradient that drives their flow is represented by batteries (E_{Na} and E_K respectively). The ion movement through other channels, such as the leakage channels, may not depend on voltage changes and its conductance is constant (g_L, current I_L and its battery E_L)**.** Adapted from Sterratt et al., 2010.

For a channel to be in an open state, all its gates must be in their permissive state. Any other gate placement keeps the channel closed. Moreover, gates are considered to be electrically charged and hence a voltage change can affect their distribution across the membrane (Hille, 2001).

The transition of gates between these two states is assumed to be governed by a first-order kinetics schema. When a gate *i* of a particular channel is considered, then a probability p_i of that gate being in a permissive state can be defined. Similarly, the probability of that gate *i* being in a non-permissive state will be $1 - p_i$. When more than only one channel is taken into account, this probability represents the fraction of gates *i* in permissive state in that channel population. The transitions between the two gating states are given by a first-order kinetic equation and are according to the voltage dependent rate constants $\alpha_i(V)$ (forward direction) and $\beta_i(V)$ (backward direction):

$$(1 - p_i) \underset{\beta_i(V)}{\overset{\alpha_i(V)}{\rightleftarrows}} p_i \qquad \textbf{Equation 3.1}$$

Given the initial value of probability p_i the subsequent values can be calculated by the rate of the reaction, which, based on the law of mass action, is given by the differential equation:

$$\frac{dp_i}{dt} = \alpha_i(V)(1 - p_i) - \beta_i(V) p_i \qquad \textbf{Equation 3.2}$$

When the membrane voltage is clamped at a fixed value *V*, after a time point the system is eventually equilibrated and reaches a steady-state value:

$$p_{i,t\to\infty} = \frac{\alpha_i(V)}{\alpha_i(V) + \beta_i(V)} \qquad \textbf{Equation 3.3}$$

The time course for this process is given by an exponential equation with the time constant (Hille, 2001):

$$\tau_i(V) = \frac{1}{\alpha_i(V) + \beta_i(V)} \qquad \textbf{Equation 3.4}$$

Time constants can be also, represented by:

$$\tau_i(V) = \left(\frac{A}{exp\left(\frac{V-B}{C}\right) + exp\left(\frac{V-D}{E}\right)} \right) + F \qquad \textbf{Equation 3.5}$$

where *A*, *B*, *C*, *D*, *E* and *F* are obtained empirically based on voltage clamp recordings (Steuber et al., 2011).

The rate constants $\alpha_i(V)$ and $\beta_i(V)$ can be described as:

$$a_i(V) = \frac{p_{i,t\to\infty}}{\tau_i(V)} \qquad \textbf{Equation 3.6}$$

and

$$b_i(V) = \frac{1 - p_{i,t\to\infty}}{\tau_i(V)} \qquad \textbf{Equation 3.7}$$

By combining the Equations 3.2, 3.3 and 3.4, the rate of change of the gate state probability with time can be expressed as:

$$\frac{dp_i}{dt} = \frac{p_{i,t\to\infty} - p_i}{\tau_i(V)} \qquad \textbf{Equation 3.8}$$

The voltage dependence of the steady-state $p_{i,t\to\infty}$ is usually represented by a Boltzmann (sigmoid) function:

$$p_{i,t\to\infty} = \left(\frac{1}{1 + exp\left(\frac{V - V_{half}}{k}\right)} \right) \qquad \textbf{Equation 3.9}$$

where *k* is the slope factor, and V_{half} is the membrane potential when the $p_{i,t\to\infty}$ is at half maximum, based on experimental voltage clamp data (Hille, 2001; Steuber et al., 2011).

The above formalism describes the behaviour of a single gate. The conductance g_c of a channel population *c* is given by the product of the individual gate probabilities p_i and a constant $\bar{g}_c$ that represents the maximum possible conductance of the channel population if all the gates were at permissive states, namely, all the channels were opened (Hille, 2001).

Hodgkin and Huxley modelled the behaviour of the sodium and the potassium channels of the squid giant axon. To bring into accordance the mathematical formulation with the experimental data, they assumed the existence of three independent types of gating particles, the activation gates, *m* and *n*, and the inactivation gate, *h* (Figures 3.7 and 3.8). Each channel

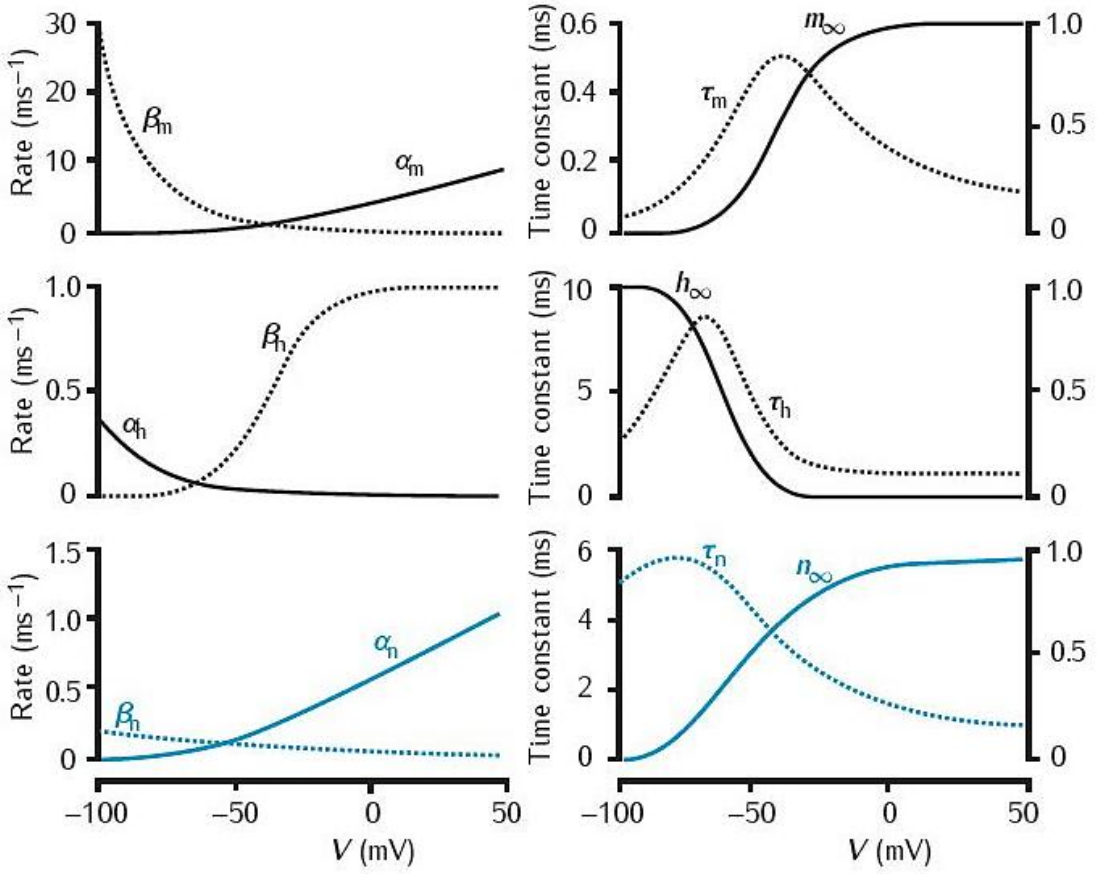

Figure 3.7 Voltage dependence of the Hodgkin–Huxley model parameters. Left panels: Forward (α_m, α_h, α_n, solid lines) and backward (β_m, β_h, β_n, dotted lines) rate constants for the sodium and potassium channels gating variables (m, n, h). Right panels: Equilibrium steady-state (m_∞, h_∞, n_∞, solid lines) and time constants (τ_m, τ_h, τ_n, dotted lines). All the parameters are calculated from the empirical equations of the Hodgkin–Huxley model for the squid giant axon membrane. Adapted from Sterratt et al., 2010.

type was modelled by a different combination and number of gating particles. Thus, the equations for the sodium and potassium channel conductances are (Hille, 2001):

$$g_{Na} = \bar{g}_{Na} m^3 h \qquad \textbf{Equation 3.10}$$

$$g_K = \bar{g}_K n^4 \qquad \textbf{Equation 3.11}$$

The definition of number and type of gating variable was based on the experimentally obtained time dependence of channel conductance. The time course of the conductance followed a sigmoid curve when a depolarizing step was applied, and an exponential decrease during a repolarization one. The proposed kinetics governing each gating variable was first-order reactions, which could reproduce the exponential part of the curve. However, for the sigmoid component of the curve, more than one first-order reactions should take place at the same time. Such an assumption favoured the idea of several independent electrically sensitive gates within

a channel. When several gates were assumed, their probability to be placed in the permissive position would rise along a sigmoid shape, and the greater the number of gating particles, the more pronounced the inflexions on the curve. Their probability to transit to a non-permissive state would fall exponentially. In the case of the potassium channel, an assumption of four independent variables *n* (Equation 3.11) would fit the exact shape of the experimentally measured curve. The time course of the sodium channel conductance suggested different gating processes for the sodium channel, activation and inactivation. The best fit to the empirically conductance time course curve was actualized by assuming three gates (*m*) to control activation and one (*h*) for inactivation (Hille, 2001) (Equation 3.10 and Figure 3.7).

When the membrane voltage *V* is clamped to another level V_{new}, the time course of p_i is described by the following exponential expression that can be derived from Equation 3.8 above:

$$p(t)_i = p_{i,t\to\infty}(V_{new}) - \left(p_{i,t\to\infty}(V_{new}) - p_i(0)\right)exp\left(-\frac{t}{\tau_i(V_{new})}\right) \qquad \textbf{Equation 3.12}$$

where V_{new} is the new voltage step, $p_{i,t\to\infty}(V_{new})$ is the new equilibrium value of p_i when $V = V_{new}$, $p_i(0)$ is the value of state p_i at $t = 0$, where $V = 0$, and $\tau_i(V_{new})$ is the value of time constant at $V = V_{new}$ (Hille, 2001).

3.2.1.1 Hodgkin-Huxley model for action potential

To fully describe the change of the membrane potential locally in the squid giant axon, Hodgkin and Huxley suggested an additional voltage-independent current, which accounted for a fixed background current flow, mostly made up of chloride ions, and was constant, that is the leakage conductance, $\bar{g}_L$ (Hille, 2001).

As mentioned, excitable membranes, in a confined area of the neuron, can be represented by an electrical equivalent circuit. The basic elements of the circuit are the membrane capacitance, which represents the phospholipid bilayer that separates the ions on the intracellular and extracellular medium, and non-linear or linear resistances, which represent the voltage gated or leak ion channels respectively (Figure 3.6). The Hodgkin-Huxley model for action potential generation can be summarized by an equation that corresponds to the equivalent electrical circuit of a membrane patch with sodium, potassium currents and leak

$$C_m\frac{dV}{dt} = -\bar{g}_{Na}m^3h(V_m - E_{Na}) - \bar{g}_K n^4(V_m - E_K) - \bar{g}_L(V_m - E_L) \qquad \textbf{Equation 3.13}$$

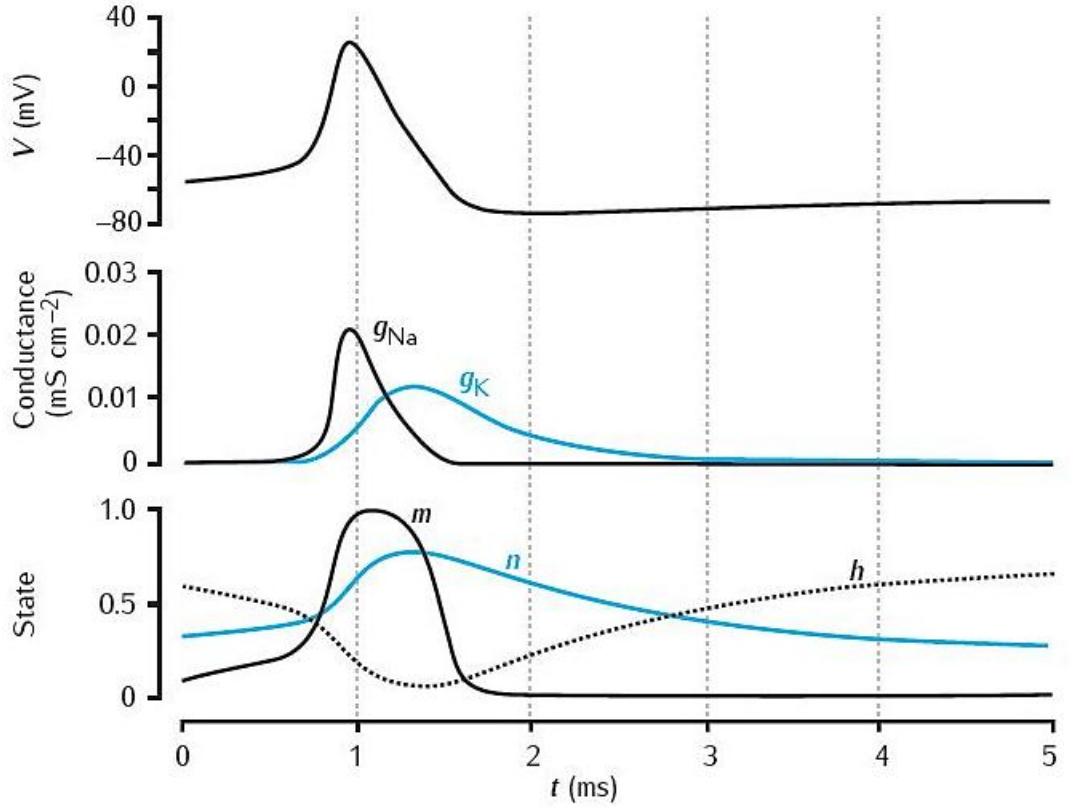

Figure 3.8 Time course of the Hodgkin–Huxley model parameters during an action potential. Upper panel: Action potential. Middle panel: Sodium (g_{Na}) and potassium (g_K) conductances. Lower panel: Gating variables (*m*, *n*, *h*). Adapted from Sterratt et al., 2010.

channels where *Vm* is the membrane potential. Each ion channel is associated with an equilibrium or reversal potential (E_{Na}, E_K and E_L, for sodium, potassium and leakage channels respectively) that is the particular voltage value where the net flow through any open channels is zero (Hille, 2001) (Figure 3.8).

3.2.2 Markov formalism

Despite the success of the Hodgkin-Huxley formalism in reproducing the behaviour of macroscopic currents, it is based on several approximations regarding the kinetics that govern ion channels, and as result there are inconsistencies with some of the experimental data, such as modelling sodium channels with resurgent current where the activation and inactivation gates are not independent, but coupled (Hille, 2001; Lewis and Raman, 2014). The Hodgkin-Huxley channel models tend to use oversimplified kinetic schemas compared to the Markov models. The latter ones take into consideration more possible conformational states, and thus the state diagrams or kinetic schemas describing a channel are more realistic and allow to study some of their stochastic behaviour (Hille, 2001).

The Markov formalism is based on three assumptions: (a) each channel can be represented by a collection of conformational states, (b) the system is memory-less (Markovian assumption), that is, the transition probability between states depends only on the current state, and not on the previous history of how the model reached that state and (c) the elementary transitions are first order schemes (Cannon and D'Alessandro, 2006; Hille, 2001; White et al., 2000).

The sequence of the conformational states can be represented by a state diagram of the form:

$$S_1 \Leftrightarrow S_2 \Leftrightarrow \cdots \Leftrightarrow S_n \qquad \textbf{Equation 3.14}$$

where $S_1, S_2 \ldots S_n$ are the discrete conformational states. In the Markov formalism, if the system has n number of states, the kinetic response will have $n - 1$ relaxation times, namely, the time ranges at which a new equilibrium occurs after a perturbation, and if there are m relaxation times, the system includes at least $m + 1$ states (Hille, 2001).

Assume that a channel is at state S_i at time t. Then the probabilities that can be defined are the probability being at that state S_i at t, $P(S_i, t)$, and the probabilities for transition from state S_i to another S_j , where $j = 1, 2 \ldots n$, $P(S_i \rightarrow S_j)$, and backwards, $P(S_j \rightarrow S_i)$. The kinetic equation for such a schema is:

$$S_i \underset{P(S_j \rightarrow S_i)}{\overset{P(S_i \rightarrow S_j)}{\rightleftharpoons}} S_j \qquad \textbf{Equation 3.15}$$

The temporal evolution of $P(S_i, t)$ is described by:

$$\frac{dP(S_i, t)}{dt} = \sum_{j=1}^{n} P(S_j, t)\, P(S_j \rightarrow S_i) - \sum_{j=1}^{n} P(S_i, t)\, P(S_i \rightarrow S_j) \qquad \textbf{Equation 3.16}$$

In a channel population these probabilities can be interpreted at a macroscopic level. Therefore, the probability $P(S_i, t)$ becomes the fraction of channels being in state S_i and the transition probabilities $P(S_i \rightarrow S_j)$, and $P(S_j \rightarrow S_i)$ become the rate constants r_{ij} and r_{ji} respectively. The revised deterministic version of the kinetic schema at the channel population level is:

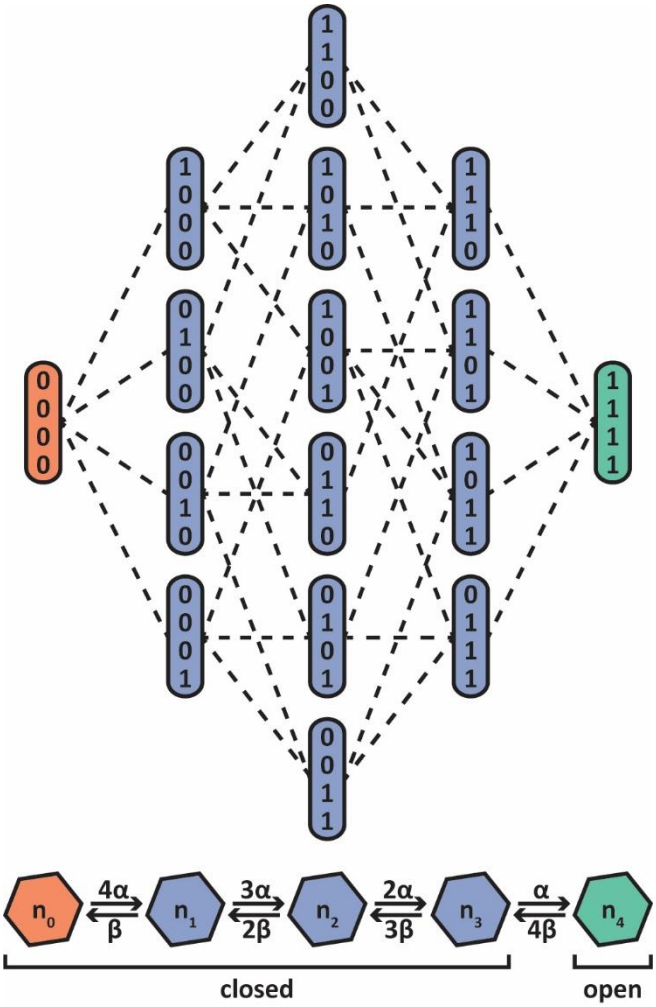

Figure 3.9 Kinetic schemas. K^+ channel is represented by four *n* activation gates. Upper panel: Full state diagram. If 1 indicates a gate to be in a permissive state and 0 to be in a non-permissive, then there would be 15 closed and a single open substates for the system, with 32 permitted transitions. Every transition (dashed lines) is governed, from left to right, by the *a* rate constant, and right to left by the *β* one. Lower panel: Reduced diagram. All the substates with the same number of gates in the same state, permissive or non-permissive, are equivalent. Thus, the system can be described by five major states (n_0, n_1, n_2, n_3 and n_4), with the transition rate constants also summarised for all the transitions and their *4α, 3α, 2α, α* and right to left: *4β, 3β, 2β, β* is kinetically equivalent to the n^4 Huxley-Hodgkin model. Adapted from Hille, 2001.

$$s_i \underset{r_{ji}}{\overset{r_{ij}}{\rightleftarrows}} s_j \qquad \textbf{Equation 3.17}$$

where s_i and s_j are the fractions of channels being in states S_i and S_j respectively. The transition rates r_{ij} and r_{ji} can be either voltage or concentration dependent, with appropriate temperature dependencies as well (Cannon and D'Alessandro, 2006; Hille, 2001).

The macroscopic time course for each state can be expressed as:

$$s(t) = C_0 + C_1\, exp\left(-\frac{t}{\tau_1}\right) + C_2\, exp\left(-\frac{t}{\tau_2}\right) + \cdots + C_m\, exp\left(-\frac{t}{\tau_m}\right) \qquad \textbf{Equation 3.18}$$

where the coefficients C_j $(j = 0, \ldots, m)$ are the initial conditions constants and τ_j are the time constants (Cannon and D'Alessandro, 2006; Hille, 2001).

Markov models are more general than Hodgkin-Huxley ones, but when channel gates are assumed to be independent, they are equivalent. As a result, ion channels can be represented by kinetic Markov diagrams of their different states and with a special sequence of rate constants, and be kinetically identical to their representation by a Hodgkin-Huxley formalism (Cannon and D'Alessandro, 2006; Hille, 2001) (Figure 3.9).

4 Gain modulation

4.1 Gain modulation: Definition

The function of the nervous system is based on its ability to transform environmental stimuli into representations of the physical world in the brain. In that context, neurons are not computing devices that merely receive and summate in an additive manner synaptic inputs followed by signal transmission, but they must also be able to combine and even dynamically transform the various pieces of information that travel across different brain regions.

Gain modulation appears to be a brain-wide principle of neuronal computation which applies to the way neurons integrate the inputs they receive from different brain areas. The response amplitude (sensitivity) of one neuronal unit (brain region, system, population or single neuron) to one set of signal inputs (driving input) can be enhanced or dampened by the concurrent input of a second unit (modulatory input). Despite the potentially different response to a driving input, due to the modulatory input activity, the neuronal selectivity and receptive field properties (that is, the region in which the presence of a stimulus will evoke a neuronal response) remain unaffected (Salinas and Sejnowski, 2001; Silver, 2010).

4.2 Gain in neuronal response functions: firing rate and tuning curves

The first step to comprehend the neuronal activity and its underlying computations is to depict it in a graph that relates the neuron's response (output) to an input stimulus. Such a graph is highly dependent on the experimental protocol applied to study the particular neuronal behaviour, which defines the nature of driving and modulatory inputs (for instance,

iontophoretic application of drugs, injected current, or synaptic inputs) or parameters (for instance, external relevant stimulus, such as contrast, head or eye orientation, attention, sound frequency, joint position etc.) that trigger a neuronal response. Hence, neuronal behaviour can be demonstrated either as an Input-Output relation graph (I-O function, I-O relationship, firing rate curve or transfer function) of a neuron or as tuning parameter curve (Salinas and Sejnowski, 2001; Silver, 2010).

The I-O function illustrates the average neuronal response (output rate) to an input (driving synaptic input rate or injected current amplitude). When a modulatory input is integrated at the same time with the driving one, the I-O relation could be shifted or tilted, and these transformations correspond to different algebraic operations (addition and multiplication, respectively). Gain modulation is equivalent to the change of the slope (but not the shape) of the I-O curve in a multiplicative (increase) or divisive (decrease) scaling (Silver, 2010) (Figure 4.1).

Furthermore, a multiplicative scaling of the I-O curve could take place on both axes. A change in the slope can be produced either along the x-axis, where the input is modulated and the maximum response of the I-O curves remains the same, or along the y-axis, where the output is modulated and the maximum response of the I-O is scaled (Silver, 2010). Additionally, the I-O function of a neuron could be either linear or nonlinear. In the case of a linear I-O graph, an additive operation is clearly illustrated as a shift of the curve along the x-axis and a gain change can be deduced from the change in slope (that is, scaling along the y-axis) (Chance and Abbott, 2009; Murphy and Miller, 2003). However, in the case of nonlinear I-O relationships, an actual additive operation could function as a multiplicative one, since the shift of a nonlinear I-O curve along the x-axis, introduces a multiplicative component too (that is, gain change as a function of the x-axis). This effect could be also enhanced by an additional nonlinear relationship between the driving input and the stimulus parameter (Brozović et al., 2008; Murphy and Miller, 2003). For that reason, a true change in gain should be quantified as a function of the y-axis, because this modulation takes place to the output and scales the neuronal dynamic range (Chance et al., 2002; Murphy and Miller, 2003; Silver, 2010).

Similarly, the tuning curve shows the neuronal average firing rate (output rate) as a function of an external tuning parameter. The peak of the tuning curve represents the highest neuronal activation that is evoked by the neuronal preferred stimulus. The tuning curves have often a bell-like shape (for instance Gaussian). In the presence of a modulatory input the

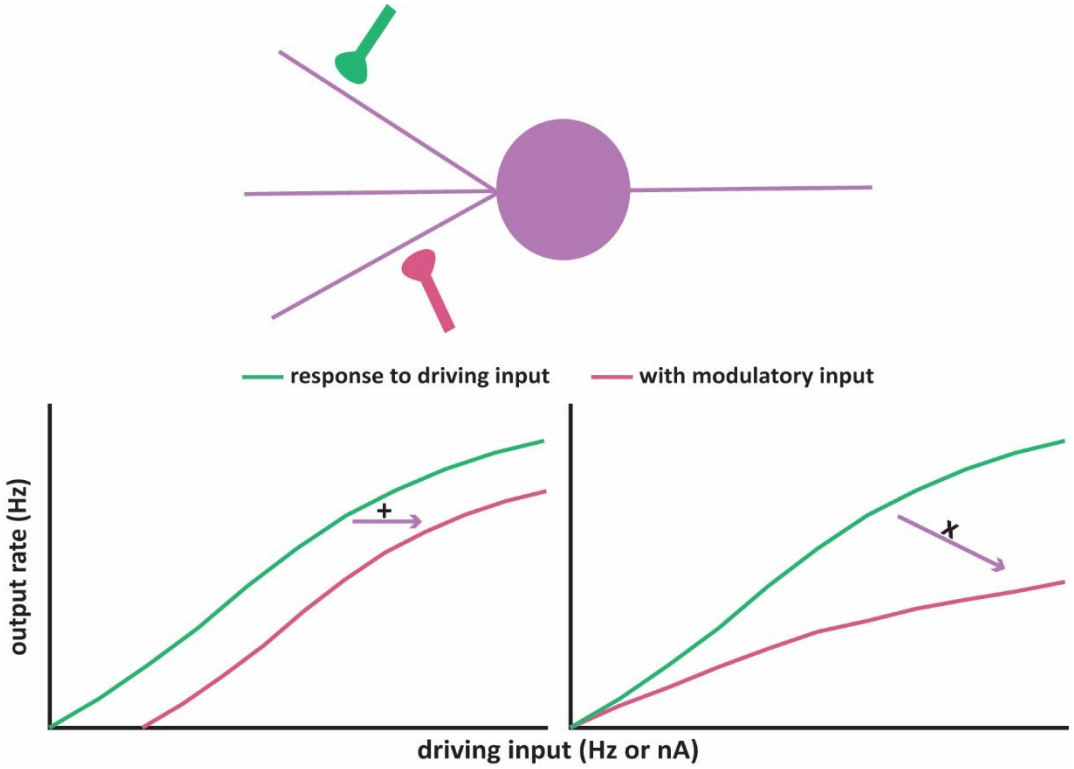

Figure 4.1 Input-Output relationships and gain modulation. Upper panel: Neurons receive numerous presynaptic signals that drive their response (green synapse). However, a second input source (pink synapse) could modify the computational operations utilized by neurons to transform their synaptic input into output firing rate. Lower left panel: A shift along the x-axis of the I-O curve in the presence of a modulatory input, such as synaptic or tonic inhibition, is an indicator of an additive operations. Lower right panel: A change in the slope (or gain) of the I-O curve in the presence of different cellular and synaptic mechanisms, such as synaptic noise, shunting inhibition and synaptic plasticity is an indicator of a multiplicative operations.

amplitude of peak response is scaled (multiplied or divided), but the tuning curve shape remains unaffected. The extent of gain modulation is then defined as the change in the peak amplitude (Butts and Goldman, 2006; Salinas and Sejnowski, 2001).

4.3 Gain modulation in different brain areas

Many cortical and subcortical areas utilize gain modulation operations to combine all the information emerging from sensory, motor or cognitive systems (Salinas and Sejnowski, 2001). Examples where gain modulation operations are applied as a neuronal computational principle exist in the parietal cortex (Andersen and Mountcastle, 1983; Andersen et al., 1985; Brotchie et al., 1995), in the occipital cortex (Bremmer et al., 1997; Galletti and Battaglini, 1989; Trotter and Celebrini, 1999), in the motor cortex (Boussaoud et al., 1998), in the temporal cortex (Winkowski and Knudsen, 2006), in the cerebellum (Herzfeld et al., 2015; Yakusheva et al., 2007), and it is also implicated in the brain stem (Khojasteh and Galiana, 2009).

Moreover, gain modulation control has been suggested in the brain of invertebrates (Baca et al, 2008).

The monkey parietal cortex was the first brain area where gain modulation was observed and as a result thoroughly studied. In that region, neuronal responses depend on the retinal location of a visual stimulus and are multiplicatively scaled by gaze direction (Andersen and Mountcastle, 1983; Andersen et al., 1985) (Figure 4.2) or head position (Brotchie et al., 1995).

Gain modulation computations are often performed during the conversion of one coordinate sensory system with a set reference frame, to another system with a differently centred reference frame, namely, during coordinate transformations (as the latter example). These transforms are necessary for object localization and visually guided reaching (Pouget and Sejnowski, 1997; Salinas and Abbott, 1995; Zipser and Andersen, 1988).

Another task where gain modulation has been implicated as its basis is the translation-invariant object recognition. Visual systems neurons are able to respond with view, size, and position (translation) invariance to objects or faces. Such responses could be gain modulated by cognitive inputs, like those representing states of attention (McAdams and Maunsell, 1999; Salinas and Abbott, 1997; Tovee et al., 1994; Treue and Martínez Trujillo, 1999). Premotor activity is also modulated by eye position during preparation of limb movements in space (Boussaoud et al., 1998). Moreover, the gaze control circuitry in the forebrain modulates the gain of midbrain auditory responses in an space-specific manner (Winkowski and Knudsen, 2006).

In the cerebellum, Purkinje cells residing in the vermal cerebellar cortex encode inertial motion. This neuronal population performs critical computations for the conversion of the head-centred frame into an earth-referenced one, by modulating the information that arises from the inner ear structures. Afferents from those organs converge onto cerebellar structures, including the (fastigial) cerebellar nuclei, the vestibular nuclei and directly on the Purkinje cells residing in the cerebellar nodulus and uvula. The latter are sensitive to translation acceleration, but not gravitational force, and their response is modulated by the angle between the motion direction (head movement towards a stimulus) and the cell's preferred direction. Yet, the cell population of vestibular and cerebellar nuclei neurons show a mixture response to translation and tilt motions (Yakusheva et al., 2007). The cerebellum can also predict in real time the speed

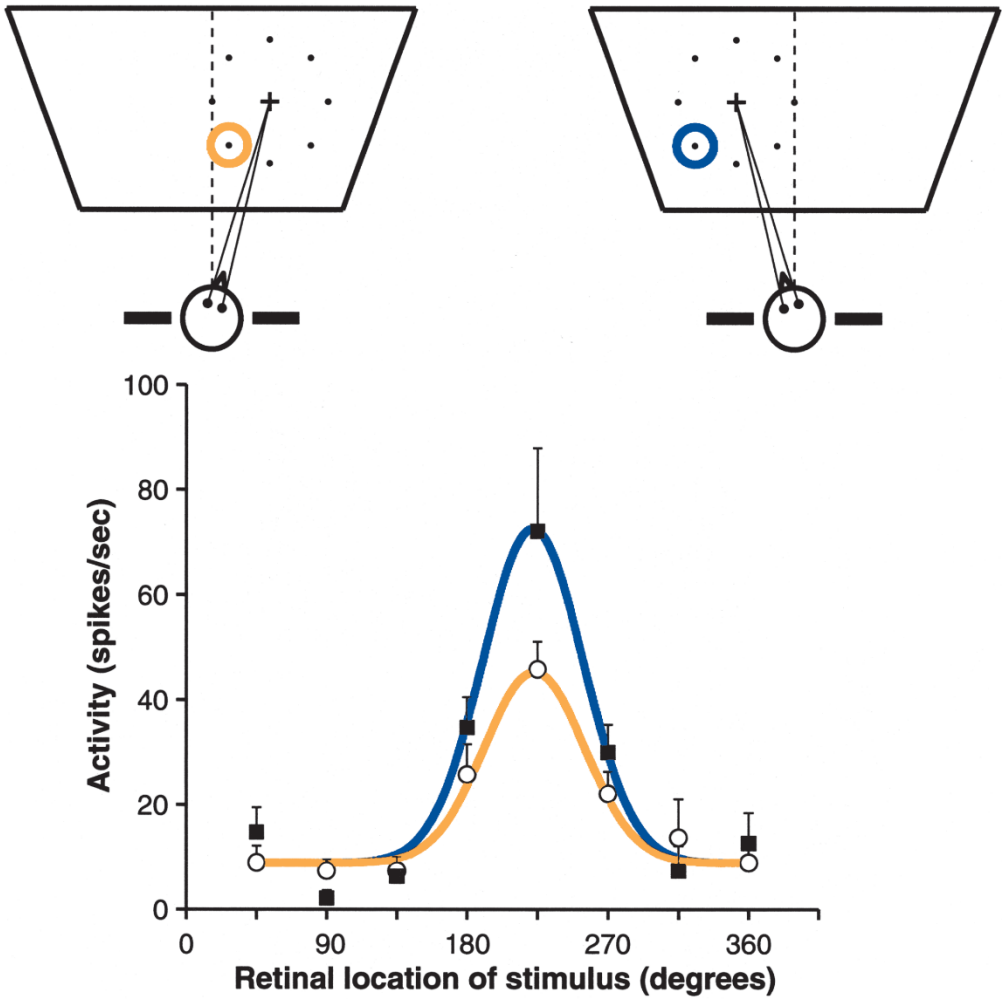

Figure 4.2 Gain modulation in parietal cortex. Upper panels: The response of the parietal cortex to a visual stimulus, depends both on the retinal location of a stimulus and on gaze direction. In these experiments, the monkey directs its gaze to the fixation point (cross), while stimuli are presented, one at a time at various locations (eight dots), within the neuron's receptive field. The retinal location of the stimuli is the same when the monkey head is turned right or left. The receptive field of a recorded neuron is indicated by the coloured (blue and orange) circles, and the direction straight ahead is indicated by the dashed lines. Lower panel: The firing rate of the recorded neuron for both conditions (right or left head turn) is plotted as a function of the position of the spot (stimulus location) in retinal coordinates. The neuronal response can be fitted by a Gaussian function (blue and orange solid lines). When the head turns, the peaks (neuron's preferred location) and shape of the response curve remains the same, but the amplitude, namely, gain, changes. Adapted from Salinas and Sejnowski, 2001.

and direction of the eye during saccadic movements, via a gain-field encoding. When Purkinje cells are organized into a mixed population of firing and bursting neurons (during saccades) that share the same complex-spike tuning preference (but not similar simple-spike receptive fields), they give rise to presynaptic simple spikes that converge onto a deep cerebellar nuclei neuron. This population response is linear to the speed of the saccade but has a cosine-shaped tuning curve in relation to the eye direction. The latter, however, is multiplicatively modulated by the speed of the saccade (Herzfeld et al., 2015).

The brainstem circuits might also utilize multiplicative gain operations in the control of the vestibulo-ocular reflex, which stabilizes images on the retina and thus, provides clear vision during head movements. The vestibulo-ocular reflex due to yaw rotations of the head is processed by a simple three-neuron circuit. The vestibular canals of the inner ear send their afferents to the vestibular nucleus of the brainstem, which in turn innervates the extraocular muscles of the eyeball. The response of the vestibular neurons to head speed, that is to the activation of the vestibular canals, could be modulated by the eye position stimulus (Khojasteh and Galiana, 2009).

An additional example of gain modulation comes from the invertebrate brain, where stereotypical species-specific behaviour can be triggered by an external stimulus/input. The amplitude of this response is gain modulated by inhibition and is proportional to the intensity of stimulation (Baca et al, 2008).

4.4 Gain modulation mechanisms

In order to clarify the mechanisms through which gain modulation occurs in single neurons, both experimental and theoretical approaches have been applied, such as dynamic-clamp electrophysiological techniques and single neuron modelling. The experimental conditions vary between the studies, but the typical methodology followed is exciting a neuron with an input that could be injection of constant current of various magnitudes, conductance steps or synaptic input and at the same time modulating its response with another input (of the same or different kind as the driving one). Both the driving and modulatory inputs can be of noisy nature.

4.4.1 Neuronal noise

The neuronal state (for instance, voltage fluctuations based on background synaptic activity) and its biophysical and synaptic determinants (for example, shunting inhibition, synaptic depression, ionic conductances) are putative key players in gain modulation. Neurons *in vivo* constantly receive synaptic inputs, which cause membrane potential fluctuations. Furthermore, events which are not evoked directly by an action potential but originate from the spontaneous release of neurotransmitters at the presynaptic terminal, are considered as a continuous background source of noise (Faisal et al., 2008; Kavalali, 2014). The neuronal response is not immune to this activity. Synaptic noise could affect the neuronal response in various ways. The background presynaptic events activate postsynaptic conductances that add

further to the mean membrane conductance. As a result, the input resistance is decreased which could decrease the neuronal responsiveness. However, the background synaptic activity introduces fluctuations to the membrane voltage. If the spiking threshold of the neuron is close to the resting potential, the subthreshold random membrane voltage fluctuations caused by the synaptic noise can cause variability in the firing rate and add additional spikes that would not occur in the absence of noise. If the membrane voltage is in a suprathreshold regime, the additional synaptic discharge affects the output, because there is a decrease in the rheobase, that is, the minimum current or conductance that triggers a spike, resulting in an increase of the spike rate (Chance et al., 2002; Faisal et al., 2008; Hô and Destexhe, 2000; Shu et al., 2003; Silver, 2010).

4.4.2 Shunting inhibition

The component of the synaptic input that is not considered noise can have a different impact on the integration properties of a neuron depending on the synaptic reversal potential and the membrane resting potential. An activated synaptic conductance could produce a depolarization, and thus it would be considered an excitatory one, if its reversal potential is above the resting potential of the neuron. Accordingly, if its reversal potential is below the resting voltage it would hyperpolarize it, and it would be an inhibitory one. In both cases, there would be an increase in the total membrane conductance due to the opening of the postsynaptic receptors, and a production of the corresponding subthreshold electrical pulse (Excitatory Post Synaptic Potential - EPSP or Inhibitory Post Synaptic Potential - IPSP) that propagates down the dendrite. There could be though the case where the synaptic reversal potential is close or equal to the resting membrane potential. In this scenario, due to the negligible driving force, there would not be any net movement of ions through the synaptic channels, and consequently no generation of a measurable postsynaptic potential. However, an increase in the local membrane conductance would occur (and hence the input resistance would decrease), which consequently would reduce (or shunt) any on path EPSPs. This effect is called shunting or silent inhibition. $GABA_A$ receptor activation is assumed to mediate the shunting inhibition, through the opening of membrane Cl^- channels (Paulus and Rothwell, 2016).

Much effort has been devoted to investigating the role of various configurations of synaptic input, background activity, leak membrane conductance/shunting inhibition in gain modulation by taking also into account different neural coding schemes, for example, firing rate coding or spatiotemporal coding (Silver, 2010). As aforementioned, shunting inhibition

scales down concurrent EPSPs and in particular, is assumed to have a divisive effect on the synaptic depolarization, due to Ohm's law. Ohm's law states that the membrane voltage (V_m) is proportional to the product of the input current (I_{in}) and the input resistance (R_{in}), and inversely proportional to the input conductance (g_{in}). Hence, the decrease in R_{in} induced by shunting inhibition attenuates the excitatory synaptic potentials and introduces divisive gain changes in the subthreshold V-I relationship. However, the role of shunting inhibition, under conditions, where a neuron responds to the input with a train of action potentials, seems to be different. Inhibitory shunting conductances alone performs a subtractive operation by causing a shift to higher input currents in the F-I curve, rather than a change in the slope. The reason behind this subtractive effect is that for prolonged periods, such as during sustained firing, the action potential train resets and "clamps" the somatic temporal-averaged membrane voltage to a new potential, above the resting one and close to the spiking threshold. Subsequently, the shunting conductance acts as a constant hyperpolarizing current source (Ayaz and Chance, 2009; Azouz, 2005; Brizzi et al., 2004; Capaday, 2002; Chance et al., 2002; Gabbiani et al., 1994; Holt and Koch, 1997; Prescott and De Koninck, 2003; Shu et al., 2003; Ulrich, 2003).

4.4.2.1 Shunting inhibition and synaptic noise

However, shunting inhibition can underlie multiplicative operations in the suprathreshold regime when certain conditions are met. Inhibition by shunt can be introduced either by a synaptic source (for instance, the background noise) or by a fixed tonic inhibitory conductance. Ongoing synaptic noise can modulate the response tuning curves (Ayaz and Chance, 2009; Murphy and Miller, 2003) or I-O relationships in a multiplicative manner (Azouz, 2005; Burkitt et al., 2003; Doiron et al., 2001; Fellous et al., 2003; Higgs et al., 2006; Hô and Destexhe, 2000; Longtin et al., 2002; Mitchell and Silver, 2003; Prescott and De Koninck, 2003; Shu et al., 2003; Tiesinga et al., 2000; Williams and Stuart, 2003).

4.4.2.2 Shunting inhibition and balanced background noise

When both the background synaptic components (excitatory and inhibitory firing rates) are concomitantly increased in a balanced manner the neuronal response is likewise modulated in a divisive manner. Such a configuration leads to enhanced shunting conductance and input noise (causing random membrane voltage fluctuations). The shunting inhibition alone results in a subtractive operation (right shift of the F-I curve) to the neuronal response. On the other hand, the increased input noise gives rise to an additive operation (left shift of the F-I curve) and decreases the gain too. During a balanced increase of the background synaptic activity both

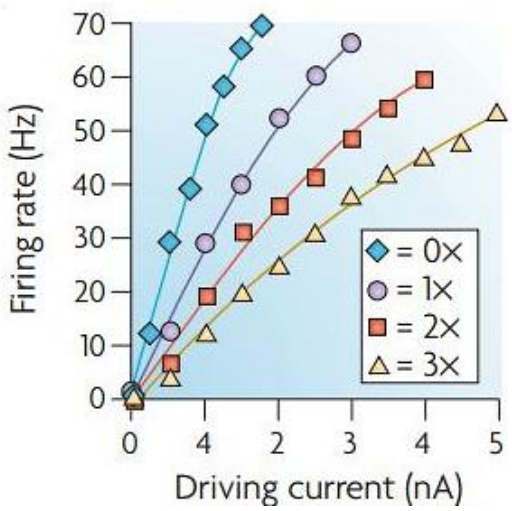

Figure 4.3 Gain modulation from background synaptic input. Changing the level of background synaptic input noise modifies the I-O relationship gain in a divisive manner. The firing rates evoked by different steps of driving input current at distinct levels of a *x* concurrent balanced increases in background excitation and inhibition together (Chance et al., 2002). Adapted from Silver, 2010.

phenomena take place. Thus, the right and left shift cancel out each other, and a pure gain change occurs (Chance et al., 2002) (Figure 4.3). This divisive gain control scheme arises also when the input stimulus is not just static, namely, its input statistics are not constant, but time-varying, where the neuronal response is represented by the mean firing rate over a time window, but also incorporates a time-varying component, that is, dynamic stimuli (Ly and Doiron, 2009). Yet, a balanced synaptic configuration might not always generate multiplicative operations (Capaday, 2002). Such inconsistencies, however, could be explained when bearing in mind that the function of a neuron in the presence of balanced synaptic noise could lie in a linear or nonlinear regime, depending on the interplay of the stochastic membrane fluctuations, membrane leakiness and the time scale that the neuron operates on (namely, the time constant of a non-passive membrane). For instance, in a conductance-based integrate-and-fire neuron model, the membrane time constant is different compared to a non-passive membrane, when synaptic conductances are present. When the background synaptic input increases, the leakiness of the membrane also increases, due to opening of more synaptic channels. The time constant of a non-passive membrane, however, decreases, and for a spiking-rate driving input, the membrane potential approaches a mean value that is decreased as well. Lower values of the mean membrane potential could cause also a decrease in the output firing rate. However, at the same time, the membrane fluctuations are more rapid (due to the decreased membrane time constant). Therefore, there are two competing processes taking place simultaneously, membrane leakiness and change in the time scale of the membrane dynamics. When these two

processes cancel each other, there is no change in gain. But, when the effect of leakiness is stronger than the effect of a small time constant, there is a change in gain (Burkitt et al., 2003).

4.4.3 Dendritic saturation

Further, the divisive effect of the combined synaptic fluctuations and shunting inhibition can be enhanced dramatically by dendritic saturation. As mentioned, the background noise enhances the probabilistic synaptic driven spiking in the subthreshold regime. Subsequently, the spike response to an input does not transit abruptly from one constant value to another, that is, a step-function, but follows a smooth course, namely, a sigmoid function. In addition, shunting inhibition acts as modulatory mechanism, when synaptic noise is present (see 4.2.2.1 Shunting inhibition and synaptic noise). This divisive control of the spike output by shunting inhibition, occurs because of the smoothing (resulting from synaptic noise), which

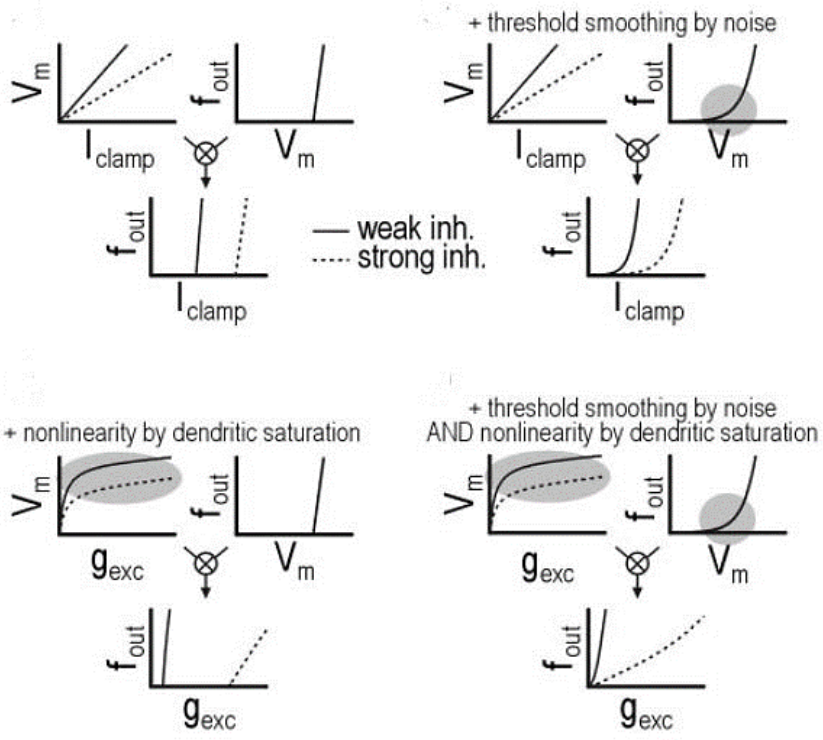

Figure 4.4 Gain modulation from shunting inhibition in the presence of synaptic noise and dendritic saturation. The effect of shunting inhibition on the spike output depends on the underling conditions. Upper left panel: Traditionally, shunting inhibition alone introduces a subtractive shift to the I-O relationship, by acting as a constant hyperpolarizing current source. Upper right panel: In the presence of a synaptic noisy source, the threshold nonlinearity is not an abrupt transition, but a smooth one. This enables shunting inhibition to perform divisive modulations. Lower left panel: Another nonlinearity observed in the relationship between the somatic voltage (V_m) and dendritic synaptic excitatory conductance (g_{exc}), due to the dendritic saturation. Again, in the absence of noise effect, the shunting inhibition modulation is translated as a subtractive operation to the firing output. Lower right panel: The gain modulation of the output firing by shunting inhibition is achieved when both threshold smoothing and dendritic saturation occurs. Adapted from Prescott and De Koninck, 2003.

is mirrored to the relationship of the firing rate with the underlying somatic depolarization. However, shunting inhibition with noise alone exhibits a mild multiplicative operation to the soma, or perisomatic areas. On the other hand, the somatic excitation from dendritic excitatory synaptic inputs usually requires strong input, due to the electrotonic attenuation of a propagating signal. But the stronger the local dendritic depolarization, the larger the reduction of the related synaptic driving force, and thus the smaller the effect of the synaptic excitation on the soma, due to the occurring dendritic saturation. Therefore, a nonlinearity is introduced between the somatic voltage and the synaptic conductance, which, in the absence of synaptic noise, is reflected as a subtractive shift in the F-I relationship. But the dendritic saturation effect, combined with the threshold smoothing mediated by the synaptic noise, produce enhanced divisive modulation (Prescott and De Koninck, 2003) (Figure 4.4).

4.4.4 Driving input features

Besides the background synaptic noise, features of the driving input could also influence gain modulation mediated by shunting inhibition. For instance, divisive gain operations occur when a neuron is driven with tonic excitation during synaptic (noisy) shunting inhibition. Nevertheless, the extent of that modulation is limited to low firing rates (Doiron et al., 2001; Hamann et al., 2002). Further, when a driving excitatory input is enriched with high variability, tonic shunting inhibition can act as a divisive mechanism with an additive shift too, due to the inhibitory effect (Mitchell and Silver, 2003). The reason behind this is that an increase in the firing rate of a non-tonic driving input will produce corresponding input noise, with similar effects as in the background noise-mediated gain modulation.

4.4.5 Excitation or inhibition alone

Nevertheless, even simple excitation or inhibition (hyperpolarising or shunting) alone can drive divisive control. In these cases, the divisive scaling is not evident in the F-I curves but when a tuning curve is considered instead. Yet, some additional conditions are required. Firstly, the background noise induces a nonlinear power-law relationship between the membrane voltage and the firing rate when the neuron is driven by an excitatory input. Secondly, the relationship between the input rate and the corresponding sensory stimulus parameter is nonlinear (for instance, sigmoidal or Gaussian). Finally, the modulatory excitatory or inhibitory input is small compared to the peak response evoked by the driving excitation (Murphy and Miller, 2003). However, for a stronger modulatory stimulus, the effect of a tonic

shunting conductance or a hyperpolarizing current on the tuning curve is subtractive. Noisy synaptic input, however, can act as a divisive mechanism (Ayaz and Chance, 2009).

The noise-mediated gain mechanisms described above are observed under *in vitro* and/or *in silico* conditions. However, *in vivo* the random synaptic driven membrane voltage fluctuations might not necessary result in gain modulation but depend on the spatiotemporal features of the synaptic activity evoked by a specific sensory context. Thus, gain modulation *in vivo* may be dynamically defined by the sensory context. Nonetheless, if the membrane fluctuations are combined with a depolarization in mean membrane voltage and a decrease in the mean input resistance, a divisive operation occurs (Cardin et al., 2008).

4.4.6 Noise-independent mechanisms

Additional putative mechanisms for gain modulation have been also suggested, where deterministic (that is, noise-independent) intrinsic processes are accountable. Gain control by synaptic inhibition can be obtained in neurons, where dendrites are enriched with active properties capable of generating backpropagation waves. A backpropagating event enhances multiplicatively the firing rate by acting as a feedback excitation process. This is because the depolarizing afterpotential resulting from a backpropagating spike is coupled with the somatic spiking rate and vice versa. The generation of dendritic spikes follows somatic action potential generation. Subsequently, the depolarizing afterpotential is spike-dependent and scales with the firing rate, but has no impact on the value of the input firing rate corresponding to the firing threshold of the neuron (rheobase). In the presence of dendritic inhibition, this multiplicative effect can be scaled down and consequently give rise to a divisive manipulation (Mehaffey, 2005).

By applying tonic inhibition at the soma, the total membrane conductance is increased and the slope of the steady-state F-I relationship is reduced, under noise-free conditions. The increase in the somatic conductance induces both an elevated spike threshold and a depolarization of mean voltage during spike generation. In neurons whose biophysical active properties support spike frequency adaptation, there is a positive correlation between this grade of depolarization and the magnitude of the steady-state spike frequency adaptation. Consequently, when a conductance is added, there is an increase in the steady-state spike frequency adaptation, which causes a decrease in gain of the steady-state F-I curve (Fernandez and White, 2010).

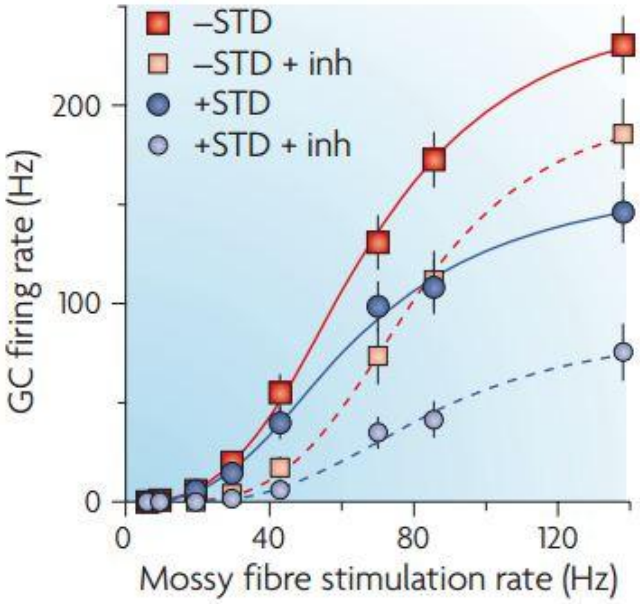

Figure 4.5 Gain modulation from Short-Term Depression. STD transforms inhibition-induced additive shifts into a multiplicative gain chain. When a tonic inhibitory conductance train (*+inh*) is introduced in a cerebellar granule cell (CGC), the I-O relationship shifts along the input (mossy fibre input rate) axis (additive operation, *-STD+inh* traces). STD adds a multiplicative component to this operation (*+STD+inh* traces) (Rothman et al., 2009). Adapted from Silver, 2010.

4.4.7 Short-Term Depression

Synaptic nonlinearities can also be the basis of gain modulation. Synapses can be dynamic, and their efficacy can be suppressed in a frequency-dependent manner (that is, Short-Term Depression - STD). When STD is present, the otherwise additive operation on the driving excitatory input by a tonic shunting inhibition is transformed, independently of noise, into a divisive modulation. The reason behind this effect is a nonlinearity in the relationship between presynaptic input firing rate and the time-averaged excitatory synaptic conductance, which is introduced by STD. The postsynaptic integration of the time-averaged excitatory synaptic conductance, however, is not affected by the presence of STD (Rothman et al., 2009) (Figure 4.5).

4.4.8 Synaptic mechanisms

Ionic cellular mechanisms, synaptic receptors or other voltage-gated channels can have a crucial role in defining gain operations. The currents that are generated in response to an input are shaped by the kinetics of the synaptic channels that are activated. Thus, their waveform characteristics, like peak amplitude, rise and decay time constants, vary accordingly, and their integration can result as well in output firing patterns with distinctive features. The abovementioned divisive effects of synaptic (shunting) inhibition are facilitated through

$GABA_A$ receptor currents. Excitatory currents are usually mediated by AMPA and NMDA receptors. AMPA-mediated gain can be obtained under noisy conditions, when the modulatory input is shunting inhibition. However, when an NMDA component is added to the excitatory driving input, the observed change in the gain is rather due to the decrease of the output firing frequency range. The presence of NMDA receptors increases the total input current, and as a result the range of input frequencies where gain modulation occurs is narrowed. A further decrease in gain modulation is added by the NMDA receptor saturation (Berends et al., 2005). In a similar way, the synaptic AMPA receptors make the dominant contribution to STD-dependent gain modulation, and not the NMDA ones. This is because the relationship between the mean input frequency and the NMDA conductance is nearly linear, so it does not add any further nonlinearity to the gain mechanism (Rothman et al., 2009).

However, the kinetics of the NMDA receptor render it capable of amplification events. The regenerative potentials that arise after the activation of NMDA synapses are characterized by a large plateau phase and long duration, favouring the temporal and spatial integration of local dendritic events (Antic et al., 2010). In light of this, there is evidence that the amplification effects due to the NMDA dendritic spikes might underlie sensory processing by combining information from different cortical areas (Palmer et al., 2014) or by multiplying excitatory postsynaptic responses to the preferred or null stimulus in a way that will remain proportional to the synaptic input, and undergo divisive operation by stimulus-tuned inhibition. As a result, the stimulus tuning (neuronal selectivity) is maintained but the fidelity of the signal is enhanced by noisy conditions (Poleg-Polsky and Diamond, 2016).

4.4.9 Ionic, voltage-gated and passive mechanisms

Furthermore, understanding how gain is modulated by the non-synaptic active and passive channel repertoire of a neuron, could provide some insight with regards to the way that neurons interpret their inputs, and subsequently how this is translated into sensory processing at a network level. The neuronal channels can be modelled by the Hodgkin-Huxley formalism where each channel current depends on the product of their maximal specific conductance, which is proportional to the channel density, and the activation and/or inactivation variables, which are voltage dependent and represent the probability of a channel to permit ion flow through the channel. Thus, at different voltage ranges, the current flowing through the channels changes according to its activation and therefore the neuronal excitability is altered. For instance, in the lobster stomato-gastric neurons, voltage-gated channels contribute to the gain

change by modulating the inter-spike interval. Increases in the maximal specific conductance of voltage-gated K^+ channels (A-type K^+ channel, delayed-rectifier K^+ channel, Ca^{2+}-activated K^+ channel) result in gain reduction. On the other hand, there is an enhancement in gain with increased channel density of slow voltage-gated Ca^{2+} channels, and no gain change has been found related to the hyperpolarization-activated (HCN) current density. Changes in passive excitatory or inhibitory channel conductances produce also no effect in gain. Moreover, changes in the density of coupled channels, like the Ca^{2+}-activated K^+ channel and the slow voltage-gated Ca^{2+} channel can perform a combined divisive gain operation (Patel and Burdakov, 2015).

4.4.10 Spike frequency adaptation

Biophysical mechanisms that generate spike frequency adaptation can also underlie gain operations. For example, Na^+ conductance inactivation lessens the spike generation and enables steady-state divisive modulation by increased tonic somatic inhibition, in the absence of noise (Fernandez and White, 2010). Yet, the ability of membrane fluctuations to control the gain, can be related to the magnitude of the spike dependent activation of slow afterhyperpolarization currents (slow afterhyperpolarization – sAHP). Noise enhances the gain in neurons with large sAHP, by reducing the suprathreshold activation of hyperpolarization (Higgs et al., 2006). Ca^{2+}-dependent potassium currents also regulate the response gain by influencing the AHP (Smith et al., 2002).

4.4.11 Neurotransmitters

The modulation of firing rates can be also carried out by neurotransmitter receptor activators, like nicotine, which increases the response gain to a given stimulus (Disney et al., 2007) and serotonin, which reduces the postsynaptic sAHP and induces a slow afterdepolarization (Higgs et al., 2006; Zhang and Arsenault, 2005).

4.4.12 Neuronal morphology

Neuronal morphology and input topology can influence the synaptic integration and the corresponding mathematical operations (Silver, 2010). The responsiveness to inputs of neurons with different complexities of dendritic trees is generally enhanced, in the presence of background synaptic noise, but the shape of their corresponding response curves varies slightly (Hô and Destexhe, 2000). Further, the capacity of a neuron to modulate its inputs is correlated

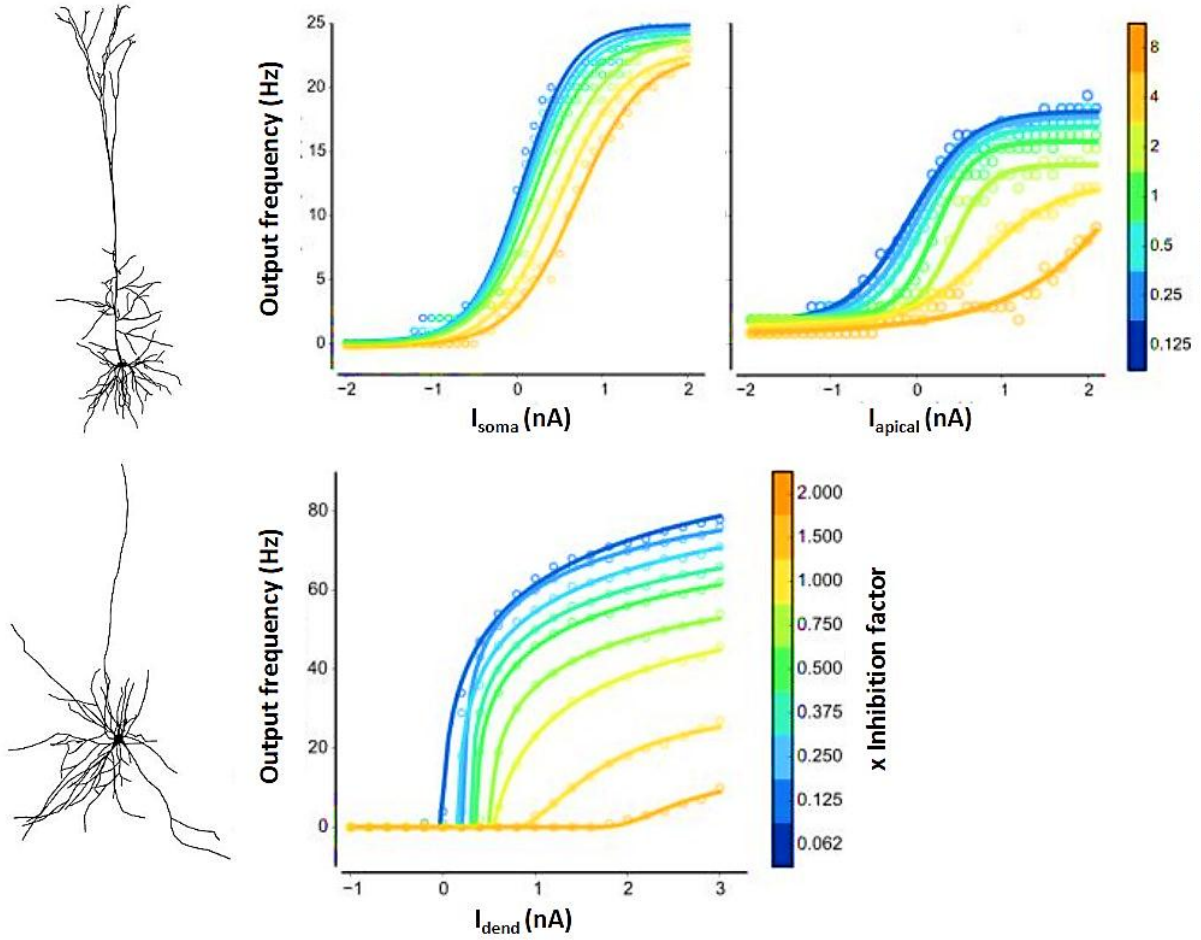

Figure 4.6 Gain modulation from dendritic morphology. Upper panels: A layer V pyramidal cell (left panel) is driven with current injections at the soma (middle panel) or dendritic tree (right panel) and modulated by altering the balance of background excitation to inhibition (x Inhibition ratio factor). Gain modulation occurs in the dendritic site, but not in the soma. Lower panels: Same for the dendritic tree of a layer II hippocampal stellate cell, where the I-O function is divisively modulated. The background balance, for both neurons, is simulated as light-coactivated opsins (excitatory and inhibitory) that are distributed along the neuron. Adapted from Jarvis et al., 2016.

to the branching pattern of its dendritic tree, and the balance between background excitatory and inhibitory synaptic inputs. The dendritic branch points attenuate the propagating currents. Therefore, the integration of synaptic inputs is affected by the branching pattern. The firing rate of neurons with a pyramidal shape (a bipolar-like neuron with an apical tree that bifurcates with moderate branching) is divisively modulated by the excitatory-inhibitory background balance, if the balance ratio is shifted towards the inhibition. In this case, neurons can be driven either with current injections in their distal apical dendrites or receive distributed throughout the dendritic tree excitatory and inhibitory synaptic inputs. In an analogous way, responses to driving injection currents to neuron with multiple dendrites emerging from the dendritic sites of stellate neurons (a multipolar soma, but with no elaborate branching pattern), are modulated by varying the excitatory-inhibitory background balance. When, however, these cells are

driven with distributed mixed excitatory and inhibitory synaptic input, there is rather a linear shift in the output response corresponding to the changes in the background amount of excitation or inhibition. Moreover, dendritic subtrees that do not receive background input, or a centrally located soma, lessen the gain modulation ability of the neuron by acting as current sinks (Jarvis et al., 2016) (Figure 4.6). Besides the aforementioned morphological properties, dendritic inputs could have distinct control on neuronal gain compared to the somatic ones, because of factors such as dendritic saturation (Prescott and De Koninck, 2003) and dendritic inhibitory conductances (Holt and Koch, 1997; Mehaffey, 2005)

4.4.13 Input topology

In addition, the topological configuration of synaptic input influences the neuronal gain. The integration of two excitatory synaptic inputs that are located on the same basal dendrite depends on their absolute and relative location. When the driving input is distal, is gain modulated by proximal to the soma synaptic inputs, which also lower the neuronal response rheobase. On the contrary, when the driving input is proximal to the soma, the distal synaptic inputs only lower the rheobase. The biophysical mechanisms underlying this process are related to the increased input resistance and signal attenuation of distal stimulus sites, as well as the voltage dependence of NMDA currents (Behabadi et al., 2012). The relevant location of inhibitory and excitatory inputs also affects their summation in the soma. Distal synaptic inhibitory input or input at the same basal compartment with a synaptic excitatory, increases the spike threshold. However, somatic inhibition applied with basal dendritic excitation causes a reduced gain operation. Basal dendritic inhibition placed on the path between basal dendritic excitation and soma has a combined effect, where both an increase in the rheobase and a decrease in the slope of the I-O relationship take place. The differential effects of inhibition depend on the interplay of the membrane leak conductance increase, due to the inhibition and the branch diameter and the voltage dependence of NMDA channels (Jadi et al., 2012). When the excitatory tonic conductance is co-localised with an inhibitory one, at a distance from the soma apical dendritic compartment, the latter causes a shift of the I-O function, whereas tonic inhibition on the proximal apical trunk performs divisive modulation, because it adds to the leakiness of the membrane (Pouille et al., 2013).

5 Channel noise in the CN neuron

5.1 Introduction

Neurons are equipped with numerous transmembrane proteins specialized to allow the bidirectional flow of ion currents from the extracellular space to the cytosol and vice versa The gating of these channels is highly probabilistic and the basis of the channel or electrical noise at the cellular level in the neuronal system, with various functional implications (see Chapter 3).

Experimental evidence shows a large variation of the electrophysiological responses of the neurons within cerebellar nuclei, *in vivo* and *in vitro* (Canto et al., 2016; Steuber et al., 2011; Uusisaari et al., 2007; Uusisaari and Knöpfel, 2012). This observed trial-to-trial variability in CN neurons belonging to the same subgroup suggests that neuronal noise could be an important contributor too. However, noise effects on the behaviour of the CN neuron have not been studied yet, since there is not any available model with integrated stochastic channel noise properties. For instance, ion channel noise could affect the neuronal computations in a distinct manner, based on the input location. Neuronal compartments with thinner diameters are expected to exhibit larger membrane voltage fluctuations in the presence of channel noise, compared to the thicker areas, such a soma or proximal dendrites. Such phenomena could be translated into multiplicative operations of distal inputs and linear summation of the ones proximal to the soma.

To explore research questions like the above, and the functional aspects of ion channel noise in the CN a stochastic model needs to be developed. This chapter describes the conversion of a detailed deterministic CN model (Steuber et al., 2011) to a stochastic one. Firstly, the CN voltage-gated ion channels are expressed by stochastic Markov formalisms and their behaviour is validated in a simple compartmental model against the original deterministic channel versions and for different conditions. Following this, a fully stochastic CN neuron is obtained, and its behaviour is compared with the deterministic CN neuron. Finally, the results are discussed.

5.2 Introducing stochasticity to deterministic CN channels

5.2.1 Deep cerebellar nucleus channel kinetics

In the current study, a morphologically and biophysically realistic computational model of a CN neuron is used (see Chapter 2). Each area is enriched with a specific set of ion channels. There are eight ion channels distributed differentially over the different regions of the model: a fast sodium current (NaF), a mixture of fast Kv3 (fKdr) and slow Kv2 (sKdr) delayed rectifiers, an SK-type calcium-gated potassium current, an HCN current, an HVA calcium current, a Cav3.1 type LVA calcium (CaT) current and a persistent sodium (NaP) current. The channels are modelled according to the Huxley-Hodgkin deterministic formalism (Table 5.1).

Current	Abbreviation	Gating schema
Fast sodium	NaF	m^3h
Persistent sodium	NaP	m^3h
Fast delayed rectifier potassium	fKdr	m^4
Slow delayed rectifier potassium	sKdr	m^4
High-voltage-activated calcium	CaHVA	m^3
Low-voltage-activated calcium	CaLVA	m^2h
HCN	HCN	m^2
Small conductance calcium-dependent potassium	SK	calcium concentration
Tonic nonspecific cation	TNC	none
Passive	pasDCN	none

Table 1 Biophysical deep cerebellar nucleus neuronal model summary. See text and Steuber et al, 2001 for details.

5.2.2 Deterministic CN channel models

The deterministic description of the CN neuron channels is based on the classic Hodgkin-Huxley model (Steuber et al., 2011) (see Chapter 3).

The macroscopic current of each channel is described by:

$$I_{channel} = \bar{g}_{channel} x (V_m - E_{channel}) \qquad \textbf{Equation 5.1}$$

where $\bar{g}_{channel}$ is the maximum channel conductance, x is the probability that all gating particles are in the permissive position, V_m the membrane potential, and $E_{channel}$ the reversal potential of the corresponding channel. In this case, the current flow varies linearly as a function of the driving force and conductance, thus the channels are considered ohmic in nature. The current through calcium channels is modelled by the Goldman-Hodgkin-Katz equation, because the calcium channels deviate from the ohmic behaviour (Hille, 2001; Steuber et al., 2011).

5.2.3 Stochastic CN channel models

The stochastic description of the CN neuron channels is based on the stochastic model, as described in a previous study (Kole et al., 2006). Each channel is represented by a chain of kinetic states, with probabilistic transitions between the states. For example, a simple channel, with only one gating variable, *m*, has two states, an open permissive state m_1, and a closed non-permissive state m_0 (Figure 5.1),

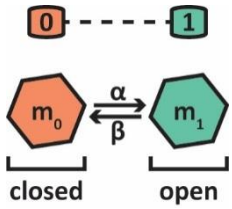

Figure 5.1 Simple channel kinetic scheme. This hypothetical channel has one gating variable *m* and consists of two gating states. If 1 indicates gate *m* to be in a permissive state and 0 to be in a non-permissive, then there would be one closed and a single open state for the system. Every transition (dashed lines) is governed, from left to right, by the *α(V)* rate constant, and right to left by the *β(V)* one. The system can be described by two major states (m_0 and m_1), with the corresponding transition rate constants shown.

where the rate constants, α and β (or $\alpha(V)$ and $\beta(V)$, which indicates their voltage dependence), are defined as in the Huxley-Hodgkin model (see Chapter 3). If this channel is open, then at any given point in time there is a probability to transit to its close state, independently of the time spent in the open state or how it acquired this state. Therefore, the system is modelled based on Markovian assumptions, namely, any event that occurs in a discrete short time interval is independent of the history of the system.

Each transition (open or close, or intermediate) depends on the rate constant of the state transition ($\alpha(V)$ and $\beta(V)$ or intermediate respectively). As the duration increases, the number

of successive transitions to m_1 can be described by an exponential decay (Sakmann and Neher, 1995).

$$f(t) = \alpha(V)exp(-\alpha(V)t) \qquad \textbf{Equation 5.2}$$

By integrating the above, the probability for the channel to transit to the m_1 state during a simulation time step dt_{sim} is defined by (see also below and Appendix A):

$$p_{m_1} = \int_{t=0}^{dt_{sim}} \alpha(V)exp(-\alpha(V)t)dt = 1 - exp(-\alpha(V)dt_{sim}) \qquad \textbf{Equation 5.3}$$

The macroscopic current density (per area of membrane A and expressed in nA/cm^2) is given by:

$$I_{channel} = \frac{N_{open}\gamma_{channel}}{A}\,(V_m - E_{channel}) \qquad \textbf{Equation 5.4}$$

The total conductance can be expressed as the product of the single channel conductance and the number of open channels per compartment, where N_{open} is the number of open channels, $\gamma_{channel}$ is the single channel conductance, and $E_{channel}$ the reversal potential of the corresponding channel (Steuber et al., 2011), and A is the neuronal (soma, dendritic or axonal) compartment area.

5.2.2.1 An example: HCN channel

In the present study, the voltage-gated channels of the CN neuron are expressed either as deterministic formalisms, based on the Hodgkin-Huxley model, or as Markov formalisms (as in Kole et al., 2006). Their behaviour is first investigated using a simple single compartmental neuronal model (one compartment cylindrical soma with length = 7 μm, diameter = 7 μm, without any axon or dendrites added, and uniformly distributed C_m = 1 μF/cm^2, R_a = 35.4 ohm/cm, V_m = -70 mV), where one type of CN channel is inserted per time, and current clamp simulations are performed. Three sets of experiments were carried out: (a) adjustment of the deterministic CN channel models and validation of their behaviour, (b) conversion of the deterministic CN channel models to stochastic ones, (c) investigation of the stochastic CN channel models' behaviour. For clarity, the conversion and validation of a channel with a simple kinetic scheme, the HCN channel (Steuber et al., 2011), is presented here.

5.2.2.1.1 Deterministic HCN model 1

The deterministic HCN channel model 1 is a part of the channel collection of the CN neuron model (Steuber et al., 2011). The formalism for this channel is a two activating (*m*) gates Hodgkin – Huxley type model. Thus, the total conductance for the HCN channel is given by:

$$g_{HCN} = \bar{g}_{HCN} m^2 \qquad \textbf{Equation 5.5}$$

Thereby, the macroscopic HCN current density is given by:

$$I_{HCN} = \bar{g}_{HCN} m^2 (V_m - E_{HCN}) \qquad \textbf{Equation 5.6}$$

where $\bar{g}_{HCN}$ = 10^{-3} S/cm^2 and E_{HCN} = -45 mV.

The temporal evolution of *m* is given by:

$$\frac{dm}{dt} = \frac{m_\infty - m}{\tau_m} \qquad \textbf{Equation 5.7}$$

where τ_m = 400 ms.

The steady-state activation m_∞ is given by:

$$m_\infty = \left(\frac{1}{1 - exp\left(\frac{V - V_{half}}{k}\right)} \right) \qquad \textbf{Equation 5.8}$$

where V_{half} = -80 mV and k = 5 mV (Steuber et al., 2011).

5.2.2.1.2 Deterministic HCN model 2

Although the deterministic HCN model 1 is based on the Hodgkin-Huxley model, the description of activation variables is given without calculating the state transition rate constants explicitly. However, the stochastic formalism of channel models, as described in the work of Kole et al. (2006), is expressed based on the rate constants. For this reason, the deterministic HCN model 1 is adjusted to a deterministic channel formalism that includes state transition rate constants, before proceeding to the stochastic conversion.

In the second deterministic HCN model (deterministic HCN model 2) the rate constants $\alpha(V)$ and $\beta(V)$ are introduced, and the temporal evolution of *m* is defined by:

$$\frac{dm}{dt} = \alpha(V)(1 - m) - \beta(V)m$$ **Equation 5.9**

The rate constants $\alpha(V)$ and $\beta(V)$ are expressed as:

$$\alpha(V) = \frac{m_\infty}{\tau_m}$$ **Equation 5.10**

and

$$\beta(V) = \frac{1 - m_\infty}{\tau_m}$$ **Equation 5.11**

5.2.2.1.3 Stochastic HCN channel model

The cerebellar HCN channel is represented by a two activating gate particles Hodgkin – Huxley model and can be represented by a Markov model with three states (Figure 5.2).

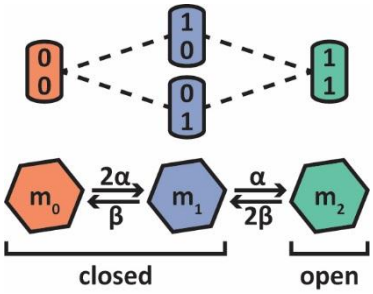

Figure 5.2 HCN channel kinetic scheme. HCN channel is represented by two *m* activation gates. Upper panel: Full kinetic diagram. If 1 indicates gate *m* to be in a permissive state and 0 to be in a non-permissive, then there would be three closed and a single open substates for the system, with four permitted transitions. Every transition (dashed lines) is governed, from left to right, by the *a(V)* rate constant, and right to left by the *β(V)* one. Lower panel: Reduced diagram. The *m* activation gates are independent and kinetically identical. As a result, all substates that share the same number of open and closed gates become equivalent and can be reduced to one major state. The system can be then described by three major states (m_0, m_1 and m_2). In a similar way, the rate constants are summarized, and their sequence (left to right: $2a$, a and right to left: 2β, β) is kinetically identical to the m^2 Huxley-Hodgkin model.

When the channel is in state m_0, where both activating gates *m* are non-permissive, or m_1, where only one activating gate *m* is permissive, it is closed, but in state m_2, where both activating gates *m* are permissive, it is open and allows the movement of ions. The probabilities for each state transition during each simulation time step dt_{sim} are:

Transition from $m_0 \rightarrow m_1$:

$$p(t) = 1 - exp(-(2\alpha)dt_{sim})$$ **Equation 5.12**

Transition from $m_1 \rightarrow m_2$:

$$p(t) = \frac{\alpha}{\alpha + \beta}(1 - exp(-(\alpha + \beta)dt_{sim})) \quad \textbf{Equation 5.13}$$

Transition from $m_1 \rightarrow m_0$:

$$p(t) = \frac{\beta}{\alpha + \beta}(1 - exp(-(\alpha + \beta)dt_{sim})) \quad \textbf{Equation 5.14}$$

Transition from $m_2 \rightarrow m_1$:

$$p(t) = 1 - exp(-(2\beta)dt_{sim})) \quad \textbf{Equation 5.15}$$

I_{HCN} is given by:

$$I_{HCN} = \frac{N_{open}\gamma_{HCN}}{A}(V_m - E_{HCN}) \quad \textbf{Equation 5.16}$$

where γ_{HCN} = 6.8 pS, and E_{HCN} = -45 and A is the neuronal compartment area. The number of open channels corresponds to the number of channels in state m_2.

5.2.3 Deterministic channel model validation

The first step towards the investigation of stochastic CN channels is to validate that the behaviours of the two deterministic formalisms are identical. Although such an outcome is expected, since the two deterministic formalisms are alternative forms of the classic Hodgkin-Huxley model, this test is still necessary as a control for the further investigation whether the behaviour of the stochastic channel models follow the same pattern as their deterministic counterparts. The deterministic HCN models exhibit the same somatic voltage responses and channel current waveforms, in response to a 100 pA current injection, and consequently they can be considered equivalent (Figure 5.3).

5.2.4 Stochastic channel model validation

The next step is to implement stochasticity in the CN channel models. This is introduced based on transition probabilities between the kinetic states. The similarity of the deterministic and stochastic channel behaviour of the CN neuron is assessed by comparing their voltage and channel current response, under the same current injection stimulation conditions. The voltage dependence of their gating variables is evaluated as well. Moreover, for the stochastic channel

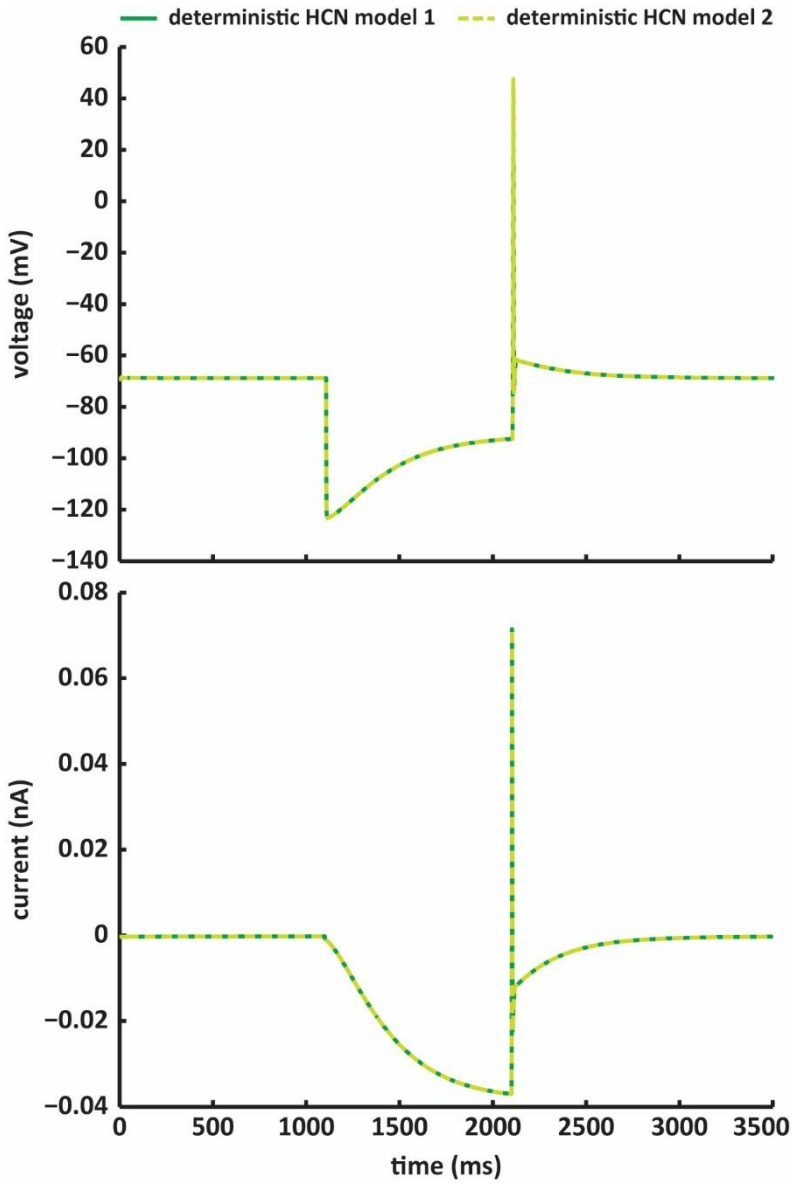

Figure 5.3 Deterministic HCN channel models. Overlay of the somatic voltage response (upper panel) and HCN current (lower panel) for both the deterministic HCN channel models, when the somatic neuronal model is current clamped. Both deterministic models exhibit the same behaviour.

models, the behaviour of all the intermediate states is evaluated during the course of the simulation, that is, before, during and after the current injection.

The stochastic version of the HCN channel displays the same behaviour as its deterministic version, as the deterministic voltage and current waveforms overlie precisely with the mean (of ten individual runs) stochastic counterparts (Figure 5.4). Additionally, the behaviour of its intermediate states is as expected, according to its kinetic schema. While the stimulus is applied, most channels are expected to transition to the open gating conformation, namely, the m_2 state. Consequently, the number of channels in the closed m_o state drops gradually, which mirrors the transition of channels to the open state. In addition, the number

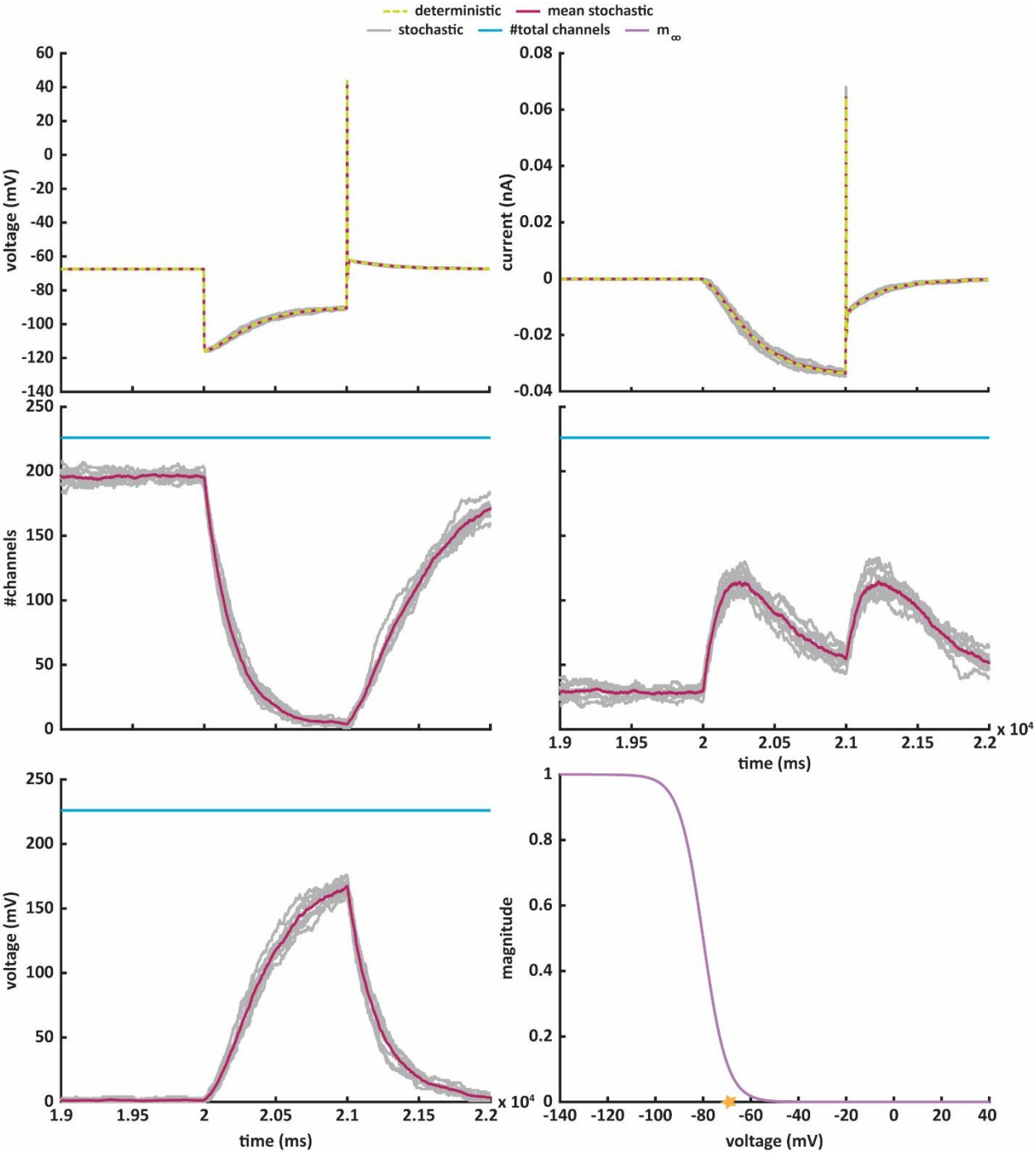

Figure 5.4 HCN channel behaviour. Upper panels: Deterministic and stochastic voltage and current response comparison. Middle panels: Time course of the closed m_0 (left) and m_1 (right) stochastic HCN channel states. Lower panels: Time course of the open m_2 (left) stochastic HCN channel state and voltage dependence of the steady-state activation gating variable (right). Asterisk: V_{rest} = -70 mV.

of channels in the intermediate m_1 state increases initially, as the channels transition from the m_o state, then drops, due the transitioning of channels from this state to the open m_2 one, and increases again, due to more channels transitioning back to the m_1 state, since the stimulus is not applied any more (Figure 5.4). While this is the case for most of the CN channels (data not shown), the behaviour of the NaF and the CaLVA channels models differ. This is further

investigated in the "5.2.7 Channels whose deterministic and stochastic models produce different results" section.

5.2.5 Effect of single channel conductance

The total channel conductance in a neuronal area (or in a compartment of a neuronal model) is the product of the single channel conductance and the number of channels in that area or compartment. Therefore, when the total conductance is kept constant and the value of the single channel conductance is altered, the number of channels in that area should alter as well (Hille, 2001; Kole et al., 2006). The role of the single channel conductance in affecting the behaviour of the stochastic HCN model is investigated here. The same experimental configuration is applied as previously, but with a 10-fold increase of the single HCN channel conductance.

The increase of the single channel HCN conductance is compensated by a decrease in the number of channels (total and therefore also open ones). Compared to the original stochastic HCN model behaviour, this results further in less averaging of the occurrence of channel openings, which is reflected in larger membrane voltage and channel current fluctuations (Figure 5.5). A larger number of channels results in flattening of the random fluctuations by evening out the single channel responses, while smaller numbers of channels and larger single channel conductances are associated with larger fluctuations, as described by previous studies (Cannon et al., 2010; Kole et al., 2006; Neishabouri and Faisal, 2014; O'Donnell and van Rossum, 2014; Steinmetz et al., 2000)

5.2.6 Channels whose deterministic and stochastic models produce different results

In the absence of any stimulus, spontaneous channel gating still takes place, resembling *in vivo* and *in vitro* single-channel recording (Faisal et al., 2008; Hille, 2001; Sakmann and Neher, 1995; White et al., 2000). To investigate further the behaviour of the two different channel models (deterministic and stochastic) the channel behaviour is studied under different conditions, that is, with or without current injection. Additionally, the measurement of a stochastic temporal mean is introduced. Firstly, the average of the current or voltage traces over a time window is calculated for each of the individual simulation trials and then these means are further averaged, resulting in the overall stochastic temporal mean. The comparison, over a defined time window, of the stochastic temporal means to the deterministic traces indicates whether the two models exhibit corresponding behaviours.

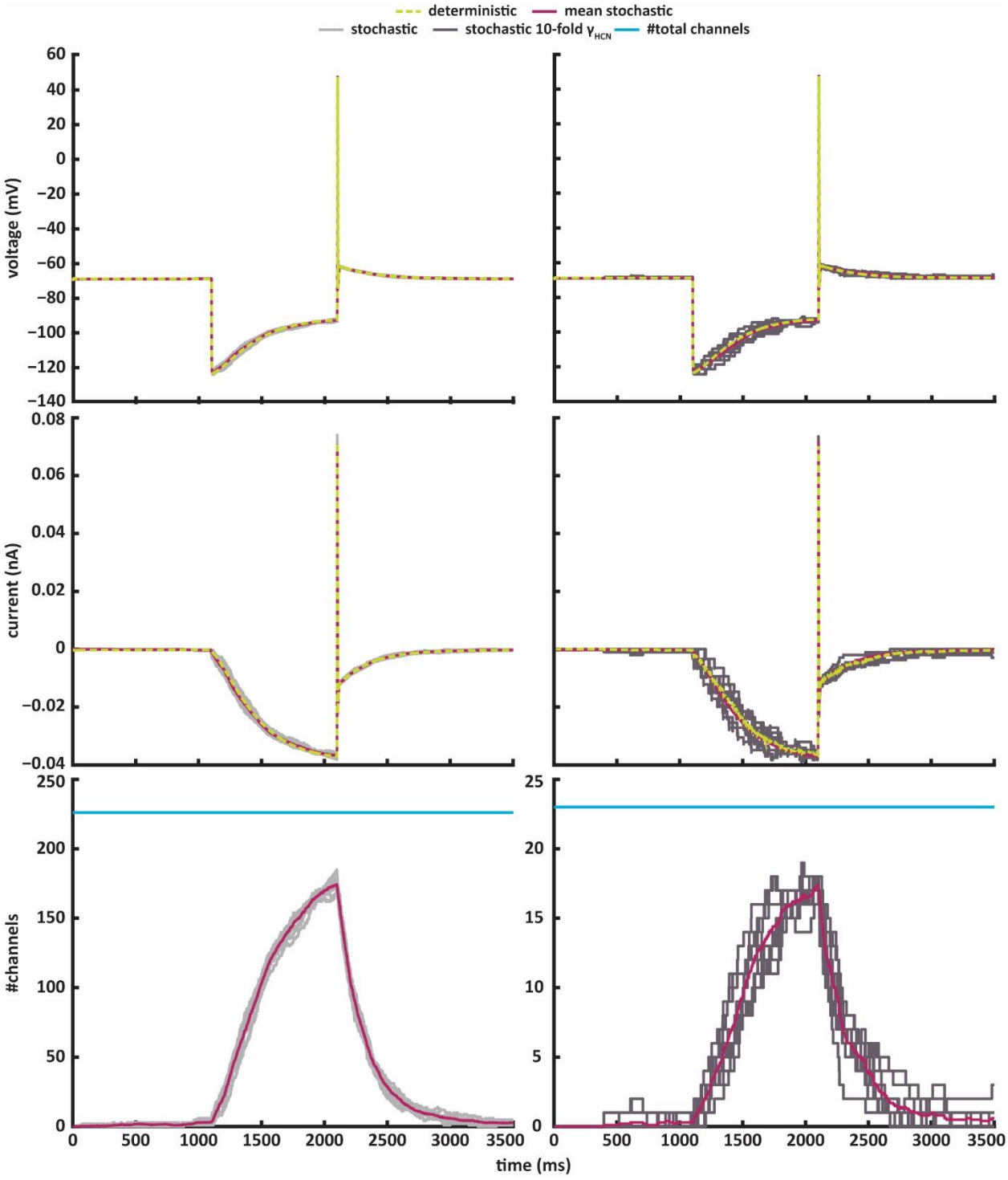

Figure 5.5 Stochastic HCN channel model. Due to the stochastic nature of the HCN channel model fluctuations between the experimental iterations are observed in the somatic voltage response (upper panels), the HCN current (middle panels) and the number of the channels that are open at every time point of the simulation (lower panels). When the single HCN channel conductance is increased 10-fold (right panels) the total number of channels and number of open channels is decreased. Overlay of ten experimental iterations. Mean stochastic is the average value of the experimental trials.

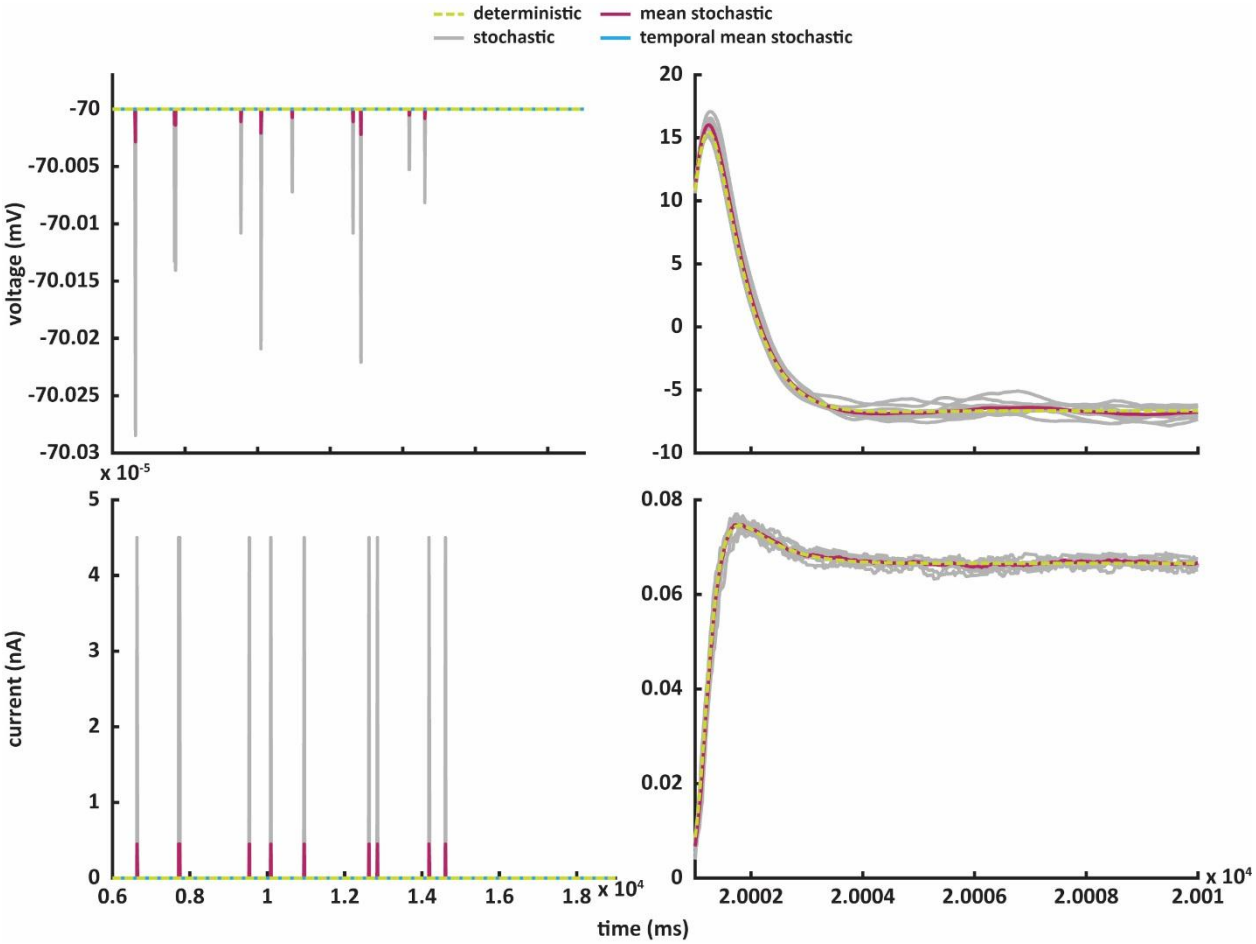

Figure 5.6 An example of deterministic and stochastic models with corresponding behaviour. The fKdr channel models showed similar behaviour under different simulation conditions. Left panels: Voltage (upper panel) and current (lower panel) response of the fKdr deterministic and stochastic models, when no current is injected. Right panels: Voltage (upper panel) and current (lower panel) response of the fKdr models when a 200 pA current pulse was injected for 1 s.

Although the majority of the stochastic CN ion channels (HCN, fKdr, sKdr, SK, CaHVA, NaP) show a similar behaviour as their deterministic counterparts (data not shown), resulting in a satisfactory overlay of the voltage and current traces for the stochastic and deterministic models (for instance HCN, Figure 5.4, and fKdr, Figure 5.6), this is not the case for the NaF and CaLVA channels (for instance NaF, Figure 5.7). Both in the presence and absence of a stimulus, the models differ in their behaviour, with the mean membrane voltage response of the stochastic model being higher than that of the deterministic one.

5.2.7 Effect of the specific channel conductance on stochastic channel behaviour

The discrepancy between two deterministic and stochastic channel models brings into question why these differences arise and whether there are conditions under which the two models could exhibit the same behaviour. The NaF channel is chosen for further investigation.

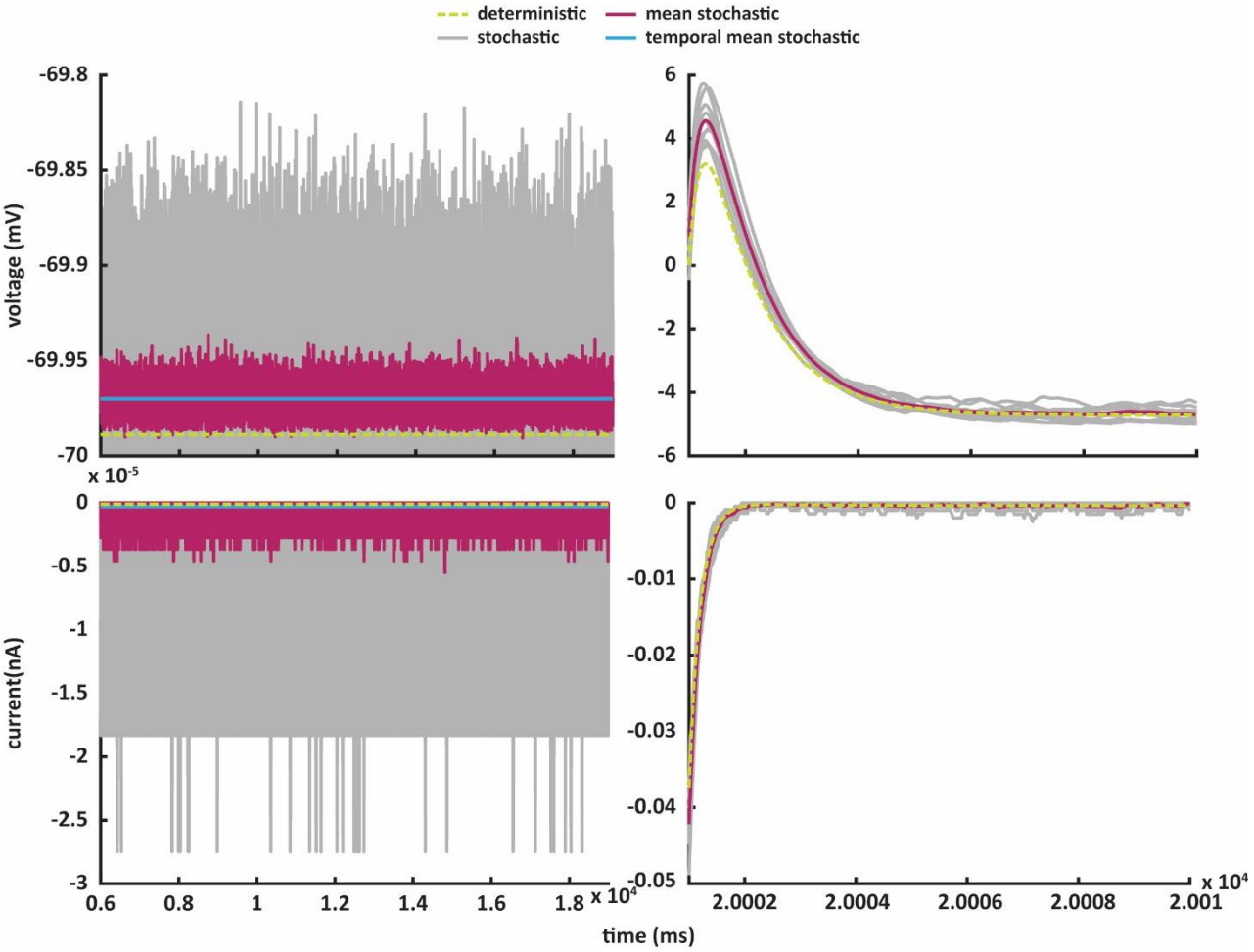

Figure 5.7 An example of deterministic and stochastic models with different behaviours. The NaF channel models under different simulation conditions. Left panels: Voltage (upper panel) and current (lower panel) response of the NaF deterministic and stochastic models, when no current is injected. Right panels: Voltage (upper panel) and current (lower panel) response of the NaF models when a 100 pA current pulse was injected for 1 s.

When no current is injected into the single compartmental model, both the deterministic and stochastic channel models eventually reach a steady-state or equilibrium voltage (and corresponding current). Due to the nature of the models, the equilibrium state of each model behaves differently. In the deterministic channel model, the equilibrium is achieved when the membrane potential stays at the exact same level of depolarization until a new event (for example, an external stimulus) is presented to the system. In the stochastic channel model, the depolarization level of the membrane alters through time as a result of the probabilistic channel gating and consequently electrical noise, expressed as fluctuations around the equilibrium point, is introduced. However, the stochastic temporal mean of the voltage (or current) gives an estimation of the average equilibrium point over a time window. Alternatively, an equilibrium value, equivalent to the stochastic temporal mean, could be reached with a very large number of channels, because the resulting fluctuations would even out.

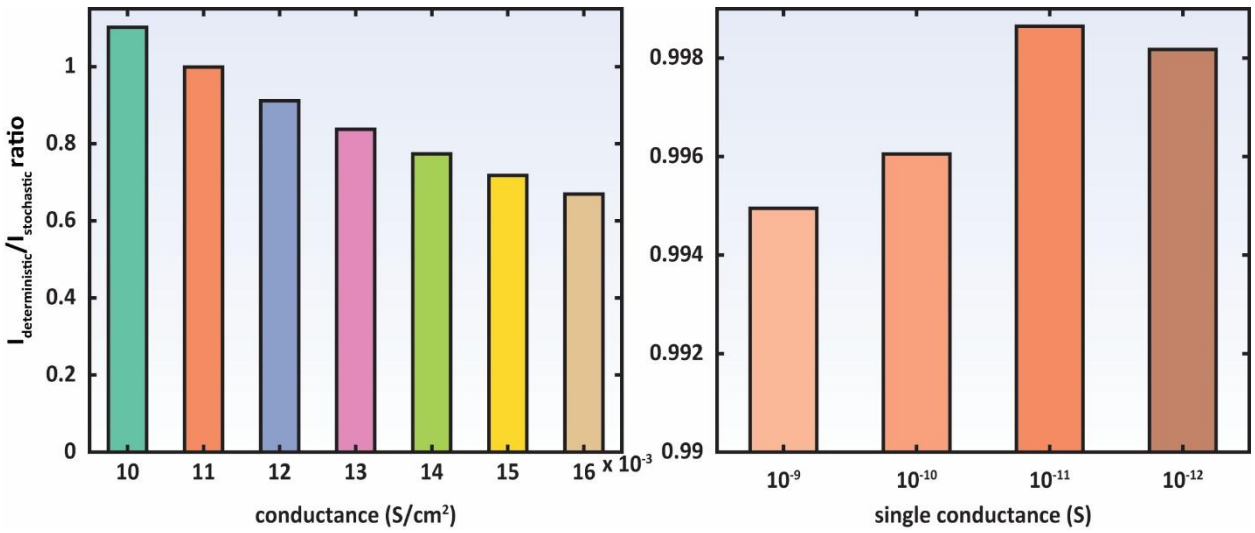

Figure 5.8 Effect of the specific or single NaF channel conductance Left panel: Adjusting the specific NaF channel conductance. The difference between the stochastic NaF channel model and the deterministic one is estimated in the absence of current injection, for the same single channel conductance (γ_{NaF} = 10^{-11} S). The numbers under the bars indicate the specific channel conductance (in S/cm^2). Right panel: Testing different single NaF channel conductances. The effect of different single NaF channel conductances is estimated in the absence of current injection, and for the same specific NaF channel conductance (g_{NaF} = 11 x 10^{-3} S/cm^2). The number of channels is inversely proportional to the single channel conductance (10^{-9} S corresponds to 169 total channels and accordingly 10^{-10} S to 1693, 10^{-11} S to 16933, 10^{-12} S to 169332).

The deterministic models of the channels used in this study are taken from the CN neuron model, which is turn is tuned to *in vitro* electrophysiological experimental data (Steuber et al., 2011). Thus, the approach applied here is to tune the stochastic channel model so that it matches the deterministic one (and therefore experimental data). The current through the open channels is proportional to the total channel conductance in both formalisms (see Equation 5.1 and 5.4). Therefore, different channel current responses indicate that the two models have different total channel conductances and consequently the specific conductance of the stochastic model is adjusted to replicate the behaviour of the deterministic model.

The ratio of the deterministic current mean ($I_{deterministic}$) to the stochastic temporal current mean ($I_{stochastic}$) is estimated for different values of the specific channel conductance in the stochastic model, when both models are equilibrated, and no current injection is applied. A current mean ratio close to one indicates that the channel models exhibit similar macroscopic current flow for this particular value of the total channel conductance (Figure 5.8).

Using the same experimental conditions (only the NaF channel type inserted into a single compartmental neuronal model), fixed current injection simulations are performed for a specific NaF conductance range of 10 - 16 x 10^{-3} S/cm^2. The behaviour of the two models is studied for the pre- and during stimulus period. For the time window when no current stimulus

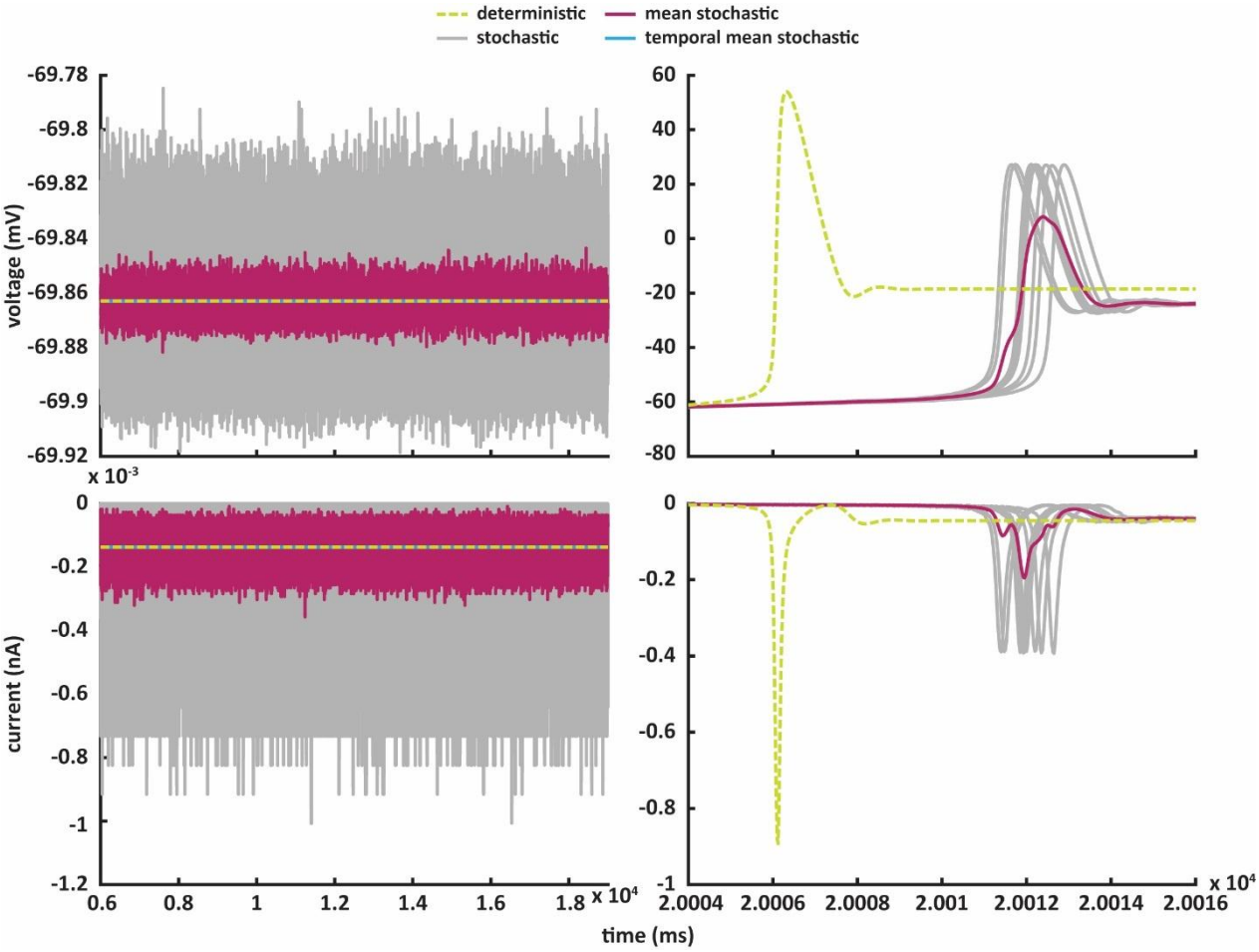

Figure 5.9 Tuning NaF channel models at g_{NaF} = 11 x 10^{-3} S/cm^2. Right panels: Voltage (upper panel) and current (lower panel) response of the deterministic and stochastic NaF models, when no current is injected (left panes) and during stimulus (100 pA current, for 1 s) (right panel).

is delivered and both channel models are equilibrated, a total specific NaF conductance of 11 x 10^{-3} S/cm^2 is enough to match the behaviour of the stochastic model to the deterministic one (Figure 5.8 and 5.9, left panels). However, during stimulus application the responses of the two models deviate, with the stochastic model showing a smaller depolarization of the membrane voltage for the same current injection (Figure 5.9, right panels). Increasing the specific channel conductance leads to a larger behavioural deviation in the pre-stimulus window, with the stochastic model having a lower temporal current mean and a higher temporal voltage response, and to a better match during the stimulus, with the stochastic model gradually getting faster. At a specific channel sodium conductance of 15 x 10^{-3} S/cm^2, the response to the stimulus of the two NaF channel models is similarly fast (Figure 5.10). Therefore, the two models could exhibit similar behaviours under different stimulation conditions, but not for the same specific channel conductance value at all conditions.

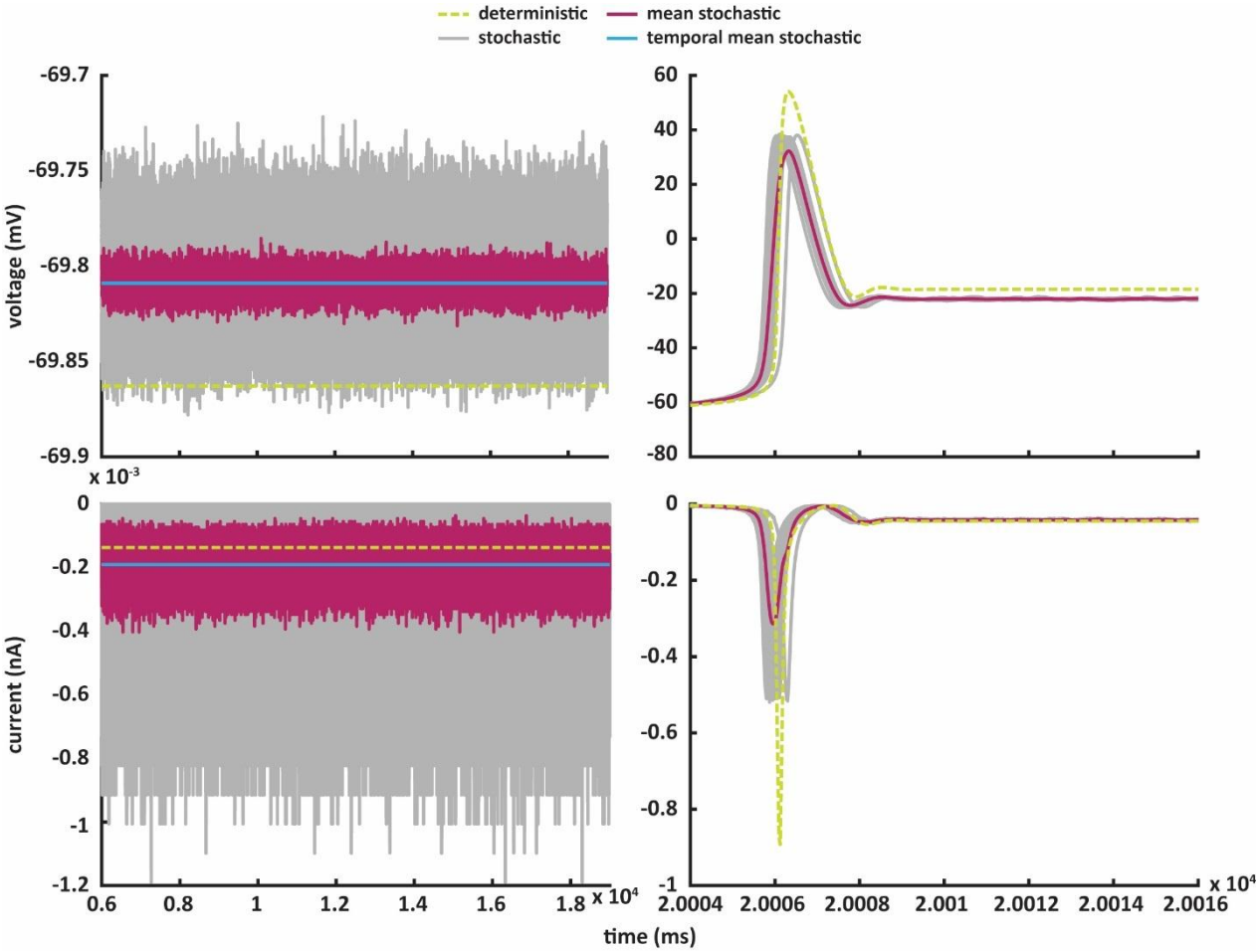

Figure 5.10 Tuning NaF channel models at g_{NaF} = 15 x 10^{-3} S/cm^2. Right panels: Voltage (upper panel) and current (lower panel) response of the NaF deterministic and stochastic models, when no current is injected (left panes) and during stimulus (100 pA current, for 1 s) (right panel).

5.2.8 Effect of the single channel conductance on the behaviour of the stochastic model

In order to explore further the behaviour of the stochastic model, the effect of the single sodium channel conductance is studied for a specific NaF conductance of 11 x 10^{-3} S/cm^2, under stimulus-free conditions. For a fixed specific channel conductance and in a confined area (that is, the area of the single compartmental neuronal model used in this study), a smaller single channel conductance represents more channels. Additionally, a larger number of channels in an area results in less noise in the membrane voltage and channel current. As a result, a large number of channels could produce a behaviour very similar to the deterministic model.

To explore this, current clamp simulations are performed for a specific NaF conductance value (11 x 10^{-3} S/cm^2) and different single NaF conductance values, namely, different numbers of total channels, since the compartment area is fixed. Larger populations of

total channels do not affect the behaviour of the stochastic model regarding its match with the deterministic one in the pre-stimulus and during stimulus time windows. However, fewer channels produce more noise, which is manifest by jitter in the spike timing (Figure 5.9 and 5.11), a common behavioural outcome of stochastic channel gating (see Chapter 3). The similarity of the two models, in terms of the temporal current mean ratio increases with smaller single channel conductances, but decreases when the single channel conductance is decreased even further (Figure 5.8). This optimum similarity condition for the two models (at 10^{-11} S) could be the result of the combined effect of two processes. Although, the simulation round-off errors for larger numbers of channels are smaller, at the same time, there is a larger number of missed state transitions. Thus, the overall behavioural convergence of the two channel models is sensitive to the number of channels.

5.2.9 The rectified distribution of open channels results in differences between the two models

The Hodgkin-Huxley model describes the collective response of a channel population. At every time point the current passing through the channels is proportional to the fraction of open channels in the overall population, given by the activation and inactivation variables and their respective exponents. This fraction is voltage dependent, because the transition rates between the open and closed channel states are voltage dependent, and it remains fixed at an equilibrium value for every steady-state voltage level. As a result, the response of the system (macroscopic membrane voltage and current) is steady, until a new event takes place. On the other hand, in the Markov model the transitions between the states are stochastic. Therefore, at any time point the transition between states is still voltage dependent, as in the Hodgkin-Huxley model, but whether it actually occurs is a stochastic event. Hence, for the same steady-state the voltage and channel current responses are not fixed, but fluctuate around a mean point, the mean response of the population. Furthermore, the behaviour of the stochastic model is affected by changes in the number of channels. The mean current measured in the stochastic model is the average of all single (unitary) channel currents. For the same channel population current per unit membrane area, a larger single channel conductance implies a smaller total number of channels, and a larger unitary current. Thus, channel populations with a larger single channel conductance will exhibit greater current flow fluctuations (Donnell and Nolan, 2014; Kole et al., 2006; White et al., 2000).

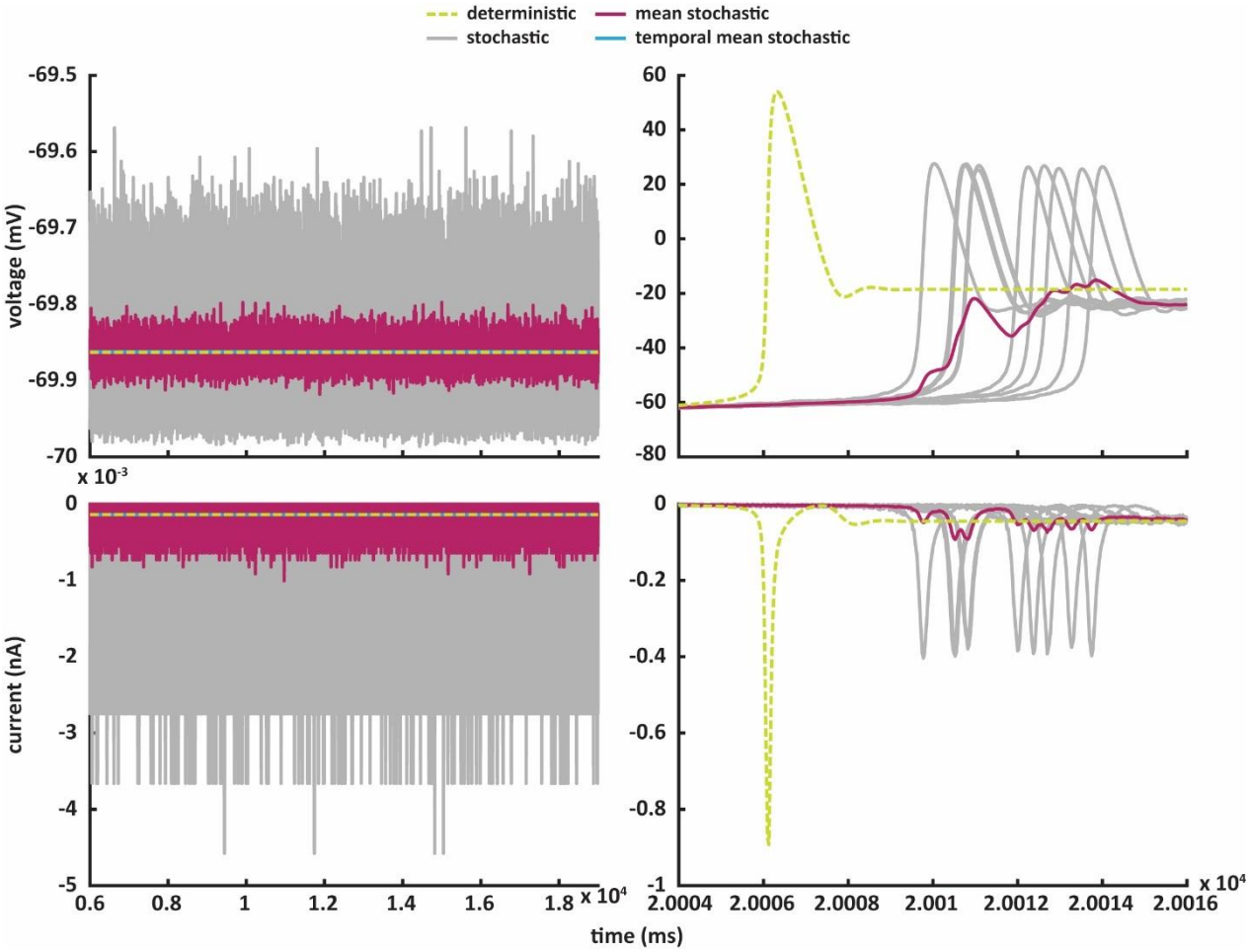

Figure 5.11 Tuning NaF channel models at g_{NaF} = 11 x 10^{-3} S/cm^2 and γ_{NaF} = 10^{-11} S. Right panels: Voltage (upper panel) and current (lower panel) response of the deterministic and stochastic NaF models, when no current is injected (left panels) and during stimulus (100 pA current, for 1 s) (right panels).

The distribution of the open channels in the Markov model can be described by a binomial distribution *B(N, p)*, where the number of trials *N* is defined by the number of channels and the success probability *p* in each trial is the probability of a channel to be open. The mean current *I* through a population of channels is the product of the unitary channel current *i*, the total number of channels *N* and their open probability, namely, *I* = *iNp*, where the product *Np* corresponds to the mean number of open channels. Thus, *I* can also be described by a binomial distribution with the standard deviation of the unitary current fluctuations $\sigma = i\sqrt{Np(1-p)}$ (Donnell and Nolan, 2014; White et al., 2000). The standard deviation σ describes the absolute amplitude of channel current noise for a given channel population. Therefore, for larger channel populations, and smaller single channel conductances, the current fluctuations will decrease, and the stochastic channel model behaviour will converge with the deterministic channel behaviour. This is due to the relationships of the σ with *i* and *N*. Smaller single channel

conductance, γ, results in smaller i, since $i = \gamma(V\text{-}E_{channel})$, which in turn will decrease the σ. On the other hand, the concurrent increase in N, could increase the σ. However, σ is not directly proportional with the N, as it is with the i, but grows proportional with the $\sqrt{N}$. Thus, the σ decreases faster with i than N (Figure 5.12).

The NaF channel models exhibit this anticipated behaviour (Figure 5.7). However, the temporal means of the voltage and current responses do not exactly match the deterministic responses under stimulus-free conditions. The stochastic model has a higher membrane voltage and current response compared to the deterministic one. The cause of this discrepancy might lie in a rectification effect emerging from a combined effect of a little overlap between the Hodgkin–Huxley steady-state activation and inactivation variables and a biologically realistic feature of the stochastic NaF channel model. There is a voltage range where the steady-state values of both sodium channel gating variables are not zero (Figure 5.12). Consequently, in this restricted voltage range, a sodium window current flows into the cell, slightly depolarizing the membrane and affecting the equilibrium value of the membrane voltage. In the case of the stochastic NaF model, the voltage (and current response) will fluctuate around the equilibrium value because the number of open channels also fluctuates, due to the probabilistic transition rates.

The stochastic current equilibrium point is the average of all fluctuating unitary channel currents. In order to be at the same level as the deterministic current equilibrium, symmetrical fluctuations around this equilibrium value would need to occur. However, this is not possible as it would require the existence of a negative number of channels, which is a biologically unrealistic condition. Consequently, the stochastic equilibrium point is estimated by averaging only the biologically allowed fluctuations, namely, a rectification effect is applied, which shifts the stochastic equilibrium up. Hence, for the observed rectification effect to take place, three conditions should apply: (a) the channel kinetics and state variable characteristics allow the generation of a window current, (b) the current equilibrium is close to zero and (c) the number of open channels exhibit fluctuations with a magnitude greater than their mean (which would be clipped at zero) (Figure 5.12).

An alternative way to depict this phenomenon is to study the distribution of open stochastic channels. Since a negative number of channels is biologically unrealistic, the distribution of the open stochastic channels is ‘forced’ to move to more positive values (for instance, 0, 1, 2), causing a rectification effect. As a result, the average fraction of open

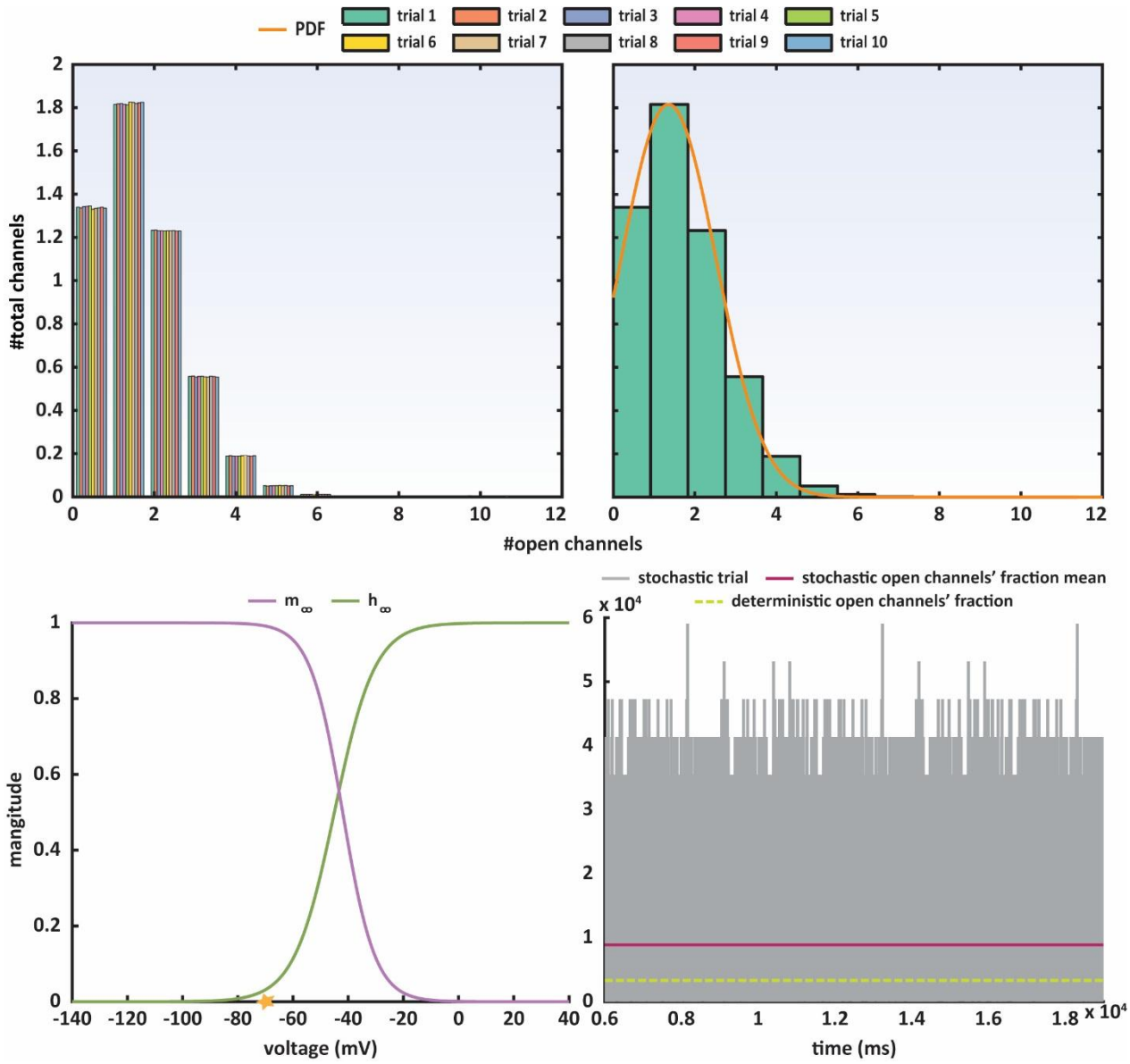

Figure 5.12 Rectification effect due to clipped distribution of open NaF channels. Upper panels: Distribution of the open channels when no current is injected (g_{NaF} = 11 x 10^{-3} S/cm^2 and γ_{NaF} = 10^{-11} S. Left panel: Channel population behaviour for all experimental trials with the stochastic NaF channel model. Right panel: Distribution for the first experimental trial and its probability density function (PDF). The distribution is clipped because there cannot be negative number of channels. Lower panels: Voltage dependence of the steady-state activation and inactivation variables of the NaF channel (left panel) and fraction of open NaF channels for both the stochastic and deterministic models (right panel). The average fraction of open stochastic channels is larger compared to the average deterministic fraction, and without any parameter correction (adjustment of the g_{NaF}), the behaviour of the two channels models (voltage and current response) will deviate. Asterisk: V_{rest} = -70 mV:

stochastic channels is higher compared to the average deterministic fraction without any parameter correction. Without such an adjustment of the total conductance the behaviour of the two models cannot match exactly (Figure 5.8, 5.9, 5.10 and 5.12).

5.2.10 Sensitivity to simulation time step

In the current study, the stochastic ion channels are modelled as memoryless chemical Markov chains, where the transition probabilities are voltage-dependent. The simulations use a fixed time step, which might impact the accuracy of the simulation results (White et al., 2000). The reason for this potential inaccuracy lies in the characteristic kinetic properties of a channel, and especially the relative magnitude of the transition lifetime from one intermediate state to another, compared to the simulation time step. Simulation methods that use a fixed time step assume that for each channel either nothing happens within a time step, or one event takes place that is, transitioning to a new state. However, in the case of the fast ion channels, where the transitioning time is significantly shorter than the simulation time step, more events could take place in the same time step. Thus, fewer events would be registered, which could lead to deviations in the number of open and close channels, resulting in less precise average

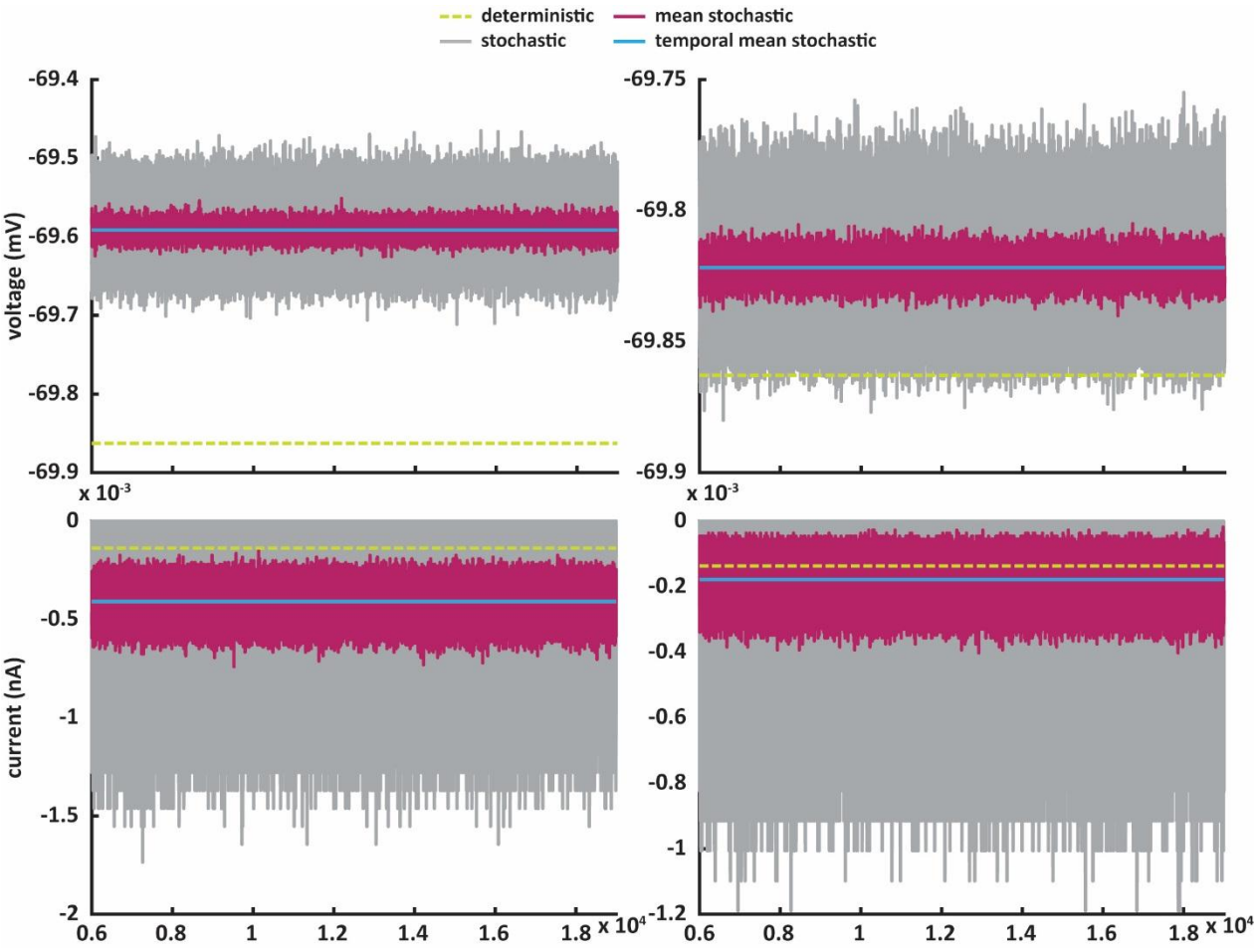

Figure 5.13 Effect of the simulation time step. Voltage (upper panels) and current (lower panels) response of the deterministic and stochastic NaF models, when the simulations step is 25 μs (left panels) and 5 μs (right panels) and no current is injected. For both, g_{NaF} = 30 x 10^{-3} S/cm2 and γ_{NaF} = 10^{-11} S.

macroscopic currents and voltages. Therefore, the behaviour of the stochastic NaF channel is investigated here for different simulation time steps.

As shown in Figure 5.13 and 5.14, the length of the time step indeed has an impact on the simulation accuracy, namely, the similarity of the stochastic and deterministic responses. Longer simulation time steps are associated with greater differences between the two formalisms. For instance, in this study at 1 or 5 μs there is a great overlap between the temporal stochastic and the deterministic voltage mean (Figure 5.14). The mean voltage difference is greater for larger time steps, such as 50 μs. The same trend can be seen in the case of the temporal current mean. However, at small time steps (1 or 5 μs) there is still a noticeable difference.

This difference between the various simulation time steps could be related to the probability of an opening or closing events occurring for a given time window. For the smallest time window (1 μs), there is still a chance of 0.12% of one opening event happening (transition from the closed state without inactivation m_2h_1 to the open state m_3h_1 with rate α_m). For greater simulation time steps, the probability of more than one event taking place increases, and for larger time steps, such as 25 or 50 μs, there is a 0.05% and 0.18% probability, respectively. Furthermore, at the same time the probability of predicted closing events taking place is greater for the transition from m_3h_1 to m_2h_1, (probability of one event: 36.67% for 25 μs and 29.14% for 50 μs and probability of more than one event: 23.59% for 25 μs and 55.07% for 50 μs, with

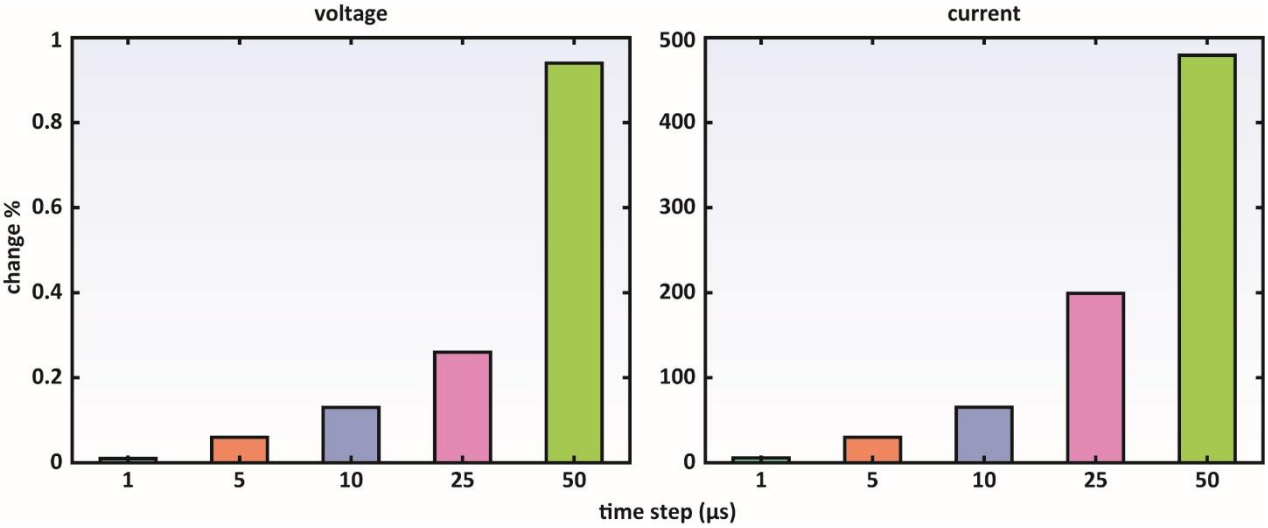

Figure 5.14 Relative change and simulation time step. Voltage (left panel) and current (right panel) temporal mean change, when the simulation time step varies. The change is defined as the relative percentage difference between the deterministic and temporal stochastic voltage or current mean. For both, the response of NaF models is shown, when no current is injected, and g_{NaF} = 30 x 10^{-3} S/cm2 and γ_{NaF} = 10^{-11} S.

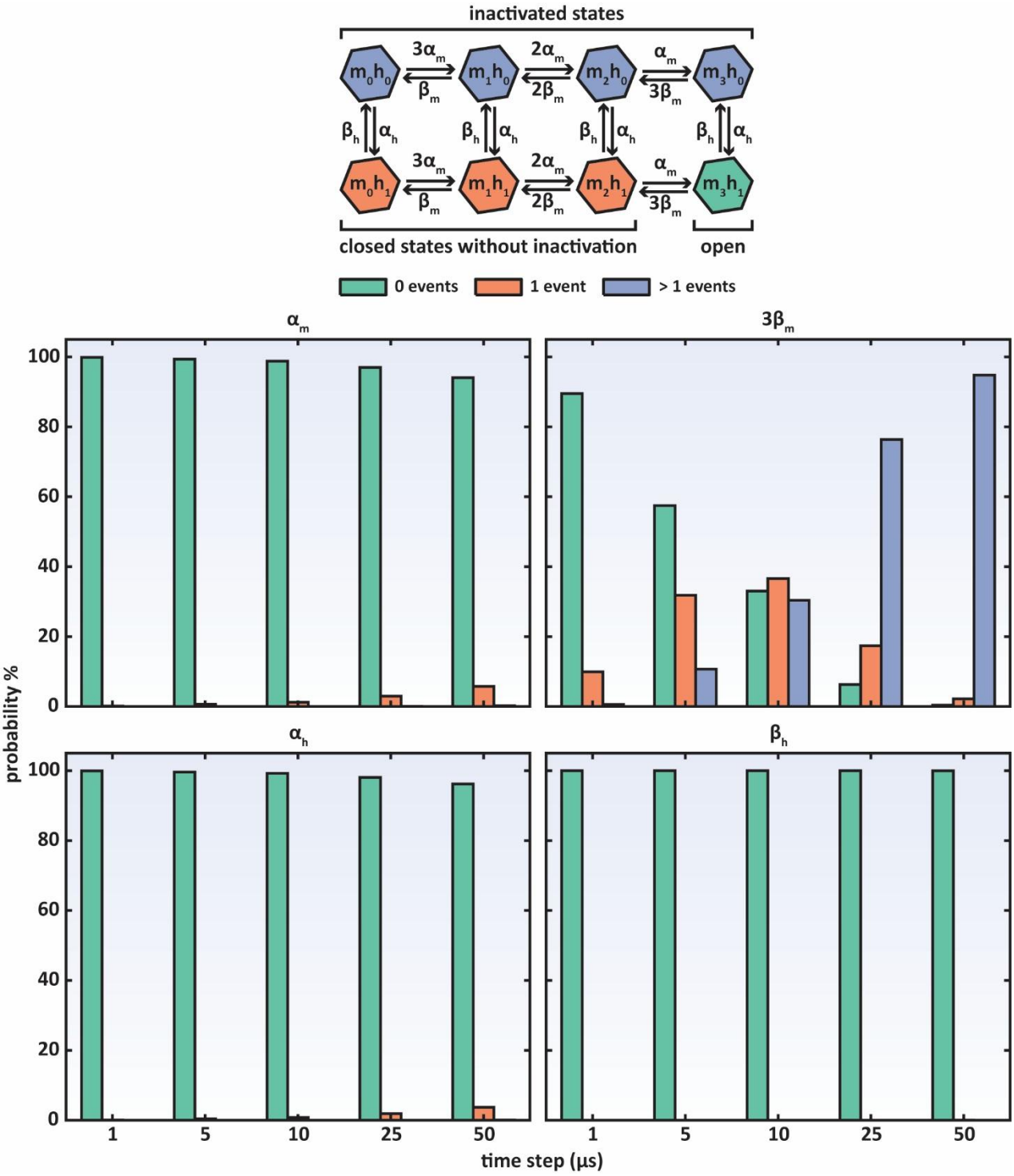

Figure 5.15 Predicted events per simulation time step according to the transition rates. Upper panel: NaF kinetic scheme. Lower panels: Probability of zero events, one event or more than one event occurring for a given time simulation step, and for the different transition rates. The probabilities are calculated based on the Poisson model, where the average number of events is given by the product of the transition rate and a given simulation time step.

rate β_m). Similar phenomena are observed for the predicted transitions between m_3h_1 and the inactivated state m_3h_0, with rates α_h and β_h (Figure 5.15). Hence, for larger time steps, due to the fast transition rates, there is a greater probability that more events will take place, in

different directions, based on the channel kinetic scheme, which can lead to the detected discrepancies.

In addition, for the case of the deterministic formalism, there is no prerequisite of considering the independent opening events occurrence for the determination of the channel response. Therefore, the channel behaviour would be recorded the same for all time steps, until a new external event, such as new stimulus is applied. However, in the stochastic formalisms, the number of opening events is important for the measurement of the channel's behaviour, for instance current flow. Each opening event is considered independent and equally contributing to the channel's population response. As a result, the impact of the predicted transitions is accumulated, and is scaled-up for simulations with large number of channels.

Thus, more accurate stochastic simulations of fast channels could be achieved with smaller time steps, as previously reported as well (Cannon et al., 2010; Kole et al., 2006). Nevertheless, smaller time steps could lead to accumulation of numerical errors and high computational cost. These factors should be all considered for the selection of the optimal time step.

5.3 Implementing stochastic channels in a CN neuron model

The output of a neuron is shaped by the interplay of its intrinsic properties and the inputs (synaptic input or current/conductance injections) it receives. On top of this, the specific morphological features of a neuron could also affect the integration of its electrical inputs (Silver, 2010). Current computational representations of CN neurons are based on deterministic descriptions (Steuber and Jaeger, 2013), neglecting the realistic stochastic nature of neuronal channels and their possible impact on the neuronal response.

To investigate the impact of the deterministic and stochastic channels on the behaviour of the CN neuron, two set of experiments are performed. Firstly, the effect on the CN behaviour of one stochastic channel type per time is investigated. Secondly, stochasticity is introduced to all the channels of the CN neuron.

5.3.1 Semi-stochastic CN neuronal models

The semi-stochastic CN models are built by introducing stochasticity to one channel type while retaining the rest as deterministic. Simulations of somatic fixed current injections

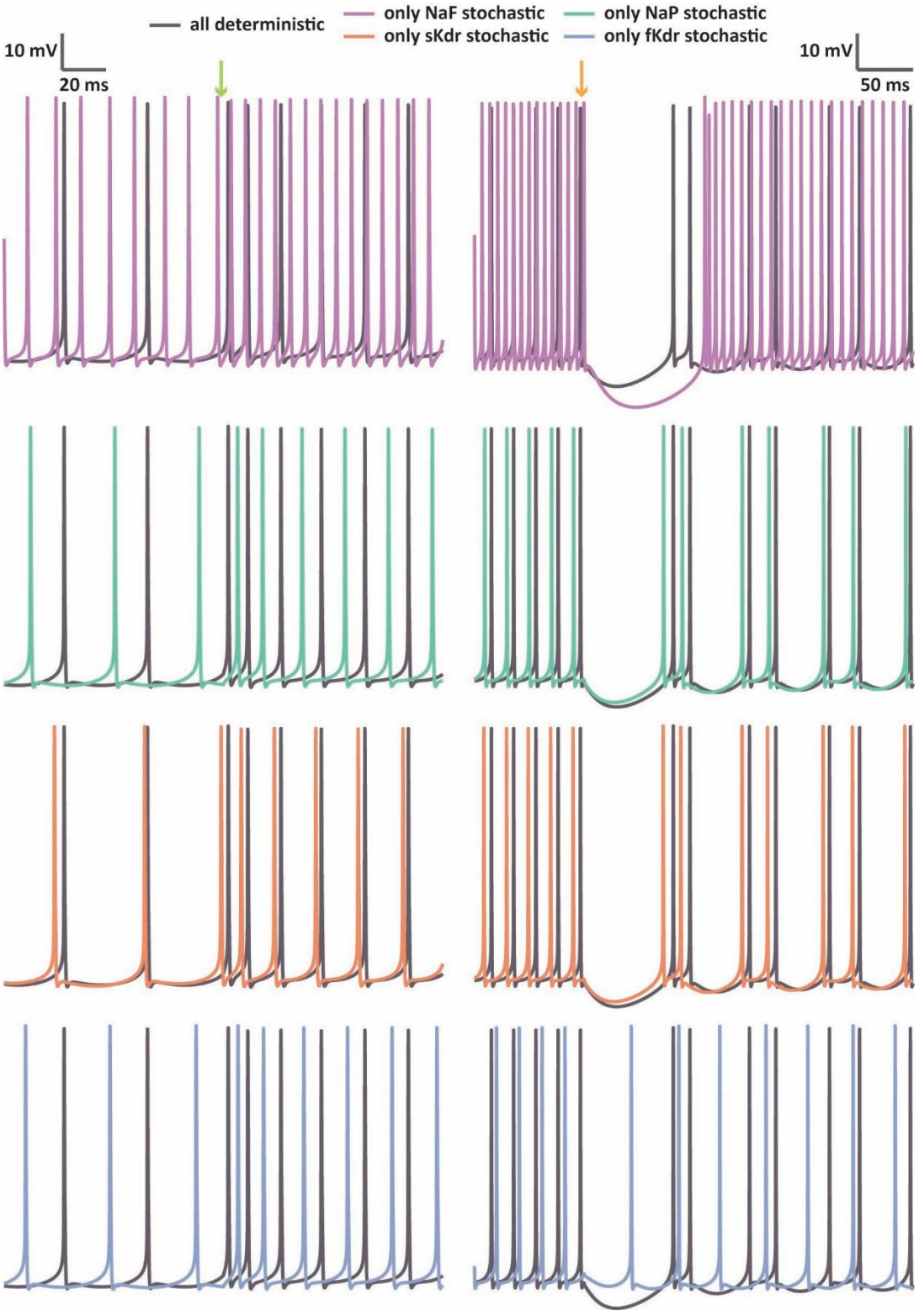

Figure 5.16 Semi-stochastic CN neuron models. Somatic voltage response of the CN neuron with no stimulus (left panels) and pre-stimulus and during 100 pA current injection for 1.5 s (right panels). Green arrow: Beginning of stimulus; Orange arrow: End of stimulus

are carried out by applying two conditions: (a) only one stochastic channel type model is investigated per time and the rest of the CN channel collection are described by their formalism,

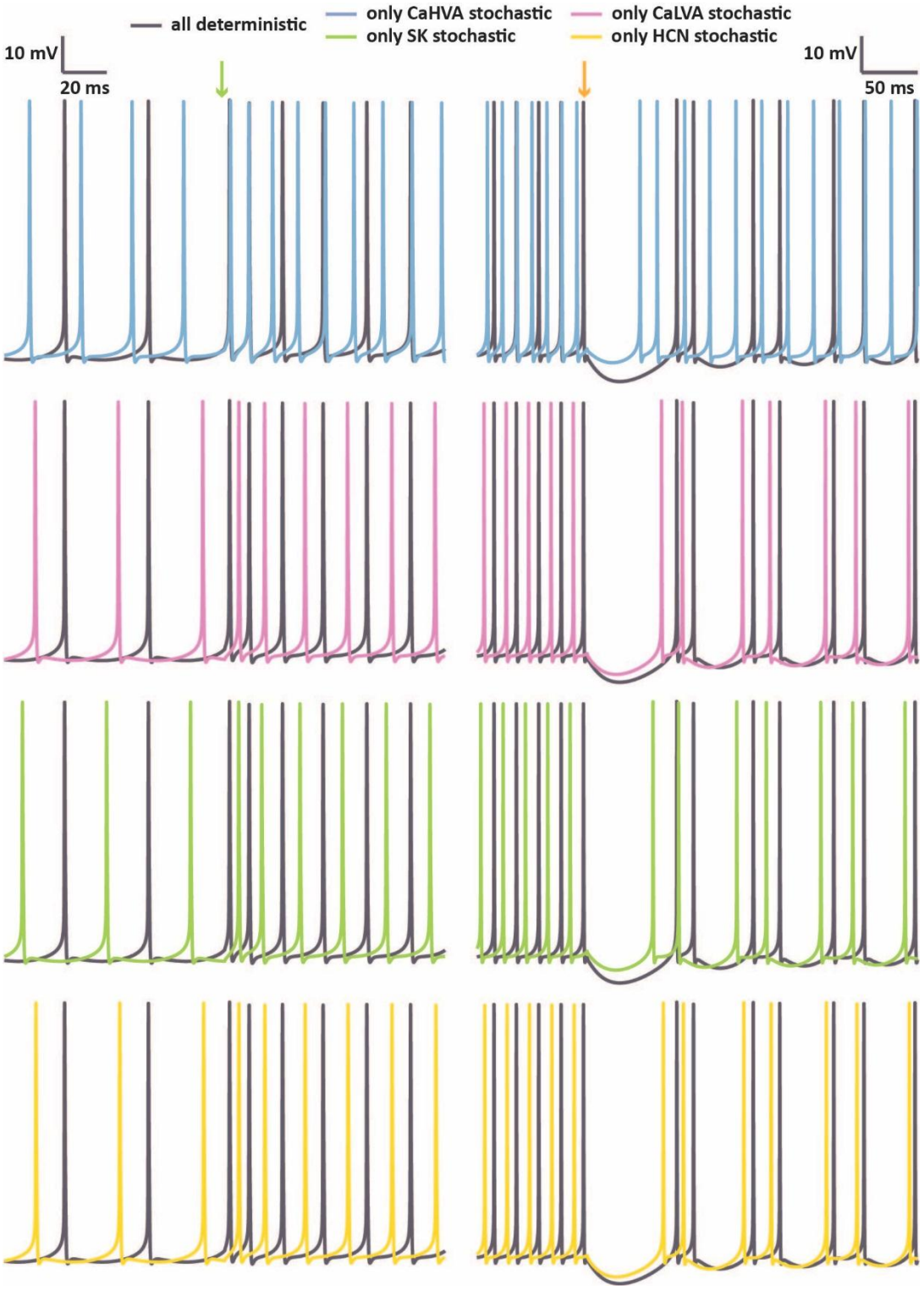

Figure 5.17 Semi-stochastic CN neuron models. Same as Figure 5.16 for the rest of the channels.

(b) the single channel conductance of the channel under investigation is adjusted so that even the smallest neuronal compartment would have at least 100 channels. By using this experimental configuration, it is possible to study the behaviour of each stochastic channel model without any interference due to the other stochastic channels. Moreover, by adjusting

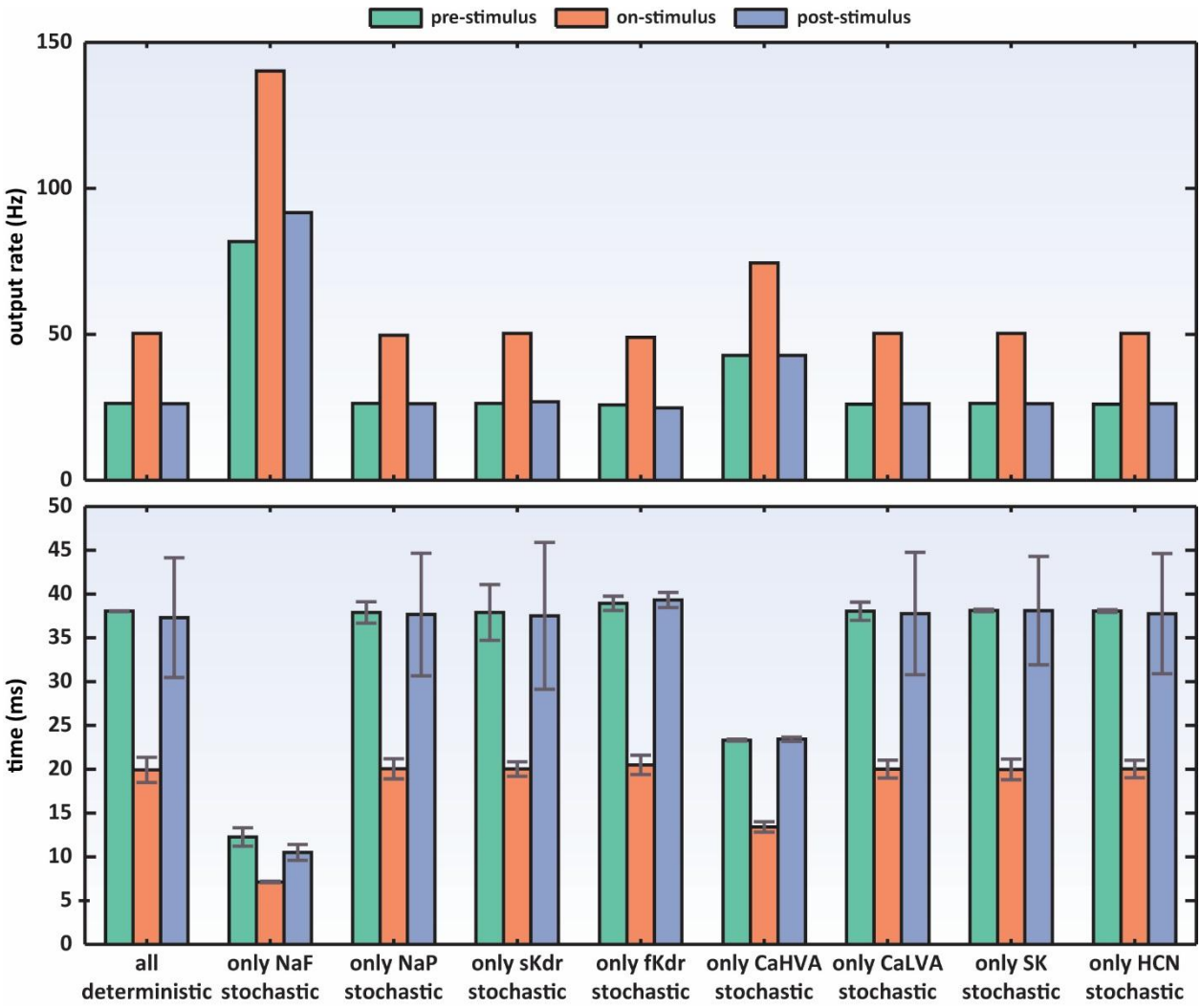

Figure 5.18 CN neuron model behaviour for different stochastic channel models. Current pulses (100 pA for 1.5 s) are injected into a CN neuron model where only one stochastic channel model type is implemented each time. Firing rate (upper panel) and interspike interval (lower panel) of the CN neuron models for different time windows during simulation.

the number of channels to a moderate population size, noise is limited but not totally eliminated.

The semi-stochastic CN neuron models exhibit qualitatively similar electrophysiological properties as their deterministic counterpart, that is, the CN neuronal model that has been tuned to match *in vitro* electrophysiological data (Steuber et al., 2011). Their behaviour is characterized by spontaneous firing in the absence of stimulus, and a regular spike pattern in response to a fixed current injection (Figure 5.16 and 5.17). However, as for the single compartmental model, the CN neuron models with stochastic NaF channels do not behave exactly like their deterministic version. Moreover, the model with stochastic CaHVA channels also exhibits a slightly faster spike response compared to the deterministic one (Figure 5.18).

5.3.2 Fully-stochastic CN neuronal models

The construction of a fully-stochastic CN neuron model is achieved by implementing stochasticity to all the voltage-gated ion channels. However, this configuration does not result in a good match of the two models, independently of the stimulation with injected current (Figure 5.19). Since the semi-stochastic CN models with only NaF or CaHVA channels are the ones with the most different behaviour compared to the deterministic model (Figure 5.16, 5.17 and 5.18), the NaF and CaHVA in an altered stochastic CN neuron model are changed back to deterministic formalisms. This new stochastic CN model, hereafter referred to as stochastic CN model, shows electrophysiological properties similar to the deterministic one, namely, the ongoing spontaneous spiking without a stimulus and a regular spike pattern in response to a fixed current injection (Figure 5.19). In addition, the spike rate as a function of injected current in the soma for both the neuronal models is similar (Figure 5.20). Therefore, this stochastic CN neuron model is chosen for further investigation in the current study.

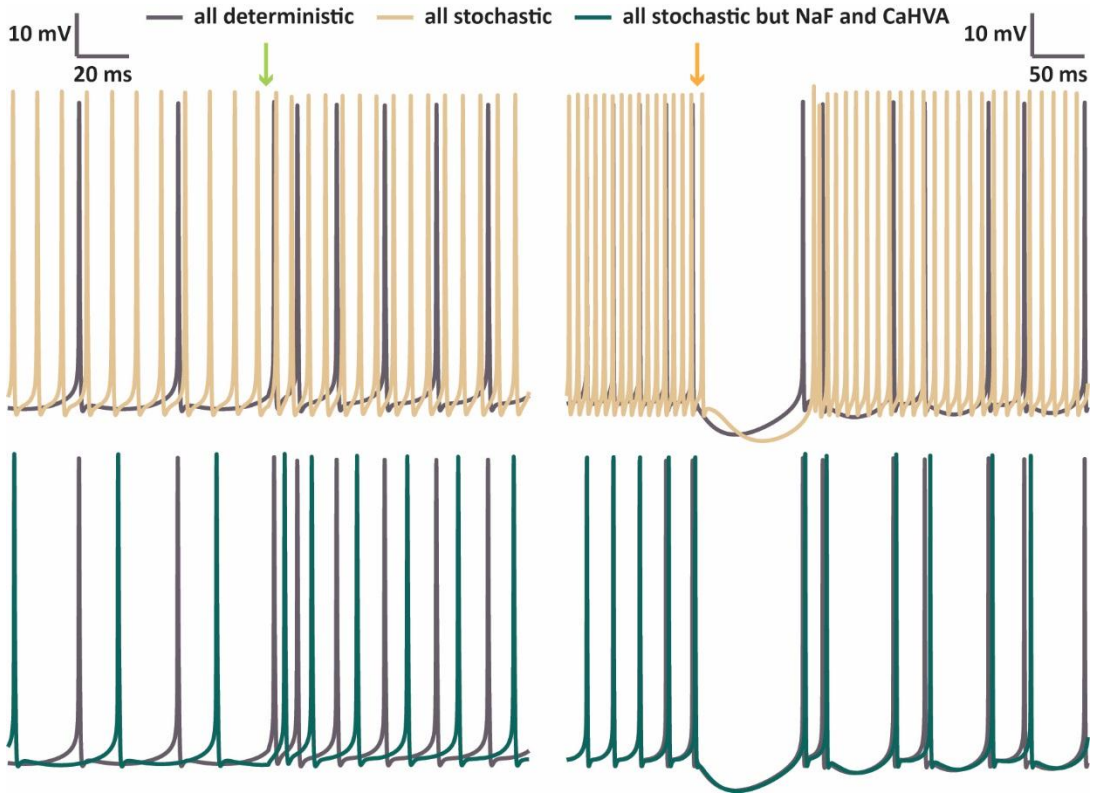

Figure 5.19 Fully-stochastic CN neuron models. Somatic voltage response of the two stochastic CN neurons with no stimulus (left panels) and pre-stimulus and during 100 pA current injection for 1.5 s (right panels). Green arrow: Beginning of stimulus; Orange arrow: End of stimulus.

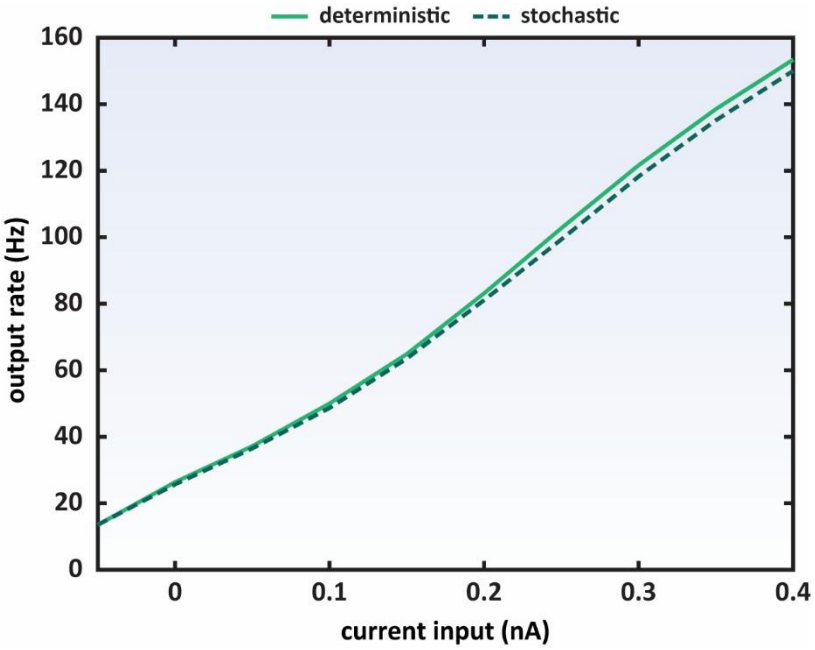

Figure 5.20 I-O relationships of CN models for current input. The CN neuronal model is injected with somatic current steps for 1.5 s.

5.4 Discussion

The aim of this chapter is to present the steps taken while constructing a stochastic CN neuron model. This study is divided into two parts: (a) conversion of all the voltage-gated ion CN channels to stochastic versions and exploration of their behaviour using a simple compartmental model, (b) implementation of a fully-stochastic CN neuron model and validation of its behaviour against a detailed deterministic CN neuron model (Steuber et al., 2011).

Several CN neuron models have been developed in order to study synaptic integration, neural coding and computation in the CN. Depending on the scientific question addressed, CN neuron models differ in their complexity and biological abstraction, but a feature they have in common is that they are all based on deterministic ion channel models (Steuber and Jaeger, 2013). Ion channel noise could play an important role in signal processing and neuronal coding. Moreover, implementing stochastic processes in voltage-gated channels of the CN neuron could lead to a more realistic model, ideal for the study of neuronal computations in the presence of ion channel noise (Faisal et al., 2008; Silver, 2010; White et al., 2000).

5.4.1 Determining the stochastic behaviour

To study the behaviour of the stochastic voltage-gated CN neuron channels, a single compartmental neuronal model is chosen for all initial simulations. A simple neuronal somatic

compartment without dendrites and axon, although unrealistic compared to real neurons or detailed single-cell neuron models, can still reveal the function of ion channels, by establishing a cause-and-effect relation of the variables in question, that is, the total or single channel conductance. This is beneficial when untangling the function of voltage-gated channels, since by nature they are coupled to membrane voltage perturbations and subsequently can be affected by the function of neighbouring ion channels. For example, in the simple model, the stochastic channel models whose behaviour differs significantly from the deterministic models are the NaF, NaP and the CaLVA channel, but in the detailed CN model, the response of the semi-stochastic CN models with NaF, CaHVA, or fKdr (and not CaLVA or NaP) channels produces a phenotype that is not similar to the deterministic CN neuron model. Hence, the behaviour of the same stochastic voltage-gated channel, in this case the NaP or CaLVA, could not always be matched to their deterministic counterparts, but this depends on the neuronal cell that is simulated. Possible factors contributing to this discrepancy could be the complex morphological features of the detailed compartmental model and the inference due the other channels, that are not present in the simple neuronal model. Nevertheless, as demonstrated, an (almost) fully-stochastic CN neuronal model where all the channels but the NaF and CaHVA channel are stochastic matches the behaviour of its deterministic counterpart. In addition, the existing variability in experimental data, as also shown in the current study, and the potential functionality it underlies (see Chapter 3), support the concept of a more realistic representation of ion channels that replicates this trial-to-trial variability.

The differences between deterministic and stochastic models that arise in some channels could also be due to the fact that the deterministic formalisms consider the behaviour of a channel population rather than taking into account the individual channel behaviour. Hence, either the deterministic formalism deviates from the real behaviour of a channel or a stochastic formalism ‘overestimates’ the behavioural impact of the probabilistic channel gating. Further, as the findings also suggest, the deterministic models might not be able to address fast kinetic processes or other phenomena such as the rectification effect described above, which could affect the single channel behaviour.

Thus, the method how stochasticity in channels is implemented is critical, and it needs to be able to represent the above phenomena or the sensitivity to the specific conductance or single channel conductance, and the transition time between states. The latter is extremely important for the decision on the simulation time step, and there is a trade-off between accuracy and computational cost. As is also highlighted in this study, the integration time step can have

a great impact on the simulation results, and its definition prior to conducting any research is critical. For instance, the discrepancy between the stochastic and deterministic behaviour for some ion channels and the hypothesis of the rectification effect could be only verified, if the simulations are repeated with stochastic algorithms and an appropriate time step. Yet, even in the absence of a rectification effect, fast transitions rates between the multiple states of the channel might still underlie the discrepancies between the two models, and for different simulation time steps, as the predicted number of events is associated with the span of the simulation time step.

Existing algorithms, such as the Gillespie algorithm, tackle some of these issues. In the Gillespie method, the time step is not fixed, but is considered as an additional continuous Markov process with a discrete state space, with the time of the next state transition being also a probabilistic choice. As a result, more events in total would register, since there is no "one or nothing event per time step" restriction that applies with algorithms that use a fixed time step, such as the backward Euler that is applied in this study. For slower channels, the probability that an event will take place within a fixed time step is usually small, and therefore, no great deviation will occur at macroscopic level. However, this can be detrimental for channels with faster kinetics where more events could take place, during a fixed time-step simulation.

Furthermore, the morphological neuronal features and the distribution of the channel type could affect the neuronal output. In the stochastic channel model, larger single channel conductances imply a smaller number of channels and greater single channel current fluctuations, namely, more noise. This phenomenon could be enhanced in narrow regions, such as thin dendrites, due to the greater input resistance, with impact on the neuronal output (Cannon and D'Alessandro, 2006; Diba et al., 2006; Faisal et al., 2005; Kole et al., 2006). In the stochastic CN neuronal model, there is also some variability in the spike pattern, which is depicted as interspike interval variability. The impact on the computational properties of CN neurons is studied in detail in Chapter 6.

6 Computational properties of the CN neuron

6.1 Introduction

As discussed (see Chapter 4), the neuronal synaptic noise, neuronal morphology and topological arrangement of the synaptic inputs on dendritic branches are amongst the mechanisms that can affect gain modulation operations. Synaptic noise can act as a modulatory input when delivered in mixed background input (for tonic driving input), be present in the driving synaptic input itself or operate in combination with other factors, such as dendritic saturation. However, noise in neurons can originate from various sources with further implications for its computational role. An important contributor to neuronal noise could be the ion channel noise, which arises from the intrinsic stochastic nature of ion channel gating (see Chapter 3) and its role can be influenced by the morphological properties of the structure that carries the channels.

Thus, important questions arise when considering the above phenomena.

(a) Does ion channel noise affect the input integration of a single neuron? If yes, in what ways?
(b) What is the role of input location in gain modulation operations? Could ion channel noise impact neuronal computations in an input location dependent way?

This chapter focuses on exploring various aspects of these questions. Initially, the impact of intrinsic noise on neuronal computations in the CN neuron is investigated. Then a

systematic study of possible effects of input location on gain modulation is carried out, in two different neuronal models (CN and LVb pyramidal neurons). Lastly, the results for the two different types of neurons are compared and discussed.

6.2 Channel noise and neuronal response

An investigation of the computational operations a neuron could undergo in the presence of intrinsic channel noise should be conducted through the prism of the channel kinetics, and the neuronal toolkit of voltage-gated channels (active properties), as well as the electrical membrane properties, such as capacitance and resistance, and the morphology of the neuron (passive properties).

Firstly, ion channel noise could impact the characteristics of the action potential output. The stochastic gating of ion channels could contribute to the variability of the neuronal firing that is observed experimentally. The mechanism is analogous to the effect of synaptic noise. Probabilistic ion channel gating leads to membrane voltage fluctuations, which subsequently affect the output fidelity of the neuron, by introducing variability in the timing and generation of action potentials (White et al., 2000). Secondly, the ion channel repertoire of the neurons is not distributed uniformly along the cell. Different ion channels can be found in the soma and the dendrites, and their number (and subsequently their total conductance) varies, too, between different neuronal compartments. On top of that, there is a third aspect, the dendritic morphology. Even if two dendrites share the same ion channel distribution, their morphological features, such as the thickness and distance of the integration compartment (axon initial segment, hillock or soma), will translate the impact of probabilistic gating differently to the neuronal output (Cannona et al., 2010; London and Häusser, 2005; Silver, 2010). Morphologically distinct neurons (or even subregions of the same neuron) that share the same density of stochastic ion channels exhibit a variability in the amplitude of membrane fluctuations, which affects the probability of a synaptic input to trigger an action potential. The intrinsic ion channel properties, namely, channel kinetics, and their open probability affect the extent of these membrane fluctuations too (Cannon et al., 2010).

Even a single type of stochastic ion channel, when inserted into a fully deterministic model, can impact greatly the amplitude of the membrane potential fluctuations. For example, the number of channels responsible for generation of the hyperpolarization-activated cation current (I_h) increases exponentially in the distal apical dendrites of the cortical layer V pyramidal neurons compared to their somatic regions. The single I_h channel properties (channel

kinetics and single channel conductance) are the same though, along all subcellular compartments. Still, the stochastic gating of the I_h channels contributes significantly to noisy fluctuations of the resting membrane potential and affects the reliability of temporal spiking pattern (Kole et al., 2006).

In addition, the contribution to membrane noise of the various types of channels is expected to vary. When, in the same deterministic neuronal model (cortical layer V pyramidal cell), a stochastic voltage-activated Na^+ channel is inserted, the impact on the resting membrane potential fluctuations is less than that of the I_h one. Although the density of the voltage-activated Na^+ channels is uniform across the somato-dendritic area, distal dendritic areas exhibit larger membrane voltage fluctuations induced by the random voltage-activated Na^+ channel gating. Moreover, when the I_h density is low and uniform across the somatic and distal dendritic compartments, the membrane noise attributed to the Na^+ channel gating is the same for both regions. This phenomenon might be attributed to colocalized high I_h channel density at these regions, which can lead to greater activation of the voltage-activated Na^+ channels due to the depolarizing I_h action (Kole et al., 2006). Thus, the output response of a neuron could be affected by the interplay of different stochastic channels and its morphological features (see also Chapter 3).

6.2.1 Deterministic CN vs Stochastic CN neuronal response

6.2.1.1 Excitatory synaptic input to one location

In order to explore the impact of channel noise on neuronal computations, a model of the CN neuron enriched with noisy ion channels (stochastic CN, see Chapter 5) is used and its behaviour is compared to a fully deterministic CN model, under a number of different experimental conditions.

In the first set of experiments, excitatory synaptic input is delivered to the stochastic and deterministic CN models, in different neuronal branches (somatic, proximal and distal) and the Input - Output relationships are identified. Both of the models show similar integration of their excitatory inputs, with distal inputs giving rise to lower firing rates, compared to the somatic and proximal ones, as it is also expected, due to the dendritic signal attenuation and low-pass filtering (London and Häusser, 2005; Papoutsi et al., 2014) (Figure 6.1). The neuronal response of the two models is also similar, indicating not a significant impact of ion channel noise on the mean firing output rate. However, such a model matching should be expected since

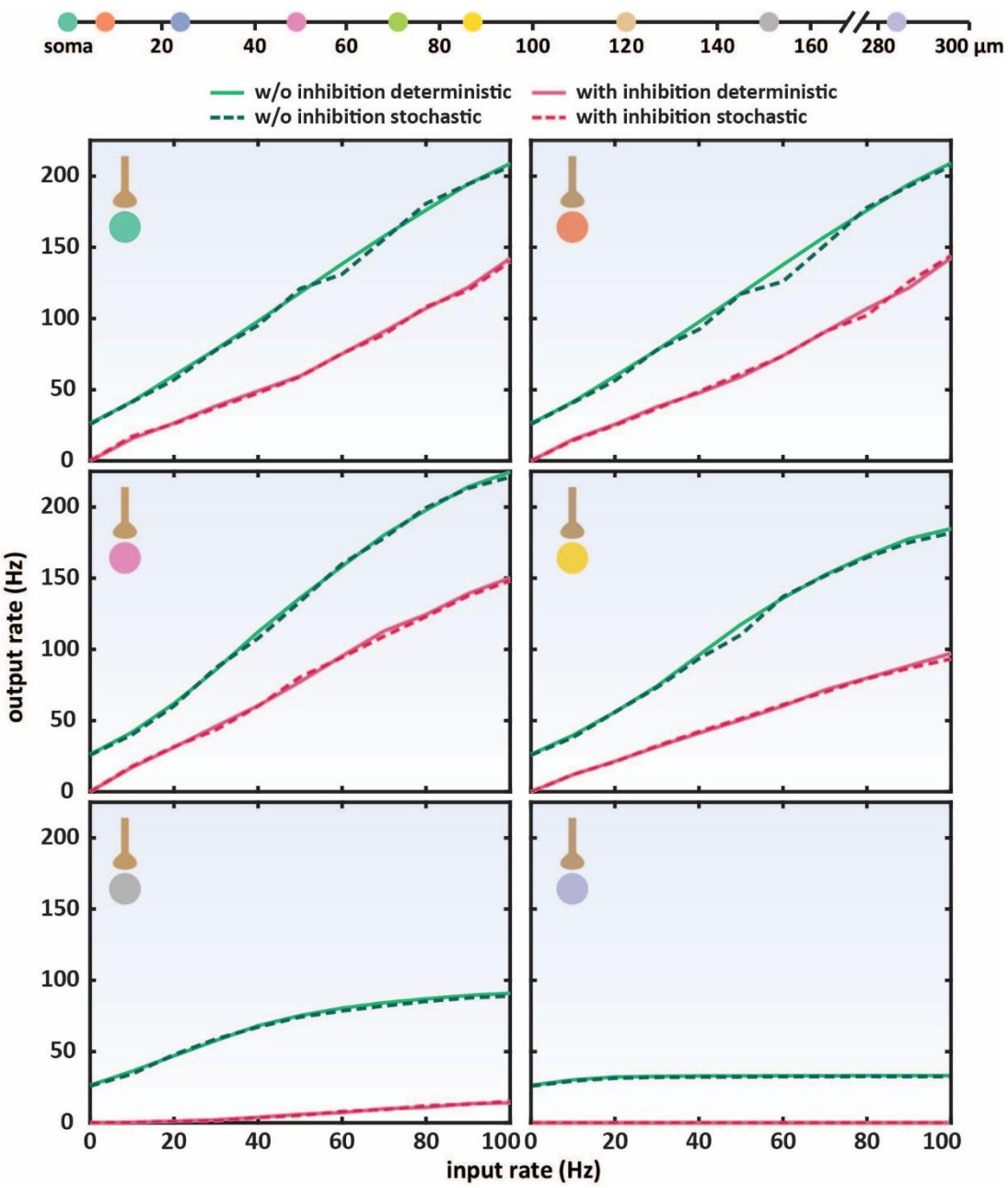

Figure 6.1 I-O relationships of CN models for synaptic inputs. The CN neuronal model is stimulated with 50 synchronous excitatory synapses confined in one dendritic compartment per time, in the presence of ion channel noise (dashed green lines) or not (solid green lines). When synaptic inhibition (450 synapses at 10 Hz) is applied (pink lines), it is distributed along the dendritic tree and soma. Top: Schematic distance map from soma of the distinct synaptic excitatory input locations.

the number of the ion channels used per compartment is probably large enough (>100) for the stochastic model to approach the deterministic behaviour (Figure 6.2). Nevertheless, a discrepancy could be observed in the most distal areas of the neuron, where the effect of the stochastic channel-induced noise could be enhanced by the higher input resistance of thinner dendritic branches, but potentially this would take place for smaller number of channels.

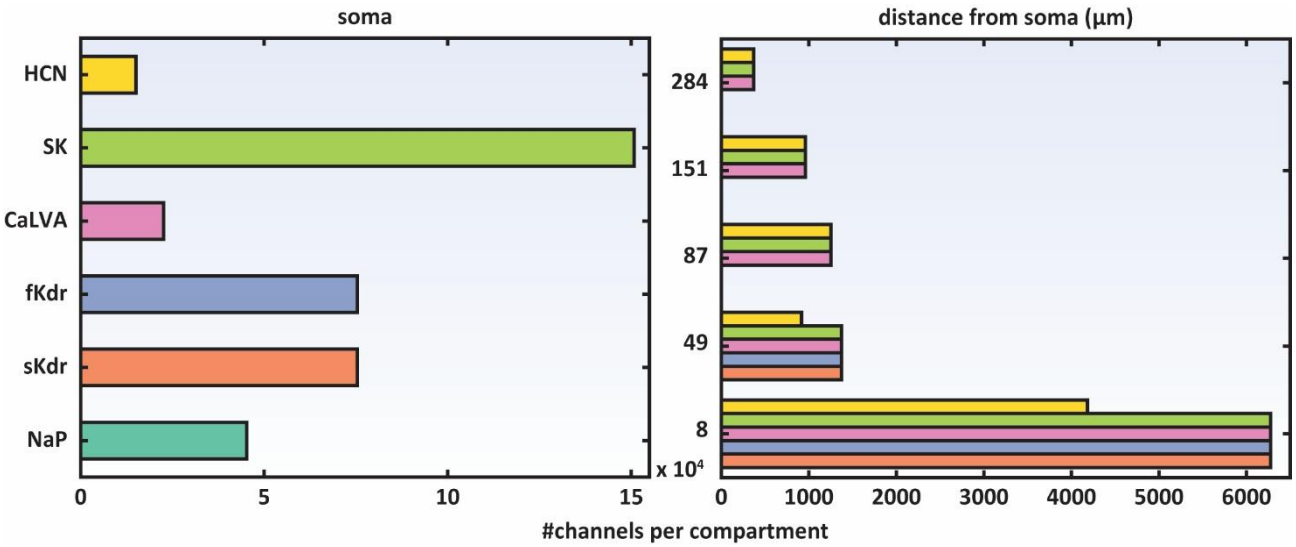

Figure 6.2 Number per channels type in the stochastic CN model. Left panel: Soma. Right panel: Dendritic compartments. The type of channels in the dendritic compartments (right panel) corresponds to the colour mapping in the soma bar chart (left panel).

6.2.1.2 Effect of single channel conductance

One of the core differences between the two CN formalisms, is the definition of the total channel specific conductance and consequently, the macroscopic channel current. In the deterministic model, the channel population is considered homogenous in terms of open channel probability, and its total specific conductance is expressed as the product of this total open channel probability and the maximum possible specific channel conductance. On the other hand, in the stochastic model it is assumed that each single channel is governed by its own independent gating probability, and channel conductance is the product of the single channel conductance and the number of open channels per neuronal segment. For a given area, the total number of channels is therefore given by the fraction of the total channel conductance divided by the single channel specific conductance (see Chapter 3). This allows for the experimental manipulation of the total number of a specific channel in a neuronal compartment, by simple changing the value of its single channel conductance (and keeping the total conductance constant).

To investigate if there are any conditions where the ion channel noise could distinguish the behaviour of the stochastic CN neuron, the number of ion channels is decreased by the same factor in all the neuronal subregions, but the total conductance of each channel type is kept the same. In that way, the mean macroscopic current generated by each cannel would be the same, but fewer channels are expected to give rise to more fluctuations in the membrane voltage (Diba et al., 2006; Kole et al., 2006; White et al., 2000). Hence, the integration of the synaptic

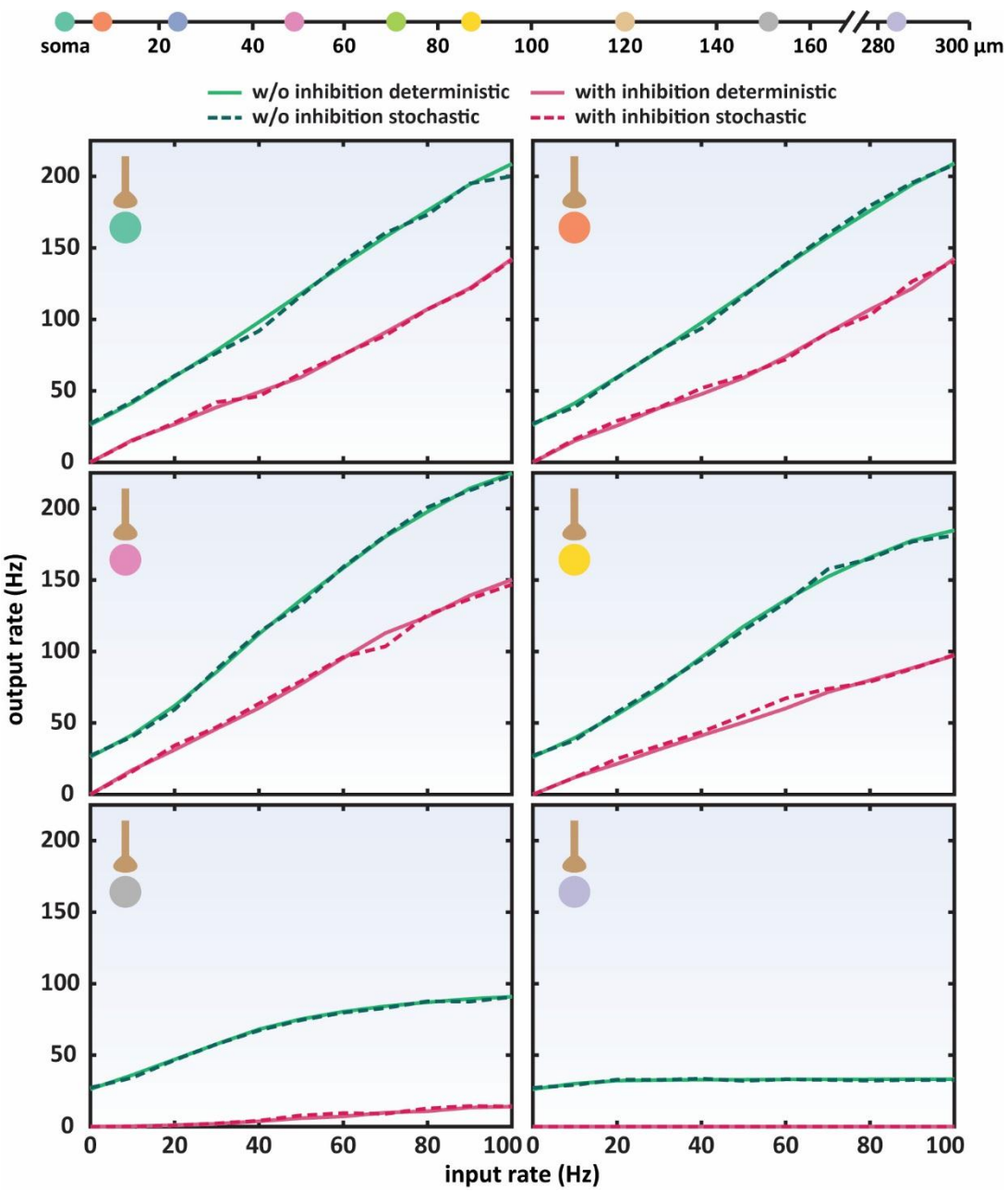

Figure 6.3 I-O relationships of CN models for synaptic inputs, and 100 fewer ion channels per compartment. Same as Figure 6.1, but for 100 times fewer channels per compartment, in the stochastic CN neuron.

inputs and the neuronal output might be affected, since the channel gating induced voltage fluctuations underlie the variability to the spiking threshold, propagation and timing (Cannon et al., 2010; Diba et al., 2006; Faisal et al., 2008; Kole et al., 2006; White et al., 2000). Moreover, thinner dendrites are expected to have greater voltage fluctuations, because they have a smaller diameter, and thus a greater input resistance. In contrast, larger compartments, like the soma, have a large capacitance, which could act as a filter for membrane fluctuations, and are expected to contain a larger number of channels, resulting in averaging out of the

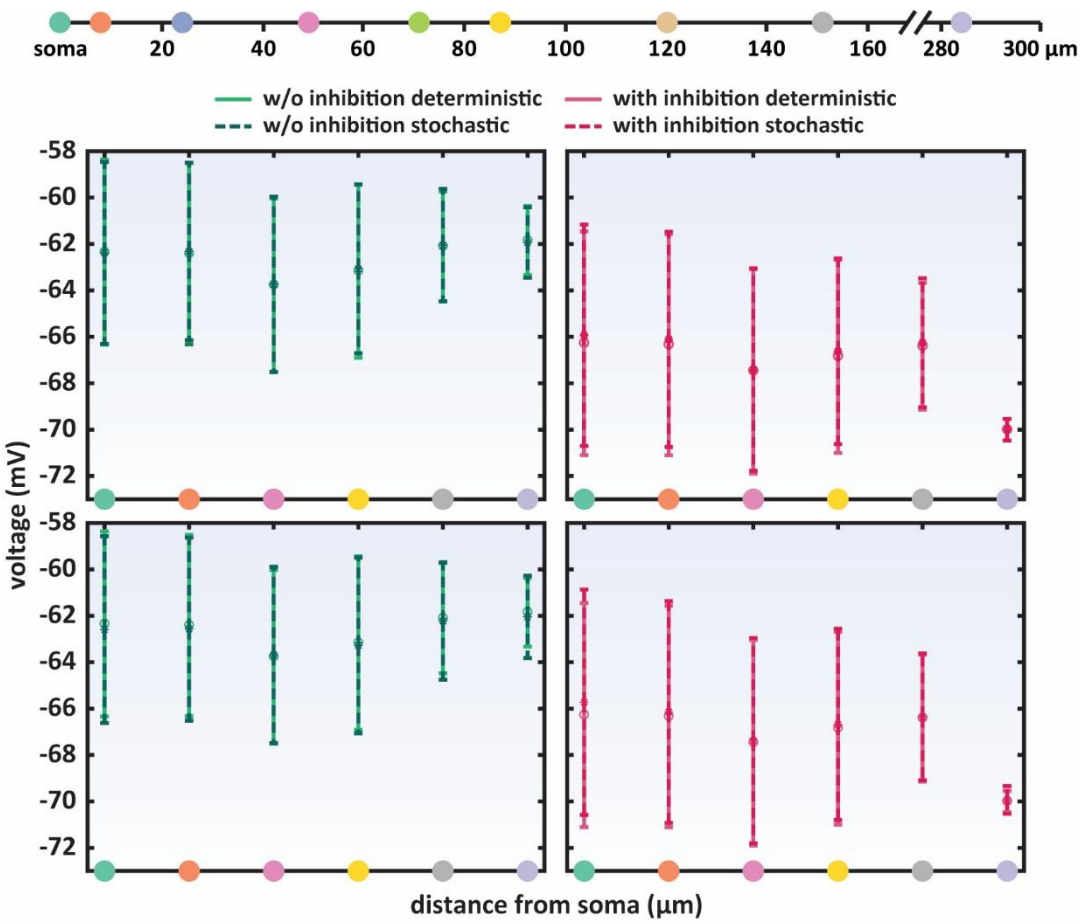

Figure 6.4 Impact of ion channel noise in the non-spiking membrane voltage. The CN neuronal model is stimulated with 50 synchronous excitatory synapses at 30 Hz, confined in one dendritic compartment per time, in the presence of ion channel noise (dashed green lines) or not (solid green lines). When synaptic inhibition (450 synapses at 10 Hz) is applied (pink lines), it is distributed along the dendritic tree and soma. The spikes were removed by applying median filter with a window of 200 points. Top: Schematic distance map from soma of the distinct synaptic excitatory input locations. Upper panels: Stochastic vs deterministic CN model, without (left panel) or with (right panel) synaptic inhibition. Lower panels: Same, but for 100 times fewer channels per compartment.

random voltage fluctuations (Cannon et al., 2010; Faisal et al., 2005; London and Häusser, 2005).

Still the stochastic CN neuron, even with 100 times fewer channels all over the neuronal compartments, exhibits similar firing rates as the deterministic one, in response to increasing firing rates of the excitatory synaptic input and for all the different synaptic locations (Figure 6.3). To explore in more detail the impact of the ion channel noise, the mean non-spiking membrane voltage and standard deviation are estimated in both models, during the stimulation with excitatory and inhibitory synaptic input. The total mean membrane voltage is similar to the deterministic CN model (Figure 6.4). A smaller number of channels per compartment is predicted to trigger more and steeper membrane fluctuations (Faisal et al., 2008; White et al., 2000). However, when the number of channels is 100 times fewer the standard deviation is still

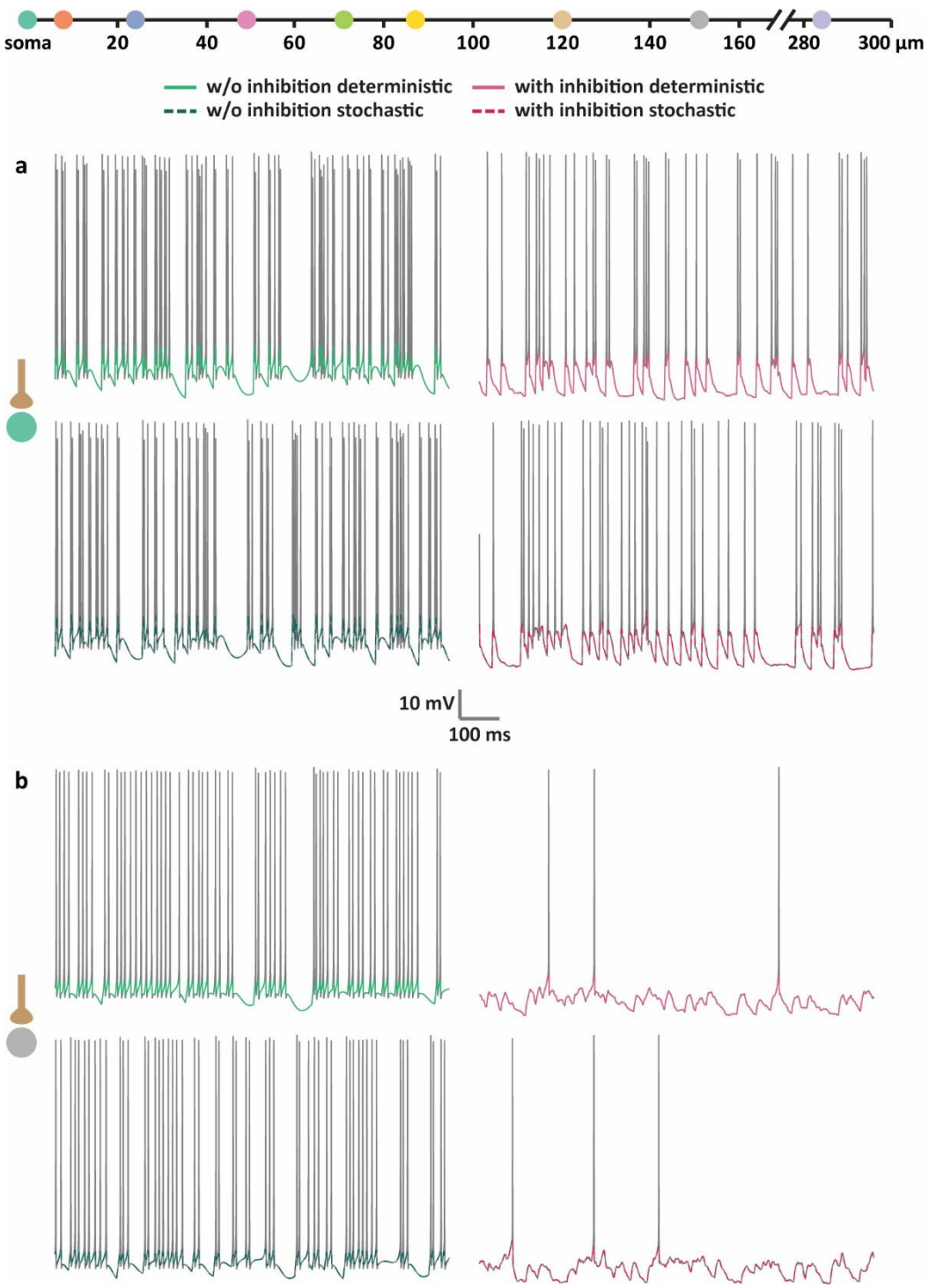

Figure 6.5 Impact of ion channel noise in the fidelity of spiking. Samples of voltage traces of the response of the deterministic and stochastic CN models at (a) soma and (b) 151 μm further form soma. As in Figure 6.4, the CN neuronal model is stimulated with 50 synchronous excitatory synapses at 30 Hz, confined in one dendritic compartment per time. The coloured lines show the spikes removed by applying median filter with a window of 200 points, in the presence of ion channel noise (dashed lines) or not (solid lines). When synaptic inhibition (450 synapses at 10 Hz) is applied (pink lines) it is distributed along the dendritic tree and soma. Top: Schematic distance map from soma of the distinct synaptic excitatory input

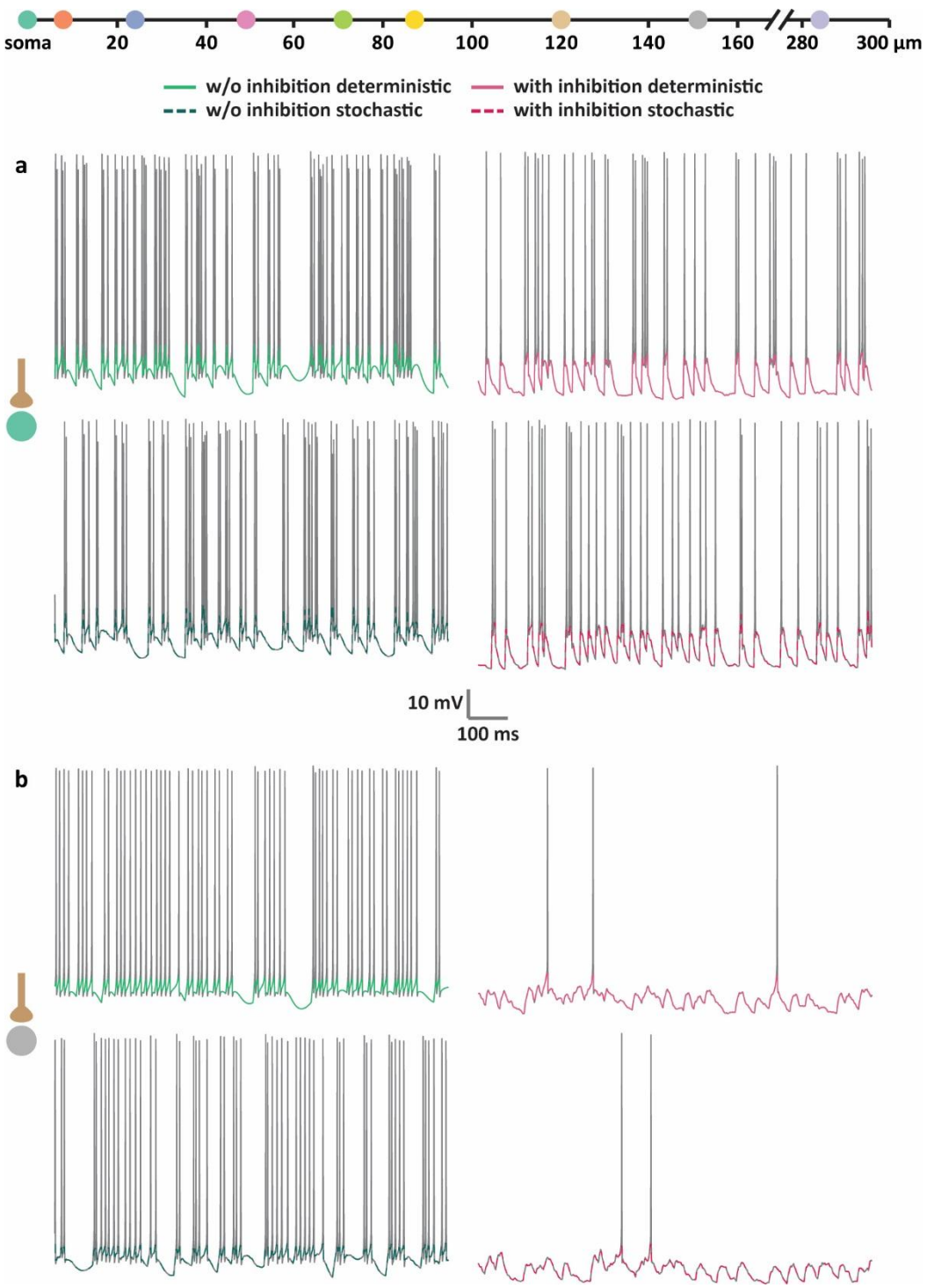

Figure 6.6 Impact of ion channel noise in the fidelity of spiking for 100 fewer channels per compartment. Same as Figure 6.5, but for 100 times fewer channels per compartment, in the stochastic CN neuron.

at similar levels with the corresponding deterministic (Figure 6.3 and 6.4) Moreover, a stochastic formulation of the ion channels in the CN model introduces some variability in the timing of individual output spikes (Figure 6.5 and 6.6) as indicated also by previous studies (Cannon et al., 2010; Diba et al., 2006; Faisal et al., 2008; Kole et al., 2006; White et al., 2000).

Thus, the level of noise generated by the random ion channel gating in the stochastic CN neuron is not sufficient to cause a change in the firing rate and the behaviour of the model might be dominated by the noisy synaptic input (Destexhe et al., 2014). Yet, the stochastic ion channel gating affects the spike timing. Furthermore, the level of the neuronal response across the different dendritic branches is also in accordance with the expected outcome, namely, the further the location of the excitatory input, the weaker the neuronal activation (London and Häusser, 2005; Papoutsi et al., 2014).

6.2.1.3 Excitatory synaptic input to different regions

So far, excitatory synaptic input is applied to one compartment per time. Yet, neurons *in vivo* receive synaptic input all over their somato-dendritic area, and different neuronal regions might be functionally compartmentalized by receiving synaptic inputs from distinct brain areas (for example, pyramidal neurons) (Spruston, 2008). Moreover, different modes of activation (clustered inputs onto one specific dendrite or dispersed onto different dendritic branches) might support diverse functions too (Stuart and Spruston, 2015).

Since the neuronal response to clustered activation is similar between the two models, it is investigated whether a distributed synaptic activation of distinct dendrites could distinguish the behaviour of the deterministic and stochastic CN neurons. For that reason, the neuronal area is divided into dendritic subregions, based on their distance from the soma (proximal, distal and dendritic tips). Each subregion is excited by synaptic inputs to distinct dendritic compartments, with one synapse per compartment. The total synaptic input is equal to the amount used for the clustered stimulation of single dendritic compartments.

Still, with this experimental configuration, the neuronal response of the two models is very similar, with weaker drive of the soma for the subregion away from it, and with no substantial effect of the channel noise (Figure 6.7). The signal attenuation is related to the distance of the input from the integration point, as with the clustered synapses (London and Häusser, 2005; Papoutsi et al., 2014). Since the same number of synapses are distributed along the dendritic compartments, and not confined in one dendritic compartment as in the previous experiments, the dampening of their signal strength from the dendritic branching (Vetter et al., 2001), could be more profound, since it applies to the signal generated by every individual synapse, which due to the experimental set-up would be weaker compared to the clustered signal, and propagates across pathways to the soma with various number of branchpoints from

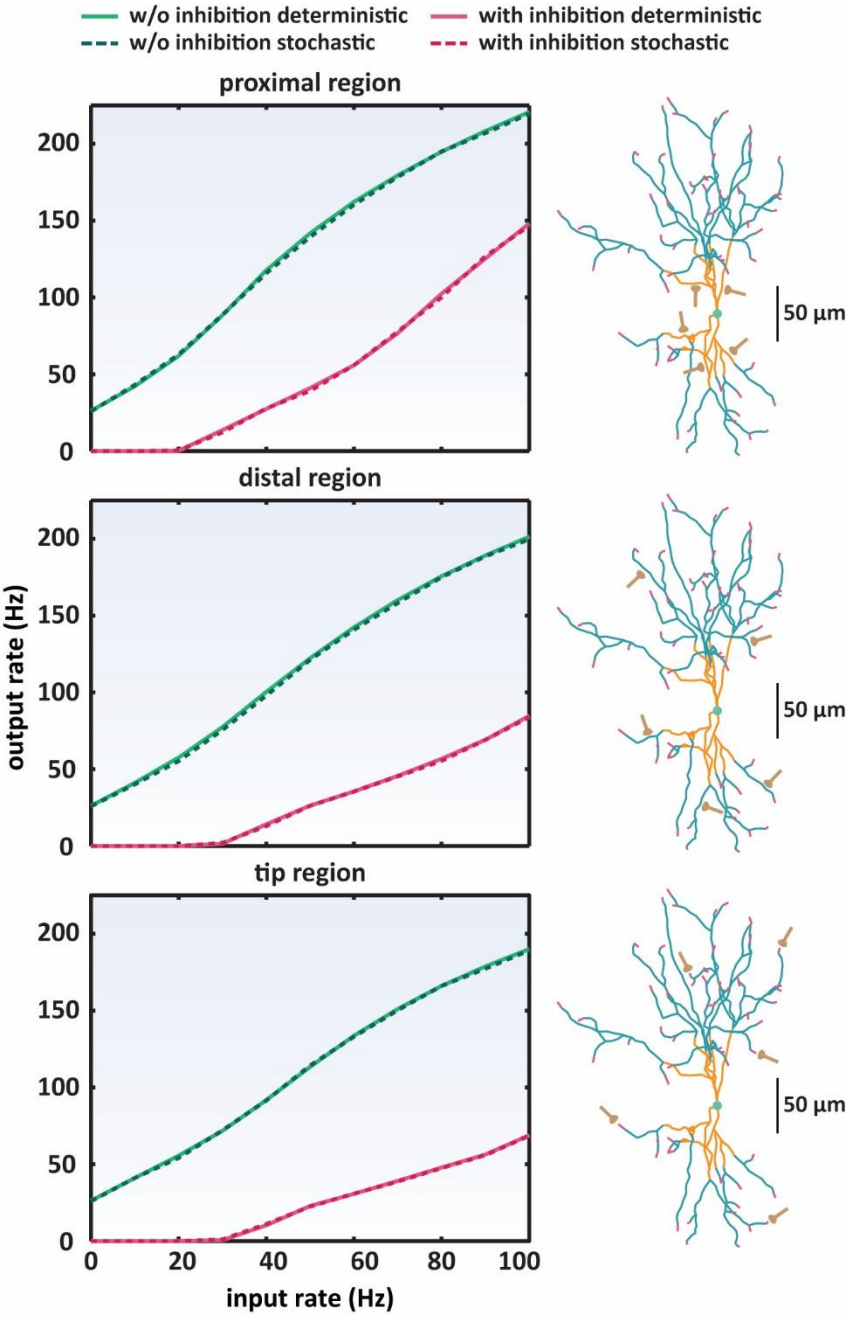

Figure 6.7 I-O relationships of CN model for distributed synaptic inputs. The CN neuronal model is stimulated with 50 synchronous excitatory synapses distributed in one neuronal subregion per time, in the presence of ion channel noise (dashed green lines) or not (solid green lines). When synaptic inhibition (450 synapses at 10 Hz) is applied (pink lines), it is distributed along the dendritic tree and soma. Right: The detailed reconstructed morphology of the CN neuron is shown, with distinct colours for the different neuronal subregions (orange: proximal, cean: distal and pink: tip subregions).

the cluster synapses. Therefore, the membrane fluctuations introduced by the channel noise are filtered out further, and do not have a great impact on the mean output firing level of the neuronal models.

6.2.1.4 Current input to one location

The findings thus far suggest that the stochastic CN neuron does not significantly deviate in behaviour from the deterministic CN neuron, under synaptic stimulation. One possible explanation is that the synaptic noise, introduced by the variability of the synaptic input, masks the ion channel noise (Destexhe et al., 2003; Faisal et al., 2008). To test this assumption, the input driving both models is changed to a non-noisy current. In this way, any noisy synaptic component is removed and the only source of noise for the generation of the membrane voltage fluctuations is the random ion channel gating.

In a comparable way to the synaptic protocol, somatic and dendritic compartments are stimulated one per time with a series of current step injections and the neuronal response of the two neuronal models is investigated. Both models respond similarly, with the spike response dependent on the distance, and with no considerable impact of the ion channel noise (Figure 6.8). Therefore, the membrane fluctuations due to ion channel noise are not adequate to impact the firing rate, either surpass or add to the already established impact of the neuronal noise related to the synaptic input, as it is also suggested by previous studies (Destexhe et al., 2003; Faisal et al., 2008).

6.3 Input-location and neuronal computations

Neurons come in different shapes and sizes, and it is likely that their morphological features could be correlated to their output firing (London and Häusser, 2005; Papoutsi et al., 2014; Psarrou et al., 2014; Silver, 2010; Spruston, 2008). On the other hand, neuronal computations could be as simple as a mere summation of the inputs, or more complicated where the input integration is nonlinear and it is dependent on combined spatial and/or temporal factors (Silver, 2010).

Gain modulation is an example of input integration, where the combination of signals from various sources (local neural circuit or other brain areas) can scale the neuronal response to an input. When neurons utilize this mechanism, their behaviour acquires a dynamic character that is correlated to the degree of gain change. Weaker inputs can be detected more easily, because a high gain change could transform them into a robust output. Stronger inputs could be mapped onto firing rates of a physiologically plausible range. Thus, while the neuronal selectivity remains unaffected, individual neurons are provided with a dynamic tool to integrate a larger range of synaptic inputs. In addition, since different input sources originate from different environmental stimuli, this adaptive scaling of neuronal input-output relationships

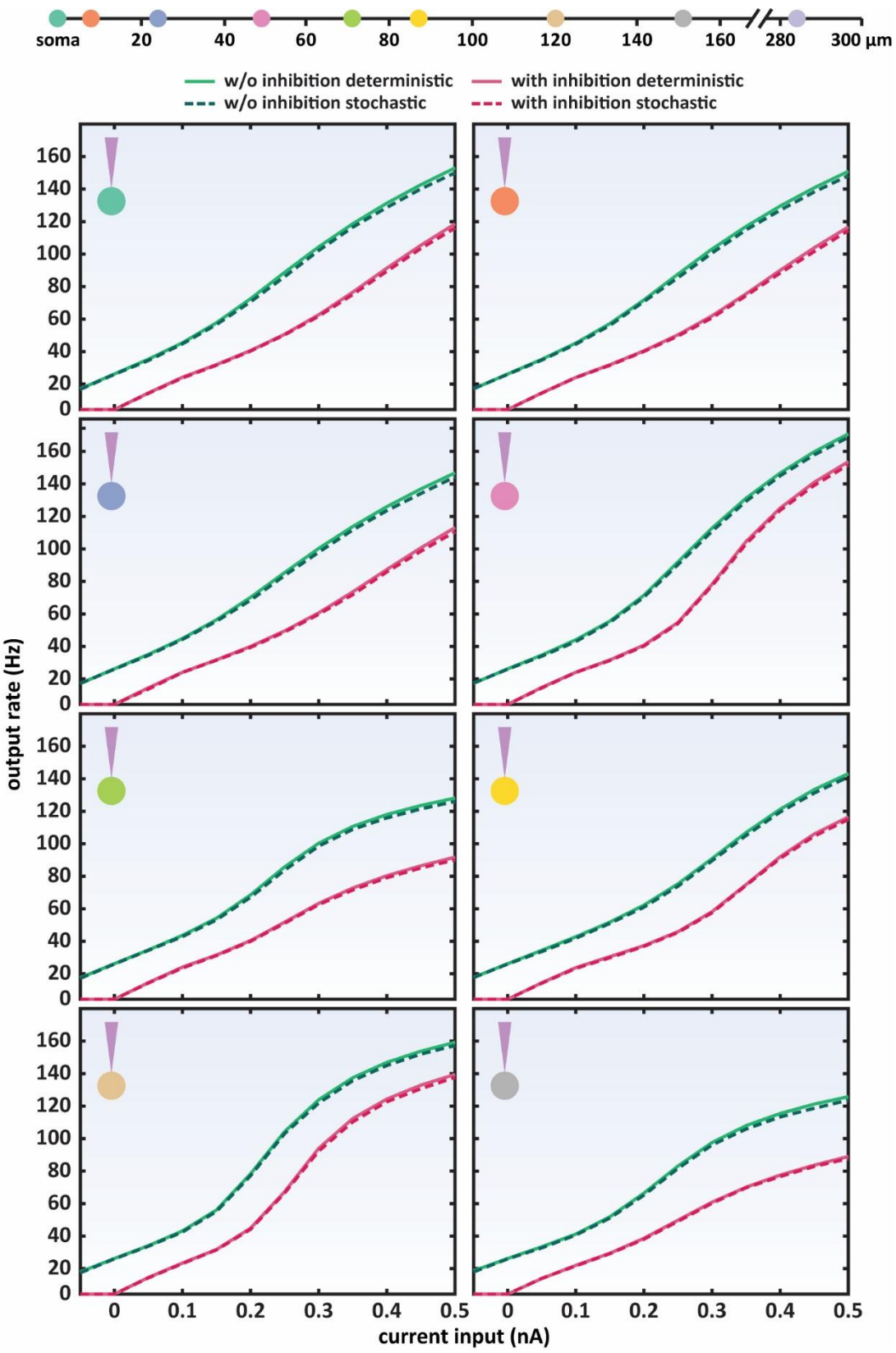

Figure 6.8 I-O relationships of CN models for non-synaptic inputs. The CN neuronal model is injected with current steps confined in one dendritic compartment per time, in the presence of ion channel noise (dashed green lines) or not (solid green lines). Tonic inhibitory conductance (9 nS) is applied (pink lines), at the soma. Top: Schematic distance map from soma of the distinct synaptic excitatory input locations.

allows for multiple encoding of input parameters in a single neuronal output pattern (Salinas and Sejnowski, 2001; Silver, 2010).

Several mechanisms have been suggested to underlie gain modulation, including noise (originating from the background synaptic activity or the input train variability), and mechanisms related to morphological or other cellular properties. Neurons can perform multiplicative gain modulation in the presence of a sufficient amount of noise, whereas additive operations occur in its absence. In addition, the neuronal morphology and topological input configuration contribute to gain operations (see Chapter 4). The previous analysis in this study does not reveal any significant effect of the channel noise in the behaviour of the CN neuronal model. However, the presence of a second source of variability, such an inhibitory synaptic input, might affect the response of a stochastic CN neuronal model.

6.3.1 Channel noise and neuronal computations

In order to characterize the effect of ion channel noise on gain modulation, a series of experiments is conducted, where the deterministic CN and stochastic CN are driven by excitatory synaptic input or current injections, on one dendritic location or one neuronal subregion, and their response is modulated either by inhibitory synaptic inputs distributed along the somato-dendritic axis, or tonic somatic inhibition.

So far, the neuronal response of both models to a driving excitatory input has been very similar. In addition, the impact of ion channel noise appears to be negligible, or to be totally masked by the fluctuations introduced by the excitatory synaptic input. However, an additional inhibitory input could still reveal variances in the integration properties of the two models. For instance, when the inhibitory synaptic input is delivered simultaneously throughout the neuronal cell, it adds a shunting factor to the signal attenuation as the excitatory input propagates from its synaptic location to the soma. Furthermore, since the inhibitory input is inherently variable and delivered all over the cell, it could be seen as source of background voltage noise, which could disguise the ion channel noise, depending on the relative magnitude of the voltage fluctuations induced by the inhibitory synaptic noise or the channel noise (see Chapter 4).

Nevertheless, the deterministic and the stochastic CN model display very similar response amplitudes, no matter the applied stimulation protocol (Figure 6.1 and 6.8), synaptic site (Figure 6.1 and 6.7) or number of channels (Figure 6.1, 6.3 and 6.4). Thus, the ion channel

noise appears not to introduce dissimilar integration operations in the CN stochastic neuron model. However, the mapping of the driving input on the output firing rate of both models, in the presence of the modulatory input, is different for proximal dendritic and somatic locations and the distal ones, implying diverse mathematical operations (Figure 6.1, 6.7 and 6.8). This phenomenon is investigated further and discussed in detail in the following sections.

6.3.2 Input-location dependent gain modulation

The input summation of the CN models seems to be independent of the ion channel noise, but not of the input delivery site, in the presence of a second input source (Figure 6.1, 6.7 and 6.8). A close observation of the I-O relationships of both CN models reveals that different mathematical operations take place for input to the somatic and perisomatic and distal dendritic areas. The dependence of the neuronal arithmetic operations on the input topology is explored systematically, both for input onto a single dendritic compartment, and input distributed across a neuronal subregion, when the neuron is driven by excitatory synaptic or current input and modulated by distributed synaptic inhibition or tonic somatic inhibition. Additionally, the behaviour of two cell models is compared, (deterministic) CN and LVb pyramidal neuron, under different input conditions.

6.3.2.1 Cerebellar nuclei neuron

6.3.2.1.1 Synaptic input to one location

When the CN neuron is driven with only excitatory input the output firing rate is correlated with the input distance from the soma. The distal input results in lower firing rates compared to the proximal to the soma and somatic one. The shape of the I-O relationship depicts this process (Figure 6.9). The neuronal response tends to saturate at lower input firing rates, when the input site is distal, due to greater reductions of the local driving force. Accordingly, the I-O curve acquires a characteristic sigmoid shape. On the other hand, the I-O shape for inputs on thicker compartments (for example, soma or proximal dendrites) is more linear and saturates in much higher firing input rates (Silver, 2010).

As soon as the modulatory inhibitory input is applied, the shape of the I-O curve remains the same for the various input sites, however, its relative position to the x- and y- axes changes (Figure 6.9). For somatic or perisomatic inputs, the I-O curve is predominately shifted along the x-axis, while for distal inputs it tilts. Thus, different neuronal computations take place in the presence of synaptic inhibition; additive shifts for inputs for somatic and proximal sites

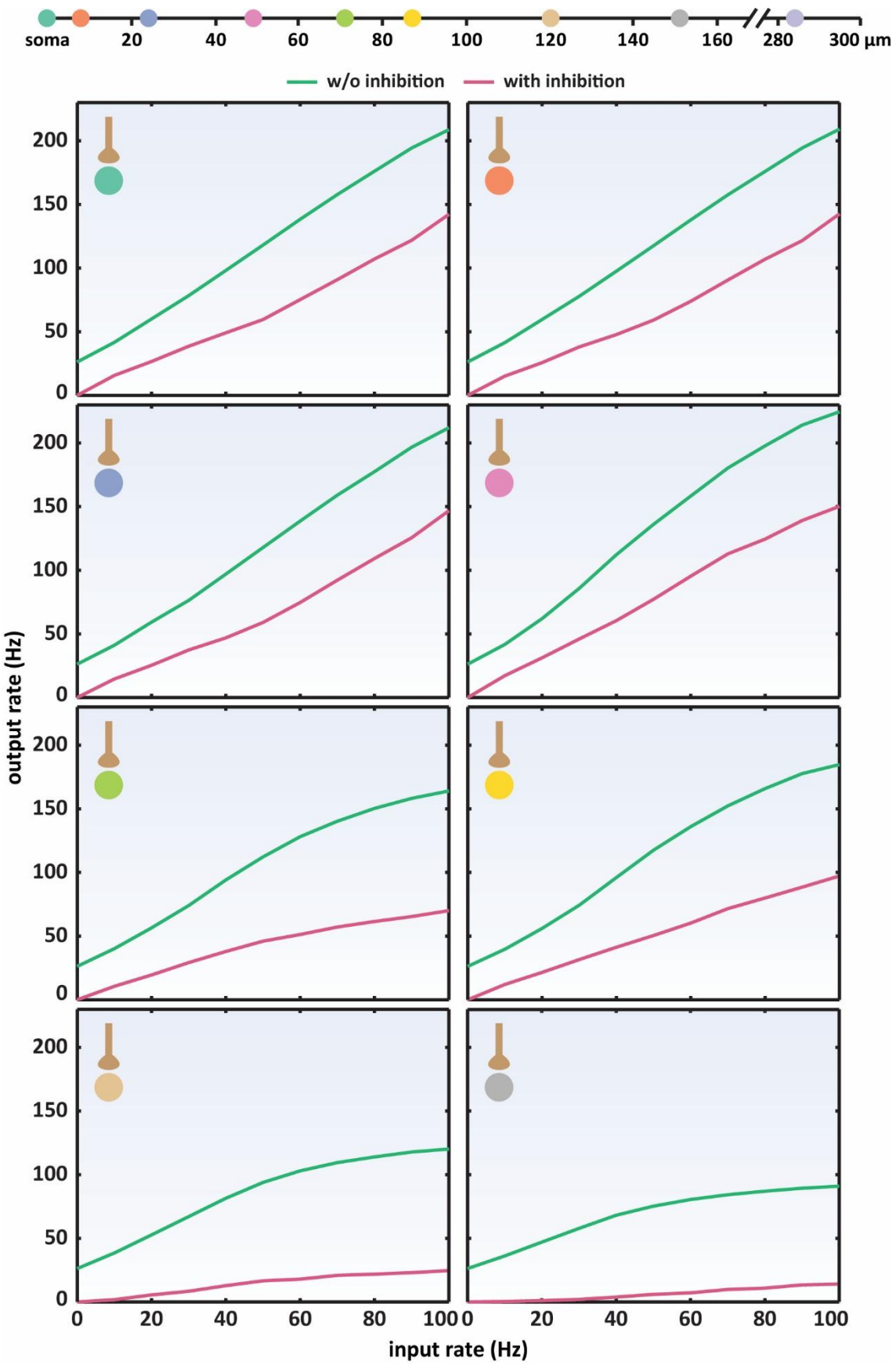

Figure 6.9 I-O relationships of CN model for synaptic inputs. The CN neuronal model is stimulated with 50 synchronous excitatory synapses confined in one dendritic compartment per time (green lines).

When synaptic inhibition (450 synapses at 10 Hz) is applied (pink lines), it is distributed along the dendritic tree and soma. Top: Schematic distance map from soma of the distinct synaptic excitatory input locations.

that transform to divisive slope changes (namely, gain change) for distal and tip locations. The change in the gain is also quantified for a series of locations, covering a distance range from the soma to very distal locations, and it is revealed that the extent of divisive operations is systematically correlated to that distance (Figure 6.10).

Moreover, in the current experiment, the inhibitory input is not colocalized with excitation only in one dendritic area (Holt and Koch, 1997; Jadi et al., 2012; Mehaffey, 2005; Pouille et al., 2013) or completely segregated (Jadi et al., 2012; Mehaffey, 2005; Pouille et al., 2013; Prescott and De Koninck, 2003), but rather distributed randomly across the somato-dendritic area. Thus, its effect is both upstream and downstream from the driving input location.

6.3.2.1.2 Synaptic input to different dendritic regions

The dendritic area of some neurons can be divided into subregions of functionally clustered inputs (Silver, 2010). In addition, different combinations of the synaptic delivery site of excitatory and inhibitory inputs affect their summation (Holt and Koch, 1997; Jadi et al., 2012; Mehaffey, 2005; Pouille et al., 2013; Prescott and De Koninck, 2003). The previous analysis shows that in CN neurons an inhibitory input distributed across the dendritic tree and the soma performs distinct modulatory operations to excitatory inputs to single compartments depending on their relative location to the soma. Hence, it is further investigated if similar

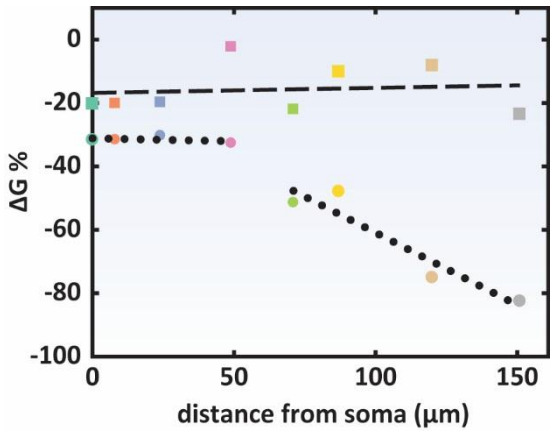

Figure 6.10 Changes in gain (ΔG%) for different neuronal locations in the CN model. As per Figure 6.9, the CN neuronal model is stimulated in different locations along the somato-dendritic area, either with synaptic driving and modulatory inputs (circles), or, as per Figure 6.14, injected with current and somatic tonic inhibitory conductance (squares). ΔG% is calculated after fitting the simulations' data (Figure 6.9 and 6.14) to sextic polynomial functions (Rothman et al., 2009). The dotted and dashed lines are linear trend fits, to the data shown in circles and squares, respectively. Mint shapes: soma. Other shapes: dendritic compartments

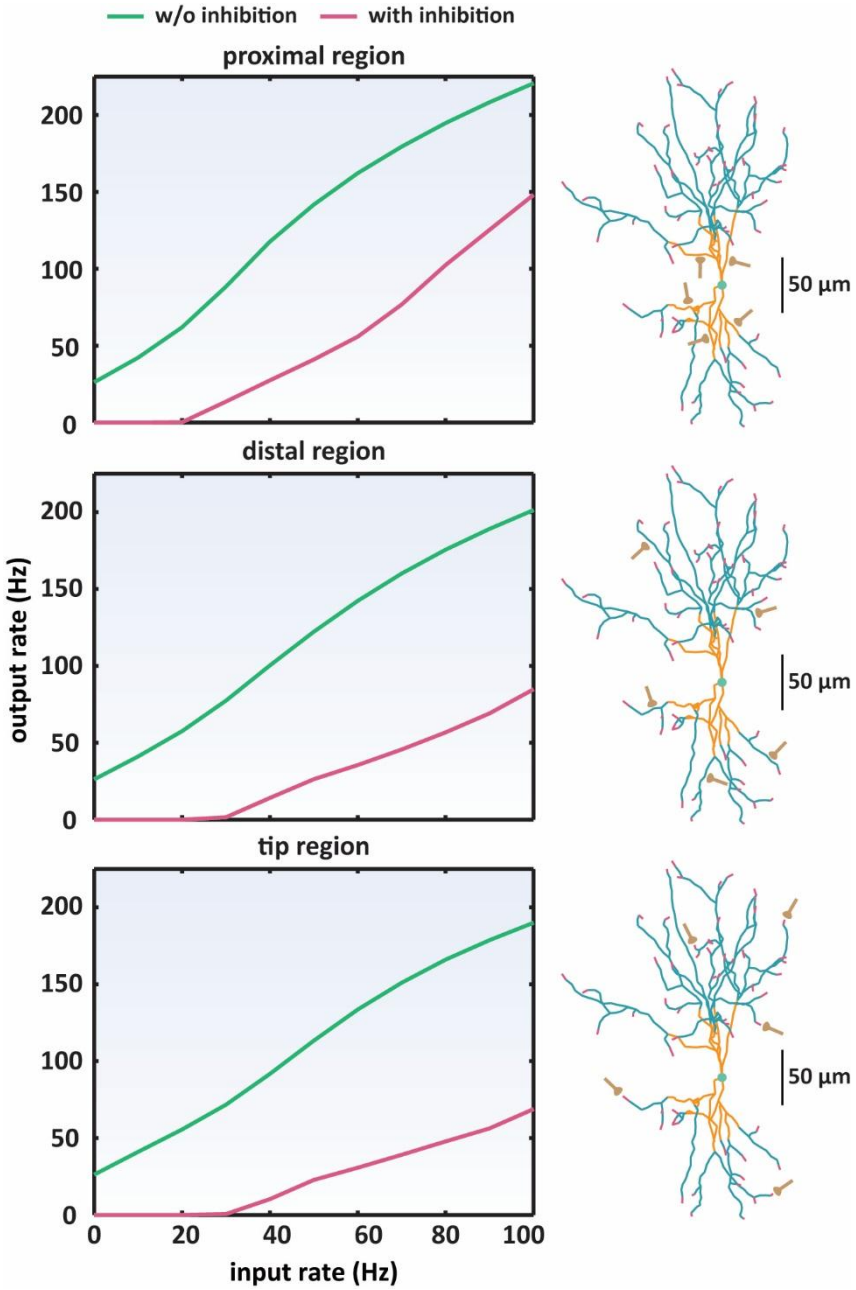

Figure 6.11 I-O relationships of CN model for distributed synaptic inputs. The CN neuronal model is stimulated with 50 synchronous excitatory synapses distributed in one neuronal subregion per time (green lines). When synaptic inhibition (450 synapses at 10 Hz) is applied (pink lines), it is distributed along the dendritic tree and soma. Right: The detailed reconstructed morphology of the CN neuron is shown, with distinct colours for the different neuronal subregions (orange: proximal, cean: distal and pink: tip subregions).

arithmetic operations occur when driving the neuron with distributed synaptic input applied to separated dendritic regions, which are distinguished based on their proximity to the soma (proximal, distal, dendritic tips).

The neuronal response follows the same pattern as before, where the excitatory synaptic inputs to the proximal to soma region undergo additive operations, and divisive operations are

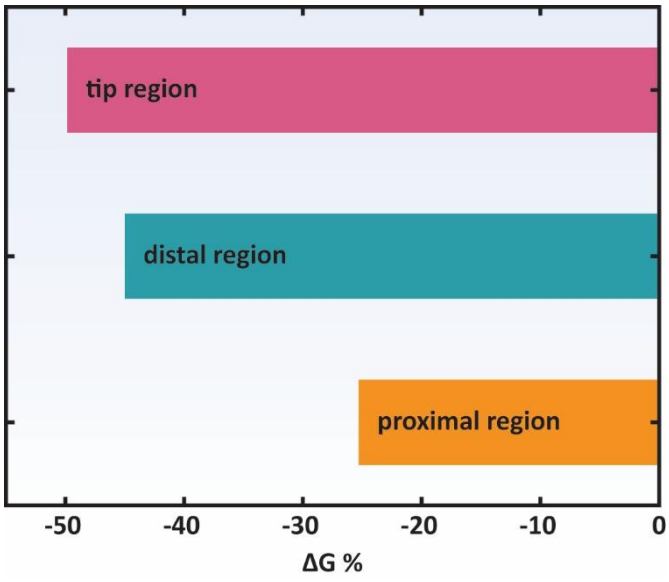

Figure 6.12 Changes in gain (ΔG%) for different neuronal subregions in the CN model. As per Figure 6.11**, t**he CN neuronal model is stimulated in different subregions with synaptic driving and modulatory inputs. ΔG% is calculated after fitting the simulations' data (Figure 6.11) to sextic polynomial functions (Rothman et al., 2009). The distinct colours in the bars correspond to the ΔG% in the different neuronal subregions (Figure 6.11).

performed in the distal and tips regions (Figure 6.11). As for inputs to single compartments, the change in gain is correlated with the distance of inputs from the soma (Figure 6.12).

Due to the experimental design, the excitatory inputs are colocalized with a fraction of the inhibitory inputs. Prior research has focused on the neuronal response under similar conditions. The modulatory effect of inhibition depends on to the relative location of inhibitory and synaptic inputs (Holt and Koch, 1997; Jadi et al., 2012; Mehaffey, 2005; Pouille et al., 2013) and on other conditions, such as the presence of background noise (Prescott and De Koninck, 2003). In particular, somatic shunting inhibition acts in a subtractive way (Holt and Koch, 1997), but in combination with dendritic saturation and background noise, can act divisively on distal dendritic inputs (Prescott and De Koninck, 2003), which is in accordance with the observed CN behaviour.

6.3.2.1.3 Dendritic saturation introduces nonlinearities

The I-O function maps the neuronal response (output) onto the driving (input). However, prior studies have shown that dissecting further this relationship, to intermediate mappings that examine the relationship of input and output, with for example the excitatory conductance, can reveal where nonlinearities are introduced. For example, a nonlinear relationship between the presynaptic input firing rate and the time-averaged excitatory synaptic

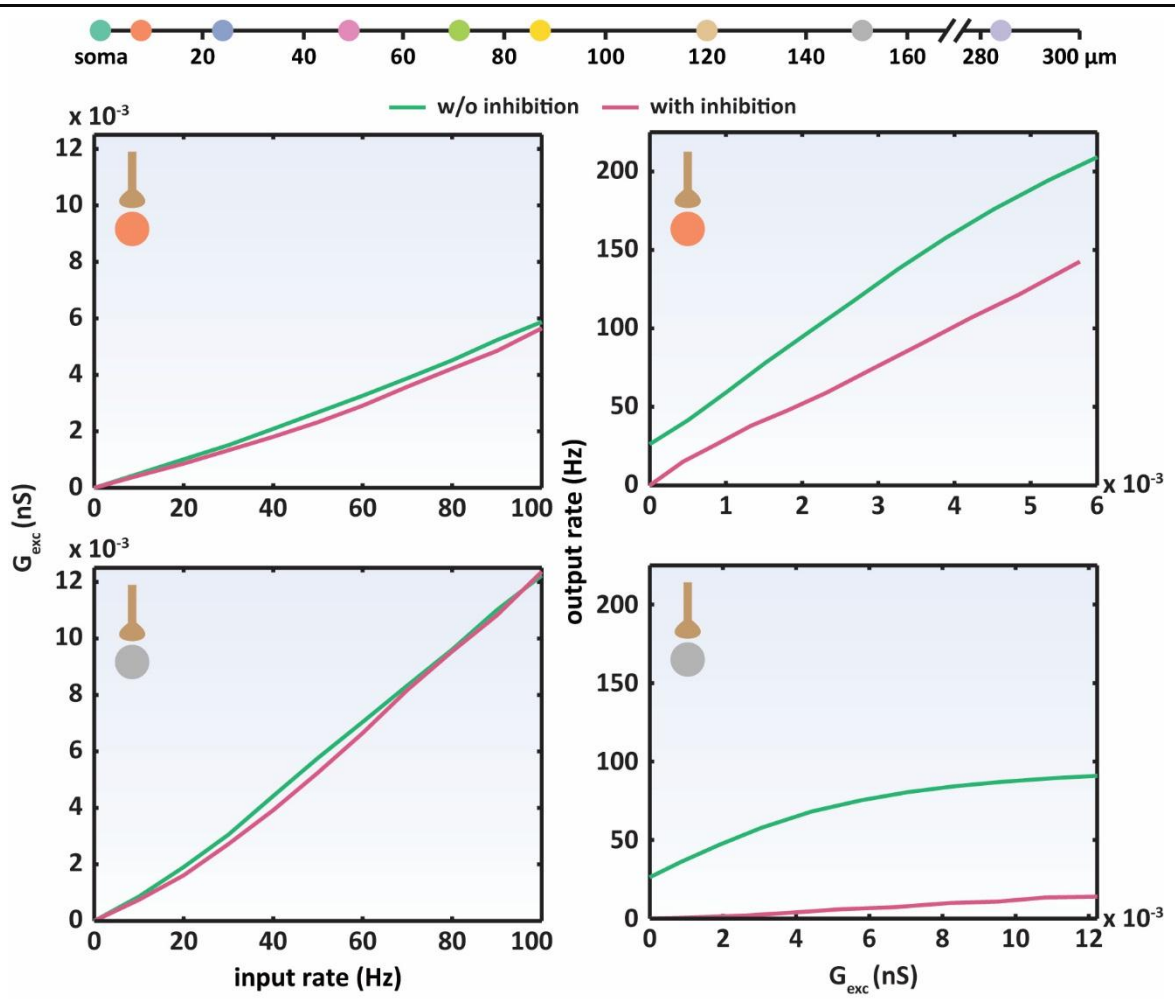

Figure 6.13 Breaking down the I-O relationship in the CN model. The I-O function of the CN model is analysed further for different dendritic locations (upper panels: 24 µm and lower panels: 151 µm) by investigating the relationships between neuronal output firing rate, synaptic excitatory conductance and synaptic excitatory input rate. The CN neuronal model is stimulated in different subregions with synaptic driving and modulatory inputs, as in Figure 6.9. Left panels: Mapping of excitatory input rate to excitatory input conductance. Right panels: Mapping of excitatory input conductance to output firing rate. Top: Schematic distance map from soma of the distinct synaptic excitatory input locations.

driving conductance underlies STD-dependent gain modulation (Rothman et al., 2009), while the nonlinear mapping between the excitatory dendritic conductance and the output firing rate caused by dendritic saturation enhances the divisive effect of shunting on the output firing rate (Prescott and De Koninck, 2003). Since the divisive modulation by inhibition in the CN model is more evident in the distal compartments, a hypothesis could be that the nonlinearity caused by dendritic saturation underlies the observed change in gain when the inhibitory modulatory input is applied.

As a first step to test this hypothesis, the relationships of the excitatory input rate to the excitatory conductance, and of the output firing rate to the excitatory input conductance are examined for two different locations, one proximal to the soma, and a very distal one (Figure

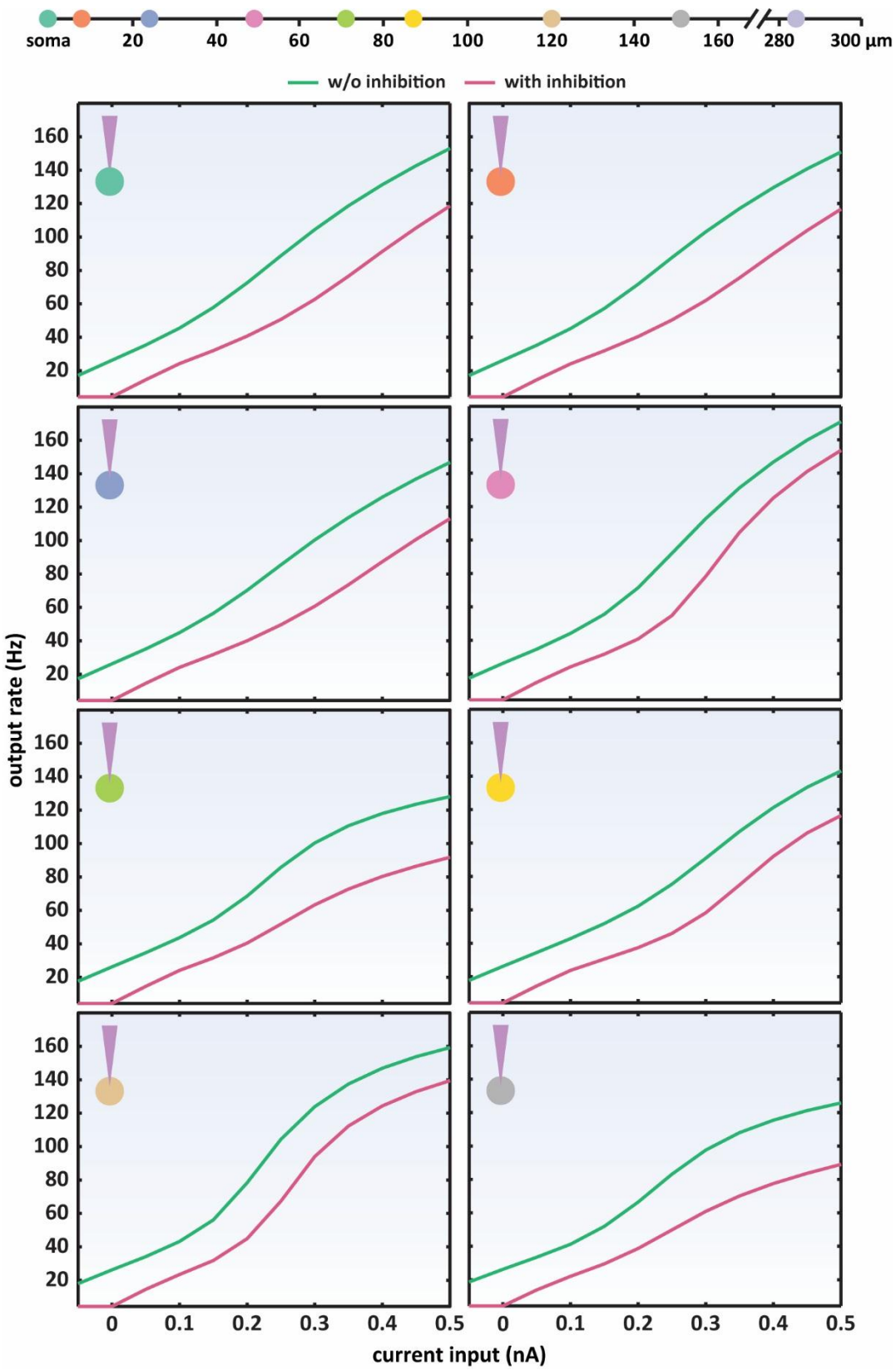

Figure 6.14 I-O relationships of CN model for non-synaptic inputs. The CN neuronal model is injected with current steps confined in one dendritic compartment per time (green lines). Tonic inhibitory conductance (9 nS) is applied (pink lines), at the soma. Top: Schematic distance map from soma of the distinct synaptic excitatory input locations.

6.13). The first mapping (excitatory input rate to excitatory input conductance) exhibits a linear relationship, independent of the presence of the modulatory input, and of the location tested. Such a result is expected, because the excitatory input conductance is direct outcome of the activation of the excitatory synapses at the given excitatory input rate, and unaffected by the delivery site or the presence of inhibition. The second mapping (excitatory input conductance to output firing rate) has a different profile for the proximal and distal location. For the proximal location, the relationship between input conductance and output rate is linear, and the effect of the excitatory input conductance is attenuated by the modulatory input in an approximately subtractive manner. In the case of the distal location, however, a nonlinearity introduced in the excitatory synaptic conductance - output firing rate relationship, resembling is the one caused by dendritic saturation (Prescott and De Koninck, 2003).

The source of the dendritic saturation is a combination of the proportionally increased leakiness of the dendrites, when conductance is added, and the input current driving force, that is, the difference between membrane potential and excitatory synaptic reversal potential, which is reduced with strong depolarization. Increasing excitatory input firing rates for thinner dendrites are saturated faster than for thicker ones, due to the higher input resistance of thinner dendrites that causes larger membrane depolarizations and reduces the driving force (London and Häusser, 2005; Papoutsi et al., 2014). Therefore, increasing excitatory input to a distal dendrite has a gradually diminishing (and eventually negligible) effect on the output firing rate, resulting in the nonlinear relationship between the excitatory synaptic conductance and output firing rate (Prescott and De Koninck, 2003).

In order to investigate further the effect of dendritic saturation on the multiplication of dendritic inputs, a series of experiments is carried out where the CN neuron is driven by a depolarizing injected current to individual compartments and modulated by a tonic inhibitory conductance step in the soma. Voltage changes in response to injected current are independent of the driving force that affects conductance-based inputs and consequently, the output firing rate of the neuron is not affected by underlying dendritic nonlinearities.

The modulation of the I-O function, resulting from the mentioned current-based experimental protocol, for all locations along the somato-dendritic axis is mainly subtractive (Figure 6.14). The resulting change in gain is very small and independent of the distance from the soma, confirming further this result (Figure 6.10). The divisive modulation of inputs to the distal areas that has been observed for synaptic conductance-based inputs has almost vanished,

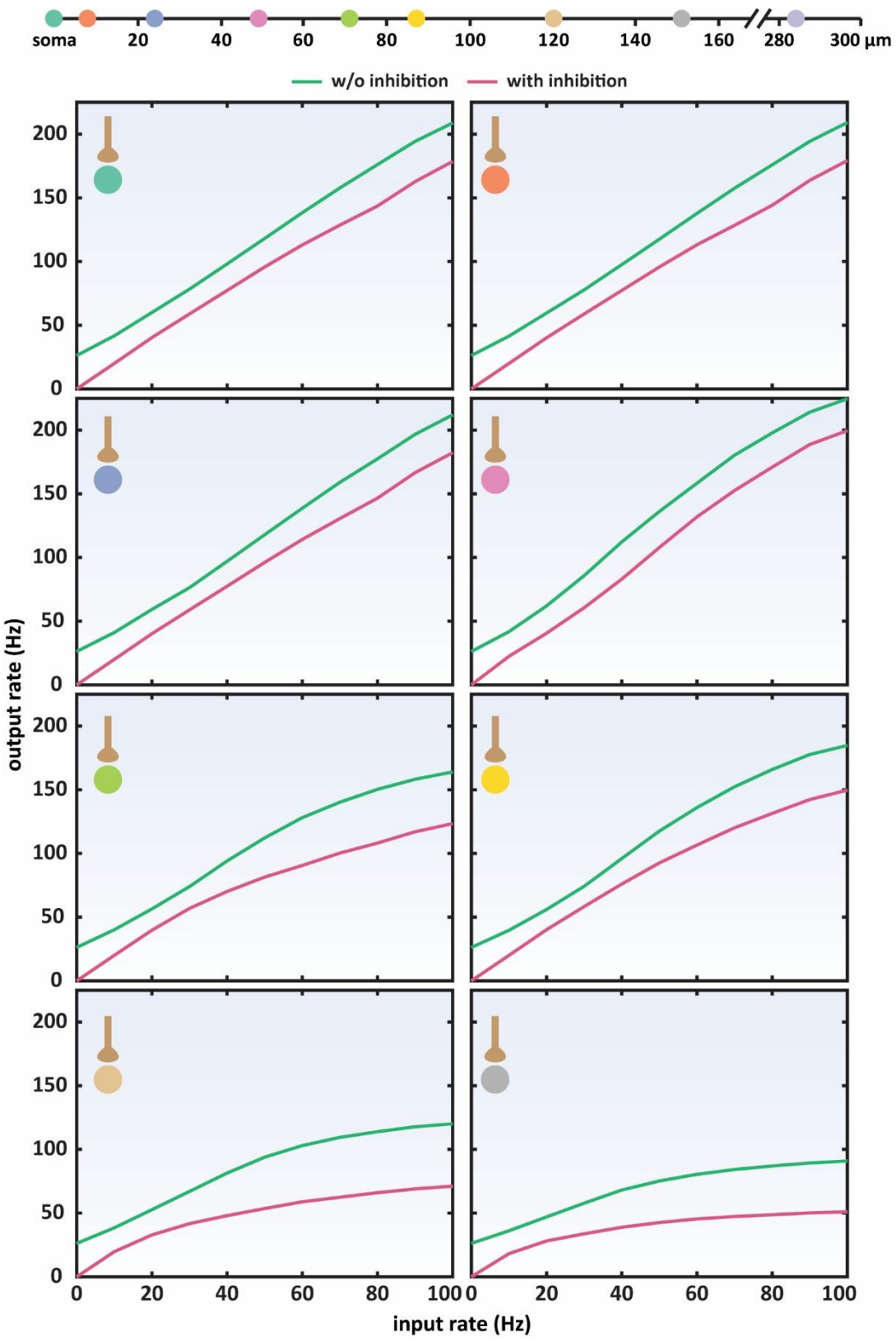

Figure 6.15 I-O relationships of CN model for synaptic and tonic inhibitory inputs. The CN neuronal model is stimulated with 50 synchronous excitatory synapses confined in one dendritic compartment per time (green lines). Tonic inhibitory conductance (9 nS) is applied (pink lines), at the soma. Top: Schematic distance map from soma of the distinct synaptic excitatory input locations.

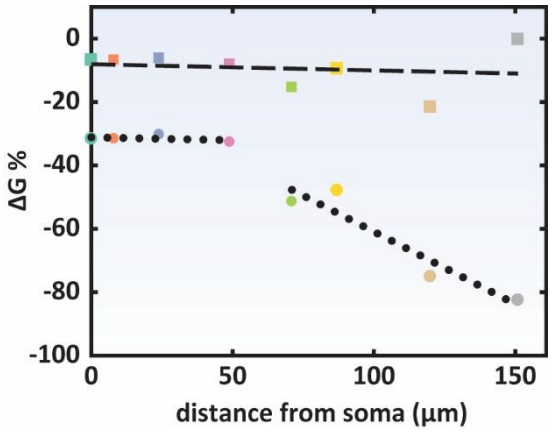

Figure 6.16 Changes in gain (ΔG%) for different neuronal locations in the CN model. As per Figure 6.10**, t**he CN neuronal model is stimulated in different locations along the somato-dendritic area, either with synaptic driving and modulatory inputs (circles), or, as per Figure 6.15, with synaptic driving and somatic tonic inhibitory conductance (squares). ΔG% is calculated after fitting the simulations' data (Figure 6.10 and 6.15) to sextic polynomial functions (Rothman et al., 2009). The dotted and dashed lines are linear trend fits, to the data shown in circles and squares, respectively. Mint shapes: soma. Other shapes: dendritic compartments

suggesting that the dendritic saturation is indeed the underlying gain modulation mechanism, as in previous studies (Prescott and De Koninck, 2003).

6.3.2.1.4 Synaptic input noise enhances gain modulation

The role of noise in gain modulation has been thoroughly researched. Both background synaptic noise and the inherently noisy synaptic driving input can contribute to gain changes in I-O relationships (see Chapter 4). In the present study, the modulatory input is synaptic and delivered ubiquitously distributed across the somatic and dendritic area of the neuron. Thus, it could account as a source of background noise too, which could enhance its divisive effect on excitatory input to the distal dendrites.

Thus far, the CN behaviour has been studied with inputs of pure synaptic or pure non-synaptic nature Figure 6.9, 6.10, 6.11 and 6.13). To evaluate the contribution of the synaptic inhibitory modulatory input as a source of background noise to the numerical operations of the CN neuron, different combinations of synaptic and tonic current or conductance inputs are applied to distinct neuronal locations: (a) synaptic excitation as driving input, and somatic tonic inhibition as modulatory input (Figure 6.15 and 6.16), (b) injected current as driving input, and synaptic inhibition as modulatory input (Figure 6.17 and 6.18).

In the first scenario, the modulation of the CN neuron does not follow a similar pattern as if the modulatory input was synaptic, but more as if the neuron was driven by current injections. This behaviour is consistent with the hypothesis that the enhanced change in gain

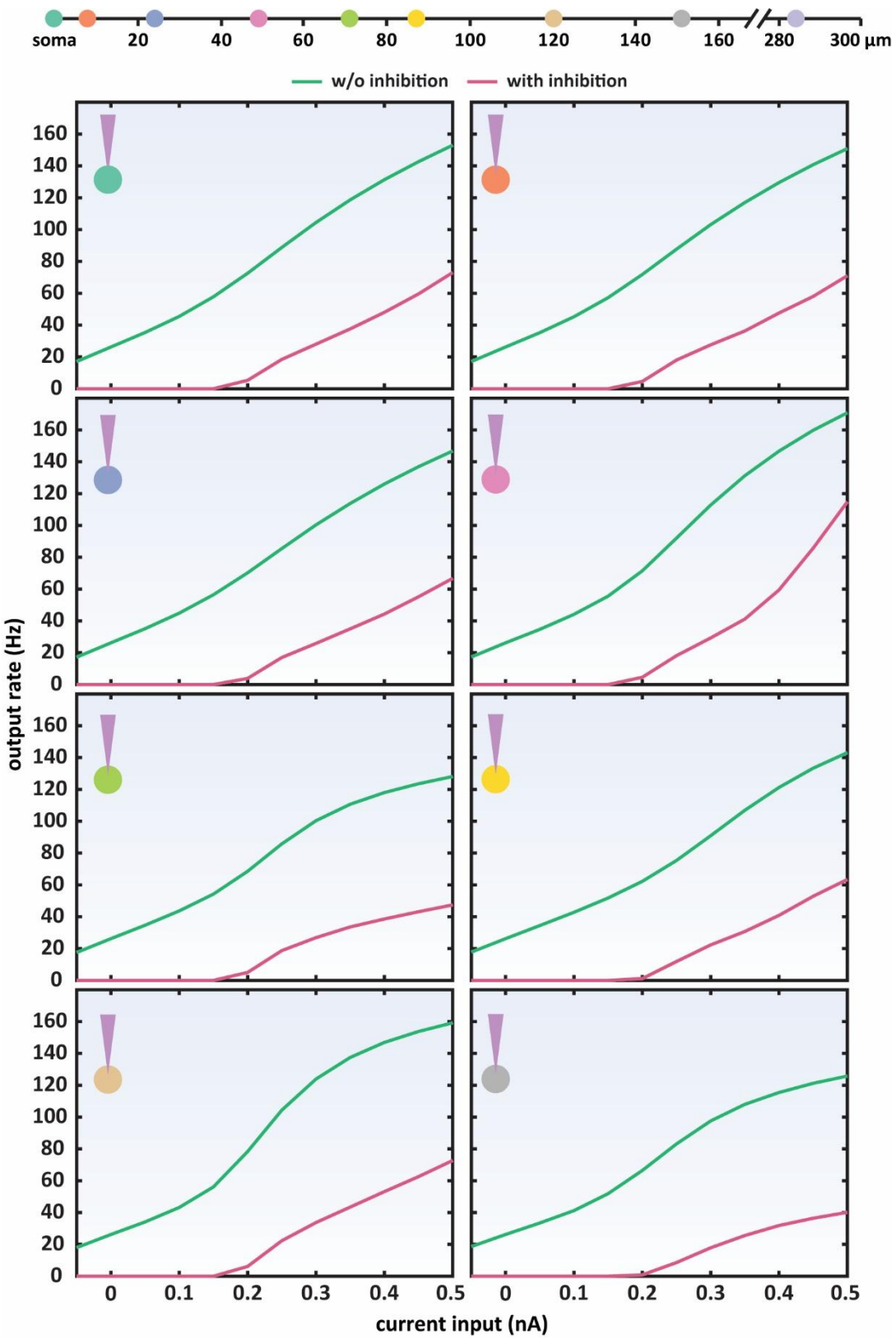

Figure 6.17 I-O relationships of CN model for current and synaptic inputs. The CN neuronal model is injected with current steps confined in one dendritic compartment per time (green lines). When synaptic inhibition (450 synapses at 10 Hz) is applied (pink lines), it is distributed along the dendritic tree and soma. Top: Schematic distance map from soma of the distinct synaptic excitatory input locations.

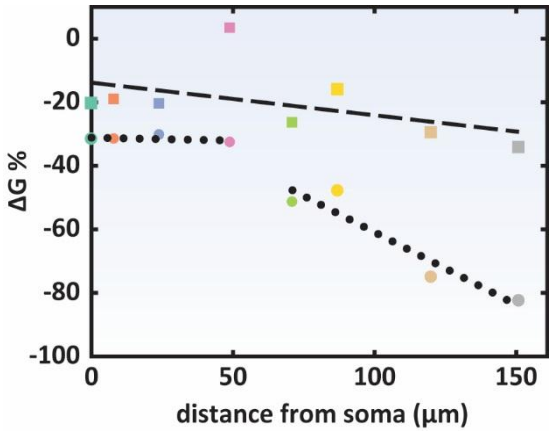

Figure 6.18 Changes in gain (ΔG%) for different neuronal locations in the CN model. As per Figure 6.10**, t**he CN neuronal model is stimulated in different locations along the somato-dendritic area, either with synaptic driving and modulatory inputs (circles), or, as per Figure 6.17, with driving current steps and synaptic inhibition distributed along the somato-dendritic area (squares). ΔG% is calculated after fitting the simulations' data (Figure 6.10 and 6.17) to sextic polynomial functions (Rothman et al., 2009). The dotted and dashed lines are linear trend fits, to the data shown in circles and squares, respectively. Mint shapes: soma. Other shapes: dendritic compartments

of the I-O function in the distal areas is caused by the nonlinearities introduced by the dendritic saturation, in the presence of a modulatory inhibitory synaptic input (Figure 6.15 and 6.16). However, there is a slight increase in the change in gain, when inspecting it individually at some distal compartments, for instance at 71 μm and 120 μm away from the soma, implying that the variability present at driving synaptic input might contribute to the distant-dependent multiplicative operations (Figure 6.16). Moreover, the synaptic inhibition appears to cause a stronger reduction of the output firing rate, compared to the tonic somatic inhibition (Figure 6.9 and 6.15). The degree of inhibition is not normalized for the two conditions, namely, the degree of the applied tonic inhibition to the soma is not adjusted to produce the same effect as the synaptic inhibition to every location. However, even for a normalized somatic tonic inhibition the activation of synaptic inhibition along the cell is expected to result in greater reduction of, the firing output, because it renders the neuronal membrane leakier.

In the second scenario, the modulation of the CN neuron is different compared to the one when the driving input is synaptic (Figure 6.9 and 6.17). It has been assumed up to now that the change in gain is introduced by dendritic nonlinearities and, hence, driving the neuron with injected current is expected to result in predominantly subtractive operations, independently of the synaptic location and the nature of the modulatory input. Still, the change in gain with modulation by the synaptic input is increased slightly in all the locations, compared to the somatic tonic inhibition, and in accordance when both driving and modulatory inputs are

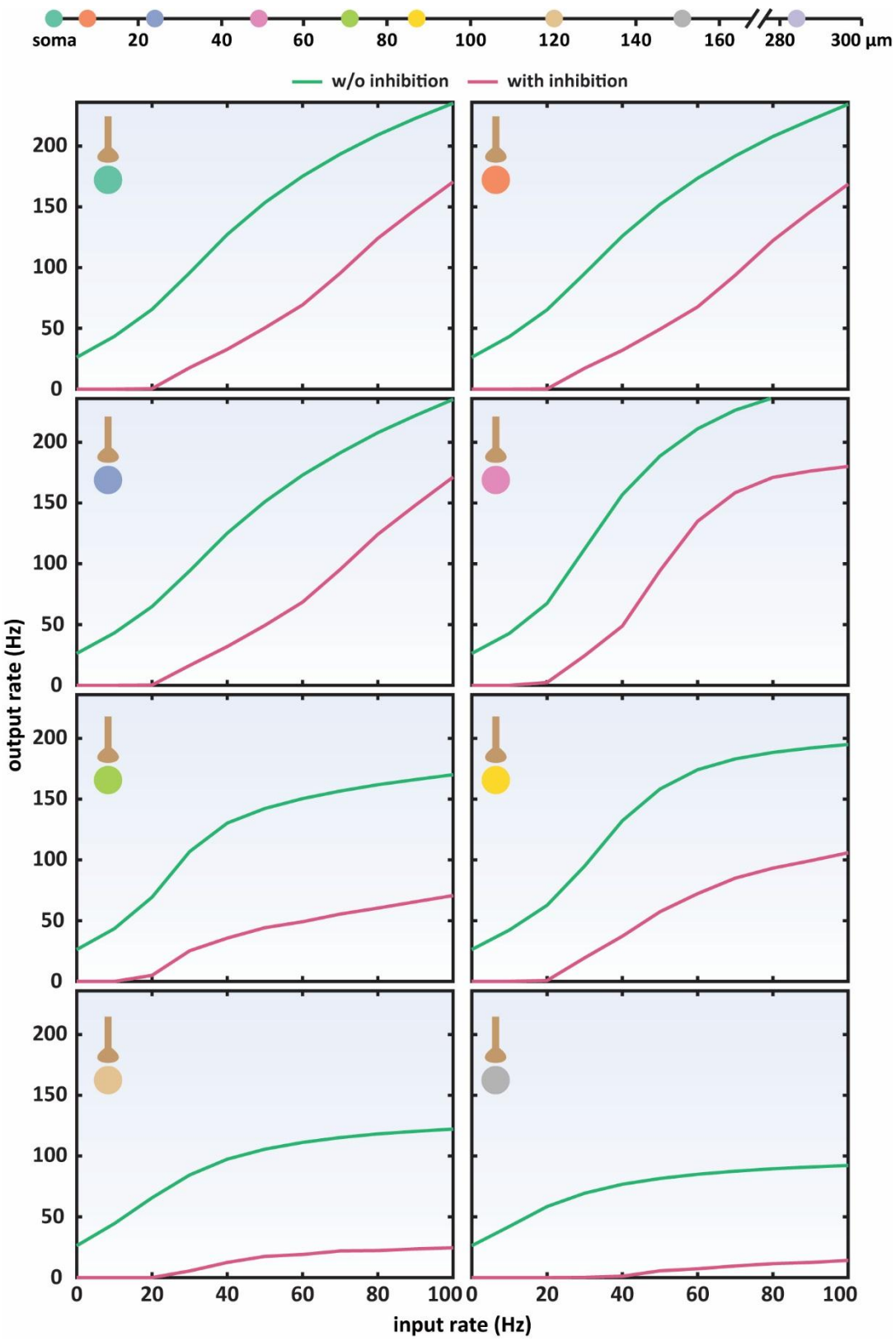

Figure 6.19 I-O relationships of CN model for synaptic inputs. The CN neuronal model is stimulated with 50 asynchronous excitatory synapses confined in one dendritic compartment per time (green lines). When synaptic inhibition (450 synapses at 10 Hz) is applied (pink lines), it is distributed along the dendritic tree and soma. Top: Schematic distance map from soma of the distinct synaptic excitatory input locations.

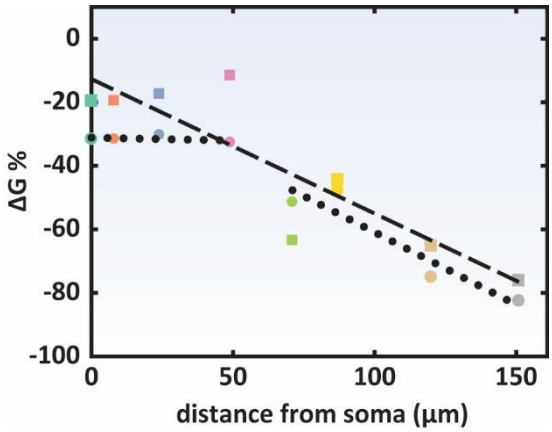

Figure 6.20 Changes in gain (ΔG%) for different neuronal locations in the CN model. As per Figure 6.10**, t**he CN neuronal model is stimulated in different locations along the somato-dendritic area, either with synaptic driving and modulatory inputs (circles), or, as per Figure 6.19, with asynchronous synaptic driving and modulatory inputs (squares). ΔG% is calculated after fitting the simulations' data (Figure 6.10 and 6.19) to sextic polynomial functions (Rothman et al., 2009). The dotted and dashed lines are linear trend fits, to the data shown in circles and squares, respectively. Mint shapes: soma. Other shapes: dendritic compartments

synaptic (Figure 6.10 and 6.18). Therefore, modulatory inhibitory synaptic input can introduce small gain changes in the absence of nonlinearities in the driving input, and it can add to the divisive modulation of the output firing rate originating from the dendritic saturation.

Since, in this experimental configuration, no other known factor could contribute to the gain changes, it is postulated that the intrinsic high variability of the inhibitory synaptic input, in combination with its distribution all over the neuron, serves as background noise, with divisive modulatory effects on the output firing rate (Chance et al., 2002; Hamann et al., 2002; Ly and Doiron, 2009; Mitchell and Silver, 2003). Nonetheless, the combination of synaptic driving and modulatory input results in the largest change in gain, for location further from the soma (Figure 6.9 and 6.10).

6.3.2.1.5 Asynchronous synaptic inputs

Thus far, in the simulation set-ups, synchronous excitatory synaptic input has been applied. The synchronous input is applied as a large excitatory synaptic conductance, which represents 50 identical and concurrent synaptic inputs. In vivo networks, however, support both synchronous and asynchronous synaptic activity with functional implications (Vogels et al., 2005). The balance between synchronous and asynchronous inputs can also affect the features of the I-O relationships. Synchronization of stimuli can lower both the gain and the rheobase and result in a more linear I-O relationship, compared to asynchronous inputs (Li and Ascoli, 2008).

To identify the impact of synchrony on the I-O relationships, the CN neuron is driven at different dendritic locations with the same level of excitatory synaptic stimuli as before, but delivered asynchronously, that is 50 independent excitatory synaptic inputs, which are delivered at the same time window, but their presynaptic trains are not simultaneous. The modulatory input is the same, namely, the distributed inhibitory synaptic input (Figure 6.19). The transformation of the I-O relationship in all locations is similar as with synchronous input: somatic and perisomatic areas are additively modulated by the inhibitory input, whereas the distal areas are modulated divisively. In a similar way, the change in gain is correlated systematically with the distance, but it is not considerably different compared to the simulation, where the excitatory synaptic input is synchronous (Figure 6.20).

6.3.2.2 LVb pyramidal neuron

The cerebral cortex is highly populated with pyramidal neurons, which are found in structures that are associated with advanced cognitive functions. They have a characteristic bipolar structure with a pyramidal shaped soma and two distinct dendritic trees that emerge from it (Spruston, 2008). Pyramidal cell-like shapes are more susceptible to gain modulation by changes in the background balance of synaptic excitatory and inhibitory inputs (Chance et al., 2002; Jarvis et al., 2016). Thus, differences in gain modulation for inputs to the proximal and distal areas of a thick-tufted LVb pyramidal neuron model (Hay et al., 2011; Ramaswamy and Markram, 2015) are investigated here.

To detect any potential differences in the arithmetic operations occurring in the LVb pyramidal neuron, similar experimental protocols as for the CN neuron are applied. The LVb pyramidal neuron is driven with excitatory synaptic inputs or injected current to one compartment (dendritic branch or soma) or inputs that are distributed across one region and modulated by inhibitory synaptic inputs that are distributed or confined to the soma, or somatic tonic inhibition. The impact of synchronicity is also investigated.

6.3.2.2.1 Synaptic input to one location

The pyramidal neuron’s behaviour is tested for input to distinct locations along the apical and basal tree and the soma. When the neuron is driven with only synaptic excitatory input, the amplitude of its output response is proportional to the distance from the spike initiation site (soma) as expected because of the electrotonic signal attenuation (London and Häusser, 2005; Papoutsi et al., 2014). In the presence of inhibitory synaptic input scattered

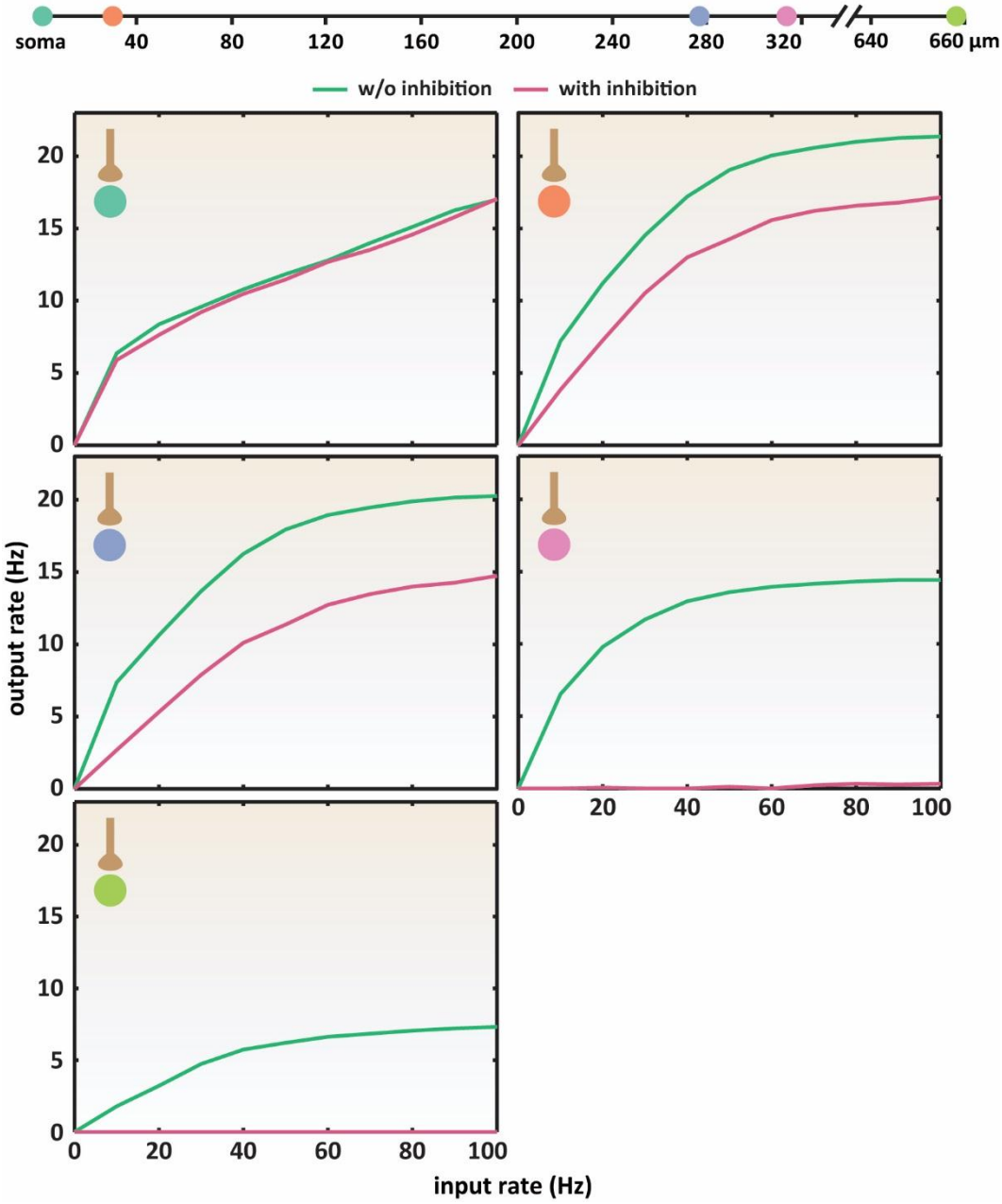

Figure 6.21 I-O relationships of LVb pyramidal model for synaptic inputs. The LVb pyramidal neuronal model is stimulated with 150 synchronous excitatory synapses confined in one dendritic compartment per time (green lines). When synaptic inhibition (178 synapses at 10 Hz) is applied (pink lines), it is distributed along the dendritic tree and soma. Top: Schematic distance map from soma of the distinct synaptic excitatory input locations. Mint: soma; Orange: basal compartment; Blue: apical trunk compartment; Pink: oblique compartment; Green: tuft compartment.

across the neuron, the I-O relationship is modulated in a divisive manner for all of the driving input site locations, but soma (Figure 6.21, 6.22 and 6.23).

The change in gain for the soma is negligible (Figure 6.20 and 6.21). When driving the soma with the same input (150 synchronous excitatory synapses) but with larger modulatory inhibitory input rate (178 synapses distributed along the somato-dendritic area at 50 Hz)

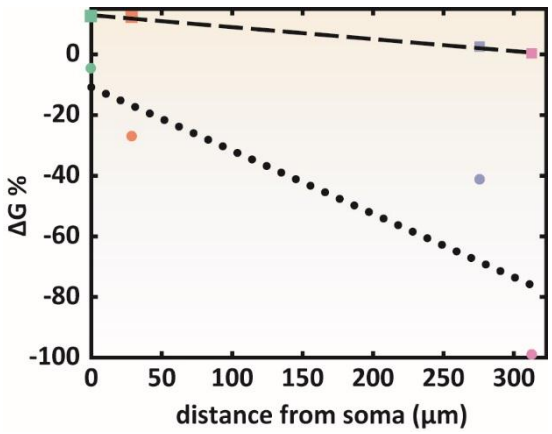

Figure 6.22 Changes in gain (ΔG%) for different neuronal locations in the LVb pyramidal model. As per Figure 6.21**, t**he pyramidal LVb neuronal model is stimulated in different locations along the somato-dendritic area, either with synaptic driving and modulatory inputs (circles), or, as in Figure 6.29, with synaptic driving and somatic tonic inhibitory conductance (squares). ΔG% is calculated after fitting the simulations' data (Figure 6.21 and 6.29) to sextic polynomial functions (except for the blue square, which is fitting to cubic polynomial function) (Rothman et al., 2009). The dotted and dashed lines are linear trend fits, to the data shown in circles and squares, respectively. Mint shapes: soma; Orange shapes: basal dendrite; Blue shapes: trunk dendrite; Pink shapes: oblique dendrite

(Figure 6.23), the arithmetic operations of the driving input, are additive (with -11% ΔG). However, the change in gain in the LVb pyramidal neuron is not correlated with the distance in a systematic way, as in the CN neuron (Figure 6.22). In the case of LVb pyramidal neuron, the change in gain for the trunk is smaller than expected for the distance from the soma (Figure 6.21 and 6.22).

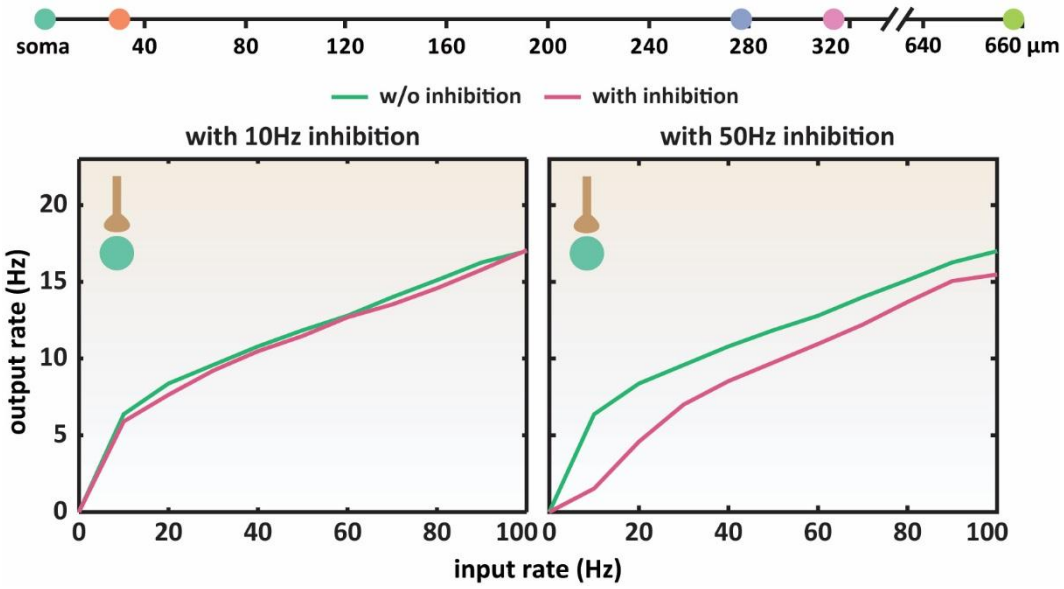

Figure 6.23 I-O relationships of LVb pyramidal model for synaptic inputs in soma. The LVb pyramidal neuronal model is stimulated with 150 synchronous excitatory synapses confined in soma (green lines). When synaptic inhibition (178 synapses) is applied (pink lines), it is distributed along the dendritic tree and soma (left panel) at 10 Hz), and (right panel) at 50 Hz. ΔG% is calculated after fitting the simulations' data to sextic polynomial functions (Rothman et al., 2009). Top: Schematic distance map from soma of the distinct synaptic excitatory input locations.

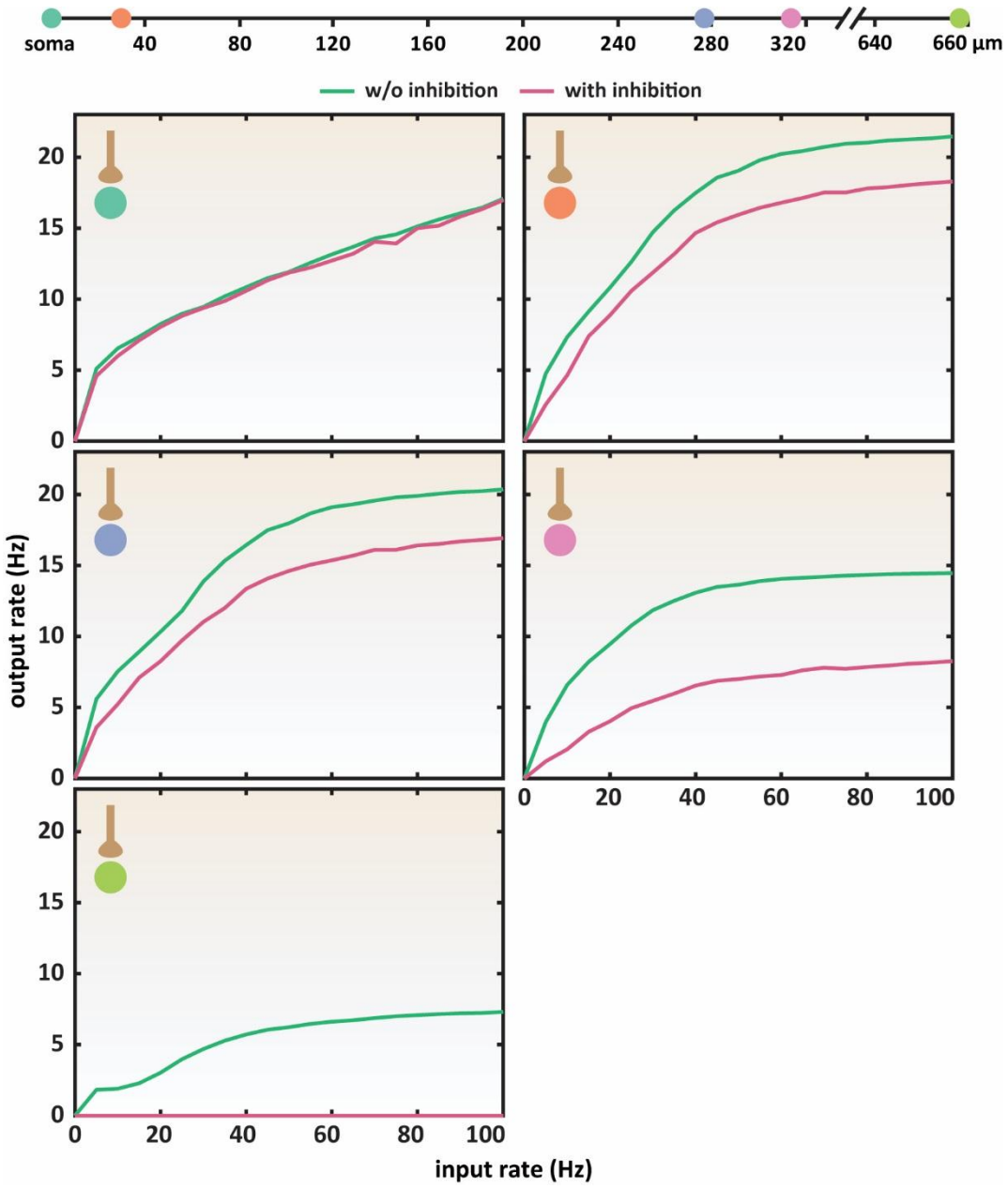

Figure 6.24 I-O relationships of LVb pyramidal model for synaptic inputs. The LVb pyramidal neuronal model is stimulated with 150 synchronous excitatory synapses confined in one dendritic compartment per time (green lines). Synaptic inhibition (50 synapses at 15 Hz) is applied (pink lines) only at soma. Top: Schematic distance map from soma of the distinct synaptic excitatory input locations. Mint: soma; Orange: basal compartment; Blue: apical trunk compartment; Pink: oblique compartment; Green: tuft compartment.

Pyramidal neurons receive most of their inhibitory inputs at the somatic and proximal dendritic areas, rather than the distal dendritic branches (Ramaswamy and Markram, 2015; Spruston, 2008). In addition, as mentioned, modulation by somatic inhibition could be additive and not multiplicative (Holt and Koch, 1997; Jarvis et al., 2016; Mehaffey, 2005; Prescott and De Koninck, 2003). To unveil the role of somatic inhibition in the modulation of somatic and dendritic inputs, the pyramidal neuron is driven with excitatory synaptic dendritic or somatic

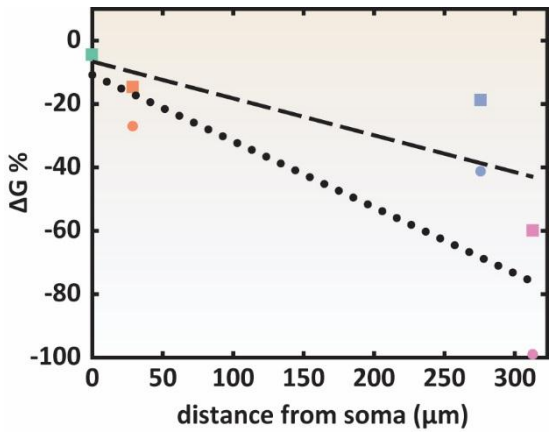

Figure 6.25 Changes in gain (ΔG%) for different neuronal locations in the LVb pyramidal model. As per Figure 6.21**, t**he LVb pyramidal neuronal model is stimulated in different locations along the somato-dendritic area, either with synaptic driving and modulatory inputs distributed along the somato-dendritic area (circles), or, as per Figure 6.24, with synaptic driving and modulatory inputs confined in soma (squares). ΔG% is calculated after fitting the simulations' data (Figure 6.21 and 6.24) to sextic polynomial functions (Rothman et al., 2009). The dotted and dashed lines are linear trend fits, to the data shown in circles and squares, respectively. Mint shapes: soma; Orange shapes: basal dendrite; Blue shapes: trunk dendrite; Pink shapes: oblique dendrite.

inputs at distinct locations and modulated by synaptic somatic inhibition only. As in the case of the distributed synaptic inhibition along the somato-dendritic area, the modulatory effect is divisive for the driving input on dendritic sites (Figure 6.24 and 6.25).

For both types of inhibition, the effect is negligible in the soma. Increasing the inhibitory input decreases the neuronal response, but it also diminishes the effect of excitatory signals arriving from the dendritic locations (data not shown), which are already electronically attenuated. Furthermore, since in this experimental set-up, the excitatory driving input is clustered on one dendritic compartment, the responses saturate fast for increasing input firing rates, especially in the thin pyramidal dendritic branches. As a result, stronger synaptic input would not boost any further the output firing rate, which in turn could make the different modulatory operations more evident (London and Häusser, 2005; Papoutsi et al., 2014). In addition, the distributed inhibitory synaptic input along the somato-dendritic area makes the dendritic membrane leakier, and in combination with the electrotonic signal attenuation could weaken the driving input more. Therefore, the effect of the neuron-wide inhibition is stronger compared to the synaptic somatic inhibition only (Figure 6.21 and 6.24).

Still, the I-O transformations triggered by the inhibitory modulatory input for excitatory input to the somatic and proximal locations are different in the two neuron models. One striking difference between the CN and LVb pyramidal neuron is their morphology. Both cells have trees with moderate branching, but the CN neuron is a multipolar neuron and the LVb is bipolar.

When neurons with different morphologies are driven with dendritic excitatory and inhibitory signals, and modulated by shifting the balance of mixed background input towards the inhibitory compound, their I-O function can undergo different neuronal arithmetic operations; in a bipolar-like neuron (for instance, pyramidal neuron) the input is divisively modulated, whereas in a multipolar-like one (for example, hippocampal stellate cell) the I-O relationship is shifted (Jarvis et al., 2016). Hence, the modulation of the CN and LVb pyramidal neuron response by a somato-dendritic wide synaptic inhibitory input, as observed in the current study, might be found in the first instance inconsistent with these results (Jarvis et al., 2016), that is, the multipolar-like CN neuron exhibits both additive and divisive arithmetic operations. However, in the mentioned study (Jarvis et al., 2016) the mixed background input is delivered by simulating an optogenetic protocol and the excitatory and inhibitory input is a photocurrent product that lacks the intrinsic synaptic variability, namely, the noisy nature of the synaptic signals. but it is in accordance with the notion that the dendritic tree morphology can affect the arithmetic operations performed by neurons.

6.3.2.2.2 Synaptic input to different dendritic regions

In an analogous way to the synaptic activation of distinct CN subregions, the LVb pyramidal neuron is stimulated with segregated synaptic excitatory (driving) input at various subregions (soma, basal, trunk, oblique and tuft), with neuron-wide distributed synaptic inhibition as modulatory input. As in the CN neuron simulations, the amplitude of the output firing rate is reduced as a function of distance of the excited subregion from the soma. The activation of the modulatory input generates multiplicative transformations of the I-O relationship for excitatory input to the distal oblique subregion, while the perisomatic basal regions and trunk are characterized of negligible change in gain (Figure 6.26 and 6.27). The activation in the tuft region does not result in neuronal spiking, due to the attenuation of the distal tuft signals (data not shown).

The experimental protocol for applying synaptic input to both neurons (CN and LVb pyramidal) follows the same principle: excitatory driving synaptic input distributed across one subregion, and inhibitory modulatory synaptic input distributed across the whole somato-dendritic area. The subregions are selected based on their proximity to the soma, so that the results are comparable to the ones when the synaptic driving input is clustered on one dendritic compartment. Nonetheless, the selection of subregions differs for the two neuronal types, due to their distinct morphology. The CN neuron is a multipolar-like neuron, with its soma located

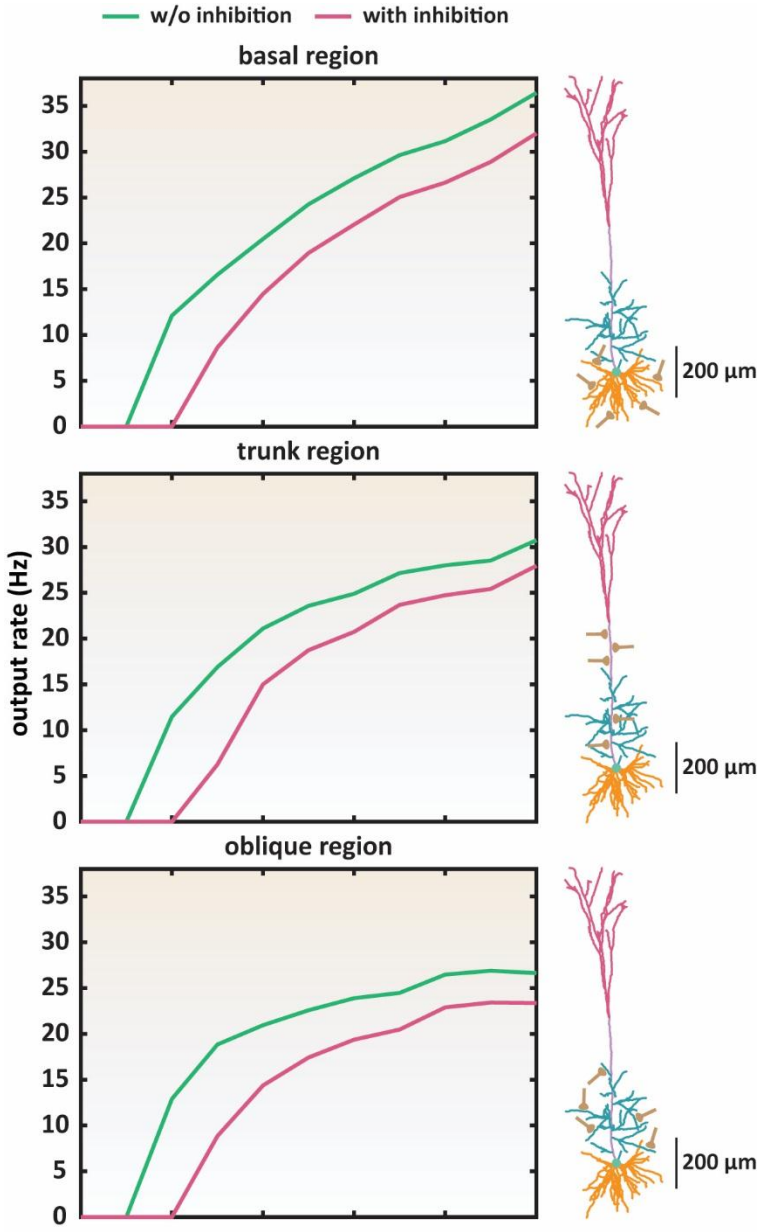

Figure 6.26 I-O relationships of LVb pyramidal model for distributed synaptic inputs. The LVb pyramidal neuronal model is stimulated with 150 synchronous excitatory synapses distributed in one neuronal subregion per time (green lines). When synaptic inhibition (178 synapses at 10 Hz) is applied (pink lines), it is distributed along the dendritic tree and soma. Right: The detailed reconstructed morphology of the LVb pyramidal neuron is shown, with distinct colours for the different neuronal subregions. Orange: basal; Cean: oblique; Purple: trunk; Pink: tuft.

centrally and the dendritic tree bifurcates around it. Thus, the division of the neuronal area based on distance results in distinct concentric zones of dendritic branches, as in a Sholl analysis (Sholl, 1953). Therefore, the signal pulses, generated by the synaptic excitation of the neuron in one subregion, propagate directly to the soma through these zones via various dendritic paths, and the change in gain is related mainly to the path length (or distance) from the soma.

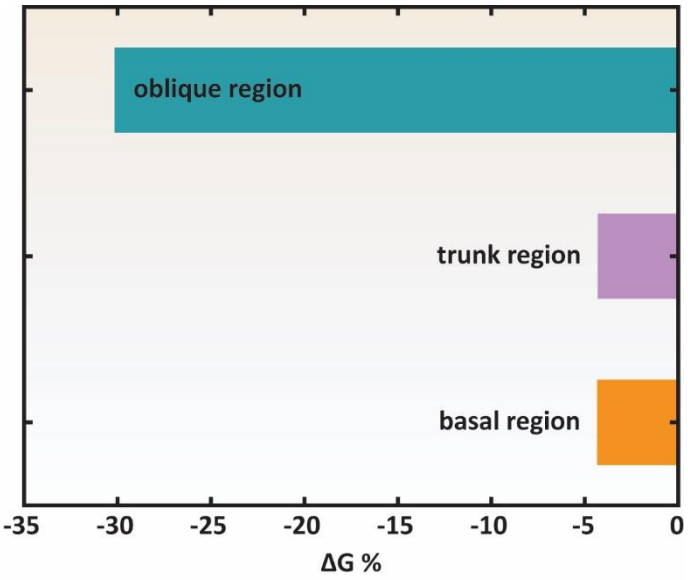

Figure 6.27 Changes in gain (ΔG%) for different neuronal subregions in the LVb pyramidal model. As per Figure 6.26**,** the LVb pyramidal neuronal model is stimulated in different subregions with synaptic driving and modulatory inputs. ΔG% is calculated after fitting the simulations' data (Figure 6.26) to sextic polynomial functions (Rothman et al., 2009). The distinct colours in the bars correspond to the ΔG% in the different neuronal subregions (Figure 6.26).

The LVb pyramidal neuron, however, is a bipolar-like neuron. The soma is located between two distinct dendritic trees with characteristic architectures. The branches of the basal tree emerge directly from the soma (like the dendritic tree of the CN neuron). The apical tree also extends from the soma, but via a large and thick dendrite (apical trunk), which bifurcates to give rise to thinner oblique dendrites, and at its end branches further to form the apical tuft. The division of subregions based on the proximity to the soma, can be matched to the already existed morphological groups of the apical and basal dendrites. However, these subregions do not give rise to concentric zones, as in the CN neuron, with putative implications for the computational operation of the synaptic inputs. As mentioned, dendritic trees with different morphological features endorse the neurons with different modulatory potential (Jarvis et al., 2016).

The change in gain in the LVb pyramidal neuron for its different subregions follows the same pattern as in the synaptic input to one location. The basal and tuft subregions have a similar extent of gain change which is much smaller compared to the oblique subregion. Therefore, the change in gain is not systematically correlated to distance, as in the CN neuron (Figure 6.26 and 6.27).

6.3.2.2.3 Dendritic saturation and synaptic input noise effect

As described in the previous sections, the LVb pyramidal neuron does not exhibit

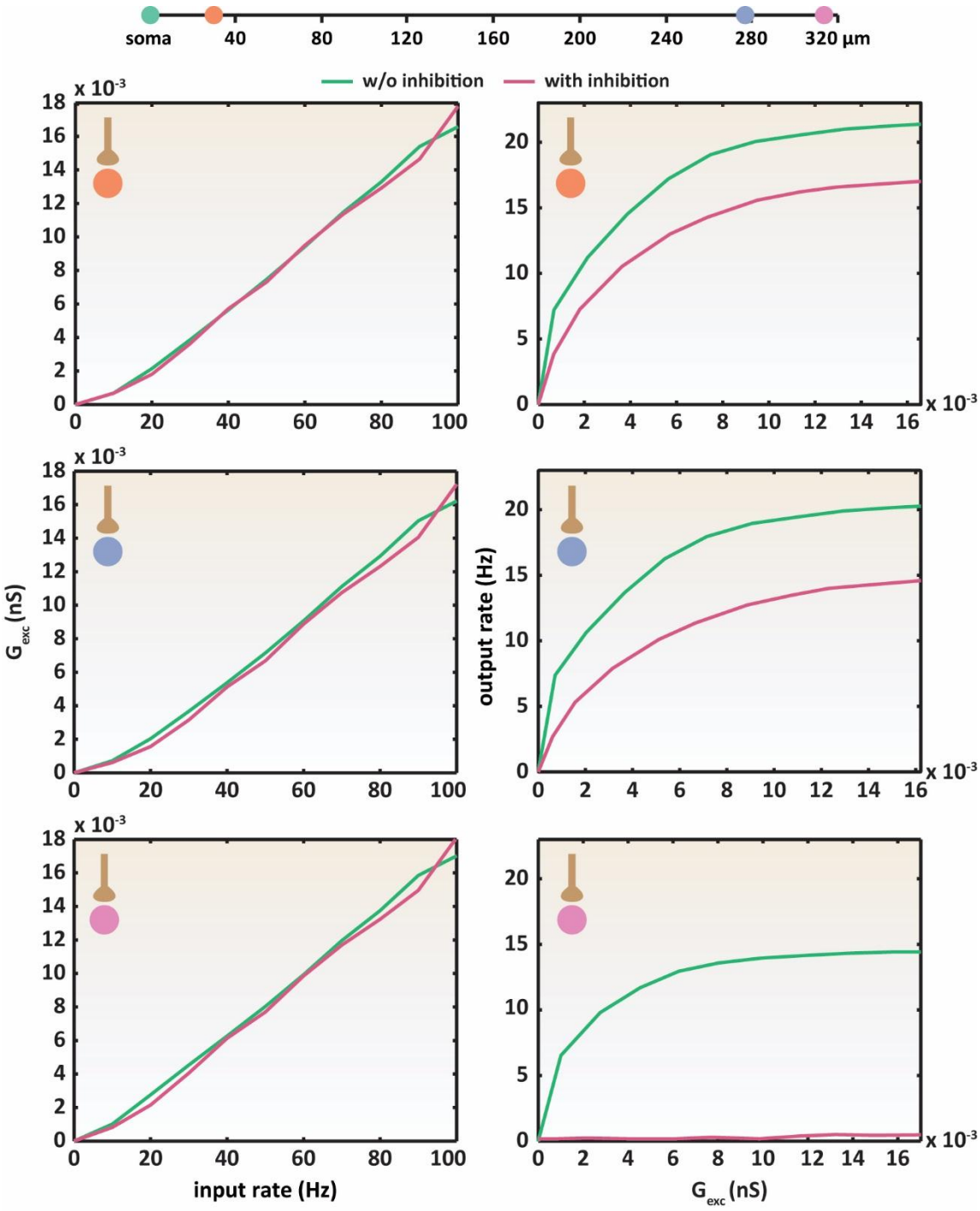

Figure 6.28 Breaking down the I-O relationship in the LVb pyramidal model. The I-O function of the pyramidal LVb model is analysed further for different dendritic locations (upper panels: 29 µm (basal), middle panels: 276 µm (trunk) and lower panels: 313 µm (oblique)) by investigating the relationships between neuronal output firing rate, synaptic excitatory conductance and synaptic excitatory input rate. The LVb pyramidal neuronal model is stimulated in different subregions with synaptic driving and modulatory inputs, as in Figure 6.21. Left panels: Mapping of excitatory input rate to excitatory input conductance. Right panels: Mapping of excitatory input conductance to output firing rate. Top: Schematic distance map from soma of the distinct synaptic excitatory input locations.

similar behaviour as the CN neuron, with multiplicative gain changes for excitatory dendritic inputs that increase systematically in magnitude with an increasing distance of the inputs from

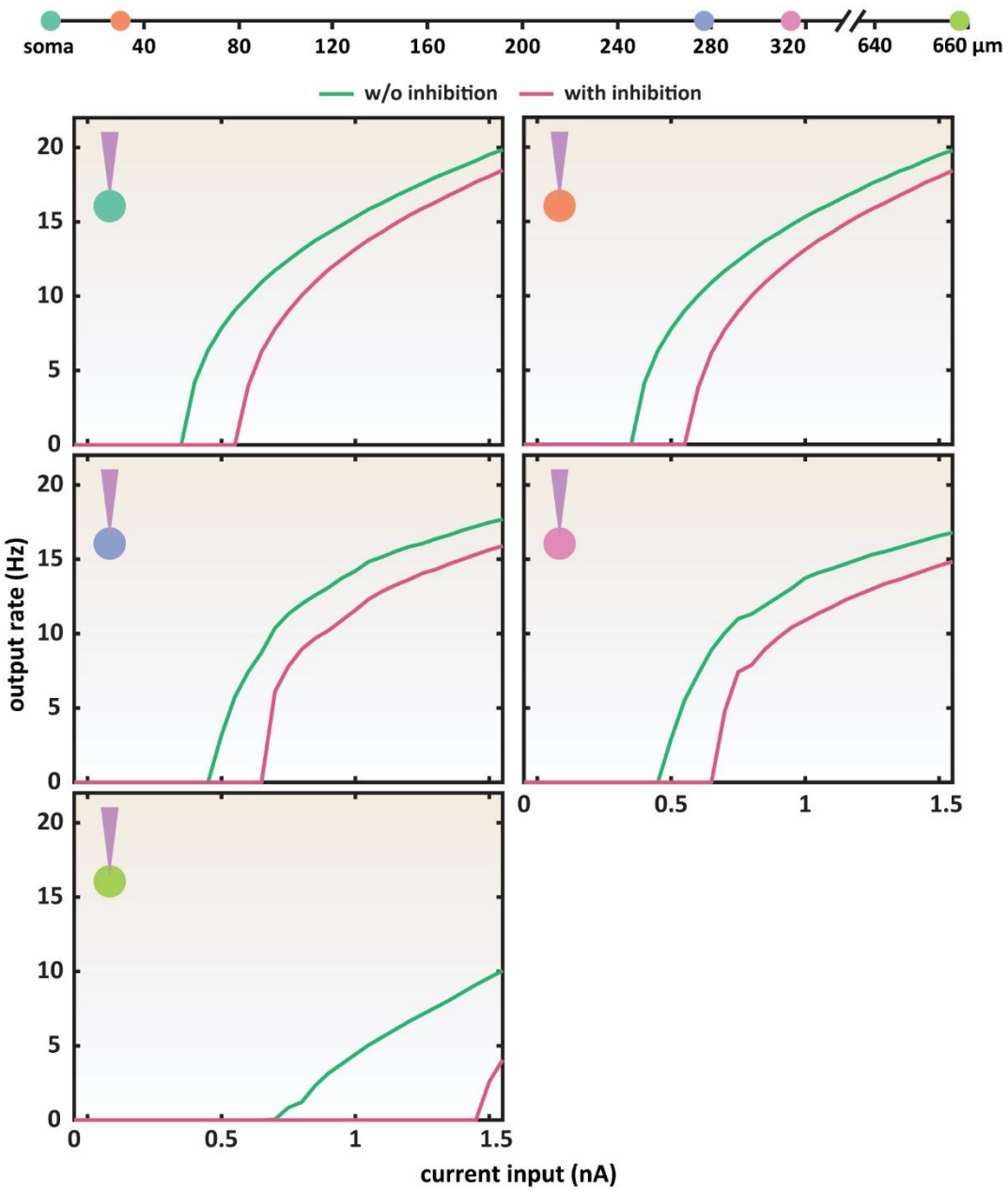

Figure 6.29 I-O relationships of LVb pyramidal model for non-synaptic inputs. The LVb pyramidal neuronal model is injected with current steps confined in one dendritic compartment per time (green lines). Tonic inhibitory conductance (12 nS) is applied (pink lines), at the soma. Top: Schematic distance map from soma of the distinct synaptic excitatory input locations. Mint: soma; Orange: basal compartment; Blue: apical trunk compartment; Pink: oblique compartment; Green: tuft compartment.

the soma. There are differences between the behaviour of the two neuronal models: (a) the excitatory inputs delivered in their perisomatic area are modulated differently by the inhibitory input. In the LVb pyramidal neuron, the divisive operations governing the integration of the synaptic excitatory inputs are also predominant in the proximal to soma locations (Figure 6.21 and 6.22), where in the CN neuron, more additive operations are found to take place (Figure 6.9 and 6.10), (b) the change in gain for the trunk area is not related to distance, and it has similar extent to the proximal basal areas.

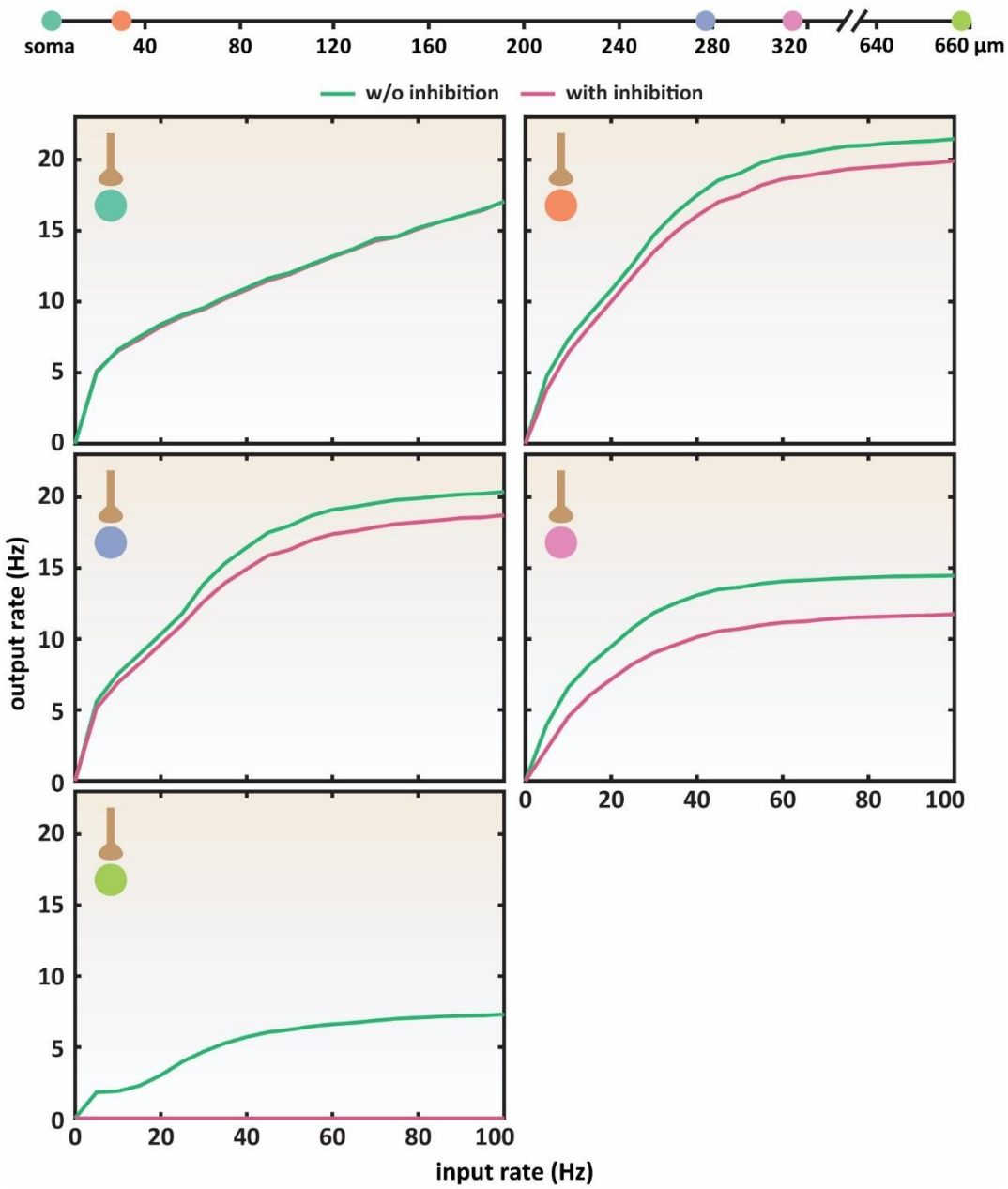

Figure 6.30 I-O relationships of LVb pyramidal model for synaptic and tonic inhibitory inputs. The LVb pyramidal neuronal model is stimulated with 150 synchronous excitatory synapses confined in one dendritic compartment per time (green lines). Tonic inhibitory conductance (12 nS) is applied (pink lines), at the soma. Top: Schematic distance map from soma of the distinct synaptic excitatory input locations. Mint: soma; Orange: basal compartment; Blue: apical trunk compartment; Pink: oblique compartment; Green: tuft compartment.

In order to shed light on the underlying cause of this difference, the mappings of the excitatory input rate to excitatory input conductance and excitatory input conductance to output firing rate are obtained for the LVb pyramidal neuron, and again as for the CN neuron, for a proximal to the soma and very distal one location. In addition, an apical trunk location is investigated (Figure 6.28).

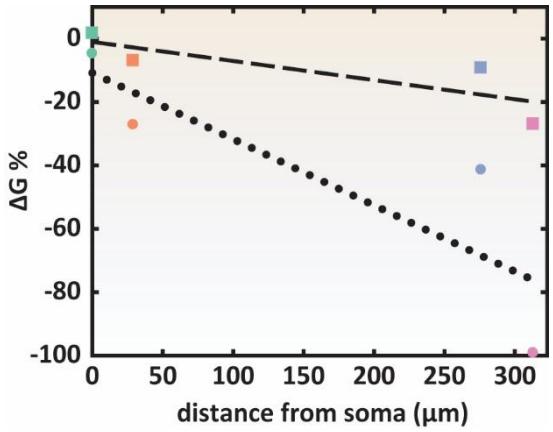

Figure 6.31 Changes in gain (ΔG%) for different neuronal locations in the LVb pyramidal model. As per Figure 6.21**, t**he LVb pyramidal neuronal model is stimulated in different locations along the somato-dendritic area, either with synaptic driving and modulatory inputs (circles), or, as per Figure 6.30, with synaptic driving and somatic tonic inhibitory conductance (squares). ΔG% is calculated after fitting the simulations' data (Figure 6.21 and 6.30) to sextic polynomial functions. The dotted and dashed lines are linear trend fits, to the data shown in circles and squares, respectively. Mint shapes: soma; Orange shapes: basal dendrite; Blue shapes: trunk dendrite; Pink shapes: oblique dendrite.

The relation between the excitatory input rate and the excitatory conductance (first mapping) exhibit the same characteristics as the CN neuron: linear and independent of the modulatory input and synaptic input delivery site. However, the relation of excitatory input conductance and output firing rate (second mapping) is different between the two neurons for the proximal (basal) to the soma location and the apical trunk one. In the case of the LVb pyramidal neuron this relation is nonlinear for both cases, and in the presence of the modulatory input is attenuated in a divisive manner. The same nonlinearity is also apparent for the distal location, like the CN neuron, and the trunk location (Figure 6.28).

However, the extent of nonlinearity for the trunk location is close to the proximal to the soma location, and not the distal one. Based on the distance from the soma, a large change in gain would be expected for input locations on the trunk. Nevertheless, the change in gain for the trunk is smaller than anticipated and closer to the extent observed in the perisomatic locations. Yet, the compartments of the apical trunk are characterized by a large diameter resulting in reduced local input resistance, which consequently could lead in reduced nonlinearities in the trunk.

Further, as in the CN neuron, it is investigated if the combination of dendritic nonlinearities and synaptic background input also underlies gain modulation by synaptic inhibition in the LVb pyramidal neuron. The neuron is either injected with a depolarizing current in different dendritic compartments and modulated by a tonic inhibitory conductance

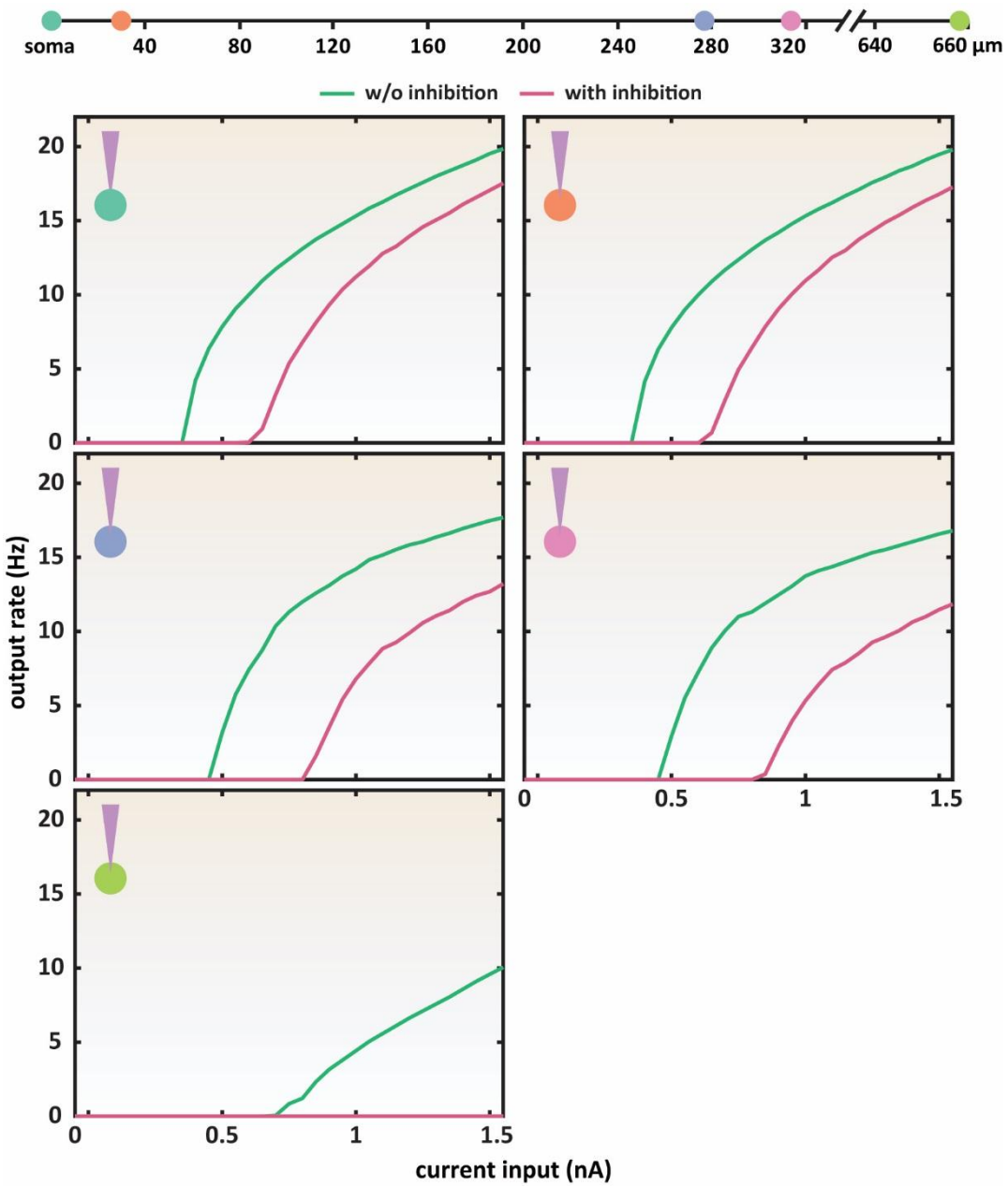

Figure 6.32 I-O relationships of LVb pyramidal model for current and synaptic inputs. The LVb pyramidal neuronal model is injected with current steps confined in one dendritic compartment per time (green lines). When synaptic inhibition (203 synapses at 5 Hz) is applied (pink lines), it is distributed along the dendritic tree and soma. Top: Schematic distance map from soma of the distinct synaptic excitatory input locations. Mint: soma; Orange: basal compartment; Blue: apical trunk compartment; Pink: oblique compartment; Green: tuft compartment.

in the soma (Figure 6.22 and 6.29) or by neuron-wide synaptic inhibitory input (Figure 6.32 and 6.33) or is excited synaptically in different dendritic locations and modulated by somatic tonic inhibition (Figure 6.30 and 6.31).

The results are similar to the CN neuron. The observed divisive operations, when synaptic input (driving and modulatory) is delivered, are substituted by additive in the presence of current inputs (Figure 6.22 and 6.29), favouring the idea that the saturation of synaptic input

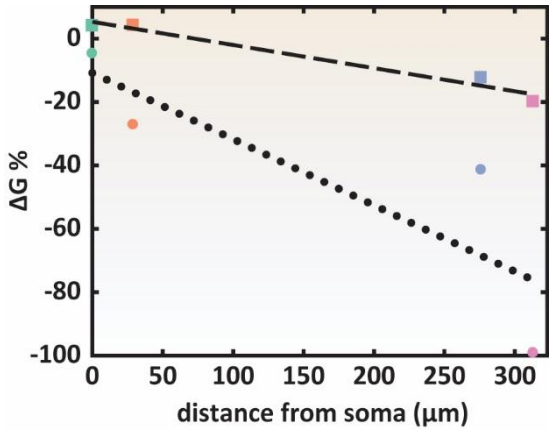

Figure 6.33 Changes in gain (ΔG%) for different neuronal locations in the LVb pyramidal model. As per Figure 6.21**,** the LVb pyramidal neuronal model is stimulated in different locations along the somato-dendritic area, either with synaptic driving and modulatory inputs (circles), or, as per Figure 6.32 with driving current steps and synaptic inhibition distributed along the somato-dendritic area (squares). ΔG% is calculated after fitting the simulations' data (Figure 6.21 and 6.32) to sextic polynomial functions (Rothman et al., 2009). The dotted and dashed lines are linear trend fits, to the data shown in circles and squares, respectively. Mint shapes: soma; Orange shapes: basal dendrite; Blue shapes: trunk dendrite; Pink shapes: oblique dendrite.

is the source of dendritic nonlinearities, and hence the underlying mechanism of the gain modulation. When the driving input is synaptic excitation and the modulatory input is tonic inhibition, the effect of dendritic nonlinearities is still present, and as for the CN neuron is additive in the proximal (and trunk) locations, compared to the distal branches (Figure 6.30 and 6.31).

Shunting input can underlie gain modulation in cerebellar granule cells when the driving input is enriched with high variability (Mitchell and Silver, 2003). An analogous divisive mechanism might be applied in the case of LVb pyramidal neuron too, and it scales, based on the input location (but not in a systematic manner), with the inhibitory synaptic input enhancing it further. When the driving input is current and the modulatory one is synaptic, there still a multiplicative component (Figure 6.32 and 6.33). As in the CN neuron, the inhibitory synaptic modulation might serve as background noise giving rise to divisive operation (Chance et al., 2002; Hamann et al., 2002; Ly and Doiron, 2009; Mitchell and Silver, 2003).Thus, the source of gain modulation in pyramidal LVb and CN neurons is both from the excitatory and inhibitory synaptic input.

6.3.2.2.4 Asynchronous synaptic inputs

In the synaptic simulations that were described previously, a synchronous driving excitatory input is applied. However, input synchronicity can have an impact on gain modulation in hippocampal pyramidal cells (Li and Ascoli, 2008), but not in the CN neuron as

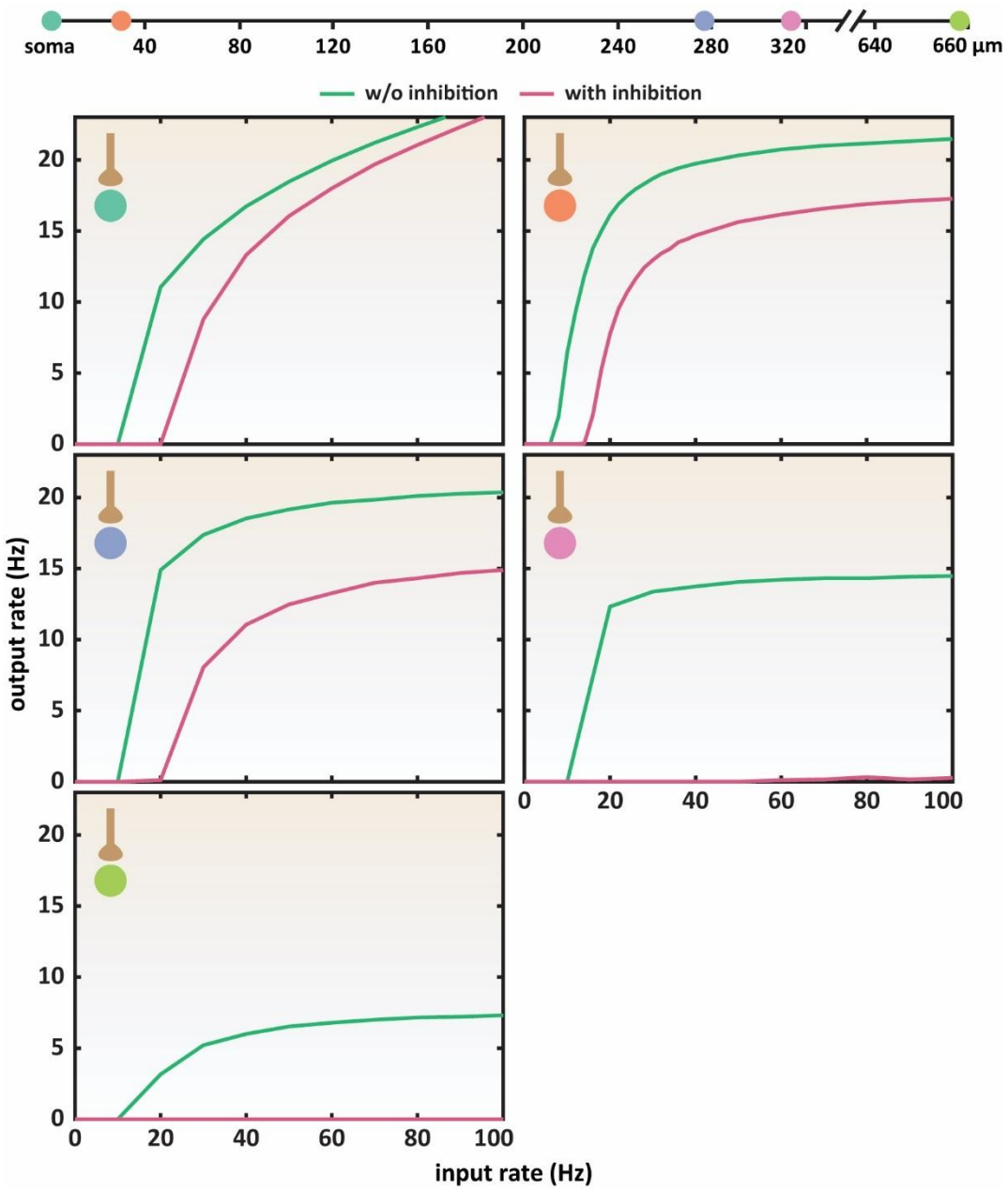

Figure 6.34 I-O relationships of pyramidal LVb model for synaptic inputs. The LVb pyramidal neuronal model is stimulated with 150 asynchronous excitatory synapses confined in one dendritic compartment per time (green lines). When synaptic inhibition (178 synapses at 10 Hz) is applied (pink lines), it is distributed along the dendritic tree and soma. Top: Schematic distance map from soma of the distinct synaptic excitatory input locations. Mint: soma; Orange: basal compartment; Blue: apical trunk compartment; Pink: oblique compartment; Green: tuft compartment.

it is shown in the current study (see 6.3.2.1.5 Asynchronous synaptic inputs).

To explore the effect of synchronicity on the neuronal response of the LVb pyramidal neuron, an analogous synaptic simulation to the CN neuron is carried out, with asynchronous excitatory driving input in somatic and various dendritic locations, and neuron-wide inhibitory modulatory synaptic input (Figure 6.34). The pattern of the neuronal computations occurring in the presence of the modulatory input, in the various cell locations, is the same with the

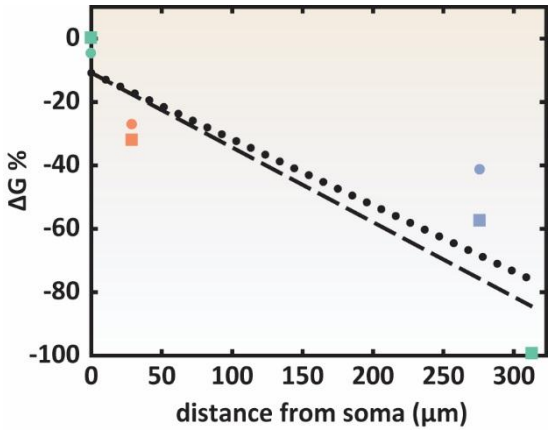

Figure 6.35 Changes in gain (ΔG%) for different neuronal locations in the pyramidal LVb model. As per Figure 6.21**,** the LVb pyramidal neuronal model is stimulated in different locations along the somato-dendritic area, either with synaptic driving and modulatory inputs (circles), or, as per Figure 6.34, with asynchronous synaptic driving and modulatory inputs (squares). ΔG% is calculated after fitting the simulations' data (Figure 6.21 and 6.34) to sextic polynomial functions, except for the blue square, which is fitting to quintic polynomial function (Rothman et al., 2009). The dotted and dashed lines are linear trend fits, to the data shown in circles and squares, respectively. Mint shapes: soma; Orange shapes: basal dendrite; Blue shapes: trunk dendrite; Pink shapes: oblique dendrite.

synchronous synaptic input (Figure 6.21 – 6.27). Nevertheless, the extent of divisive change is larger for the asynchronous input in the layer LVb pyramidal neuron (Figure 6.35), as in previous studies (Li and Ascoli, 2008).

6.4 Discussion

The aim of this chapter is to investigate the location dependent gain changes in two types of neurons, CN and pyramidal LVb. Two possible players are considered: ion channel noise and modulation by inhibitory synaptic input. The rationale to study these factors lies in the nature of the CN neuron itself. The cell is enriched with an elaborate dendritic tree and a plethora of ion channels that shape its unique electrophysiological properties (Steuber et al., 2011; Steuber and Jaeger, 2013; Uusisaari et al., 2007). CN neurons receive excitatory input from climbing and mossy fibres and inhibitory input from the Purkinje cells, across their soma and dendritic tree. In addition, they fire spontaneously action potentials without requiring the presence of synaptic input and during behavioural tasks their firing frequency increases. Their position in the cerebellar circuit is central since they provide the major output of the cerebellum (Knöpfel, 2013).

Considering that even a single type of stochastic channel located in thin dendrites can affect the generation of actions potentials and the fidelity of spiking (see Chapter 3), the question arises which mathematical operations on its inputs could a fully stochastic CN neuron

perform, when the excitatory input is delivered in various locations and a second inhibitory input is present. For that reason, the behaviour of a detailed morphological conductance-based compartmental deterministic model of CN is compared to a stochastic counterpart. Further to investigate the generality of some of the results, a parallel comparison is carried out for a LVb pyramidal neuron.

6.4.1 CN neuronal arithmetic and noise

The putative impact of noise on the mathematical operations occurring during synaptic integration in the CN neuron is addressed at two distinct levels, ion channel noise and synaptic noise.

Ion channel noise can affect the characteristics of neuronal output firing patterns, by introducing substantial fluctuations in the membrane voltage. The interplay between factors such as channel kinetics, single channel conductance, cellular distribution and density, open probability and electrical membrane properties (for example, capacitance) and dendritic morphology influence the stochastic membrane potential fluctuations. Subsequently, they can affect the initiation and propagation of dendritic spikes that is translated to a probabilistic generation of somatic spikes, in the firing pattern (Cannon et al., 2010; Kole et al., 2006). The current study is focused more on the quantitative feature of the output firing, namely, if the probabilistic generation of spikes is reflected by higher firing rates, rather than the time fidelity of spiking. Thus, an analysis of the temporal features of the firing pattern is not carried out here.

The simulations of the stochastic CN model confirm that a stochastic implementation of ion channels results in the generation of noisy membrane potential fluctuations. Nevertheless, the comparison to a deterministic counterpart CN model shows no substantial difference in the firing rates in response to synaptic input between the two models. Equivalent results are also obtained when the synaptic noise is not present, and both models are driven with injected current, or when the synaptic input is distributed across a cellular subregion, rather than delivered to a single branch location. Further, the impact of the single channel conductance on the membrane potential fluctuations is in agreement with previous studies, namely, for a constant current density increasing the single channel conductance and scaling down the total number of channels will increase the amplitude of the voltage fluctuations (Diba et al., 2006; Faisal et al., 2008; Kole et al., 2006; White et al., 2000). This impact of stochastic ion channel gating on voltage fluctuations, however, is not translated into a change in the mean

output firing rate of the stochastic CN neuronal model. Therefore, the membrane voltage fluctuations due to the random gating of the ion channels are not adequate to change the I-O relationship, by means of altering the mean output firing rate, even if they are expected to modify the fidelity of spiking (Cannon et al., 2010; Diba et al., 2006; Faisal et al., 2008; Kole et al., 2006; White et al., 2000). One possible explanation is that the noise generated by the stochastic ion channels is either too small (Chance et al., 2002; Kole et al., 2006) or in some cases masked by the synaptic input noise (Destexhe et al., 2003; Faisal et al., 2008). However, since the response of the stochastic CN model to current injection is also similar to the deterministic one, it is more likely that the ion channel noise is not adequate to affect the mean output firing of the CN neuron. Further, dendritic morphology shapes the impact of ion channel noise on membrane potential fluctuations. The fluctuations of the resting membrane potential are increased with distance from the soma for neurons enriched with stochastic ion channels. However, this phenomenon depends on the specific channel kinetics, and the ion channel distribution and density across the neuronal cell (Cannon et al., 2010). Hence, ion channel driven membrane voltage fluctuations in neurons with different morphologies and channel profiles from the stochastic CN neuron might have a different influence on the mean output firing rate.

On the other hand, the synaptic noise has a more profound effect on the neuronal response of the CN neuron. When the CN neuron is driven with excitatory synaptic input or injected current and a second inhibitory input is delivered along the somato-dendritic axis, the gain of the neuronal response is modulated in an input location-dependent manner. The synaptic noise, generated by the inhibitory input, appears to contribute to this divisive effect by acting as a neuron-wide background source of noise (Chance et al., 2002; Hamann et al., 2002; Ly and Doiron, 2009; Mitchell and Silver, 2003). The modulatory effect of the inhibition is independent of the presence of ion channel noise; the amplitude of the membrane potential fluctuations in the full stochastic ion channel model is too small to affect the mean spiking output rate.

Therefore, a dual functional role of neuronal noise is identified for the CN neuron. The first is the effect of the ion channel noise on the fidelity of the CN spike trains. While this phenomenon is not studied thoroughly in the current investigation, evidence from previous studies support it (Cannon et al., 2010; Diba et al., 2006; Faisal et al., 2008; Kole et al., 2006; White et al., 2000). Hence, the ion channel noise could affect temporal coding in CN neurons (Steuber and Jaeger, 2013).

The second is the introduction of divisive modulations to the neuronal I-O relationship, via the synaptic input variability. This is evident in both the CN and LVb pyramidal neurons. The functional impact of noise arises both from the excitatory and inhibitory synaptic inputs Thus, synaptic noise has an impact on rate coding in the CN and LVb pyramidal neuron (Silver, 2010; Steuber and Jaeger, 2013).

6.4.2 Input-location dependent gain modulation

A systematic investigation of an already proposed mechanism of gain modulation (Prescott and De Koninck, 2003) is carried out. The mechanism assumes the synaptic noise and dendritic saturation as key players for gain modulating the mean firing output rate. The approach undertaken in the current study, unveils further the impact of the morphology and the background noise on the integration of synaptic inputs.

The morphological influence is evident in many aspects. Firstly, it is via the relation of neuronal response with the input distance from the soma. The output firing rate of a neuron depends on the input site delivery, since the input signals attenuate as they propagate to the soma. Thus, the lower mean firing rates of the CN and PN neurons for distal inputs are in agreement with previous studies (London and Häusser, 2005; Papoutsi et al., 2014) and only being reduced further by the presence of the inhibitory input. However, the presence of active ion Ca^{2+} channels in the dendrites of the Purkinje cell, amplify the distal synaptic signals by generating dendritic spikes, in a non-NMDA dependent manner. As a result, the somatic response to excitatory synaptic inputs is independent of the exact synaptic delivery site (De Schutter and Bower, 1994). Such a phenomenon, though, is not apparent for both neurons, in the current study. Moreover, distal synaptic inputs are usually located on thinner dendrites, compared to the thicker perisomatic and proximal branches or the soma itself. Therefore, the effect of dendritic saturation that is more evident in thinner compartments, could trigger distinct types of modulation (Prescott and De Koninck, 2003). This is the case in the current study for the CN neuron, where distal inputs are divisively modulated in a distance systematic way, in the CN neuron. For the LVb pyramidal neuron, the extent of modulation is not systematically correlated to the distance from the soma.

Secondly, via the structure of the cell. The mechanism is tested in two neuronal types (CN and LVb pyramidal neuron) with characteristic distinct dendritic morphology. Although, the distant-dependent divisive gain modulation of excitatory inputs occurs in both neurons in the presence of neuron-wide inhibitory input, the mathematical operations taking place for

input to the somatic and perisomatic sites of the CN neuron are mainly additive. This is not the case, however, for the LVb pyramidal neuron, where proximal to the soma dendritic operations are divisive too. In addition, the extent of change in gain for the trunk is smaller than it would be expected for the distance from the soma. Nevertheless, the same nonlinear mechanism, namely, dendritic saturation, appears to underlie multiplicative operations in both neuronal models. In the LVb pyramidal neuron, the thick structure of trunk dendritic compartments, and the resulting reduced local input resistance, might attenuate these nonlinearities. Hence, the cellular architecture might have a stronger impact, by not only facilitating dendritic saturation effects, but also allowing similar underlying nonlinearities of the relation of excitatory input conductance to output firing rate occur in other neuronal regions, such as proximal to soma locations, leading to different modulatory operations in different neurons.

However, pyramidal neurons can exhibit different gain operations for similar input locations and the stimulation parameters are critical, because different experimental conditions can mask or unveil mathematical operations. Colocalized excitatory and inhibitory inputs in an apical or basal pyramidal neuron region have a subtractive effect on the I-O relationship. But, when inhibition is placed after the excitation and on the path to the soma, it performs a divisive modulation of the neuronal firing rate (Jadi et al., 2012; Pouille et al., 2013). In the electric brown ghost knife fish pyramidal cell in the electrosensory lateral line lobe (EEL), excitation placed on different apical (distal or more proximal to the soma) sites or on basal dendrites is divisively modulated by apical dendritic inhibition. Somatic inhibition, however, has a subtractive effect on apical or basal inputs (Mehaffey, 2005). Similarly, somatic shunting inhibition acts in a subtractive way (Holt and Koch, 1997), but in combination with dendritic saturation and background noise, can act divisively to the distal dendritic inputs (Prescott and De Koninck, 2003). Moreover, the background balance of (dendritic) synaptic and inhibitory inputs modulates only dendritic inputs in a divisive manner (Jarvis et al., 2016). Such impact of the relative distribution of the driving and modulatory input on the CN neuronal arithmetic is not known to date. Regardless, neurons might be able to adjust their gain operations, according to the colocalization or not of their inputs.

Third, the dendritic morphology, and in particular the various dendritic subregions, are suggested to be modulated by the neuron-wide inhibition to a different extent and manner between the two neuronal types. As mentioned above, prior studies have indicated the role of specific subregions in gain modulation. The different configuration of excitatory and inhibitory inputs in different regions of the pyramidal neuron can give rise to distinct computations (Jadi

et al., 2012; Mehaffey, 2005; Pouille et al., 2013). In addition, removing background (noisy-free) excitatory and inhibitory input from dendritic subregions, transforms them to current sinks and consequently lessens the gain modulation potential of a neuron (Jarvis et al., 2016). This suggests that the background input could perform different types of arithmetic operation to the driving input to different regions, as it is also shown in the current study.

Further, it implies a functional compartmentalization of the neuron, dependent on the subregion where the excitatory inputs are delivered. Such functional distinct domains are found in pyramidal neurons, which receive inputs from different cortical layers or brain regions (Spruston, 2008). An equivalent compartmentalization in the CN neuron is yet to be discovered. However, CN neurons receive excitatory input from different sources (mossy and climbing fibers) that could be organized in functional distinct regions. In addition, CN neurons show a mixture response, including being gain modulated, to translation and tilt head motions (Yakusheva et al., 2007). Input organization could take place for the excitatory inputs of the CN that could converge onto one subregion and undergo multiplicative operations.

The noise, originating from the intrinsic synaptic input variability, results in enhanced divisive gain modulation, for both neuronal models. Consequently, stronger or more noisy Purkinje input onto the CN neurons (or equivalent synaptic excitation or inhibition onto the LVb pyramidal neuron) would cause a greater change in gain between the different synaptic locations or regions. Therefore, an additional level of gain control is available. Nevertheless, gain mechanism is robust in the presence of ion channel noise, in the CN neuronal model.

The input-location dependent change in gain is correlated to the input synchronicity in LVb pyramidal neuron. Asynchronous excitatory inputs enhance the divisive modulatory effect in LVb pyramidal neuron (Li and Ascoli, 2008), without the requirement of the dendrites to be equipped with active properties that support regenerative events or spike adaptation (Fernandez and White, 2010; Li and Ascoli, 2008; Mehaffey, 2005). On the other hand, introducing asynchronicity in the synaptic excitatory inputs delivered in the CN neuronal model does not result in enhanced change in gain, compared to the asynchronous synaptic excitatory input. Nonetheless, both neurons are characterized by a distinguished morphology (Hay et al., 2011; Steuber et al., 2011), and the structural properties of dendritic trees are known to impact the spatiotemporal summation of the excitatory postsynaptic potentials (London and Häusser, 2005; Papoutsi et al., 2014). Even, in the same neuron, for instance, the rat CA1 pyramidal neuron, subtle differences in the geometrical features of oblique branch points, alter the branch

excitability, synchrony of synaptic inputs originating from different branches, and coupling between dendritic and somatic spikes (Ferrante et al., 2013). Thus, diversity in the morphological features between neuronal types, could affect drastically their computational properties.

7 Conclusions

7.1 General discussion

The aim of this thesis is to provide an insight into the computational properties of CN neurons. The key focus is set on two related objectives, the role of ion channel noise and the mechanism of gain modulation. To study the first one, stochasticity is implemented in the gating of the voltage-gated ion channels of a detailed conductance-based CN neuronal model. The second objective is investigated in both the deterministic and stochastic CN neuronal models, but as a control also in a detailed deterministic conductance-based LVb pyramidal neuron.

7.1.1 CN neuronal model with ion channel noise

In this study, conductance-based CN and LVb pyramidal neuronal models with detailed biophysical and morphological properties are utilized. The use of compartmental models to elucidate nervous system function has been proven extremely valuable, by providing predictions and insights that shape new avenues for nervous system research. Experimental evidence is always the reference point for theoretical and computational neuroscience. Therefore, the implementation of ion channel noise, an existing biological phenomenon, in a computational CN model already tuned to replicate experimental data is a step further to produce a more realistic computational model. In that context, one of the outcomes of this thesis is a more biologically accurate CN neuronal model.

To develop the mentioned stochastic CN model, a systematic approach is applied. Each of the known CN voltage-gated ion channels is modelled to reproduce the stochastic gating. The modelling strategy is based on Markovian assumptions, because it offers a more realistic representation of the ion channel kinetic scheme, compared to the classic Hodgkin-Huxley formalism, and therefore the simulation results have in principle the potential to be closer to experimental recordings. The behaviour of each voltage-gated channel is tested both in a simple compartmental model and in the detailed CN model. In order to validate the translation from deterministic channels, the temporal stochastic voltage or current mean of an ion channel population is compared to the deterministic one. An approach like this allows the observation of the stochastic behaviour and its dependence on parameters, such as the single channel conductance. This thesis provides a systematic analysis of the correlation of these parameters with the CN voltage-gated ion channel and consequently neuronal behaviour. In addition, it is highlighted that the main effect of ion channel noise on the CN neuronal behaviour is the probabilistic generation of actions potentials in the output spike pattern.

However, the temporal mean voltage (and current) behaviour of the NaF channel, which a voltage-gated channel with fast kinetics, could not match its deterministic counterpart. One possible explanation could be the choice of appropriate integration method and integration time step for the simulation. Indeed, as the findings of this research confirm again, smaller integration time steps give more accurate results, because they allow the registration of faster gating events. However, smaller time steps are associated with accumulation of numerical errors and high computational cost. It is suggested here that an integration method with a dynamic time step would be a wiser choice for fast kinetics modelling.

Nonetheless, the investigation in this thesis indicates that the match of the stochastic and the deterministic representation of a voltage-gated channel with fast kinetics might not be possible under specific conditions, even if the integration time step is small enough. A hypothesis is that the distribution of the open channels of voltage-gated ion channels might be rectified if their channel kinetics and state variable characteristics allow the generation of a window current in the absence of any external stimulus such as synaptic input or injected current. For this to occur, the equilibrium current should be close to zero and the number of open channels exhibit fluctuations with a magnitude greater than zero. The result would be a shift of the stochastic equilibrium up, compared to the deterministic one. An additional explanation could be that multiple events could take place in a given time step due to the fast transition rates between the kinetic states. Both effects could take place simultaneously, adding

to the observed discrepancy between the response of the stochastic and the deterministic models. However, to verify, the hypothesis of the rectification effect and the impact of fast transition rates more investigation is needed, extending the research undertaken in this thesis.

7.1.2 Gain modulation

The study of single neuron arithmetic is fundamental to comprehend brain function. Such studies have been mainly conducted in pyramidal neurons, due to their presence in areas usually associated with higher cognitive functions, or for reasons related to experimental constraints, such as the thick apical trunk that allowed experimental manipulations, before more refined methods of exploring electrical excitability were developed. The cerebellum has a pluripotent function as well, extending from motor control and coordination to visual processing, memory and decision making, and CN neurons are assigned with processing the cerebellar output. Therefore, the study of their computational properties could unravel how the cerebellum carries out its important functions for the organism.

The main objective of this thesis is to study in a systematic way the computational properties of a stochastic CN neuronal model. As reviewed, ion channel noise can have functional implications for neuronal function, and its impact is related to the neuronal morphology. Ion channel noise causes larger membrane voltage fluctuations in thin neuronal compartments favouring probabilistic spiking, compared to the thick ones proximal to the soma. Thus, a gradient of multiplicative integration could exist along the neuronal dendrite, with strong multiplicative operations taking place at distal locations, which are replaced with linear summation for proximal to somatic ones. However, as the findings of this study demonstrate, the introduction of ion channel noise to a CN neuronal model only affects the spiking fidelity, but the mean output firing and rate-coded neuronal computations remain unaffected.

Nevertheless, the input location defines the arithmetic operations of the neuron. The main finding of this thesis is that the CN neuron utilizes different integration modes for the inputs in distinct locations, in a systematic manner. In particular, distal excitatory synaptic inputs undergo a multiplicative modulation by inhibitory synaptic input, which becomes systematically less apparent when the input location is shifted towards to the somatic and perisomatic areas. The underlying mechanism is the combined effect of dendritic saturation and synaptic noise, arising from both the excitatory and inhibitory synaptic input. In particular, dendritic saturation is crucial as it introduces a nonlinear relationship between the excitatory

input conductance and output firing rate. Although this multiplicative process takes place in the distal areas of both CN and LVb pyramidal neurons, the two types of neurons exhibit different arithmetic operations for input to their proximal regions. In the pyramidal neuron, more apparent multiplicative operations occur along the perisomatic area. In addition, the extent of gain modulation in the LVb pyramidal neurons appears not to be systematically related to the input location as in the CN neuron. In the LVb pyramidal neuron the change in gain for trunk is smaller than it would be expected for the distance from the soma. This is due the reduced local input resistance, as the trunk is characterized by large diameter. Hence, the results of this thesis indicate that different neurons might apply the same gain mechanism in distinct ways.

In pyramidal neurons, functional compartmentalization based on the origin of synaptic inputs is a popular concept. A similar hypothesis has not been expressed for the CN neuron, so far. Nonetheless, the outputs of this study suggest that different neuronal regions might support different function since they vary in the extent of change in gain modulation.

Moreover, it is shown that synchronicity of the driving synaptic input has a different effect on the extent of gain change between the two neuronal models. The change in gain is sensitive to the synchronicity of the excitatory synaptic input only in the LVb pyramidal neuronal model, implying that neurons might apply this as a second level of shaping the integration of their inputs.

Lastly, since both neuronal models used in this study share similar types of ion channels, but distinct morphologies, it is implied that the latter might contribute greatly to the differences in the computational properties of both neurons.

7.2 Future work

The following future avenues to explore can be considered:

- The simulations in the current study are performed in the NEURON simulation environment (Hines and Carnevale, 1997), and the integration method to solve the set of the model's ordinary differential equations is backward Euler. As shown in this thesis, such an algorithm might not be suitable for the description of the stochastic gating of the CN ion channels. Therefore, it is suggested that the same analysis performed here is repeated with the implementation of a stochastic simulation

algorithm, such as Gillespie. Then, the hypothesis of the effect of the rectified open channel distribution could be examined in detail.

- The findings of this thesis indicate that ion channel noise introduces variability to the timing of the spikes in the CN output rate, with each stochastic voltage-gated channel affecting the CN firing pattern differently. Thus, an analysis of the temporal features of the firing pattern could be carried out here, when the CN model is enriched with stochastic voltage-gated channels.
- Functional compartmentalization, as it is demonstrated here, might also be applied in the CN neurons. Further experimental and theoretical investigation, where the synaptic stimulation of specific regions is associated with a specific behavioural task could shed light on this.
- An important future study would be the experimental testing of the arithmetic operations predicted in this thesis for the CN and LVb pyramidal neurons, aiming to verify the relation of change in gain to the input location.
- The findings here suggest that the shape of the dendritic tree might affect the extent of change in gain. Therefore, a systematic theoretical study could confirm this and identify related morphological patterns or features.
- There is a great variability in the morphology of the CN neurons. A step further to this research could be the building of a cerebellar neural network, including CN neurons with distinct morphology and studying the impact of their computational properties on the network activity

8 Bibliography

Adolphs, R., 2015. The unsolved problems of neuroscience. Trends Cogn. Sci. doi:10.1016/j.tics.2015.01.007

Aizenman, C.D., Linden, D.J., 1999. Regulation of the rebound depolarization and spontaneous firing patterns of deep nuclear neurons in slices of rat cerebellum. J. Neurophysiol. doi:10.1152/jn.1999.82.4.1697

Alexander, S.P.H., Striessnig, J., Kelly, E., Marrion, N. V., Peters, J.A., Faccenda, E., Harding, S.D., Pawson, A.J., Sharman, J.L., Southan, C., Davies, J.A., 2017. The concise guide to PHARMACOLOGY 2017/18: Voltage-gated ion channels. Br. J. Pharmacol. doi:10.1111/bph.13884

Andersen, R. a, Mountcastle, V.B., 1983. The influence of the angle of gaze upon the excitability of the light-sensitive neurons of the posterior parietal cortex. J. Neurosci. 3, 532–48.

Andersen, R.A., Essick, G.K., Siegel, R.M., 1985. Encoding of spatial location by posterior parietal neurons. Science 230, 456–458. doi:10.1126/science.4048942

Antic, S.D., Zhou, W.L., Moore, A.R., Short, S.M., Ikonomu, K.D., 2010. The decade of the dendritic NMDA spike. J. Neurosci. Res. 88, 2991–3001. doi:10.1002/jnr.22444

Apps, R., Garwicz, M., 2005. Anatomical and physiological foundations of cerebellar information processing. Nat. Rev. Neurosci. 6, 297–311. doi:10.1038/nrn1646

Ayaz, A., Chance, F.S., 2009. Gain modulation of neuronal responses by subtractive and

divisive mechanisms of inhibition. J. Neurophysiol. 101, 958–68. doi:10.1152/jn.90547.2008

Azouz, R., 2005. Dynamic spatiotemporal synaptic integration in cortical neurons: neuronal gain, revisited. J. Neurophysiol. 94, 2785–2796. doi:10.1152/jn.00542.2005

Baranauskas, G., Tkatch, T., Nagata, K., Yeh, J.Z., Surmeier, D.J., 2003. Kv3.4 subunits enhance the repolarizing efficiency of Kv3.1 channels in fast-spiking neurons. Nat. Neurosci. 6, 258–266. doi:10.1038/nn1019

Baranauskas, G., Tkatch, T., Surmeier, D.J., 1999. Delayed rectifier currents in rat globus pallidus neurons are attributable to Kv2.1 and Kv3.1/3.2 K+ channels. J Neurosci 19, 6394–6404.

Baumel, Y., Jacobson, G.A., Cohen, D., 2009. Implications of functional anatomy on information processing in the deep cerebellar nuclei. Front. Cell. Neurosci. 3, 14. doi:10.3389/neuro.03.014.2009

Behabadi, B.F., Polsky, A., Jadi, M., Schiller, J., Mel, B.W., 2012. Location-Dependent Excitatory Synaptic Interactions in Pyramidal Neuron Dendrites. PLoS Comput. Biol. 8, e1002599. doi:10.1371/journal.pcbi.1002599

Berends, M., Maex, R., Schutter, E. De, 2005. The Effect of NMDA Receptors on Gain Modulation. Neural Comput. 17, 2531–2547. doi:10.1162/089976605774320520

Bezanilla, F., 2008. How membrane proteins sense voltage. Nat. Rev. Mol. Cell Biol. 9, 323–332. doi:10.1038/nrm2376

Boussaoud, D., Jouffrais, C., Bremmer, F., 1998. Eye position effects on the neuronal activity of dorsal premotor cortex in the macaque monkey. J. Neurophysiol. 80, 1132–1150.

Bremmer, F., Ilg, U.J., Thiele, A., Distler, C., Hoffmann, K.P., 1997. Eye position effects in monkey cortex. I. Visual and pursuit-related activity in extrastriate areas MT and MST. J. Neurophysiol. 77, 944–961.

Brizzi, L., Meunier, C., Zytnicki, D., Donnet, M., Hansel, D., D'Incamps, B.L., Van Vreeswijk, C., 2004. How shunting inhibition affects the discharge of lumbar motoneurones: a dynamic clamp study in anaesthetized cats. J. Physiol. 558, 671–683. doi:10.1113/jphysiol.2003.059964

Brotchie, P.R., Andersen, R.A., Snyder, L.H., Goodman, S.J., 1995. Head position signals used by parietal neurons to encode locations of visual stimuli. Nature 375, 232–235. doi:10.1038/375232a0

Brozović, M., Abbott, L.F., Andersen, R.A., 2008. Mechanism of gain modulation at single neuron and network levels. J. Comput. Neurosci. 25, 158–168. doi:10.1007/s10827-007-0070-6

Burkitt, A.N., Meffin, H., Grayden, D.B., 2003. Study of neuronal gain in a conductance-based leaky integrate-and-fire neuron model with balanced excitatory and inhibitory synaptic input. Biol. Cybern. 89, 119–125. doi:10.1007/s00422-003-0408-8

Butts, D.A., Goldman, M.S., 2006. Tuning curves, neuronal variability, and sensory coding. PLoS Biol. 4, 639–646. doi:10.1371/journal.pbio.0040092

Cannon, R.C., D'Alessandro, G., 2006. The ion channel inverse problem: neuroinformatics meets biophysics. PLoS Comput. Biol. 2, e91. doi:10.1371/journal.pcbi.0020091

Cannon, R.C., O'Donnell, C., Nolan, M.F., 2010. Stochastic ion channel gating in dendritic neurons: morphology dependence and probabilistic synaptic activation of dendritic spikes. PLoS Comput. Biol. 6. doi:10.1371/journal.pcbi.1000886

Canto, C.B., Witter, L., De Zeeuw, C.I., 2016. Whole-cell properties of cerebellar nuclei neurons in vivo. PLoS One 11, 1–19. doi:10.1371/journal.pone.0165887

Capaday, C., 2002. A re-examination of the possibility of controlling the firing rate gain of neurons by balancing excitatory and inhibitory conductances. Exp. Brain Res. 143, 67–77. doi:10.1007/s00221-001-0970-z

Cardin, J.A., Palmer, L.A., Contreras, D., 2008. Cellular Mechanisms Underlying Stimulus-Dependent Gain Modulation in Primary Visual Cortex Neurons In Vivo. Neuron 59, 150–160. doi:10.1016/j.neuron.2008.05.002

Chance, F., Abbott, L.F., 2009. Simulating in vivo background activity in a slice with the dynamic clamp. Dyn. From Princ. to Appl. 73–87. doi:10.1007/978-0-387-89279-5

Chance, F.S., Abbott, L.F., Reyes, A.D., 2002. Gain modulation from background synaptic input. Neuron 35, 773–82.

Cuntz, H., Remme, M.W.H., Torben-Nielsen, B., 2014. The Computing Dendrite From

Structure to Function, in: The Computing Dendrite. pp. 1–110. doi:10.1007/978-1-4614-8094-5

D'Angelo, E., Antonietti, A., Casali, S., Casellato, C., Garrido, J.A., Luque, N.R., Mapelli, L., Masoli, S., Pedrocchi, A., Prestori, F., Rizza, M.F., Ros, E., 2016. Modeling the Cerebellar Microcircuit: New Strategies for a Long-Standing Issue. Front. Cell. Neurosci. 10, 1–29. doi:10.3389/fncel.2016.00176

D'Angelo, E., Casali, S., 2013. Seeking a unified framework for cerebellar function and dysfunction: from circuit operations to cognition. Front. Neural Circuits 6, 1–23. doi:10.3389/fncir.2012.00116

De Schutter, E., Bower, J.M., 1994. Simulated responses of cerebellar Purkinje cells are independent of the dendritic location of granule cell synaptic inputs. Proc. Natl. Acad. Sci. U. S. A. 91, 4736–4740. doi:10.1073/pnas.91.11.4736

De Zeeuw, C.I., Hoebeek, F.E., Bosman, L.W.J., Schonewille, M., Witter, L., Koekkoek, S.K., 2011. Spatiotemporal firing patterns in the cerebellum. Nat. Rev. Neurosci. 12, 327–344. doi:10.1038/nrn3011

Destexhe, A., Paré, D., Willmore, B.D.B., Cooke, J.E., King, A.J., Physiol, J., 2014. Impact of Network Activity on the Integrative Properties of Neocortical Pyramidal Neurons In Vivo Impact of Network Activity on the Integrative Properties of Neocortical Pyramidal Neurons In Vivo 1531–1547.

Destexhe, A., Rudolph, M., Paré, D., 2003. The high-conductance state of neocortical neurons in vivo. Nat. Rev. Neurosci. 4, 1019–1019. doi:10.1038/nrn1289

Diba, K., Koch, C., Segev, I., 2006. Spike propagation in dendrites with stochastic ion channels. J. Comput. Neurosci. 20, 77–84. doi:10.1007/s10870-006-4770-0

Diba, K., Lester, H., Koch, C., 2004. Intrinsic Noise in Cultured Hippocampal Neurons: Experiment and Modeling. J. Neurosci. 24, 9723–9733. doi:10.1523/JNEUROSCI.1721-04.2004

Disney, A.A., Aoki, C., Hawken, M.J., 2007. Gain Modulation by Nicotine in Macaque V1. Neuron 56, 701–713. doi:10.1016/j.neuron.2007.09.034

Doiron, B., Longtin, a, Berman, N., Maler, L., 2001. Subtractive and divisive inhibition: effect of voltage-dependent inhibitory conductances and noise. Neural Comput. 13, 227–48.

Donnell, C.O., Nolan, M.F., 2014. The Computing Dendrite. Springer Series in Computational Neuroscience 11. doi:10.1007/978-1-4614-8094-5

Dorval, A.D., 2005. Channel Noise is Essential for Perithreshold Oscillations in Entorhinal Stellate Neurons. J. Neurosci. 25, 10025–10028. doi:10.1523/JNEUROSCI.3557-05.2005

Dudman, J.T., Nolan, M.F., 2009. Stochastically gating ion channels enable patterned spike firing Through activity-dependent modulation of spike probability. PLoS Comput. Biol. 5. doi:10.1371/journal.pcbi.1000290

Ermentrout, G.B., Galán, R.F., Urban, N.N., 2008. Reliability, synchrony and noise. Trends Neurosci. 31, 428–434. doi:10.1016/j.tins.2008.06.002

Faisal, A.A., Selen, L.P.J., Wolpert, D.M., 2008. Noise in the nervous system. Nat. Rev. Neurosci. 9, 292–303. doi:10.1038/nrn2258

Faisal, A.A., White, J.A., Laughlin, S.B., 2005. Ion-channel noise places limits on the miniaturization of the brain's wiring. Curr. Biol. 15, 1143–1149. doi:10.1016/j.cub.2005.05.056

Fellous, J.M., Rudolph, M., Destexhe, A., Sejnowski, T.J., 2003. Synaptic Background Noise Controls the Input / Output Characteristics of Single Cells in an in Vitro Model of in Vivo Activity 122, 811–829. doi:10.1016/j.neuroscience.2003.08.027

Fernandez, F.R., White, J.A., 2010. Gain Control in CA1 Pyramidal Cells Using Changes in Somatic Conductance. J. Neurosci. 30, 230–241. doi:10.1523/JNEUROSCI.3995-09.2010

Ferrante, M., Migliore, M., Ascoli, G.A., 2013. Functional impact of dendritic branch-point morphology. J. Neurosci. 33, 2156–65. doi:10.1523/JNEUROSCI.3495-12.2013

Gabbiani, F., MIDTGAARD, J., Knopfel, T., 1994. Synaptic Integration in a Model of Cerebellar Granule Cells. J. Neurophysiol. 72, 999–1009.

Galletti, C., Battaglini, P.P., 1989. Gaze-dependent visual neurons in area V3A of monkey prestriate cortex. J. Neurosci. 9, 1112–1125.

Gauck, V., Thomann, M., Jaeger, D., Borst, a, 2001. Spatial distribution of low- and high-voltage-activated calcium currents in neurons of the deep cerebellar nuclei. J. Neurosci. 21, RC158. doi:20015463 [pii]

Halloran, C.J.O., Kinsella, G.J., Storey, E., 2011. Journal of Clinical and Experimental Neuropsychology The cerebellum and neuropsychological functioning : A critical review The cerebellum and neuropsychological functioning : A critical review 37–41.

Hamann, M., Rossi, D.J., Attwell, D., 2002. Tonic and spillover inhibition of granule cells control information flow through cerebellar cortex. Neuron 33, 625–633. doi:10.1016/S0896-6273(02)00593-7

Harris, K.D., Shepherd, G.M.G., 2015. The neocortical circuit: themes and variations. Nat. Neurosci. 18, 170–181. doi:10.1038/nn.3917

Hay, E., Hill, S., Schürmann, F., Markram, H., Segev, I., 2011. Models of neocortical layer 5b pyramidal cells capturing a wide range of dendritic and perisomatic active properties. PLoS Comput. Biol. 7. doi:10.1371/journal.pcbi.1002107

Hay, E., Segev, I., 2015. Dendritic excitability and gain control in recurrent cortical microcircuits. Cereb. Cortex 25, 3561–3571. doi:10.1093/cercor/bhu200

Heck, D.H., 2015. The Neuronal Codes of the Cerebellum. The Neuronal Codes of the Cerebellum 33, 1–264. doi:10.1016/C2013-0-23273-6

Herzfeld, D.J., Kojima, Y., Soetedjo, R., Shadmehr, R., 2015. Encoding of action by the Purkinje cells of the cerebellum. Nature 526, 439–42. doi:10.1038/nature15693

Higgs, M.H., Slee, S.J., Spain, W.J., 2006. Diversity of Gain Modulation by Noise in Neocortical Neurons: Regulation by the Slow Afterhyperpolarization Conductance. J. Neurosci. 26, 8787–8799. doi:10.1523/JNEUROSCI.1792-06.2006

Hille, B., 2001. Ion Channels of Excitable Membranes, 3rd ed, Sinauer Associates, Sunderland. doi:10.1007/3-540-29623-9_5640

Hines, M.L., Carnevale, N.T., 1997. The NEURON simulation environment. Neural Comput. 9, 1179–1209. doi:10.1162/neco.1997.9.6.1179

Hines, M.L., Morse, T., Migliore, M., Carnevale, N.T., Hines, M.L., 2004. ModelDB: A Database to Support Computational Neuroscience. J. Comput. Neurosci. 17, 7–11. doi:10.1023/B:JCNS.0000023869.22017.2e

Hô, N., Destexhe, a, 2000. Synaptic background activity enhances the responsiveness of neocortical pyramidal neurons. J. Neurophysiol. 84, 1488–1496.

Holt, G.R., Koch, C., 1997. Shunting inhibition does not have a divisive effect on firing rates. Neural Comput. 9, 1001–13.

Jacobson, G.A., Diba, K., Yaron-Jakoubovitch, A., Oz, Y., Koch, C., Segev, I., Yarom, Y., 2005. Subthreshold voltage noise of rat neocortical pyramidal neurones. J. Physiol. 564, 145–60. doi:10.1113/jphysiol.2004.080903

Jadi, M., Polsky, A., Schiller, J., Mel, B.W., 2012. Location-dependent effects of inhibition on local spiking in pyramidal neuron dendrites. PLoS Comput. Biol. 8. doi:10.1371/journal.pcbi.1002550

Jahnsen, H., 1986. Extracellular activation and membrane conductances of neurones in the guinea-pig deep cerebellar nuclei in vitro. J. Physiol. doi:10.1113/jphysiol.1986.sp016002

Jarvis, S., Nikolic, K., Schultz, S., 2016. Neuronal gain modulability is determined by dendritic morphology: a computational optogenetic study. bioRxiv.

Johansson, S., Arhem, P., 1994. Single-channel currents trigger action potentials in small cultured hippocampal neurons. Proc. Natl. Acad. Sci. U. S. A. 91, 1761–5.

Kaas, J.H., 2011. Neocortex in early mammals and its subsequent variations. Ann. N. Y. Acad. Sci. 1225, 28–36. doi:10.1111/j.1749-6632.2011.05981.x

Kandel, E.R., Schwartz, J.H., Jessell, T.M., Siegelbaum, S.A., Hudspeth, A.J., 2014. Principles of Neural Science, Fifth Edition, Neurology. doi:10.1036/0838577016

Kavalali, E.T., 2014. The mechanisms and functions of spontaneous neurotransmitter release. Nat. Rev. Neurosci. 16, 5–16. doi:10.1038/nrn3875

Khojasteh, E., Galiana, H.L., 2009. Implications of gain modulation in brainstem circuits: VOR control system. J. Comput. Neurosci. 27, 437–451. doi:10.1007/s10827-009-0156-4

Knöpfel, T., 2013. Handbook of the Cerebellum and Cerebellar Disorders. doi:10.1007/978-94-007-1333-8

Kole, M.H.P., Hallermann, S., Stuart, G.J., 2006. Single Ih channels in pyramidal neuron dendrites: properties, distribution, and impact on action potential output. J. Neurosci. 26, 1677–87. doi:10.1523/JNEUROSCI.3664-05.2006

Le Bé, J.V., Silberberg, G., Wang, Y., Markram, H., 2007. Morphological, electrophysiological, and synaptic properties of corticocallosal pyramidal cells in the

neonatal rat neocortex. Cereb. Cortex 17, 2204–2213. doi:10.1093/cercor/bhl127

Lewis, A.H., Raman, I.M., 2014. Resurgent current of voltage-gated Na^+ channels. J. Physiol. 592, 4825–4838. doi:10.1113/jphysiol.2014.277582

Li, X., Ascoli, G.A., 2008. Effects of Synaptic Synchrony on the Neuronal Input-Output Relationship. Neural Comput. 20, 1717–1731. doi:10.1162/neco.2008.10-06-385

Lodish, H., Berk, A., Matsudaira, P., Kaiser, C., Krieger, M., Scott, M., Zipursky, S.L., Darnell, J., 2003. Molecular Cell Biology, 5th ed. W.H.Freeman & Co Ltd, Gordonsville, Virginia, USA.

London, M., Häusser, M., 2005. Dendritic computation. Annu. Rev. Neurosci. 28, 503–32. doi:10.1146/annurev.neuro.28.061604.135703

Longtin, A., Doiron, B., Bulsara, A.R., 2002. Noise-induced divisive gain control in neuron models. Biosystems. 67, 147–56.

Luthman, J., Hoebeek, F.E., Maex, R., Davey, N., Adams, R., De Zeeuw, C.I., Steuber, V., 2011. STD-dependent and independent encoding of input irregularity as spike rate in a computational model of a cerebellar nucleus neuron. Cerebellum 10, 667–82. doi:10.1007/s12311-011-0295-9

Ly, C., Doiron, B., 2009. Divisive gain modulation with dynamic stimuli in integrate-and-fire neurons. PLoS Comput. Biol. 5, e1000365. doi:10.1371/journal.pcbi.1000365

Magistretti, J., Alonso, A., 1999. Biophysical Properties and Slow Voltage-Dependent Inactivation of a Sustained Sodium Current in Entorhinal Cortex Layer-II Principal Neurons. J. Gen. Physiol. doi:10.1085/jgp.114.4.491

Marín-Padilla, M., 2014. The mammalian neocortex new pyramidal neuron: a new conception. Front. Neuroanat. 7, 51. doi:10.3389/fnana.2013.00051

McAdams, C.J., Maunsell, J.H., 1999. Effects of attention on orientation-tuning functions of single neurons in macaque cortical area V4. J Neurosci 19, 431–441.

Mehaffey, W.H., 2005. Deterministic Multiplicative Gain Control with Active Dendrites. J. Neurosci. 25, 9968–9977. doi:10.1523/JNEUROSCI.2682-05.2005

Mitchell, S.J., Silver, R.A., 2003. Shunting inhibition modulates neuronal gain during synaptic excitation. Neuron 38, 433–45.

Moberget, T., Ivry, R.B., 2016. Cerebellar contributions to motor control and language comprehension: Searching for common computational principles. Ann. N. Y. Acad. Sci. 1369, 154–171. doi:10.1111/nyas.13094

Molineux, M.L., McRory, J.E., McKay, B.E., Hamid, J., Mehaffey, W.H., Rehak, R., Snutch, T.P., Zamponi, G.W., Turner, R.W., 2006. Specific T-type calcium channel isoforms are associated with distinct burst phenotypes in deep cerebellar nuclear neurons. Proc. Natl. Acad. Sci. 103, 5555–5560. doi:10.1073/pnas.0601261103

Mountcastle, V.B., 1997. The columnar organization of the neocortex. Brain 120, 701–722. doi:10.1093/brain/120.4.701

Murphy, B.K., Miller, K.D., 2003. Multiplicative gain changes are induced by excitation or inhibition alone. J. Neurosci. 23, 10040–51. doi:23/31/10040 [pii]

Neishabouri, A., Faisal, a A., 2014. Axonal noise as a source of synaptic variability. PLoS Comput. Biol. 10, e1003615. doi:10.1371/journal.pcbi.1003615

O'Donnell, C., van Rossum, M.C.W., 2014. Systematic analysis of the contributions of stochastic voltage gated channels to neuronal noise. Front. Comput. Neurosci. 8, 105. doi:10.3389/fncom.2014.00105

Palmer, L.M., Shai, A.S., Reeve, J.E., Anderson, H.L., Paulsen, O., Larkum, M.E., 2014. NMDA spikes enhance action potential generation during sensory input. Nat. Neurosci. 17. doi:10.1038/nn.3646

Papoutsi, A., Kastellakis, G., Maria, P., Anastasakis, S., Poirazi, P., Psarrou, M., Anastasakis, S., Poirazi, P., 2014. Coding and decoding with dendrites. J. Physiol. Paris 108, 18–27. doi:10.1016/j.jphysparis.2013.05.003

Patel, A.X., Burdakov, D., 2015. Mechanisms of Gain control by voltage-gated channels in intrinsically-firing neurons. PLoS One 10, 1–26. doi:10.1371/journal.pone.0115431

Paulus, W., Rothwell, J.C., 2016. Membrane resistance and shunting inhibition: where biophysics meets state-dependent human neurophysiology. J. Physiol. 594, 2719–28. doi:10.1113/JP271452

Poleg-Polsky, A., Diamond, J.S., 2016. NMDA Receptors Multiplicatively Scale Visual Signals and Enhance Directional Motion Discrimination in Retinal Ganglion Cells. Neuron 89, 1277–1290. doi:10.1016/j.neuron.2016.02.013

Pouget, A., Sejnowski, T.J., 1997. Spatial Transformations in the Parietal Cortex Using Basis Functions. J. Cogn. Neurosci. doi:10.1162/jocn.1997.9.2.222

Pouille, F., Watkinson, O., Scanziani, M., Trevelyan, A.J., 2013. The contribution of synaptic location to inhibitory gain control in pyramidal cells. Physiol. Rep. 1, 1–9. doi:10.1002/phy2.67

Prescott, S. a, De Koninck, Y., 2003. Gain control of firing rate by shunting inhibition: roles of synaptic noise and dendritic saturation. Proc. Natl. Acad. Sci. U. S. A. 100, 2076–81. doi:10.1073/pnas.0337591100

Psarrou, M., Stefanou, S.S., Papoutsi, A., Tzilivaki, A., Cutsuridis, V., Poirazi, P., 2014. A simulation study on the effects of dendritic morphology on layer V prefrontal pyramidal cell firing behavior. Front. Cell. Neurosci. 8, 287. doi:10.3389/fncel.2014.00287

Purves, D., Augustine, G.J., Fitzpatrick, D., Hall, W.C., Lamantia, A.-S., Mcnamara, J.O., Willians, S.M., 2004. Neuroscience, Sunderland. doi:978-0878937257

Raman, I.M., Gustafson, A.E., Padgett, D., 2000. Ionic currents and spontaneous firing in neurons isolated from the cerebellar nuclei. J. Neurosci. 20, 9004–16. doi:20/24/9004 [pii]

Ramaswamy, S., Markram, H., 2015. Anatomy and physiology of the thick-tufted layer 5 pyramidal neuron. Front. Cell. Neurosci. 9, 233. doi:10.3389/fncel.2015.00233

Ramnani, N., 2006. The primate cortico-cerebellar system: anatomy and function. Nat. Rev. Neurosci. 7, 511–522. doi:10.1038/nrn1953

Rothman, J.S., Cathala, L., Steuber, V., Silver, R.A., 2009. Synaptic depression enables neuronal gain control. Nature 457, 1015–8. doi:10.1038/nature07604

Saab, C.Y., Willis, W.D., 2003. The cerebellum: organization, functions and its role in nociception. Brain Res. Brain Res. Rev. 42, 85–95.

Sailer, C.A., Kaufmann, W.A., Marksteiner, J., Knaus, H.G., 2004. Comparative immunohistochemical distribution of three small-conductance Ca2+-activated potassium channel subunits, SK1, SK2, and SK3 in mouse brain. Mol. Cell. Neurosci. 26, 458–469. doi:10.1016/j.mcn.2004.03.002

Sakmann, B., Neher, E., 1995. Single-Channel Recording, 2nd ed. Springer, Boston, MA, New York, NY. doi:doi.org/10.1007/978-1-4419-1229-9

Salinas, E., Abbott, L.F., 1997. Invariant visual responses from attentional gain fields. J. Neurophysiol. 77, 3267–72.

Salinas, E., Abbott, L.F., 1995. Transfer of coded information from sensory to motor networks. J. Neurosci. 15, 6461–74.

Salinas, E., Sejnowski, T.J., 2001. Gain modulation in the central nervous system: where behavior, neurophysiology, and computation meet. Neuroscientist 7, 430–440. doi:10.1177/107385840100700512

Sastry, B.R., Morishita, W., Yip, S., Shew, T., 1997. Pergamon GABA-ERGIC TRANSMISSION IN DEEP CEREBELLAR NUCLEI. Science (80-.). 53, 259–271. doi:10.1016/S0301-0082(97)00033-6

Schaller, K.L., Caldwell, J.H., 2003. Expression and distribution of voltage-gated sodium channels in the cerebellum. Cerebellum. doi:10.1080/14734220309424

Schlick, B., Flucher, B.E., Obermair, G.J., 2012. Voltage-Activated Calcium Channel Expression Profiles in Mouse Brain and Cultured Hippocampal Neurons. Neuroscience 167, 786–798. doi:10.1016/j.neuroscience.2010.02.037.VOLTAGE-ACTIVATED

Sholl, D. a., 1953. Dendritic organization in the neurons of the visual and motor cortices of the cat. J. Anat. 87, 387–406.1.

Shu, Y., Hasenstaub, A., Badoual, M., Bal, T., McCormick, D. a, 2003. Barrages of synaptic activity control the gain and sensitivity of cortical neurons. J. Neurosci. 23, 10388–10401. doi:23/32/10388 [pii]

Sigworth, F.J., 1980. The variance of sodium current fluctuations at the node of Ranvier. J. Physiol. 97–129.

Silver, R.A., 2010. Neuronal arithmetic. Nat Rev Neurosci 11, 474–489. doi:10.1038/nrn2864

Smith, M.R., Nelson, A.B., Du Lac, S., 2002. Regulation of firing response gain by calcium-dependent mechanisms in vestibular nucleus neurons. J. Neurophysiol. 87, 2031–42. doi:10.1152/jn.00821.2001

Sokolov, A.A., Miall, R.C., Ivry, R.B., 2017. The Cerebellum: Adaptive Prediction for Movement and Cognition. Trends Cogn. Sci. 21, 313–332. doi:10.1016/j.tics.2017.02.005

Spruston, N., 2008. Pyramidal neurons: dendritic structure and synaptic integration. Nat. Rev.

Neurosci. 9, 206–21. doi:10.1038/nrn2286

Stein, R.B., Gossen, E.R., Jones, K.E., 2005. Neuronal variability: noise or part of the signal? Nat. Rev. Neurosci. 6, 389–397. doi:10.1038/nrn1668

Steinmetz, P.N., Manwani, A., Koch, C., London, M., Segev, I., 2000. Subthreshold voltage noise due to channel fluctuations in active neuronal membranes. J. Comput. Neurosci. 9, 133–148. doi:10.1023/A:1008967807741

Sterratt, D., Graham, B., Science, C., Gillies, A., Limited, P., Willshaw, D., Neurobiology, C., 2010. Principles of Computational Modelling.

Steuber, V., Jaeger, D., 2013. Modeling the generation of output by the cerebellar nuclei. Neural Netw. 47, 112–9. doi:10.1016/j.neunet.2012.11.006

Steuber, V., Schultheiss, N.W., Silver, R.A., De Schutter, E., Jaeger, D., 2011. Determinants of synaptic integration and heterogeneity in rebound firing explored with data-driven models of deep cerebellar nucleus cells. J. Comput. Neurosci. 30, 633–58. doi:10.1007/s10827-010-0282-z

Stuart, G.J., Spruston, N., 2015. Dendritic integration: 60 years of progress. Nat. Neurosci. 18, 1713–1721. doi:10.1038/nn.4157

The Mathworks Inc., 2016. MATLAB - MathWorks [WWW Document]. www.mathworks.com/products/matlab. doi:2016-11-26

Tiesinga, P.H.E., José, J. V., Sejnowski, T.J., 2000. Comparison of current-driven and conductance-driven neocortical model neurons with Hodgkin-Huxley voltage-gated channels. Phys. Rev. E - Stat. Physics, Plasmas, Fluids, Relat. Interdiscip. Top. 62, 8413–8419. doi:10.1103/PhysRevE.62.8413

Tovee, M.J., Rolls, E.T., Azzopardi, P., 1994. Translation invariance in the responses to faces of single neurons in the temporal visual cortical areas of the alert macaque. J. Neurophysiol. 72, 1049–1060. doi:10.1002/9780470148150.ch12

Treue, S., Martínez Trujillo, J.C., 1999. Feature-based attention influences motion processing gain in macaque visual cortex. Nature 399, 575–579. doi:10.1038/21176

Trotter, Y., Celebrini, S., 1999. Gaze direction controls response gain in primary visual-cortex neurons. Nature 398, 239–242. doi:10.1038/18444

Ulrich, D., 2003. Differential arithmetic of shunting inhibition for voltage and spike rate in neocortical pyramidal cells. Eur. J. Neurosci. 18, 2159–2165. doi:10.1046/j.1460-9568.2003.02942.x

Uusisaari, M., Obata, K., Knöpfel, T., 2007. Morphological and electrophysiological properties of GABAergic and non-GABAergic cells in the deep cerebellar nuclei. J. Neurophysiol. 97, 901–911. doi:10.1152/jn.00974.2006

Uusisaari, M.Y., Knöpfel, T., 2012. Diversity of neuronal elements and circuitry in the cerebellar nuclei. Cerebellum 11, 420–421. doi:10.1007/s12311-011-0350-6

van Rossum, M.C.W., Turrigiano, G.G., Nelson, S.B., 2002. Fast propagation of firing rates through layered networks of noisy neurons. J. Neurosci. 22, 1956–1966. doi:22/5/1956 [pii]

Vetter, P., Roth, A., Häusser, M., Ledergerber, D., Larkum, M.E., 2001. Propagation of Action Potentials in Dendrites Depends on Dendritic Morphology Propagation of Action Potentials in Dendrites Depends on Dendritic Morphology 926–937.

White, J. a, Klink, R., Alonso, a, Kay, a R., 1998. Noise from voltage-gated ion channels may influence neuronal dynamics in the entorhinal cortex. J. Neurophysiol. 80, 262–269. doi:10.1038/342175a0

White, J. a, Rubinstein, J.T., Kay, a R., 2000. Channel noise in neurons. Trends Neurosci. 23, 131–7.

Williams, S.R., Stuart, G.J., 2003. Role of dendritic synapse location in the control of action potential output. Trends Neurosci. 26, 147–54. doi:10.1016/S0166-2236(03)00035-3

Winkowski, D.E., Knudsen, E.I., 2006. Top-down gain control of the auditory space map by gaze control circuitry in the barn owl. Nature 439, 336–339. doi:10.1038/nature04411

Yakusheva, T. a, Shaikh, A.G., Green, A.M., Blazquez, P.M., Dickman, J.D., Angelaki, D.E., 2007. Purkinje cells in posterior cerebellar vermis encode motion in an inertial reference frame. Neuron 54, 973–85. doi:10.1016/j.neuron.2007.06.003

Yarom, Y., Hounsgaard, J., 2011. Voltage Fluctuations in Neurons: Signal or Noise? Physiol. Rev. 91, 917–929. doi:10.1152/physrev.00019.2010

Zhang, Z., Arsenault, D., 2005. Gain modulation by serotonin in pyramidal neurones of the rat

prefrontal cortex. J. Physiol. 566, 379–94. doi:10.1113/jphysiol.2005.086066

Zipser, D., Andersen, R.A., 1988. A back-propagation programmed network that simulates response properties of a subset of posterior parietal neurons. Nature 331, 679–684. doi:10.1038/331679a0

Appendix A

A.1 Neuronal models

Both neuron models were obtained from ModelDB database (Hines et al., 2004). The simulations were carried out in NEURON (Hines and Carnevale, 1997). The data analysis was performed in Matlab (The Mathworks Inc., 2016).

A.1.1 CN neuronal model

A.1.1.1 Deterministic model

The CN neuronal model was developed originally by Steuber et al., 2011, and translated in NEURON by Luthman et al., 2011 (accession numbers: 136175 and 144523, respectively).

A.1.1.2 Stochastic model

A.1.1.2.1 Transition state probabilities

A.1.1.2.1.1 Fast sodium (NaF) and persistent sodium (NaP) channels

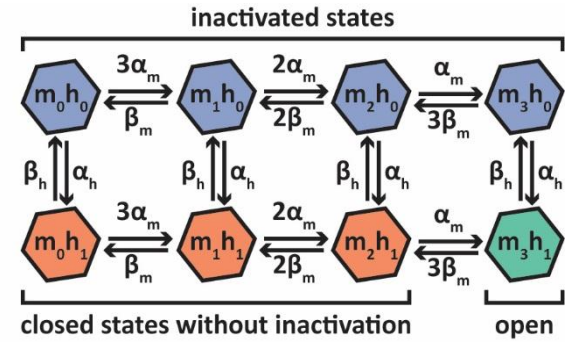

Figure A1 NaF and NaP channels reduced kinetic diagram. The system can be described by eight major states. The rate constants are summarized, and their sequence is kinetically identical to the m^3h Huxley-Hodgkin model.

The transition probabilities are:

Transition from $m_0h_0 \rightarrow m_1h_0$:

$$p(t) = \frac{3\alpha_m}{\alpha_h + 3\alpha_m}(1 - exp(-(\alpha_h + 3\alpha_m)dt_{sim})) \qquad \textbf{Equation A.1}$$

Transition from $m_0h_0 \rightarrow m_0h_1$:

$$p(t) = \frac{\alpha_h}{\alpha_h + 3\alpha_m}(1 - exp(-(\alpha_h + 3\alpha_m)dt_{sim})) \qquad \textbf{Equation A.2}$$

Transition from $m_1h_0 \rightarrow m_1h_1$:

$$p(t) = \frac{\alpha_h}{\alpha_h + 2\alpha_m + \beta_m}(1 - exp(-(\alpha_h + 2\alpha_m + \beta_m)dt_{sim})) \qquad \textbf{Equation A.3}$$

Transition from $m_1h_0 \rightarrow m_2h_0$:

$$p(t) = \frac{2\alpha_m}{2\alpha_m + \beta_m}(1 - exp(-(2\alpha_m + \beta_m)dt_{sim})) \qquad \textbf{Equation A.4}$$

Transition from $m_1h_0 \rightarrow m_0h_0$:

$$p(t) = \frac{\beta_m}{2\alpha_m + \beta_m}(1 - exp(-(2\alpha_m + \beta_m)dt_{sim})) \qquad \textbf{Equation A.5}$$

Transition from $m_2h_0 \rightarrow m_2h_1$:

$$p(t) = \frac{\alpha_h}{\alpha_h + \alpha_m + 2\beta_m}(1 - exp(-(\alpha_h + \alpha_m + 2\beta_m)dt_{sim})) \qquad \textbf{Equation A.6}$$

Transition from $m_2h_0 \rightarrow m_3h_0$:

$$p(t) = \frac{\alpha_m}{\alpha_m + 2\beta_m}(1 - exp(-(\alpha_m + 2\beta_m)dt_{sim})) \quad \textbf{Equation A.7}$$

Transition from $m_2h_0 \rightarrow m_1h_0$:

$$p(t) = \frac{2\beta_m}{\alpha_m + 2\beta_m}(1 - exp(-(\alpha_m + 2\beta_m)dt_{sim})) \quad \textbf{Equation A.8}$$

Transition from $m_3h_0 \rightarrow m_3h_1$:

$$p(t) = \frac{\alpha_h}{\alpha_h + 3\beta_m}(1 - exp(-(\alpha_h + 3\beta_m)dt_{sim})) \quad \textbf{Equation A.9}$$

Transition from $m_3h_0 \rightarrow m_2h_0$:

$$p(t) = \frac{3\beta_m}{\alpha_h + 3\beta_m}(1 - exp(-(\alpha_h + 3\beta_m)dt_{sim})) \quad \textbf{Equation A.10}$$

Transition from $m_0h_1 \rightarrow m_0h_0$:

$$p(t) = \frac{\beta_h}{3\alpha_m + \beta_h}(1 - exp(-(3\alpha_m + \beta_h)dt_{sim})) \quad \textbf{Equation A.11}$$

Transition from $m_0h_1 \rightarrow m_1h_1$:

$$p(t) = \frac{3\alpha_m}{3\alpha_m + \beta_h}(1 - exp(-(3\alpha_m + \beta_h)dt_{sim})) \quad \textbf{Equation A.12}$$

Transition from $m_1h_1 \rightarrow m_1h_0$:

$$p(t) = \frac{\beta_h}{2\alpha_m + \beta_m + \beta_h}(1 - exp(-(2\alpha_m + \beta_m + \beta_h)dt_{sim})) \quad \textbf{Equation A.13}$$

Transition from $m_1h_1 \rightarrow m_2h_1$:

$$p(t) = \frac{2\alpha_m}{2\alpha_m + \beta_m}(1 - exp(-(2\alpha_m + \beta_m)dt_{sim})) \quad \textbf{Equation A.14}$$

Transition from $m_1h_1 \rightarrow m_0h_1$:

$$p(t) = \frac{\beta_m}{2\alpha_m + \beta_m}(1 - exp(-(2\alpha_m + \beta_m)dt_{sim})) \quad \textbf{Equation A.15}$$

Transition from $m_2h_1 \rightarrow m_2h_0$:

$$p(t) = \frac{\beta_h}{\alpha_m + 2\beta_m + \beta_h}(1 - exp(-(\alpha_m + 2\beta_m + \beta_h)dt_{sim})) \quad \textbf{Equation A.16}$$

Transition from $m_2h_1 \rightarrow m_3h_1$:

$$p(t) = \frac{\alpha_m}{\alpha_m + 2\beta_m}(1 - exp(-(\alpha_m + 2\beta_m)dt_{sim})) \quad \textbf{Equation A.17}$$

Transition from $m_1h_1 \rightarrow m_1h_0$:

$$p(t) = \frac{2\beta_m}{\alpha_m + 2\beta_m}(1 - exp(-(\alpha_m + 2\beta_m)dt_{sim})) \quad \textbf{Equation A.18}$$

Transition from $m_3h_1 \rightarrow m_3h_0$:

$$p(t) = \frac{\beta_h}{3\beta_m + \beta_h}(1 - exp(-(3\beta_m + \beta_h)dt_{sim})) \quad \textbf{Equation A.19}$$

Transition from $m_3h_1 \rightarrow m_2h_1$:

$$p(t) = \frac{3\beta_m}{3\beta_m + \beta_h}(1 - exp(-(3\beta_m + \beta_h)dt_{sim})) \quad \textbf{Equation A.20}$$

A.1.1.2.1.2 Fast delayed rectifier potassium (fKdr) and slow delayed rectifier potassium (sKdr) channels

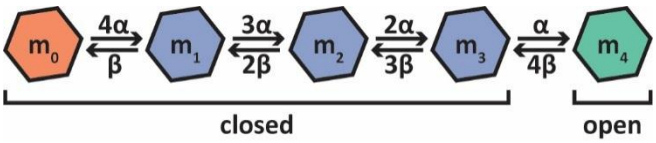

Figure A2 fKdr and sKdr channels reduced kinetic diagram. The system can be described by five major states. The rate constants are summarized, and their sequence is kinetically identical to the m^4 Huxley-Hodgkin model.

The transition probabilities are:

Transition from $m_0 \rightarrow m_1$:

$$p(t) = 1 - exp(-(4\alpha)dt_{sim}) \quad \textbf{Equation A.21}$$

Transition from $m_1 \rightarrow m_2$:

$$p(t) = \frac{3\alpha}{3\alpha + \beta}(1 - exp(-(3\alpha + \beta)dt_{sim})) \quad \textbf{Equation A.22}$$

Transition from $m_1 \rightarrow m_0$:

$$p(t) = \frac{\beta}{3\alpha + \beta}(1 - exp(-(3\alpha + \beta)dt_{sim})) \quad \textbf{Equation A.23}$$

Transition from $m_2 \rightarrow m_3$:

$$p(t) = \frac{2\alpha}{2\alpha + 2\beta}(1 - exp(-(2\alpha + 2\beta)dt_{sim})) \quad \textbf{Equation A.24}$$

Transition from $m_2 \rightarrow m_1$:

$$p(t) = \frac{2\beta}{2\alpha + 2\beta}(1 - exp(-(2\alpha + 2\beta)dt_{sim})) \quad \textbf{Equation A.25}$$

Transition from $m_3 \rightarrow m_4$:

$$p(t) = \frac{\alpha}{\alpha + 3\beta}(1 - exp(-(\alpha + 3\beta)dt_{sim})) \quad \textbf{Equation A.26}$$

Transition from $m_3 \rightarrow m_2$:

$$p(t) = \frac{3\beta}{\alpha + 3\beta}(1 - exp(-(\alpha + 3\beta)dt_{sim})) \quad \textbf{Equation A.27}$$

Transition from $m_4 \rightarrow m_3$:

$$p(t) = 1 - exp(-(4\beta)dt_{sim}) \quad \textbf{Equation A.28}$$

A.1.1.2.1.3 High-voltage-activated calcium (CaHVA) channel

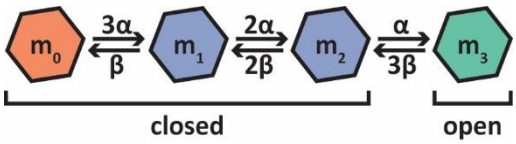

Figure A3 CaHVA channel reduced kinetic diagram. The system can be described by four major states. The rate constants are summarized, and their sequence is kinetically identical to the m^3 Huxley-Hodgkin model.

The transition probabilities are:

Transition from $m_0 \rightarrow m_1$:

$$p(t) = 1 - exp(-(3\alpha)dt_{sim}) \quad \textbf{Equation A.29}$$

Transition from $m_1 \rightarrow m_2$:

$$p(t) = \frac{2\alpha}{2\alpha + \beta}(1 - exp(-(2\alpha + \beta)dt_{sim})) \quad \textbf{Equation A.30}$$

Transition from $m_1 \rightarrow m_0$:

$$p(t) = \frac{\beta}{2\alpha + \beta}(1 - exp(-(2\alpha + \beta)dt_{sim})) \quad \textbf{Equation A.31}$$

Transition from $m_2 \rightarrow m_3$:

$$p(t) = \frac{\alpha}{\alpha + 2\beta}(1 - exp(-(\alpha + 2\beta)dt_{sim})) \quad \textbf{Equation A.32}$$

Transition from $m_2 \rightarrow m_1$:

$$p(t) = \frac{2\beta}{\alpha + 2\beta}(1 - exp(-(\alpha + 2\beta)dt_{sim})) \quad \textbf{Equation A.33}$$

Transition from $m_3 \rightarrow m_2$:

$$p(t) = 1 - exp(-(3\beta)dt_{sim}) \quad \textbf{Equation A.34}$$

A.1.1.2.1.4 Low-voltage-activated calcium (CaLVA) channel

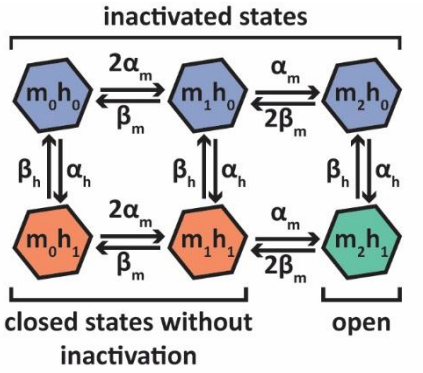

Figure A4 CaLVA channel reduced kinetic diagram. The system can be described by six major states. The rate constants are summarized, and their sequence is kinetically identical to the m^2h Huxley-Hodgkin model.

The transition probabilities are:

Transition from $m_0h_0 \rightarrow m_1h_0$:

$$p(t) = \frac{2\alpha_m}{\alpha_h + 2\alpha_m}(1 - exp(-(\alpha_h + 2\alpha_m)dt_{sim})) \quad \textbf{Equation A.35}$$

Transition from $m_0h_0 \rightarrow m_0h_1$:

$$p(t) = \frac{\alpha_h}{\alpha_h + 2\alpha_m}(1 - exp(-(\alpha_h + 2\alpha_m)dt_{sim})) \quad \textbf{Equation A.36}$$

Transition from $m_1h_0 \rightarrow m_1h_1$:

$$p(t) = \frac{\alpha_h}{\alpha_h + \alpha_m + \beta_m}(1 - exp(-(\alpha_h + \alpha_m + \beta_m)dt_{sim})) \quad \textbf{Equation A.37}$$

Transition from $m_1h_0 \rightarrow m_2h_0$:

$$p(t) = \frac{\alpha_m}{\alpha_m + \beta_m}(1 - exp(-(\alpha_m + \beta_m)dt_{sim})) \quad \textbf{Equation A.38}$$

Transition from $m_2h_0 \rightarrow m_2h_1$:

$$p(t) = \frac{\alpha_h}{\alpha_h + 2\beta_m}(1 - exp(-(\alpha_h + 2\beta_m)dt_{sim})) \quad \textbf{Equation A.39}$$

Transition from $m_2h_0 \rightarrow m_1h_0$:

$$p(t) = \frac{2\beta_m}{\alpha_h + 2\beta_m}(1 - exp(-(\alpha_h + 2\beta_m)dt_{sim})) \quad \textbf{Equation A.40}$$

Transition from $m_0h_1 \rightarrow m_1h_1$:

$$p(t) = \frac{2\alpha_m}{2\alpha_m + \beta_h}(1 - exp(-(2\alpha_m + \beta_h)dt_{sim})) \quad \textbf{Equation A.41}$$

Transition from $m_0h_1 \rightarrow m_0h_0$:

$$p(t) = \frac{\beta_h}{2\alpha_m + \beta_h}(1 - exp(-(2\alpha_m + \beta_h)dt_{sim})) \quad \textbf{Equation A.42}$$

Transition from $m_1h_1 \rightarrow m_1h_0$:

$$p(t) = \frac{\beta_h}{\alpha_m + \beta_m + \beta_h}(1 - exp(-(\alpha_m + \beta_m + \beta_h)dt_{sim})) \quad \textbf{Equation A.43}$$

Transition from $m_1h_1 \rightarrow m_2h_1$:

$$p(t) = \frac{\alpha_m}{\alpha_m + \beta_m}(1 - exp(-(\alpha_m + \beta_m)dt_{sim})) \quad \textbf{Equation A.44}$$

Transition from $m_1h_1 \rightarrow m_0h_1$:

$$p(t) = \frac{\beta_m}{\alpha_m + \beta_m}(1 - exp(-(\alpha_m + \beta_m)dt_{sim})) \quad \textbf{Equation A.45}$$

Transition from $m_2h_1 \rightarrow m_2h_0$:

$$p(t) = \frac{\beta_h}{2\beta_m + \beta_h}(1 - exp(-(2\beta_m + \beta_h)dt_{sim})) \quad \textbf{Equation A.46}$$

Transition from $m_2h_1 \rightarrow m_1h_1$:

$$p(t) = \frac{2\beta_m}{2\beta_m + \beta_h}(1 - exp(-(2\beta_m + \beta_h)dt_{sim})) \quad \textbf{Equation A.47}$$

A.1.1.2.1.5 Small conductance calcium-dependent potassium (SK) channel

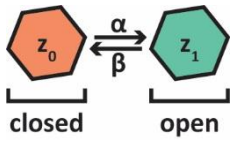

Figure A5 SK channel reduced kinetic diagram. The system can be described by four major states. The rate constants are summarized, and their sequence is kinetically identical to the *z* Huxley-Hodgkin model.

The transition probabilities are:

Transition from $z_0 \rightarrow z_1$:

$$p(t) = 1 - exp(-\alpha)dt_{sim} \quad \textbf{Equation A.48}$$

Transition from $z_1 \rightarrow z_0$:

$$p(t) = 1 - exp(-\beta)dt_{sim} \quad \textbf{Equation A.49}$$

A.1.1.2.2 Single channel conductance

For the simple compartment simulations, the values of the specific channel conductances are based on the model files of each voltage gated channel based on the CN model by Steuber et al., 2011, and as translated in NEURON by Luthman et al., 2011. However, some values are corrected so there would be a response (spike) to injected current (Table A1). The single channel conductance is chosen arbitrary based on values as in Hille, 2001, except for the HCN channel which is based on the value from the Kole et al., 2006.

Current	Specific channel conductance (S/cm^2)	Single channel conductance (S)
NaP	1.0e-02	1.0e-12
NaF	2.5e-03	1.0e-12
fKdr	1.0e-03	1.0e-12
sKdr	1.0e-03	1.0e-12
SK	1.0e-05	1.0e-13
CaLVA	1.77e-02	1.0e-12
CaHVA	7.5e-06	1.0e-16
HCN	1.0e-05	6.8e-12

Table A1 Single compartmental model

In the fully stochastic CN model, the total channel conductance values are as in Steuber et al., 2011. The single channel conductance for each stochastic channel is adjusted (Table A2) so in each neuronal compartment there would be at least 100 channels of each type, which is a moderate population size, so the impact of noise is limited but not totally eliminated. There are not known data for the numbers of each channel type in reality.

Current	Single channel conductance (S)
NaP	3.06626e-13
NaF	3.83283e-12
fKdr	3.44954e-12
sKdr	2.87462e-12
SK	2.52967e-14
CaLVA	1.35682e-14
CaHVA	1.91641e-15
HCN	2.2997e-13

Table A2 CN detailed compartmental model

A.1.1.2.3 Ion channel families

The model used in this study is a conductance based multicompartmental model, which is tuned to replicate experimentally observed electrophysiological characteristics of excitatory projection CN neuron. Ion channel subunit heterogeneity is omitted from the description of this model (Steuber et al., 2011) and it was not also taken into account for this study. However, a possible identification of the CN ion channels' families is shown in the table below (Table A3)

Current	Family	References
NaP	$Na_v1.1$, $Na_v1.6$, Naβ1	(Alexander et al., 2017; Magistretti and Alonso, 1999; Schaller and Caldwell, 2003; Steuber et al., 2011)
NaF	$Na_v1.1$, $Na_v1.6$, Naβ1	(Alexander et al., 2017; Raman et al., 2000; Schaller and Caldwell, 2003; Steuber et al., 2011)
fKdr	K_v3	(Alexander et al., 2017; Baranauskas et al., 1999, 2003; Steuber et al., 2011)

sKdr	K_v2	(Alexander et al., 2017; Baranauskas et al., 1999, 2003; Steuber et al., 2011)
SK	SK1, SK2l, SK3	(Aizenman and Linden, 1999; Alexander et al., 2017; Jahnsen, 1986; Raman et al., 2000; Sailer et al., 2004; Steuber et al., 2011)
CaLVA	$Ca_v3.1$	(Alexander et al., 2017; Gauck et al., 2001; Molineux et al., 2006; Steuber et al., 2011)
CaHVA	$Ca_v1.2$, $Ca_v1.3$, $Ca_v2.1$, $Ca_v2.2$, $Ca_v2.3$	(Alexander et al., 2017; Gauck et al., 2001; Schlick et al., 2012; Steuber et al., 2011)
HCN	HCN2	(Alexander et al., 2017; Raman et al., 2000; Steuber et al., 2011)

Table A3 CN Ion channel families

A.1.2 PN neuronal model

The PN neuronal model is based on the model by Hay et al., 2011 (accession number: 139653) and enriched with the dual-exponential synaptic conductance models for AMPA, NMDA and GABA, with their properties acquired from the model by Hay and Segev, 2015 (accession number: 156780).